Πανεπιστήμιο Ιωαννίνων
Σχολή Θετικών Επιστημών
Τμήμα Φυσικής

Ακτινοβολία **Hawking** και εντοπισμός μελανών οπών στα πλαίσια πολυδιάστατων θεωριών βαρύτητας

Θωμάς Παππάς

Διδακτορική Διατριβή

Ιωάννινα 2018

University of Ioannina
School of Natural Sciences
Department of Physics

Hawking radiation and black-hole localization in the context of higher-dimensional gravitational theories

Thomas Pappas

PhD Thesis

Ioannina 2018

Three-member advisory committee:

1. Panagiota Kanti (supervisor) – Professor, Physics Department, University of Ioannina
2. Kyriakos Tamvakis – Professor, Physics Department, University of Ioannina
3. Ioannis Rizos – Professor, Physics Department, University of Ioannina

Seven-member PhD thesis examination committee:

1. Panagiota Kanti (supervisor) – Professor, Physics Department, University of Ioannina
2. Kyriakos Tamvakis – Professor, Physics Department, University of Ioannina
3. Ioannis Rizos – Professor, Physics Department, University of Ioannina
4. Athanasios Dedes – Professor, Physics Department, University of Ioannina
5. Georgios Leontaris – Professor, Physics Department, University of Ioannina
6. Leandros Perivolaropoulos – Professor, Physics Department, University of Ioannina
7. Theodoros Tomaras - Professor, Department of Physics, University of Crete

Αφιερωμένο στη Μάνα και τον Πατέρα μου, τον Ευριπίδη και την Αθηνά, τη Γιαγιά μου, τους κοντινούς μου φίλους και την Carmen.

Abstract

In the first part of this thesis, we study the emission of Hawking radiation (HR) by higher-dimensional Schwarzschild-de Sitter (SdS) black holes in the context of the large extra dimensions scenario. Focusing on the emission of a scalar field, both on the brane and in the bulk, that is non-minimally coupled to gravity, we perform a thorough study of the corresponding greybody factors (GFs), i.e the transmission probability of the field in a given spacetime. The expressions for the GFs are derived both analytically and numerically by developing the appropriate numerical code. With our exact numerical results for the GFs, we then study in depth the HR spectra both in the brane and bulk channels of emission. Also, the effect of various definitions for the temperature of the SdS spacetime on the HR spectra is also investigated. The second part of this thesis is dedicated to the search for an exact analytic 5-dimensional black-hole solution, that is localized close to the brane in the context of the warped extra dimensions scenario. In the model we study, the line-element is of the Vaidya-type with a mass that depends on the radial, temporal and extra dimension coordinates. For the bulk content we consider various scalar field theories with one or multiple scalars, (non-)minimally coupled to gravity and with general kinetic and general potential terms.

ΠΕΡΙΛΗΨΗ

Η Γενική θεωρία της Σχετικότητας (ΓΘΣ) του Albert Einstein αποτελεί την ακριβέστερη θεωρία που διαθέτουμε για την περιγραφή της βαρύτητας. Στα πλαίσια της ΓΘΣ, η βαρύτητα περιγράφεται ως καμπύλωση στο χωρόχρονο η οποία προκαλείται από την παρουσίας μάζας. Οι εξισώσεις κίνησης για το βαρυτικό πεδίο $g_{\mu\nu}$ είναι οι ακόλουθες:

$$G_{\mu\nu} \equiv R_{\mu\nu} - \frac{1}{2}\, g_{\mu\nu}\, R = \kappa_D^2\, T_{\mu\nu}\,, \tag{1}$$

όπου στο αριστερό μέλος έχουμε τον τανυστή του Einstein, $G_{\mu\nu}$ και στο δεξί έχουμε τον τανυστή ορμής-ενέργειας $T_{\mu\nu}$.

Σύγχρονες αστρονομικές παρατηρήσεις υποδηλώνουν πως το Σύμπαν μας διανύει μια φάση επιταχυνόμενης διαστολής η οποία μπορεί να αποδοθεί στην παρουσία μιας θετικής κοσμολογικής σταθεράς η οποία επάγει ένα επιπλέον όρο $+g_{\mu\nu}\Lambda$ στο αριστερό μέλος των εξισώσεων του Einstein.

Μια από τις πιο συναρπαστικές προβλέψεις της ΓΘΣ είναι η ύπαρξη περιοχών στο χωρόχρονο όπου η καμπύλωση είναι τόσο έντονη ώστε τίποτε, ούτε το ίδιο το φως, να μην μπορεί να διαφύγει της βαρυτικής έλξης. Οι περιοχές αυτές επομένως δεν εκπέμπουν τίποτε, παρά μόνο απορροφούν ύλη και ακτινοβολία με αποτέλεσμα να φαίνονται μαύρες για ένα μακρινό παρατηρητή, εξού και η ονομασία τους ως μελανές οπές.

Οι εξισώσεις Einstein είναι υπερβολικά πολύπλοκες εξισώσεις και έτσι για να βρεθεί αναλυτικά μια ακριβής λύση για το βαρυτικό πεδίο απαιτείται η υπόθεση υψηλού βαθμού συμμετρίας για το σύστημα που μελετούμε. Το 1916, μόλις ένα χρόνο μετά τη δημοσίευση της ΓΘΣ, ο Karl Schwarzschild θεωρώντας μια στατική, σφαιρικά συμμετρική και αφόρτιστη κατανομή μάζας βρήκε την πρώτη λύση μελανής οπής η οποία έχει το ακόλουθο στοιχείο μήκους:

$$ds^2 = g_{\mu\nu}dx^\mu dx^\nu = -h(r)dt^2 + h(r)^{-1}dr^2 + r^2\left(d\theta^2 + \sin\theta^2 d\phi^2\right)\,,\; h(r) \equiv \left(1 - \frac{r_h}{r}\right)\,, \tag{2}$$

Σε αυτό το σύστημα συντεταγμένων, ο ορίζοντας γεγονότων της μελανής οπής βρίσκεται στην ακτινική απόσταση $r = r_h$ για την οποία η μετρική δεν είναι καλά ορισμένη καθώς η συνάρτηση

της μετρικής μηδενίζεται $h(r_h) = 0$. Η νοητή σφαιρική επιφάνεια ακτίνας $r = r_h$ ορίζει το "σημείο χωρίς επιστροφή", καθώς κανένα φωτεινό σήμα δεν μπορεί να εκπεμφθεί με $r \leqslant r_h$ και να φτάσει σε έναν παρατηρητή ο οποίος βρίσκεται μακριά από την μελανή οπή.

Η εικόνα που είχαμε για τις μελανές οπές ως τους απόλυτους απορροφητές του Σύμπαντος άλλαξε ριζικά στα μέσα της δεκαετίας του 1970 όταν ο Βρετανός φυσικός Stephen Hawking απέδειξε πως, αν λάβουμε υπόψη κβαντικά φαινόμενα τότε η μελανές οπές εκπέμπουν σωματίδια με θερμικό φάσμα. Η θερμοκρασία της μελανής οπής είναι ανάλογη της επιφανειακής βαρύτητας του ορίζοντα γεγονότων της, ενώ η ακτινοβολία των μελανών οπών ονομάζεται ακτινοβολία Hawking.

Η διαδικασία εκπομπής σωματιδίων από τη μελανή οπή μπορεί να περιγραφεί ως εξής. Το κενό γεννά συνεχώς ζεύγη σωματιδίων-αντισωματιδίων τα οποία εμφανίζονται για πολύ μικρό χρονικό διάστημα πριν ξανά εξαϋλωθούν. Όταν ένα τέτοιο ζεύγος σχηματιστεί κοντά στον ορίζοντα γεγονότων, το ένα σωματίδιο μπορεί να απορροφηθεί από την μελανή οπή αφήνοντας έτσι το άλλο σωματίδιο του ζεύγους ελεύθερο. Αν το σωματίδιο αυτό έχει αρκετή ενέργεια για να διαπεραστεύσει μέχρι το άπειρο, ένας μακρινός παρατηρητής θα αντιληφθεί την παραπάνω διαδικασία ως ακτινοβολία προερχόμενη από τη μελανή οπή.

Σύντομα μετά τη διατύπωση της ΓΘΣ, σε μια προσπάθεια για την ενοποίηση της βαρύτητας με τον ηλεκτρομαγνητισμό, οι Kaluza και Klein υπέθεσαν την ύπαρξη μιας επιπλέον χωρικής διάστασης πέρα των τριών που παρατηρούμε. Ο λόγος που η επιπλέον διάσταση δε γίνεται αντιληπτή είναι γιατί είναι καμπυλωμένη με πολύ μικρή ακτίνα συμπαγοποίησης. Στα τέλη του προηγούμενου αιώνα, η υπόθεση πως το Σύμπαν μας διαθέτει επιπλέον χωρικές διαστάσεις βρέθηκε ξανά στο προσκήνιο στα πλαίσια των μοντέλων βρανών (brane-world models). Σε αυτά τα μοντέλα ο χωρόχρονος είναι $(1+3+D)$-διάστατος, ενώ το Σύμπαν που παρατηρούμε μπορεί να θεωρηθεί ως μια μεμβράνη $1+3$ διαστάσεων η οποία είναι εμβαπτισμένη μέσα στον πλήρη $(1+3+D)$-διάστατο υπερχώρο.

Το πρώτο μέρος της διατριβής είναι αφιερωμένο στη μελέτη της ακτινοβολίας Hawking από πολυδιάστατες (HD) μελανές οπές τύπου Schwarzschild de-Sitter (SdS) οι οποίες περιγράφουν σφαιρικά συμμετρικές μελανές οπές παρουσία θετικής κοσμολογικής σταθεράς. Η ύπαρξη μιας θετικής κοσμολογικής σταθεράς έχει ως αποτέλεσμα την εμφάνιση ενός κοσμολογικού ορίζοντα (σε ακτινική απόσταση $r = r_c$ από την αρχή των συντεταγμένων) επιπλέον του ορίζοντα της μελανής οπής. Οι δύο ορίζοντες αποτελούν τα όρια του αιτιατού μέρους του Σύμπαντος για ένα αδρανιακό παρατηρητή που βρίσκεται σε μια θέση $r = r_0$ ανάμεσα από τους δύο ορίζοντες $r_h \leqslant r_0 \leqslant r_c$.

Στο πρώτο κεφάλαιο, κάνουμε μια σύντομη εισαγωγή σε βασικές έννοιες της ΓΘΣ, της θερμοδυναμικής των μελανών οπών και στην ακτινοβολία Hawking καθώς και στις θεωρίες επιπλέον χωρικών διαστάσεων. Στη συνέχεια, στο δεύτερο κεφάλαιο, επικεντρωνόμαστε στον αναλυτικό υπολογισμό των Συντελεστών Γκρίζου Σώματος (ΣΓΣ) (greybody factors) για ένα βαθμωτό

πεδίο σε μη-ελάχιστη σύζευξη με τη βαρύτητα, το οποίο διαδίδεται στο γεωμετρικό υπόβαθρο μιας μελανής οπής HDSdS. Οι ΣΓΣ αποτελούν πολύ βασικές ποσότητες μεταξύ άλλων και για τη μελέτη της ακτινοβολίας Hawking από μια μελανή οπή καθώς το φάσμα της εκπομπής διαφέρει από αυτό ενός τέλειου μέλανος σώματος κατά ένα παράγοντα ίσο με τον ΣΓΣ.

Για τον αναλυτικό υπολογισμό των ΣΓΣ επιλύουμε ένα πρόβλημα σκέδασης στο ενεργό δυναμικό Regge-Wheeler του βαρυτικού πεδίου της HDSdS μελανής οπής. Οι ΣΓΣ αντιστοιχούν στην πιθανότητα διέλευσης από το φράγμα δυναμικού για σωματίδια που γεννώνται από τη μελανή οπή και διαδίδονται προς μεγαλύτερες τιμές της ακτινικής συντεταγμένης. Υποθέτοντας σφαιρικά συμμετρικό πεδίο και χρησιμοποιώντας τη μέθοδο χωρισμού των μεταβλητών επιτυγχάνουμε την αποσύζευξη των ακτινικών μερών των εξισώσεων κίνησης του πεδίου για διάδοση περιορισμένη πάνω στη μεμβράνη καθώς και για διάδοση στον υπερχώρο. Οι δύο ακτινικές διαφορικές εξισώσεις που προκύπτουν είναι πολύ δύσκολο να επιλυθούν ακριβώς αναλυτικά και συνεπώς καταφύγαμε στην χρήση μιας προσεγγιστικής μεθόδου γνωστής και ως ΜΕθόδου Ταύτισης των Ασυμπτωτικών Λύσεων (ΜΕΤΑΛ). Με τη ΜΕΤΑΛ κάτω από κατάλληλους μετασχηματισμούς της ακτινικής συντεταγμένης και επανορισμό του πεδίου μπορούμε να φέρουμε την εξίσωση κίνησης σε μορφή γνωστής διαφορικής εξίσωσης κοντά στους ορίζοντες οπότε και μπορούμε να τη λύσουμε. Στη συνέχεια, για να διασφαλίσουμε την ύπαρξη λύσης σε όλο το εύρος της ακτινικής συντεταγμένης κάνουμε ταύτιση των δύο ασυμπτωτικών λύσεων στην ενδιάμεση περιοχή κάτω από κατάλληλα αναπτύγματα.

Κοντά στους ορίζοντες, και συναρτήσει της λεγόμενης tortoise συντεταγμένης μπορούμε να γράψουμε τις λύσεις των εξισώσεων κίνησης για το πεδίο με τη μορφή επίπεδων ελεύθερων κυμάτων και από το λόγο των πλατών των εξερχόμενων και εισερχόμενων κυμάτων να υπολογίσουμε τους ΣΓΣ. Στην ανάλυση μας για τη λύση κοντά στον ορίζοντα της μελανής οπής, σε αντίθεση με παρόμοιες μελέτες, καταφέραμε να βρούμε ένα κατάλληλο μετασχηματισμό για την ακτινική συντεταγμένη ο οποίος λαμβάνει υπόψη και την κοσμολογική σταθερά. Κατ' αυτόν τον τρόπο, τα αναλυτικά μας αποτελέσματα έχουν μεγαλύτερη ακρίβεια.

Τα αναλυτικά μας αποτελέσματα για τους ΣΓΣ (στη μεμβράνη και τον υπερχώρο) είναι ακριβή για χαμηλές ενέργειες, μικρές τιμές της κοσμολογικής σταθεράς (Λ), και για μικρές τιμές της σταθεράς σύζευξης του βαθμωτού πεδίου (ξ) με το βαθμωτό καμπυλότητας του Ricci. Ωστόσο είναι έγκυρα για αυθαίρετο αριθμό επιπλέον χωρικών διαστάσεων και για κβαντικό αριθμό τροχιακής στροφορμής του πεδίου (l).

Και στα δύο "κανάλια εκπομπής " (στη μεμβράνη και στον υπερχώρο) βρήκαμε πως οι ΣΓΣ καταστέλονται με τη σταθερά μη-μηδενικής σύζευξης του πεδίου, με τον κβαντικό αριθμό της τροχιακή στροφορμής καθώς και με τον αριθμό των επιπλέον χωρικών διαστάσεων (n). Όσον αφορά την επίπτωση στους ΣΓΣ της τελευταίας παραμέτρου του συστήματος , δηλαδή της θετικής κοσμολογικής σταθεράς, διαπιστώσαμε πως ο ρόλος της είναι δυικός. Ανάλογα με την τιμή του ξ,

η αύξηση της Λ μπορεί να ενισχύσει ή να καταστείλει την εκπομπή σωματιδίων. Η συμπεριφορά αυτή οφείλεται στον τρόπο που η κοσμολογική σταθερά εμφανίζεται στις εξισώσεις. Από τη μια μεριά, εμφανίζεται στη συνάρτηση της μετρικής ως πυκνότητα ενέργειας του κενού και συνεπώς ενισχύει την εκπομπή σωματιδίων. Από την άλλη μεριά, εμφανίζεται στην έκφραση της ενεργού μάζας για τα βαθμωτά σωματίδια μέσω ενός γινομένου με το ξ και έτσι, όσο πιο βαριά γίνονται τα σωματίδια τόσο πιο δύσκολο είναι να εκπεμφθούν από την μελανή οπή. Για μικρές τιμές του ξ η πρώτη συνεισφορά της Λ ως ενέργειας κενού κυριαρχεί με αποτέλεσμα οι ΣΓΣ να ενισχύονται, ενώ για μεγαλύτερες τιμές της σταθεράς μη-ελάχιστης σύζευξης τα σωματίδια αποκτούν αρκετά μεγάλη ενεργή μάζα προκαλώντας την καταστωλή των ΣΓΣ.

Η μελέτη των αναλυτικών εκφράσεων των ΣΓΣ στο χαμηλοενεργειακό όριο αποκάλυψε πως το γνωστό μη-μηδενικό γεωμετρικό όριο για το κυρίαρχο mode του πεδίου χάνεται όταν το πεδίο δεν είναι σε ελάχιστη σύζευξη με τη βαρύτητα, ένα αποτέλεσμα που ισχύει εξίσου για τη μεμβράνη και τον υπερχώρο. Οι πρώτες διορθώσεις και στις δύο περιπτώσεις είναι τάξης $\mathcal{O}(\omega^2)$ στην ενέργεια, (ω) ενώ τις ακριβείς εκφράσεις των διορθώσεων συναρτήσει των παραμέτρων του συστήματος έχουμε υπολογίσει και παρουσιάζουμε.

Για την πλήρη μελέτη της ακτινοβολίας Hawking σε όλο το ενεργειακό φάσμα, είναι απαραίτητο να έχουμε την ακριβή μορφή των ΣΓΣ και επομένως τα προσεγγιστικά αναλυτικά αποτελέσματα που υπολογίσαμε δεν είναι αρκετά. Για το λόγο αυτό, στο τρίτο κεφάλαιο αναπτύξαμε έναν αριθμητικό κώδικα για την επίλυση των ακτινικών εξισώσεων κίνησης στη μεμβράνη και στον υπερχώρο, προκειμένου να λάβουμε τις ακριβείς εκφράσεις για τους ΣΓΣ. Η σύγκριση ανάμεσα σε αναλυτικά και αριθμητικά αποτελέσματα φανέρωσε εντυπωσιακή συμφωνία ανάμεσα στα δύο σετ στη χαμηλοενεργειακή περιοχή (σε κάποιες περιπτώσεις και πέρα από αυτή) ενώ αποκλίσεις εφανίζονται όταν τα Λ και ξ αποκτούν μεγάλες τιμές.

Έχοντας τις ακριβείς εκφράσεις των ΣΓΣ στη διάθεση μας, υπολογίσαμε στη συνέχεια το φάσμα της ακτινοβολίας Hawking για την HDSdS μελανή οπή στη μεμβράνη και στον υπερχώρο. Για τη θερμοκρασία της μελανής οπής χρησιμοποιήσαμε την κανονικοποίηση των Bousso και Hawking, η οποία λαμβάνει υπόψη την απουσία του ασυμπτωτικά επίπεδου ορίου της μετρικής SdS. Βρήκαμε πως και στα δύο κανάλια εκπομπής, το φάσμα ενισχύεται με τον αριθμό των επιπλέον χωρικών διαστάσεων, ενώ η αύξηση του ξ προκαλεί καταστολή της εκπομπής σε όλο το ενεργειακό φάσμα. Επίσης, ο δυικός ρόλος της κοσμολογικής σταθεράς που παρατηρήθηκε στους ΣΓΣ μεταβιβάζεται και στην ακτινοβολία Hawking καθώς, ανάλογα με την τιμή του ξ, η κοσμολογική σταθερά ενισχύει ή καταστέλλει την ακτινοβολία.

Ακολούθως, υπολογίσαμε το λόγο των ολικών εκπεμπτικοτήτων της μελανής οπής στον υπερχώρο και στη μεβράνη για διάφορες τιμές των παραμέτρων. Με αυτό τον τρόπο μπορούμε να αποφανθούμε για το ποιο είναι το προτιμητέο κανάλι εκπομπής, δηλαδή μπορούμε να διαπιστώσουμε πού εκπέμπει η μελανή οπή το μεγαλύτερο μέρος της ακτινοβολίας της. Η μελέτη του λόγου των

ολικών εκπεμπτικοτήτων φανερώνει πως η εκπομπή στον υπερχώρο είναι αυτή που κυριαρχεί όταν οι τιμές της σταθεράς μη-ελάχιστης σύζευξης και του αριθμού των επιπλεόν διαστάσεων είναι ταυτόχρονα μεγάλες. Αξίζει να σημειωθεί πως αυτή είναι μια από τις ελάχιστες φορές όπου το κανάλι εκπομπής στον υπερχώρο κυριαρχεί του αντίστοιχου στη μεμβράνη και ο λόγος που συμβαίνει αυτό είναι ο μη τετριμμένος τρόπος με τον οποίο το πεδίο συζευγνύεται με τη βαρύτητα.

Στο κεφάλαιο 4, επικεντρωθήκαμε στην επίδραση της θερμοκρασίας στην ακτινοβολία Hawking της HDSdS μελανής οπής. Η παρουσία ενός δεύτερου ορίζοντα στο χωρόχρονο πέραν του ορίζοντα της μελανής οπής δημιουργεί προβλήματα στον ακριβή ορισμό της θερμοδυναμικής των ασυμπτωτικά de-Sitter μελανών οπών. Αρχικά η απουσία ενός ασυμπτωτικά επίπεδου ορίου σύμφωνα με το οποίο κανονικοποιείται η επιφανειακή βαρύτητα και κατά συνέπεια και η θερμοκρασία απαιτεί να ορίσουμε τη θερμοκρασία με βάση έναν αδρανειακό παρατηρητή που βρίσκεται στην περιοχή ανάμεσα από τους δυο ορίζοντες. Επιπλέον, καθώς εν γένει οι δυο ορίζοντες έχουν διαφορετική θερμοκρασία, ο χωρόχρονος SdS δε βρίσκεται σε θερμοδυναμική ισορροπία καθώς υπάρχει μια μόνιμη ροή θερμότητας από το θερμότερο ορίζοντα της μελανή οπής προς τον ψυχρότερο κοσμολογικό ορίζοντα. Για το λόγο αυτό πρόσφατα έχει προταθεί η ενεργός προσέγγιση στη θερμοδυναμική των ασυμπτωτικά de-Sitter μελανών οπών όπου, αντί καθένας από τους δυο ορίζοντες να έχει το δικό του πρώτο θερμοδυναμικό νόμο, ορίζουμε έναν τέτοιο νόμο για ολόκληρο το σύστημα και με αυτό τον τρόπο παίρνουμε μια έκφραση για την θερμοκρασία.

Για την αντιμετώπιση των προαναφερθέντων προβλημάτων, έχουν προταθεί στη βιβλιογραφία διάφοροι ορισμοί ως οι κατάλληλοι για τη θερμοκρασία της SdS μελανής οπής. Χρησιμοποιώντας τα ακριβή αριθμητικά αποτελέσματα για τους ΣΓΣ που υπολογίσαμε στο προηγούμενο κεφάλαιο, συγκρίναμε τα φάσματα εκπομπής για 6 διαφορετικές θερμοκρασίες μια εκ των οποίων προτείνουμε για πρώτη φορά. Η σύγκριση των φασμάτων καταδεικνύει πως η έκφραση της θεμοκρασίας που επιλέγεται για τη μελέτη της ακτινοβολίας Hawking επηρεάζει σημαντικά το απορρέον φάσμα εκπομπής. Κάποιες από τις θερμοκρασίες αδυνατούν να οδηγήσουν σε σημαντική εκπομπή ακτινοβολίας, ενώ άλλες το επιτυγχάνουν μόνο για μικρές ή μεγάλες τιμές της κοσμολογικής σταθεράς. Σε κάθε περίπτωση, διαπιστώσαμε πως η επιλογή της θερμοκρασίας που έχει προταθεί από τους Bousso και Hawking είναι αυτή που οδηγεί στο πιο έντονο φάσμα εκπομπής.

Στο δεύτερο μέρος της διατριβής, στραφήκαμε στο πρόβλημα εντοπισμού των μελανών οπών πάνω στη μεμβράνη σε μοντέλα καμπύλων επιπλέον διαστάσεων (ΚΕΔ) (warped extra dimensions). Σε αντίθεση με τα μοντέλα μεγάλων επιπλέον διαστάσεων (large extra dimensions) όπου αναλυτικές λύσεις μελανών οπών είναι γνωστές εδώ και δεκαετίες, στα μοντέλα ΚΕΔ μέχρι σήμερα δεν έχουν βρεθεί ακριβείς αναλυτικές λύσεις πεντα-διάστατων μελανών οπών εντοπισμένες πάνω στη μεμβράνη. Προς αυτό το στόχο, επεκτείνοντας προηγούμενες δουλειές, θεωρήσαμε ένα ansatz για τη μετρική τύπου Vaidya η οποία εκφυλίζεται σε μια μετρική τύπου Schwarzschild πάνω στη μεμβράνη.

Προκειμένου να προσδώσουμε μεγαλύτερη ευελιξία στις εξισώσεις, επιλέξαμε η παράμετρος μάζας να εμφανίζει εξάρτηση από τη χρονική και την ακτινική συντεταγμένη καθώς και από τη συντεταγμένη της επιπλέον διάστασης. Για να υποστηρίξουμε μια τέτοια λύση μέσω των εξισώσεων Einstein χρειάζεται να έχουμε ένα μη-μηδενικό τανυστή ορμής-ενέργειας $(T_{\mu\nu})$ στον υπερχώρο.

Έτσι, θεωρήσαμε διάφορες κατανομές πεδίων για τον $T_{\mu\nu}$ του υπερχώρου ξεκινώντας από την πιο απλή μη-τετριμμένη περίπτωση όπου ο υπερχώρος εμπεριέχει μόνο μια κοσμολογική σταθερά. Ακολούθως, θεωρήσαμε ένα βαθμωτό πεδίο με κανονικό ή και με μη-κανονικό κινητικό όρο στη Λαγκρανζιανή και μετά μελετήσαμε την περίπτωση όπου δυο αλληλεπιδρώντα πεδία υπάρχουν στον υπερχώρο με απλούς και μικτούς κινητικούς όρους. Τέλος, θεωρήσαμε την περίπτωση όπου στη Λαγκρανζιανή έχουμε μια γενική συνάρτηση σύζευξης $f(\Phi)$ ανάμεσα στο βαθμωτό πεδίο Φ και το βαθμωτό Ricci μαζί με ένα γενικό δυναμικό καθώς και ένα όρο κοσμολογικής σταθεράς.

Σε κάποιες από τις παραπάνω περιπτώσεις βρήκαμε συναρτήσεις μάζας οι οποίες είναι συμβατές με τις εξισώσεις περιορισμού (constraints). Η αντικατάσταση αυτών των λύσεων στη συνάρτηση μετρικής γεννά διάφορους ενδιαφέροντες όρους τύπου Schwarzschild (r^{-1}), (anti)de-Sitter (r^2) ή τύπου Reissner-Nordstrom (r^{-2}). Ωστόσο, όποτε τέτοιες λύσεις υπάρχουν το προφίλ της συνάρτησης μάζας κατά μήκος της επιπλέον διάστασης δεν είναι το κατάλληλο για τον εντοπισμό της ιδιομορφίας κοντά στη μεμβράνη και κατά συνέπεια οι λύσεις αυτές δεν οδηγούν σε εντοπισμένες μελανές οπές.

Στο κεφάλαιο 6 παρουσιάζουμε αναλυτικά τα συμπεράσματα της διατριβής.

List of Publications

Within the context of my PhD studies, five peer-reviewed articles have been produced. They are listed here for reference in descending chronological order.

1. **Greybody factors for scalar fields emitted by a higher-dimensional Schwarzschild-de Sitter black hole**, Panagiota Kanti, Thomas Pappas and Nikolaos Pappas [1]
2. **On the localisation of four-dimensional brane-world black holes: II. The general case**, Panagiota Kanti, Nikolaos Pappas and Thomas Pappas [2]
3. **Hawking radiation spectra for scalar fields by a higher-dimensional Schwarzschild-de Sitter black hole**, Thomas Pappas, Panagiota Kanti and Nikolaos Pappas [3]
4. **Effective temperatures and radiation spectra for a higher-dimensional Schwarzschild-de Sitter black hole**, Panagiota Kanti and Thomas Pappas [4]
5. **Schwarzschild-de Sitter spacetime: The role of temperature in the emission of Hawking radiation**, Thomas Pappas and Panagiota Kanti [5]

During the final stages of my PhD studies, I also worked in parallel on the following two articles:

6. **Frame-dependence of higher-order inflationary observables in scalar-tensor theories**, Alexandros Karam, Thomas Pappas and Kyriakos Tamvakis [6]
7. **Constant-Roll (Quasi-)Linear Inflation**, Alexandros Karam, Luca Marzola, Thomas Pappas, Antonio Racioppi and Kyriakos Tamvakis [7]

Acknowledgements

First of all, I thank my supervisor Professor Panagiota Kanti for her continuous guidance and support all these years. I would also like to thank the rest of my collaborators Alexandros Karam, Luca Marzola, Nikos Pappas, Antonio Racioppi, and Kyriakos Tamvakis for the fruitful collaboration.

Part of the research presented in this thesis has been cofinanced by the European Union (European Social Fund - ESF) and Greek national funds through the Operational Program Education and Lifelong Learning of the National Strategic Reference Framework (NSRF) - Research Funding Program: ARISTEIA - Investing in the society of knowledge through the European Social Fund.

I also acknowledge financial support by the Alexander S. Onassis Public Benefit Foundation during the final stages of my PhD studies.

Abbreviations

r.h.s.	**r**ight-**h**and **s**ide
l.h.s.	**l**eft-**h**and **s**ide
SR	**S**pecial **R**elativity
GR	**G**eneral **R**elativity
CT	**C**onformal **T**ransformation
EH	**E**vent **H**orizon
HD	**H**igher **D**imensional
QFT	**Q**uantum **F**ield **T**heory
ADD	**A**rkani-Hamed-**D**imopoulos-**D**vali, referring to [8–10]
LED	**L**arge **E**xtra **D**imensions
RS	**R**andall-**S**undrum, referring to [11, 12]
WED	**W**arped **E**xtra **D**imensions
DOF	**D**egrees **O**f **F**reedom
BH	**B**lack **H**ole
HR	**H**awking **R**adiation
GF	**G**reybody **F**actor
EER	**E**nergy **E**mission **R**ate
EOM	**E**quations **O**f **M**otion
SdS	**S**chwarzschild-**d**e **S**itter
KVF	**K**illing **V**ector **F**ield
TE	**T**otal **E**missivity

Contents

Chapter 1

Introduction

1.1 General theory of relativity

The General Theory of Relativity (GR) was formulated over a century ago by Albert Einstein [13] and to date, it provides the most accurate description of gravity[1]. In Einstein's theory the Newtonian force of gravity has been replaced by curvature in space and time. The presence of matter causes spacetime to "curve" and in turn, the curvature of spacetime dictates the way matter moves in it along geodesics. In this section we introduce some basic concepts of GR and refer the interested reader to an indicative list of text on the subject for further details [15–23].

1.1.1 Geometry and gravity

The mathematical framework upon which GR has been formulated is that of differential geometry [24–26] that constitutes a generalization of the usual Euclidean geometry by considering properties of vectors and curves on *curved* surfaces. In the language of differential geometry, the gravitational field, corresponds to a symmetric rank-2 tensor (endowed with some special properties) called the *metric tensor* $g_{\mu\nu}$, or simply the "metric". Let us now define some important geometric quantities more rigorously.

Starting with the most basic concept in relativity, we have the notion of *spacetime* that is defined as a manifold with a metric on it (M, g). Vectors p^a in curved spacetime are understood as differential operators and are defined as tangents to curves on M. Inversely, curves on M are defined by vector fields. Dual vectors (also termed as one-forms) are symbolized with lower indices p_α and are defined as linear operations acting on vectors and giving numbers (complex in general). A combination between a dual vector and a vector corresponds to the *inner product*. One of the important roles of the metric is to provide a way to combine a vector and a dual vector to produce a number.

The generalization of vectors and dual vectors in this abstract language are *tensors*, that are defined as operations on vectors and dual vectors that produce numbers. In order for an object $T^{a_1,\ldots,a_r}{}_{b_1,\ldots,b_s}$ to be a tensor of type (s, r) it has to transform appropriately under coordinate transformations. Under a general coordinate transformation of the form $x^a \to x'^a(x)$ the tensor components between the two

[1] For a review on the status of the experimental tests of GR see [14] and references therein.

coordinate systems are related as

$$T'^{a_1,\ldots,a_r}{}_{b_1,\ldots,b_s} = \left(\frac{\partial x'^a}{\partial x^c}\right)\cdots\left(\frac{\partial x^d}{\partial x'^b}\right) T^{c_1,\ldots,c_r}{}_{d_1,\ldots,d_s} \,. \tag{1.1}$$

By including a metric tensor $g_{\mu\nu}$ on a manifold we have a *metric space*. This gives birth to the notion of distances in spacetime which are encoded in the so-called *line element*

$$ds^2 = g_{ab}dx^a dx^b \,. \tag{1.2}$$

With this, yet another important feature of the metric is uncovered, namely that it converts coordinate increments (differentials) into physical distances. Points on a metric space are termed *events* and are usually specified by a "time coordinate" and a number (depending on the dimensionality of spacetime) of "space coordinates".

Once we have a metric we can lower and raise indices between vectors and dual vectors as follows:

$$g^{ab}p_a = p^b \quad , \quad g_{ab}p^a = p_b \,. \tag{1.3}$$

It is important to notice that before we introduce a metric on the manifold to make it a metric space the two notions of vectors are independent and so the inclusion of the metric provides a relation between the two. As a consequence, it is common that both vectors and dual vectors are referred to simply as "vectors" when dealing with metric spaces.

Another important quantity is the *inverse metric* that corresponds to the inverse matrix of the matrix representation of the original metric

$$g^{ab}g_{bc} = \delta^a_{\ c} \,. \tag{1.4}$$

Aside from the metric we may also assign another independent (in general) structure to the manifold, called the *connection* $\Gamma^a_{\ bc}$. This quantity is not a tensor as it does not transform like one under coordinate transformations. For the record, it is possible, in abstract differential geometry terms, to have a manifold with a connection and no metric on it. In this case we would have an *affine manifold*. Usually in GR it is common to have both a metric and a connection on the manifold. It is also very common to *choose* a connection that is *metric compatible*. This means that the connection is completely tied to the metric and is obtained via first derivatives of the metric in the following way:

$$\Gamma^a_{\ bc} = \frac{1}{2}g^{a\,d}\left(\partial_b g_{d\,c} + \partial_c g_{d\,b} - \partial_d g_{b\,c}\right) \,. \tag{1.5}$$

In this case the connection is called the *Christoffel symbols* which are also symmetric in the lower indices. This last property is a feature enjoyed by the connection in torsion-free theories. The role of the connection is to give us a "transport rule" to move vectors on the manifold from one point to the

other, then be able to take the difference between the two vectors and by dividing with the distance between the vectors be able to get a covariant derivative.

In covariant differentiation we distinguish two cases. There are cases where you have a vector field defined only on a curve and cases where a vector field is defined in an open region in spacetime. So, suppose that we have a vector field on a curve γ. The vector field on the curve means that for each point on the curve we know what the vector is. So the vector is defined everywhere on the curve and only on the curve. If the field is defined only on the curve we can only differentiate it only along the curve. To do that we need a parameter description of the curve which essentially is just giving the coordinate description of the curve in terms of some running parameter

$$\gamma : x^{\mu}(\lambda). \tag{1.6}$$

So, for each value of the parameter λ we know the coordinates of the curve and in this way we can "build" the curve. As an example, if we talk about the world-line of an observer the role of λ would be played by proper time (τ).

What we are looking for is to create a notion for

$$\frac{dA^{\mu}}{d\lambda}\,, \tag{1.7}$$

the derivative of a vector field with respect to the parameter. If we didn't have a problem with dealing with vectors in different points the derivative would be straight-forward. We define the *covariant derivative along a curve* as follows:

$$\frac{DA^{a}}{\partial\lambda} = \frac{\partial A^{a}}{\partial\lambda} + \Gamma^{a}_{bc}A^{b}\frac{\partial x^{c}}{\partial\lambda}\,. \tag{1.8}$$

When we calculate the covariant derivative along the curve we don't need to know anything about the vector field away from the curve! We also introduce the notion of the *tangent vector* to the curve

$$\gamma : t^{a} \equiv \frac{\partial x^{a}}{\partial\lambda}\,, \tag{1.9}$$

as the derivative of the coordinate description of the curve with respect to the parameter λ. In this notation we can re-write the expression for the covariant derivative along a curve as

$$\frac{DA^{a}}{\partial\lambda} = \frac{\partial A^{a}}{\partial\lambda} + \Gamma^{a}_{bc}A^{b}t^{c}. \tag{1.10}$$

Now we turn to the broader case where we have a vector field defined in an open region $A^{a}(x^{\mu})$ and not only on a curve and calculate its covariant derivative. We are now able to take its derivative in all directions. In that case we define the covariant derivative with respect to any coordinate direction β as

$$\boxed{A^{a}_{;\beta} = \nabla_{\beta}A^{a} = A^{a}_{,\beta} + \Gamma^{a}_{\beta c}A^{c}}\,. \tag{1.11}$$

Finally, by comparing (1.10) and (1.11), we see that we can write the covariant derivative along a curve as the full covariant derivative multiplied by the tangent to the curve as

$$\frac{DA^a}{\partial\lambda} = A^a_{;\beta} t^\beta \,. \tag{1.12}$$

In GR the paths that point-particles follow in the curved spacetime correspond to *geodesic curves* when no other force apart from gravity is exerted on them. These are curves with the very special property that they extremize the distance between two events. Depending on the sign of the norm of their tangent vector t^a, there are three types of geodesics, namely spacelike (when $t^a t_a > 0$), timelike (when $t^a t_a < 0$) and lightlike or null (when $t^a t_a = 0$). Massive particles follow timelike trajectories while massless particles (such as photons) move along null trajectories. Finally, spacelike geodesics do not have a physical interpretation and so we will not consider them any further.

Let us focus on timelike geodesics. They are timelike curves in spacetime with the fundamental property of the extremum of proper time between two events. Proper time is defined as the negative spacetime interval

$$d\tau^2 \equiv -ds^2 \,, \tag{1.13}$$

and we take the minus sign because we have the dominance of the time direction versus the space one in timelike curves. So the proper time between two events A and B is going to be

$$\tau(A \to B) = \int_A^B \sqrt{-g_{ab} \frac{dx^a}{d\lambda} \frac{dx^b}{d\lambda}} d\lambda \,, \tag{1.14}$$

and this integral is called proper time functional. It is a functional of the path A to B because we have to calculate the metric along the path we have chosen as well as the coordinate differentials along the path. Notice that the parameter λ in eq. (1.14) is not necessarily the proper time τ, but rather an arbitrary parameter. Employing the Euler-Lagrange method with the Lagrangian

$$\mathcal{L} = \sqrt{-g_{ab} \frac{dx^a}{d\lambda} \frac{dx^b}{d\lambda}} \,, \tag{1.15}$$

we end up with the *geodesic equation*

$$\frac{d^2x^a}{d\lambda} + \Gamma^a_{bc} \frac{dx^b}{d\lambda} \frac{dx^c}{d\lambda} = \kappa \frac{dx^a}{d\lambda} \quad , \quad \kappa \equiv \frac{1}{\mathcal{L}} \frac{d\mathcal{L}}{d\lambda} \,. \tag{1.16}$$

In general, when $\lambda \neq \tau$ the quantity κ is non-zero. If now we choose τ to parametrize the curve, we have that $\mathcal{L} = 1 \;\; \to \kappa = 0$. In fact this is true for any parameter λ that is *linearly* related to the proper time parameter i.e. $\lambda = a\tau + b$, for arbitrary constants a and b. This special class of parameters correspond to the so-called *affine parametrization*.

Using the tangent vector to a curve (1.9) we may also write eq. (1.16) using the covariant derivative in the following way:

$$t^a \nabla_a t^b = \kappa\, t^b \quad , \quad t^a \equiv \frac{dx^a(\lambda)}{d\lambda}\,. \tag{1.17}$$

The left hand side (l.h.s.) of the above equation can be geometrically understood as the projection of the acceleration of the curve on to the direction of the speed of the curve. Physical observers follow timelike geodesics and the "natural choice" of parametrization for the curve is their proper time (τ). Thus, the right hand side (r.h.s.) of eq. (1.17) vanishes and so we see that geodesics are curves of zero acceleration.

When it comes to null geodesics, i.e. the path that light takes in curved spacetime, the affine parameterization of the curve is no longer a good choice of parameter. This is due to the fact that for null curves $ds^2 = 0$ and so the proper time interval vanishes as well. Thus, null geodesics are in general described in terms of non-affine parameters. In general we define null geodesics as the integral curves of vectors k^a that satisfy

$$k^a \nabla_a k^b = f(x)\, k^b \quad , \quad k^a k_a = 0\,, \tag{1.18}$$

where $f(x)$ is a function of spacetime.

1.1.2 Einstein's field equations

The field equations for the gravitational field are obtained from the variation of the Einstein-Hilbert action

$$\mathcal{S} = \int \left(\frac{R}{2\kappa_D^2} + \mathcal{L}_m \right) \sqrt{-g} d^D x\,, \tag{1.19}$$

with respect to the metric tensor $g_{\mu\nu}$. In the above, R is the Ricci scalar, $\kappa_D^2 \equiv 8\pi G/c^4$ where G is the gravitational constant and c is the speed of light; $\mathcal{L}_m$ is the Lagrangian describing the matter content of spacetime, g is the metric determinant and $D = 4 + n$ is the total number of dimensions, where an arbitrary number n of extra spacelike dimensions has been introduced.

The variation of eq. (1.19) with respect to the metric yields the Einstein's Field Equations (EFEs)

$$G_{\mu\nu} \equiv R_{\mu\nu} - \frac{1}{2}\, g_{\mu\nu}\, R = \kappa_D^2\, T_{\mu\nu}\,, \tag{1.20}$$

where $G_{\mu\nu}$ is the Einstein tensor given in terms of the Ricci tensor $R_{\mu\nu}$ (involving second derivatives of the metric tensor). Finally, on the right-hand side (r.h.s.) of the Einstein equations we have the *energy-momentum* tensor $T_{\mu\nu}$ that describes the distribution of energy and momentum and is defined via

$$T_{\mu\nu} \equiv \frac{2}{\sqrt{-g}} \frac{\delta(\sqrt{-g}\,\mathcal{L}_m)}{\delta g^{\mu\nu}}\,. \tag{1.21}$$

When the action (1.19) is extended to include a positive cosmological constant[2] term ($-\Lambda/\kappa_D^2$, $\Lambda > 0$) that may be interpreted as a contribution from the field-theory part originating from $\mathcal{L}_m$ or as a geometric term in the same way that R enters the action, the EFEs are then

$$G_{\mu\nu} + g_{\mu\nu}\Lambda = \kappa_D^2\, T_{\mu\nu}\,. \tag{1.22}$$

1.1.3 Some exact solutions

To obtain the form of the metric tensor, one has to solve the EFE. In four dimensions, eq. (1.20) corresponds to ten non-lineal differential equations with respect to the metric tensor components and, in general, obtaining an analytic solution is nearly impossible unless some symmetry conditions are imposed in order to simplify the form of the equations.

The first and simplest vacuum solution ($T_{\mu\nu} = 0$)[3] to the EFEs was found by (and named after) Karl Schwarzschild [28] shortly after Einstein introduced GR. The Schwarzschild solution has a line element that in spherical coordinates (t, r, θ, ϕ) is given by

$$ds^2 = g_{\mu\nu}dx^\mu dx^\nu = -\left(1 - \frac{r_h}{r}\right)dt^2 + \left(1 - \frac{r_h}{r}\right)^{-1} dr^2 + r^2\left(d\theta^2 + \sin\theta^2 d\phi^2\right)\,, \tag{1.23}$$

where $r_h \equiv \frac{2Gm}{c^2}$ is the *Schwarzschild radius* given in terms of the mass m. In the limit $m \to 0$ the above line element reduces to the Minkowski metric of flat spacetime. One of the important properties of this spacetime is its time-independence. The latter is immediately evident since the time coordinate (t) does not appear in any of the metric components. Due to its simplicity, we will often refer to the four dimensional Schwarzschild metric when introducing various quantities in this introduction.

According to Birkhoff's theorem [29], the Schwarzschild solution corresponds to the *unique* spherically symmetric and uncharged vacuum solution to the EFEs. Notice, that the metric[4] becomes "problematic" in two specific values of the radial coordinate, $r = 0$ and $r = r_h$. These values cause the divergence and vanishing, respectively, of the so-called *metric function* associated with the element g_{tt} of the metric

$$-g_{tt} \equiv h(r) = \left(1 - \frac{r_h}{r}\right)\,. \tag{1.24}$$

Therefore, the line element (1.23) becomes inappropriate for the description of physics in this region since we have the appearance of singularities. Not both of these singularities are of the same type though. Consider the Kretschmann scalar $R^{\mu\nu\rho\sigma}R_{\mu\nu\rho\sigma}$ corresponding to the square of the Riemann tensor. Since it is a *scalar quantity* constructed out of the Riemann tensor, it measures the curvature in a way that does not depend on the coordinate system. For the Schwarzschild metric, it has the

[2] Initially introduced by A. Einstein in order to support a static universe [27].
[3] This means that no matter or non-gravitational fields are present.
[4] Often the term "metric" is used to refer to the line element as well.

following form:

$$R^{\mu\nu\rho\sigma}R_{\mu\nu\rho\sigma} = \frac{48G^2m^2}{r^6}\,, \tag{1.25}$$

and clearly diverges at $r \to 0$. Thus the singularity located at $r = 0$ in the Schwarzschild metric is a *physical* one since it causes the divergence of the scalar invariant of the curvature tensor; therefore it cannot be eliminated by any coordinate transformation. All observers agree that the physical singularity is there and physics breaks down at its location. On the other hand, at $r = r_h$ we have a *coordinate* singularity because the curvature scalars are well behaved there. Under appropriate coordinate transformations these types of singularities can be eliminated. So it becomes clear that the distinguishing characteristic between different types of singularities is whether or not they cause the curvature scalars to diverge.

When one includes the cosmological constant term into the 4-dimensional Einstein-Hilbert action, the metric (1.23) is generalized to the Schwarzschild-de Sitter (SdS) line element

$$ds^2 = g_{\mu\nu}dx^\mu dx^\nu = -\left(1 - \frac{r_h}{r} - \frac{\Lambda}{3}r^2\right)dt^2 + \left(1 - \frac{r_h}{r} - \frac{\Lambda}{3}r^2\right)^{-1}dr^2 + r^2\left(d\theta^2 + \sin\theta^2 d\phi^2\right)\,, \tag{1.26}$$

where the extra "cosmological constant term" $-\Lambda r^2$ appears in the metric function. The SdS metric can be generalized to an arbitrary number of extra space-like dimensions [30] and thus the Higher-dimensional (HD) SdS metric is obtained

$$ds^2 = G_{MN}dx^M dx^N = -h(r)\,dt^2 + \frac{dr^2}{h(r)} + r^2 d\Omega^2_{2+n}\,. \tag{1.27}$$

In the above, the metric function is

$$h(r) = 1 - \frac{\mu}{r^{n+1}} - \frac{2\kappa_D^2\Lambda}{(n+2)(n+3)}r^2\,, \tag{1.28}$$

and $d\Omega^2_{2+n}$ is the surface element of a $(2+n)$-dimensional unit sphere given by

$$d\Omega^2_{2+n} = d\theta^2_{n+1} + \sin^2\theta_{n+1}\left(d\theta_n^2 + \sin^2\theta_n\left(\,... + \sin^2\theta_2\left(d\theta_1^2 + \sin^2\theta_1\, d\varphi^2\right)...\right)\right)\,, \tag{1.29}$$

with $0 \le \varphi < 2\pi$ and $0 \le \theta_i \le \pi$, for $i = 1, ..., n+1$.

The line element of eq. (1.27) will play a very important role in this thesis as it constitutes the basis for the majority of the analysis performed.

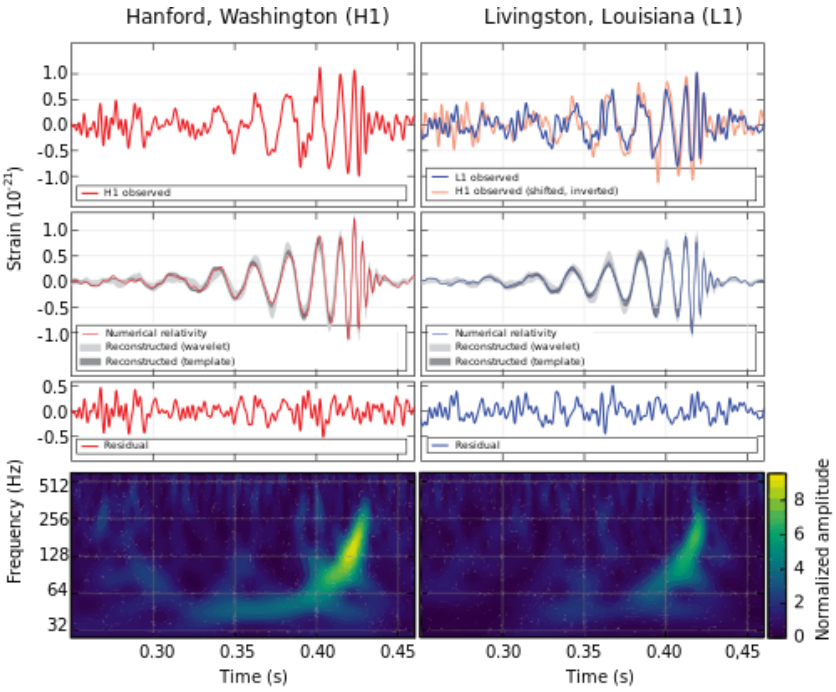

FIGURE 1.1: The "echo" of the merging of black holes as detected in the form of gravitational waves by the LIGO collaboration. Credit: [38]

1.2 Black holes

In this section we introduce some of the basic concepts of *black holes* (BHs). Black holes are definitely amongst the most exciting predictions of GR [26, 31–36]. They are regions of spacetime so intensely curved that nothing, not even light, can escape. Classical BHs are solutions to the EFE and are characterized by the existence of an event horizon at the boundary and a singularity at its core. The solutions (1.23), (1.26) and (1.27) presented above describe static, spherically-symmetric and uncharged black holes either in the absence or presence of a cosmological constant. The existence of singularities in GR is an indication that the predictive power of the theory breaks down in this region and a description based on a yet to be found complete theory of quantum gravity becomes necessary.

Even though we have never *directly* observed a black hole, the observational indications seem to strongly support the existence of BHs; from the orbits of stars close to the center of our galaxy that hint towards a super massive black hole [37] to the most recent indirect observation coming from a series of detected signals of gravitational waves [38], that are in stunning agreement with the predictions of GR, generated by the coalescing of black holes (see Fig. 1.1). Finally, the Event Horizon Telescope (EHT) [39] is set to capture the first "image" of a black-hole horizon by creating a virtual Earth-sized telescope and targeting Sgr A^* at the center of our galaxy.

1.2.1 Symmetries and Killing vectors

In GR it is often very important to be able to express the invariance of a tensor under translations along a direction in spacetime (as we shall see this is related with conserved quantities along geodesics). To this end it will prove useful to introduce yet another type of differentiation that is more "primitive" than the covariant derivative (1.11), in the sense that it does not require the extra structure of the connection in order to be defined. This new type of differentiation is the *Lie derivative* $\mathcal{L}_U$ that is defined along the integral curves of a given vector field U^a, in an open region of a manifold. The Lie derivative with respect to a vector field U^a acting on another vector field A^a is written as

$$\mathcal{L}_U A^a = U^b \partial_b A^a - A^b \partial_b U^a = -\mathcal{L}_A U^a \,. \tag{1.30}$$

Geometrically we can understand eq. (1.30) as the projection of the partial derivative of the vector A^a along the vector U^a minus the projection of the partial derivative of U^a along A^a. Even though we used partial derivatives to illustrate that Lie derivative is defined *independently* of a connection, it is clear that due to the minus sign between the two terms if we simply replace the partial differentiations with covariant ones, the Christoffel symbols that appear cancel out. This is why we may use instead the following expression as the "definition":

$$\boxed{\mathcal{L}_U A^a = U^b \nabla_b A^a - A^b \nabla_b U^a} \,. \tag{1.31}$$

From the above equation it becomes clear that Lie differentiation is a covariant operation since both terms on the r.h.s. are tensors. As is usually the case with any differential operator, $\mathcal{L}_U$ obeys the product rule of differentiation. When acting upon scalar quantities it reduces to partial differentiation i.e. $\mathcal{L}_U \Phi = U^a \partial_a \Phi$, while acting on one forms and mixed tensors it has the following effects:

$$\mathcal{L}_U B_a = U^b \nabla_b B_a + B_b \nabla_a U^b \,, \tag{1.32}$$

$$\mathcal{L}_U T^a_{\ b} = U^c \nabla_c T^a_{\ b} - T^c_{\ b} \nabla_c U^a + T^a_{\ c} \nabla_b U^c \,. \tag{1.33}$$

Let us now see how to use the Lie derivative to state that an object[5] is invariant under translations along a direction in the manifold in a covariant, i.e. coordinate independent, manner.

Consider a *specific* coordinate system in four dimensions $x^a = (x^0, x^1, x^2, x^3)$ and suppose that a vector A^a does not depend on the first of the coordinates (x^0). Then in the coordinate system x^a this is stated as $\partial A^a / \partial_{x^0} = 0$. Of course this last condition will not hold in an arbitrary coordinate system. Now, in x^a, the vector that points along the direction of x^0-changes will be $U^a = (1, 0, 0, 0)$. Since the components of U^a are constant, its partial derivative along any direction in x^a will be

$$\partial_b U^a = 0 \,. \tag{1.34}$$

[5] Here we will consider a vector, but this idea is generalized to arbitrary tensor fields.

With the above it is clear that the "x^0-independence condition" $\partial A^a/\partial_{x^0} = 0$ can be written equivalently as

$$U^b \partial_b A^a = 0\,. \tag{1.35}$$

Turning now to the definition of the Lie derivative (1.30) and using eqs. (1.34) and (1.35) we have that

$$\mathcal{L}_U A^a = U^b \partial_b A^a - A^b \partial_b U^a = 0\,. \tag{1.36}$$

Even though the above result has been derived for the specific coordinate system x^a, the covariant nature of $\mathcal{L}_U$ guarantees that this holds in *any coordinate system*. We may thus conclude that the invariance of a vector A^a along translations in the direction of U^b is stated in a coordinate-independent way by the vanishing of its Lie derivative

$$\mathcal{L}_U A^a = 0\,. \tag{1.37}$$

The condition of eq. (1.37) is of course not only restricted to vector fields but is generalized to tensors.

Assume now that the Lie derivative of an arbitrary metric g_{ab} vanishes along the direction of a vector ξ^a

$$\mathcal{L}_\xi g_{ab} = 0 = \xi^c \nabla_c g_{ab} + g_{cb}\nabla_a \xi^c + g_{ac}\nabla_b \xi^c\,, \tag{1.38}$$

where in the last step we used the definition for the Lie derivative. The first term in eq. (1.38) vanishes due to metric compatibility $\nabla_c g_{ab} = 0$ and so we have

$$g_{cb}\nabla_a \xi^c + g_{ac}\nabla_b \xi^c = \nabla_a\left(g_{cb}\xi^c\right) + \nabla_b\left(g_{ac}\xi^c\right)\,, \tag{1.39}$$

which eventually leads to *Killing's equation*

$$\boxed{\nabla_b \xi_a + \nabla_a \xi_b = 0}\,. \tag{1.40}$$

Any vector field satisfying eq. (1.40) is called a *Killing Vector Field* (KVF) and "points" along a direction that the metric remains invariant. For any symmetry of the metric there is a corresponding KVF associated with it. In D dimensions, the maximum number of linearly independent KVFs is $D(D+1)/2$ and when a metric has the maximum number of KVFs we have a *maximally symmetric space* for which the Riemann tensor is given simply by

$$R_{abcd} = \frac{R}{D(D-1)}\left(g_{ac}g_{bd} - g_{ad}g_{bc}\right)\,, \tag{1.41}$$

where R is the Ricci scalar. Some characteristic examples of maximally symmetric spaces are the Minkowski and de-Sitter spaces.

In general, in order to find the KVFs of a given metric one has to solve eq. (1.40) explicitly but often, there are cases where one can "read" the KVFs simply by inspection of the metric. Based on the

discussion above, it is clear that if in a given coordinate system the metric does not depend on one of the coordinates there is a KVF associated with translations along that coordinate.

A linear combination of KVFs still satisfies Killing's equation and this implies that KVFs are defined up to a normalization constant. In chapter 4 we discuss different approaches to the normalization of the KVFs depending on the asymptotic structure of the spacetime.

The symmetries of the metric and the associated Killing vectors that go with them give rise to conserved quantities along the geodesics of the spacetime. Assume a KVF ξ^a and a geodesic parametrized affinely by $x^a(\lambda)$ with tangent vector $t^a(\lambda) \equiv dx^a(\lambda)/d\lambda$. Then the following holds:

$$\frac{d}{d\lambda}\left(t^a\xi_a\right) = t^b\nabla_b\left(t^a\xi_a\right) = \xi_a t^b\nabla_b t^a + t^a t^b\nabla_b\xi_a = 0\,. \tag{1.42}$$

The first term vanishes due to the geodesic equation $t^b\nabla_b t^a = 0$ and the second by virtue of Killing's equation that constitutes the term $\nabla_b\xi_a$ antisymmetric. The result of eq. (1.42) then implies that the quantity $t^a\xi_a$ is a constant of motion along the geodesic. Another useful result, that is trivial to prove, is that for the energy momentum tensor T^{ab} and a KVF ξ^a the quantity $T_{ab}\xi^a \equiv P_b$ is also conserved.

1.2.2 Event horizons and surface gravity

The coordinate singularity at $r = r_h$ in the Schwarzschild geometry corresponds to the location of the *Event Horizon* (EH) of the black hole. This two-dimensional spherical surface with radius r_h is the outer boundary of the black hole. Anything that approaches the singularity to a distance smaller than r_h can never escape the gravitational attraction. According to the so-called cosmic-censorship conjecture [40], any singularity in nature, with the only exception being the big-bang singularity, remains "cloaked" behind an event horizon. This is a necessary requirement in order to preserve the predictability of classical GR.

We have defined the event horizon loosely, as the outer boundary of the black hole. A horizon usually appears for an observer ($\mathcal{O}$) when there is gravity involved (curved spacetime) or even in the absence of gravity (flat spacetime) when an observer undergoes constant proper acceleration (Rindler observer) [41]. The effect of acceleration (or gravity) is to cause some regions of spacetime to become "causally disconnected". The same holds for in the case of "repulsive gravity" effect of the cosmological constant (Λ). In the presence of a positive cosmological constant, the spacetime expands. As a result, at distances larger than the typical scale of $r_c \equiv \left(\sqrt{\Lambda}\right)^{-1}$ the expansion of space is so rapid that signals beyond this point can never reach the location of the observer. This way we have the appearance of a cosmological horizon. For the current, exceptionally small value of the cosmological constant $\Lambda \sim 10^{-52}\,m^{-2}$ the radius of the cosmological horizon is $r_c \sim 10^{26}\,m$ or roughly $3Gpc$!

There are different types of horizons in black-hole physics including trapped surfaces, apparent horizons, event horizons and dynamical horizons (see [23, 42] for more details). In static spacetimes the event horizon and the so-called, Killing horizon are identified.

A *Killing horizon*, that we shall denote with $\mathcal{H}$, is defined as a null hypersurface $S(x^a) = 0$ that is everywhere tangent to a Killing vector field K^μ which becomes null ($K^\mu K_\mu = 0$) on $\mathcal{H}$.

The defining property of a null hypersurface $S(x^a) = 0$ is that its normal vector $n_a \sim \partial_a S$ is null and so we have the condition

$$g^{ab}\partial_a S \partial_b S = 0\,. \tag{1.43}$$

It can be shown that the integral curves of the KVF that becomes null on the location of the Killing horizon $\mathcal{H}$, are geodesics everywhere on $\mathcal{H}$. This gives the parameter κ on the r.h.s. of the geodesic equation (1.16), that measures the deviation from affinity of the parametrization of the geodesic, the interpretation of the *surface gravity* [15, 22, 26] of the black-hole horizon. Explicitly on the location of the Killing horizon it is given by

$$\kappa_h^2 = -\frac{1}{2}\nabla^b K^a \nabla_b K_a|_{\mathcal{H}}\,. \tag{1.44}$$

Surface gravity plays a very important role in black-hole thermodynamics since it is related to the temperature of Hawking radiation as we shall see in the following sections.

1.3 Black-hole thermodynamics

In this section, we present the four laws of black hole mechanics and compare them to the laws of thermodynamics. Then we derive an expression for the physical temperature of a Killing-horizon valid for an arbitrary spherically-symmetric spacetime. Finally, after introducing some basic tools of quantum field theory in curved spacetime, we move on to sketch Stephen Hawking's original calculation, and obtain the famous Hawking formula for the spectrum of the black-hole radiation.

1.3.1 The four laws of black-hole mechanics

A striking similarity between black-hole mechanics and thermodynamics was uncovered in the classical level in the early 70s in the form of the "four laws of black-hole mechanics" [43]. These laws state the following

The four laws of black-hole mechanics

- **Zeroth law:** The surface gravity κ_h of a stationary black hole is constant everywhere on the surface of the event horizon.

- **First law:** Perturbing a stationary black hole with mass m, charge Q and angular momentum J respectively by δm, δQ and δJ, the new state is described by $(m+\delta m, Q++\delta Q, J+\delta J)$ and the variations are related via

$$\delta m = \frac{\kappa_h}{8\pi}\delta A + \Phi_h \delta Q + \Omega_h \delta J\,, \tag{1.45}$$

  where κ_h and A are respectively the surface gravity and surface area of the event horizon,Φ_h is the electric potential on the horizon and Ω_h is the angular velocity of the horizon.

- **Second law:** In any (classical) process the surface area of the event horizon is non-decreasing

$$\delta A \geqslant 0\,. \tag{1.46}$$

- **Third law:** It is impossible to reduce the surface gravity κ_h of the event horizon to zero under a finite sequence of operations, no matter how idealized the procedure.

———————— ⋆ ————————

There is a clear resemblance between the four laws given above and the corresponding laws of thermodynamics. In thermodynamics, the zeroth law states

For a system in thermal equilibrium, the temperature (T) remains constant.

Thus we see that the surface gravity behaves similarly to the temperature, $\kappa_h \leftrightarrow T$. In the first law for a thermodynamic system, small variations in the internal energy U and entropy S between equilibrium states are related by

$$\delta U = T\delta S + \textit{work terms}\,. \tag{1.47}$$

Then, by the forms of eqs. (1.45) and (1.47) it is tempting to identify the black-hole mass with the internal energy $m \sim U$, and the surface area of the event horizon with the entropy $A \sim S$. In fact the entropy of the black hole was found to correspond to a quarter of the total surface area of the event horizon $S = A/4$ [44] and in this way, the analogy between the laws suggests the identification of the temperature with the surface gravity as $T = \kappa_h/(2\pi)$.

The second law of thermodynamics states that

For a closed system the change in entropy is non-negative i.e. $\delta S \geqslant 0$.

Given that we have related the surface area of the black-hole horizon with the entropy of the black hole, the second law of thermodynamics becomes reminiscent of Hawking's area theorem.

The aforementioned analogy between the laws of black-hole mechanics and thermodynamics when first realized certainly appeared to be simply a formal one. This is due to the fact that classically a black hole is a perfect absorber and thus it cannot be endowed with temperature. Also, the entropy of a thermodynamic system is a measure of the number of microstates that lead to the same macrostate with a given volume, pressure and temperature. On the other hand, according to the no-hair theorems [45–47], black holes are completely characterized only by a few parameters: mass, charge, and angular momentum.

It was Hawking who first realized [48] that, when quantum effects are taken into account, the black hole is endowed with entropy and non-vanishing temperature and in this way behaves exactly like a thermodynamic system [44, 48–50]. The entropy is proportional to the surface area of the event horizon and corresponds to the information that is "hidden" behind the event horizon. The black-hole temperature is related to the surface gravity at the location of the event horizon (a proof of this statement is provided in the next subsection).

1.3.2 The black-hole temperature

In this section we shall derive a very general expression for the Hawking temperature using a method that is based on the analogy between systems at a finite temperature and path integrals with periodic time [50, 51]. The obtained result is valid for any spherically-symmetric metric in arbitrary number of extra spacelike dimensions.

Let us begin by writing down the line element for such a metric in D-dimensions

$$ds^2 = -h(r)dt^2 + \frac{1}{h(r)}dr^2 + r^2 d\Omega_{D-2}^2\,, \tag{1.48}$$

where $h(r)$ is the so-called *metric function* and $d\Omega_{D-2}^2$ is the surface element of a $(D-2)$-dimensional hyper-sphere with unit radius. The roots of the metric function correspond to the locations of the Killing horizons in the above spacetime.

We now perform a Wick rotation i.e. $t \to i\tau$, and omit the angular part of the metric (1.48) by virtue of the spherical symmetry to obtain the Euclidean form of the metric

$$ds^2 = h(r)d\tau^2 + \frac{1}{h(r)}dr^2\,. \tag{1.49}$$

Assume now the location r_h of an event horizon for the above metric, i.e. the metric function satisfies the equation $h(r_h) = 0$. Infinitesimally close to the location of the horizon $r = r_h + \epsilon \to dr = d\epsilon$, where $0 < \epsilon \ll 1$ we may Taylor expand the metric function to obtain

$$h(r_h + \epsilon) \approx h(r_h) + \epsilon\, \partial_r h(r)|_{r=r_h} + \mathcal{O}(\epsilon^2) = \epsilon\, \partial_r h(r)|_{r=r_h} + \mathcal{O}(\epsilon^2)\,. \tag{1.50}$$

In the last step we employed the fact that the metric function vanishes at the location of the horizon. To first order in ϵ the metric is then written as

$$ds^2 = \epsilon\, h'(r_h) d\tau^2 + \frac{1}{\epsilon\, h'(r_h)} d\epsilon^2 \,, \tag{1.51}$$

where we have denoted $\partial_r h(r)$ by $h'(r)$. Finally, under the following coordinate redefinition:

$$w = \frac{2\sqrt{\epsilon}}{\sqrt{h'(r_h)}} \;\rightarrow dw = \frac{d\epsilon}{\sqrt{\epsilon\, h'(r_h)}} \,, \tag{1.52}$$

we may recast the metric to the form

$$ds^2 = w^2 \frac{h'(r_h)^2}{4} d\tau^2 + dw^2 \,. \tag{1.53}$$

The form of eq. (1.53) is that of the metric of a $2D$ Euclidean plane in polar coordinates (r, ϕ) i.e. $ds^2 = dr^2 + r^2 d\phi^2$ if the rescaled time coordinate

$$\phi \equiv \frac{h'(r_h)}{2} \tau \tag{1.54}$$

is identified with the angular coordinate with period 2π

$$0 < \frac{h'(r_h)}{2} \tau \leqslant 2\pi \;\longrightarrow\; 0 < \tau \leqslant \frac{4\pi}{h'(r_h)} \equiv \beta \,. \tag{1.55}$$

With the imposed periodicity in the time coordinate we made sure that the conical singularity at $w = 0$ (or equivalently at $r = r_h$) corresponds to merely a coordinate singularity, as it should. The true merit of the identification $\phi \rightarrow \phi + 2\pi$ is that we may now use the path integral approach to the quantization of a scalar field to obtain the black-hole temperature [50].

In the path integral formulation, for a given action $S[\phi(t)]$, the amplitude for the field ϕ to go from a state ϕ_1 at time t_1 to a state ϕ_2 at time t_2 is

$$\langle \phi_2, t_2 \,|\, \phi_1, t_1 \rangle = \int d\,[\phi] \exp\left(iS[\phi]\right) \,, \tag{1.56}$$

where the integration runs over all field configurations that take the values ϕ_1 and ϕ_2 at time t_1 and t_2 respectively. The left hand side of the last equation may equivalently be obtained by means of the time evolution operator as

$$\langle \phi_2, t_2 \,|\, \phi_1, t_1 \rangle = \langle \phi_2 \,|\, \exp\left[-i\mathcal{H}(t_2 - t_1)\right] |\, \phi_1 \rangle \,, \tag{1.57}$$

where $\mathcal{H}$ is the Hamiltonian. Upon setting $t_2 - t_1 = -i\beta$ and $\phi_2 = \phi_1$ and summing over all ϕ_1 we end up with

$$Tr \exp\left(-\beta \mathcal{H}\right) = \int d\,[\phi] \exp\left(iS[\phi]\right) \,. \tag{1.58}$$

This time, the path integral is restricted to fields that are periodic with period β in imaginary time. Also, the left hand side of the above equation is by definition the partition function for the canonical ensemble of the field ϕ at temperature given by $T = \beta^{-1}$.

Returning now to eq. (1.55), we conclude that the temperature of an horizon located at r_h will be given by

$$\boxed{T_h = \frac{1}{\beta} = \frac{h'(r_h)}{4\pi} = \frac{\kappa_h}{2\pi}}, \tag{1.59}$$

where $\kappa_h = h'(r_h)/2$ is the surface gravity for the Killing horizon.

As an illustrative example, for the $4D$ Schwarzschild black hole (1.23), the temperature has the following expression in terms of the mass m of the black hole:

$$T_h = \frac{\hbar c^3}{8\pi G m k_B}\,, \tag{1.60}$$

where $\hbar$ is the reduced Planck constant, c is the speed of light, k_B is the Boltzmann constant and G is the gravitational constant. It is clear that in the classical limit $\hbar \to 0$ the black-hole temperature vanishes. The interesting feature of this expression is that the temperature of the BH is inversely proportional to its mass. It is then clear that large black holes, such the ones generated in astrophysical processes, have a very small temperature. On the other hand, mini-black holes, such as the ones theorized to emerge in high-energy particle collisions, are extremely hot due to the smallness of their mass.

1.3.3 Quantum field theory in curved spacetime

The aim of this section is to develop the basic formalism of semiclassical gravity that is necessary in order to derive the Hawking radiation spectrum in a following section. In the semiclassical treatment of gravity, it is assumed that at energy scales much lower than the Planck scale it is a very good approximation to treat gravity classically and matter quantum mechanically. This is realized in the context of Quantum Field Theory (QFT) in curved spacetime [52–62] where one considers a classical solution to the Einstein equations as the *fixed* curved background and performs QFT calculations on it.

Consider the Equation Of Motion (EOM) for a free scalar field ϕ propagating in a curved background described by a metric $g_{\mu\nu}$

$$g^{\mu\nu}\nabla_\mu\nabla_\nu\phi = 0\,. \tag{1.61}$$

In analogy to the usual QFT in flat spacetime, the canonical quantization proceeds by promoting the field to an operator, imposing the canonical equal time commutation relations

$$\left[\phi\left(t,x^i\right),\phi\left(t,y^i\right)\right]=\delta^3\left(x^i-y^i\right)\,, \tag{1.62}$$

and defining the Hilbert space upon which the operators act. The observable quantities are then obtained as expectation values of their respective operators in this space.

We are specifically interested in the notion of particles which correspond to the positive frequency excitations of the vacuum "defined" with respect to an observer's time. In flat space, Lorentz invariance of QFT ensures that all *inertial* observers define the same vacuum and thus agree in the particle content. In curved space, the vacuum state of the theory is not uniquely defined since Lorentz invariance is replaced by general covariance and every observer's proper time is a legitimate choice of time with respect to which the vacuum may be defined. It is the non-uniqueness of the vacuum in combination with the presence of an horizon that will result in the phenomenon of particle creation.

Let us now return to the Klein-Gordon equation for the scalar field, (1.61) and consider two complex solutions f and h. We then define the *Klein-Gordon inner product* as

$$\langle f,h\rangle=\int_\Sigma d\Sigma n_\mu j^\mu\ \ ,\ \ j^\mu(f,h)=-i\sqrt{-g}g^{\mu\nu}\left[f^*\partial_\nu h-\left(\partial_\nu f^*\right)h\right]\,, \tag{1.63}$$

where Σ is a *spacelike* (hyper-)surface, n^μ is the (future-directed) unit normal vector to Σ and we indicate complex conjugation with the superscript "$*$". Notice that due to the fact that f and h are solutions to the EOM (1.61) the current in (1.63) is conserved ($\partial_\mu j^\mu=0$). As a consequence, we obtain the very important property that the Klein-Gordon inner product $\langle f,h\rangle$ is independent of the choice of the boundary Σ

$$\langle f,h\rangle\left|_{\Sigma_1}=\langle f,h\rangle\right|_{\Sigma_2}\ \ \forall\ \ \Sigma_1,\Sigma_2\,. \tag{1.64}$$

In other words, the Klein-Gordon inner product is conserved. Since the vector n^μ is a future directed vector, eq. (1.63) assumes the following simplified expression

$$\langle f,h\rangle=-i\int dx^3\sqrt{-g}\left(f\dot{h^*}-\dot{f}h^*\right)\,, \tag{1.65}$$

where we used a dot to denote time differentiation $\dot{f}\equiv\partial_t f$. Consider now a complete basis of solutions f_ω, which are orthonormal $\langle f_\omega,f_{\omega'}\rangle=\delta(\omega-\omega')$ with respect to the inner product (1.65). We may then write the field operator in this basis as

$$\phi=\int d\omega\left(\hat{\mathbf{a}}_\omega f_\omega+\hat{\mathbf{a}}_\omega^\dagger f_\omega^*\right)\,, \tag{1.66}$$

in terms of the creation ($\hat{\mathbf{a}}^\dagger$) and anihilation ($\hat{\mathbf{a}}$) operators that obey the following commutation relations

$$[\hat{\mathbf{a}}_\omega, \hat{\mathbf{a}}^\dagger_{\omega'}] = \delta(\omega - \omega') \ , \ [\hat{\mathbf{a}}_\omega, \hat{\mathbf{a}}_{\omega'}] = [\hat{\mathbf{a}}^\dagger_\omega, \hat{\mathbf{a}}^\dagger_{\omega'}] = 0 \, . \tag{1.67}$$

The vacuum state of the theory ($|0\rangle_{in}$) is defined by the condition

$$\hat{\mathbf{a}}_\omega \, |0\rangle_{in} = 0 \ , \ \forall \omega > 0 \, , \tag{1.68}$$

where the subscript "*in*" is introduced for consistency with the discussions of the following sections. By acting consecutively upon the vacuum state with the creation operator we obtain states that contain particles. For example the state $\hat{\mathbf{a}}^{\dagger\, n}_\omega \, |0\rangle = |n\rangle$ contains n particles, each with energy ω. The total number of particles in the state $|n\rangle$ is then calculated as usual, by means of the number operator

$$\hat{\boldsymbol{N}}^{in}_\omega \equiv \hat{\mathbf{a}}^\dagger_\omega \hat{\mathbf{a}}_\omega \ \longrightarrow \langle 0 | \hat{\mathbf{a}}^n_\omega \hat{\boldsymbol{N}}^{in}_\omega \hat{\mathbf{a}}^{\dagger\, n}_\omega | 0 \rangle_{in} = n \, . \tag{1.69}$$

We can always expand the field operator in a second set of solutions to the Klein-Gordon equation (p_ω, p^*_ω) as

$$\phi = \int d\omega \left(\hat{\boldsymbol{b}}_\omega p_\omega + \hat{\boldsymbol{b}}^\dagger_\omega p^*_\omega \right) \, . \tag{1.70}$$

In this basis, the respective creation ($\hat{\boldsymbol{b}}^\dagger_\omega$) and annihilation ($\hat{\boldsymbol{b}}_\omega$) operators obey the following commutation relations:

$$[\hat{\boldsymbol{b}}_\omega, \hat{\boldsymbol{b}}^\dagger_{\omega'}] = \delta(\omega - \omega') \ , \ [\hat{\boldsymbol{b}}_\omega, \hat{\boldsymbol{b}}_{\omega'}] = [\hat{\boldsymbol{b}}^\dagger_\omega, \hat{\boldsymbol{b}}^\dagger_{\omega'}] = 0 \, , \tag{1.71}$$

and they define a vacuum state, different from $|0\rangle_{in}$, by the condition

$$\hat{\boldsymbol{b}}_\omega \, |0\rangle_{out} = 0 \ , \ \forall \omega > 0 \, . \tag{1.72}$$

From the ladder operators $\hat{\boldsymbol{b}}^\dagger_\omega$ and $\hat{\boldsymbol{b}}_\omega$ we define the corresponding number operator $\hat{\boldsymbol{N}}^{out}_\omega$ that measures the particle content in an excited state of the vacuum $|0\rangle_{out}$.

The two sets of modes (f_ω, f^*_ω) and (p_ω, p^*_ω) are solutions to the same equation and constitute complete orthonormal bases. It is then possible to relate the two sets by expressing one in terms of the other in the following way:

$$p_\omega = \int d\omega' \left(\alpha_{\omega\omega'} f_{\omega'} + \beta_{\omega\omega'} f^*_{\omega'} \right) \, , \tag{1.73}$$

and

$$f_\omega = \int d\omega' \left(\alpha^*_{\omega'\omega} p_{\omega'} - \beta_{\omega'\omega} p^*_{\omega'} \right) \, . \tag{1.74}$$

The quantities $\alpha_{\omega\omega'}$ and $\beta_{\omega\omega'}$ are the so-called *Bogoliubov coefficients* [63] and they can be isolated from the above integrals by using the inner product (1.65) as follows:

$$\alpha_{\omega\omega'} = \langle p_\omega, f_{\omega'} \rangle \ , \ \beta_{\omega\omega'} = - \langle p_\omega, f^*_{\omega'} \rangle \, . \tag{1.75}$$

They obey the following normalization conditions:

$$\int d\omega_k \left(\alpha_{\omega_i\omega_k}\alpha^*_{\omega_j\omega_k} - \beta_{\omega_i\omega_k}\beta^*_{\omega_j\omega_k}\right) = \delta(\omega_i - \omega_j)\,, \tag{1.76}$$

and

$$\int d\omega_k \left(\alpha_{\omega_i\omega_k}\beta_{\omega_j\omega_k} - \beta_{\omega_i\omega_k}\alpha_{\omega_j\omega_k}\right) = 0\,. \tag{1.77}$$

The Bogoliubov coefficients have been introduced to relate different sets of the field modes. Consequently they can also be used to relate their corresponding creation and annihilation operators as

$$\hat{\mathbf{a}}_\omega = \int d\omega' \left(\alpha_{\omega'\omega}\hat{\mathbf{b}}_{\omega'} + \beta^*_{\omega'\omega}\hat{\mathbf{b}}^\dagger_{\omega'}\right)\,, \tag{1.78}$$

and

$$\hat{\mathbf{b}}_\omega = \int d\omega' \left(\alpha^*_{\omega\omega'}\hat{\mathbf{a}}_{\omega'} - \beta^*_{\omega\omega'}\hat{\mathbf{a}}^\dagger_{\omega'}\right)\,. \tag{1.79}$$

These last two equations are the most important expressions of this section since they make possible the comparison between the particle content of a given state as it is perceived by different observers. Finally, due to the fact that the basis functions are orthonormal, we have the following important relation between the Bogoliubov coefficients:

$$\int d\omega' \left(|\alpha_{\omega\omega'}|^2 - |\beta_{\omega\omega'}|^2\right) = \delta(\omega - \omega')\,. \tag{1.80}$$

Consider now the vacuum state with respect to the modes (f_ω, f^*_ω) namely $|0\rangle_{in}$. Then, obviously the corresponding number operator $\hat{\boldsymbol{N}}^{in}_\omega \equiv \hat{\mathbf{a}}^\dagger_\omega\,\hat{\mathbf{a}}_\omega$ gives zero particles for this state

$$\langle 0|\hat{\boldsymbol{N}}^{in}_\omega|0\rangle_{in} = \hat{\mathbf{a}}^\dagger_\omega\,\hat{\mathbf{a}}_\omega = 0\,. \tag{1.81}$$

The ladder operators $\hat{\mathbf{b}}^\dagger_\omega$ and $\hat{\boldsymbol{b}}_\omega$ corresponding to the basis (p_ω, p^*_ω) of eq. (1.70) can be expressed via eq. (1.79) in terms of the operators $\hat{\mathbf{a}}^\dagger_\omega$ and $\hat{\mathbf{a}}_\omega$ and in this way, the vacuum expectation value for the number operator $\hat{\boldsymbol{N}}^{out}_\omega \equiv \hat{\boldsymbol{b}}^\dagger_\omega\,\hat{\boldsymbol{b}}_\omega$ in the *same* state $|0\rangle_{in}$ is

$$\begin{aligned}\langle 0|\hat{\boldsymbol{b}}^\dagger_\omega\,\hat{\mathbf{b}}_\omega|0\rangle_{in} = \;& \langle 0|\int d\omega_i \int d\omega_j [\alpha_{\omega\omega_j}\alpha^*_{\omega\omega_i}\hat{\mathbf{a}}^\dagger_{\omega_j}\hat{\mathbf{a}}_{\omega_i} - \alpha_{\omega\omega_j}\beta^*_{\omega\omega_i}\hat{\mathbf{a}}^\dagger_{\omega_j}\hat{\mathbf{a}}^\dagger_{\omega_i} \\ & -\beta_{\omega\omega_i}\alpha^*_{\omega\omega_i}\hat{\mathbf{a}}_{\omega_j}\hat{\mathbf{a}}_{\omega_i} + \beta_{\omega\omega_i}\beta^*_{\omega\omega_i}\hat{\mathbf{a}}_{\omega_j}\hat{\mathbf{a}}^\dagger_{\omega_i}]\,|0\rangle_{in}\,.\end{aligned} \tag{1.82}$$

The first three terms in the above equation are vanishing because they give zero when acting upon the state $|0\rangle_{in}$ and so we have

$$\langle 0|\hat{\boldsymbol{N}}^{out}_\omega|0\rangle_{in} = \int d\omega_i d\omega_j |\beta_{\omega\omega_i}|^2\,\langle 0|\hat{\mathbf{a}}_{\omega_j}\hat{\mathbf{a}}^\dagger_{\omega_i}|0\rangle\,. \tag{1.83}$$

After using the commutation relations (1.67) and relabeling the integration parameter $\omega_i \to \omega'$ we finally obtain that

$$\boxed{\langle 0|\hat{\boldsymbol{N}}_{\omega}^{out}|0\rangle_{in} = \int d\omega' |\beta_{\omega\omega'}|^2} \,. \tag{1.84}$$

This is a striking physical consequence of considering QFT in curved spacetime! A state that is empty of particles for one observer is interpreted as a non-vacuum state by another observer. An equivalent way to interpret this result is that the gravitational field creates particles!

It is clear then by the form of eq. (1.84) that particles will be created whenever any of the coefficients $\beta_{\omega\omega'}$ are non-zero.

1.3.4 Particle creation by black holes

Hawking Radiation [48] is undoubtedly one of the most remarkable predictions of semiclassical gravity and plays a pivotal role in providing the link between the laws of black-hole mechanics and classical thermodynamics discussed in the previous section. In the absence of a complete theory of quantum gravity, the Hawking effect emerges as a semiclassical phenomenon of QFT in curved spacetime.

In this section we will derive the famous thermal spectrum for the Hawking radiation emitted by a black hole following along the lines of Hawking's original work [48, 64]. We start by considering a massless scalar field ϕ, that propagates in the gravitational background of a black hole formed by gravitational collapse (see Fig. 1.2). The scalar field's equation of motion is

$$\frac{1}{\sqrt{-g}}\partial_\mu \left[\sqrt{-g}g^{\mu\nu}\partial_\nu \phi\right] = 0 \,. \tag{1.85}$$

Sufficiently far away from the black hole we may write the field in terms of a complete set of orthonormal solutions f_ω of the EOM (1.85) as

$$\phi = \int d\omega \left(f_\omega \hat{\mathbf{a}}_\omega + f_\omega^* \hat{\mathbf{a}}_\omega^\dagger\right) \,, \tag{1.86}$$

where the operators $\hat{\mathbf{a}}_\omega$ and $\hat{\mathbf{a}}_\omega^\dagger$ are the annihilation and creation operators respectively. With the above decomposition of the scalar field we describe the *incoming* modes of the field originating from past null infinity. The vacuum for these modes i.e. the ground state that corresponds to no incoming particles is defined as usually via

$$\hat{\mathbf{a}}_\omega \,|0\rangle = 0 \,. \tag{1.87}$$

Turning now to the near-black-hole region the field will be "mixed" in the sense that there will be field modes moving towards the black hole and field modes moving away from it after scattering. Thus

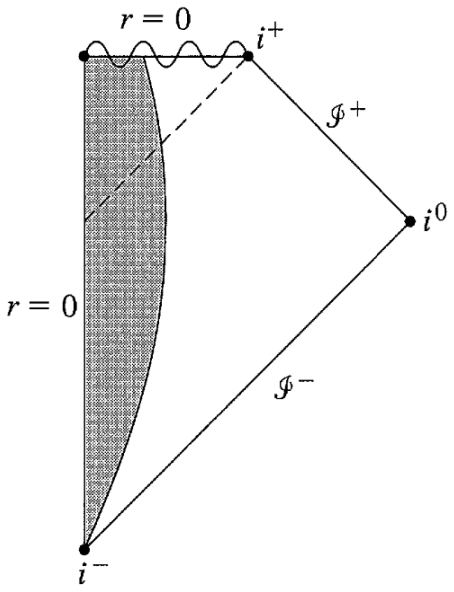

FIGURE 1.2: Carter-Penrose diagram of a collapsing star that results in the formation of a black hole. The shaded region corresponds to the interior of the star. Credit: [15]

we may write the field as

$$\phi = \int d\omega \left(p_i \hat{\mathbf{b}}_\omega + p^*_\omega \hat{\mathbf{b}}^\dagger_\omega + q_\omega \hat{\mathbf{c}}_\omega + q^*_\omega \hat{\mathbf{c}}^\dagger_\omega \right) , \tag{1.88}$$

in terms of the two sets of orthonormal functions p_ω (outgoing modes) and q_ω (incoming modes) that are also solutions to eq. (1.85). The corresponding creation and anihilation operators for these solutions are $\hat{\mathbf{b}}^\dagger_\omega, \hat{\mathbf{c}}^\dagger_\omega$ and $\hat{\mathbf{b}}_\omega, \hat{\mathbf{c}}_\omega$ respectively. The outgoing modes will eventually reach the distant observer in the future and they may be expressed as a linear combination of the original field decomposition in terms of the f_ω modes as

$$p_\omega = \int d\omega' \left(\alpha_{\omega'\omega} f_{\omega'} + \beta_{\omega'\omega} f^*_{\omega'} \right) , \tag{1.89}$$

where the coefficients $\alpha_{\omega'\omega}$ and $\beta_{\omega'\omega}$ are the Bogoliubov coefficients. This last equation leads to the following relation between the operators $\hat{\mathbf{a}}_\omega$ and $\hat{\mathbf{b}}_\omega$:

$$\hat{\mathbf{b}}_\omega = \int d\omega' \left(\alpha^*_{\omega\omega'} \hat{\mathbf{a}}_{\omega'} - \beta^*_{\omega\omega'} \hat{\mathbf{a}}^\dagger_{\omega'} \right) . \tag{1.90}$$

We thus conclude that the vacuum expectation value for the number operator of the outgoing field modes $\hat{\mathbf{b}}^\dagger_\omega \hat{\mathbf{b}}_\omega$ will be given by

$$\langle 0 | \, \hat{\mathbf{b}}^\dagger_\omega \hat{\mathbf{b}}_\omega \, | 0 \rangle = \sum_{\omega'} |\beta_{\omega\omega'}|^2 . \tag{1.91}$$

This last equation yields the total number of particles that are generated by the gravitational field of the collapsing black hole, manage to escape the gravitational attraction and reach the distant observer. It is clear that this number is determined by the Bogoliubov coefficient $\beta_{\omega\omega'}$. We may now take advantage of the spherical symmetry of spacetime and Fourier expand the solutions f_ω and p_ω

as

$$f = \frac{F_\omega(r)}{\sqrt{2\pi\omega}} \frac{e^{i\omega v}}{r} Y_{l\,m}(\theta,\phi) \ , \ p = \frac{P_\omega(r)}{\sqrt{2\pi\omega}} \frac{e^{i\omega u}}{r} Y_{l\,m}(\theta,\phi) \ , \tag{1.92}$$

in terms of the *advanced* and *retarded* coordinates given respectively by

$$v \equiv t + r + 2m \log|\frac{r}{2m} - 1| \,, \tag{1.93}$$

$$u \equiv t - r - 2m \log|\frac{r}{2m} - 1| \,. \tag{1.94}$$

Consider now an outgoing field mode p_ω at the location of the observer and trace it back to the near black hole region. There, part of the field will get scattered by the gravitational potential of the black hole and move again towards the distant observer with its frequency unaltered ω. This part of the field will contribute to the $\alpha_{\omega\omega'}$ Bogoliubov coefficient. The rest of the field that does not get back-scattered by the potential will tunnel through it and as a consequence will be highly red-shifted due to the intense gravitational field. This part of the field contributes to the $\beta_{\omega\omega'}$ Bogoliubov coefficient. Then, if $(1-\Gamma)$ is the part of the field that back-scatters of the potential, the part that goes through it will be Γ and is explicitly given in terms of the Bogoliubov coefficients as

$$\Gamma = \int_0^\infty \left(|\alpha_{\omega\omega'}|^2 - |\beta_{\omega\omega'}|^2\right) d\omega' \,. \tag{1.95}$$

The expectation value of the number of particles that are generated and escape to the location of the observer are

$$n = \int_0^\infty |\beta_{\omega\omega'}| d\omega' \tag{1.96}$$

while the following relation between the coefficients holds

$$|\alpha_{\omega\omega'}| = e^{\pi\omega/\kappa_h} |\beta_{\omega\omega'}|. \tag{1.97}$$

Finally, after combining eqs. (1.95) and (1.97) one obtains

$$n = \frac{\Gamma}{e^{2\pi\omega/\kappa_h} - 1} \,. \tag{1.98}$$

This last equation tells us that the energy profile of the particle flux generated by the gravitational field of the black hole, as it is detected by a distant observer, resembles that of black body radiation at temperature determined by the value of the surface gravity of the black-hole horizon κ_h. More presisely the temperature for the Schwarzschild black hole will be given by eq. (1.60).

As any thermodynamic system with temperature, black holes radiate by emitting particles in the form of *Hawking radiation* (HR). The vacuum is constantly generating particle-antiparticle pairs that "pop" into existence for a very short period of time before annihilating. The number of pairs generated is larger in regions of spacetime where the curvature is more intense. Such a region is the vicinity of the horizon of a mini-black hole. For large BHs the region close to the event horizon is relatively "flat".

When a pair of particles forms close to the horizon, the pair gets "pulled apart" by tidal forces and the antiparticle may get absorbed by the BH. In this way, the mass of the black hole gets reduced by the tinniest amount. The other particle of the pair is then able to move away from the black hole (if it overcomes the gravitational barrier, that is) and as such a distant observer detects a flux of particles originating from the horizon. Over time, through this process, the mass of the black hole decreases until it eventually evaporates completely. This has lead to the *information paradox* [65] since if the black hole indeed evaporates completely in the final stages of Hawking radiation and no "quantum gravity effect" prevents this from happening, all the information that went into the black hole during its lifetime is lost. This is in contradiction with one of the most fundamental principles of physics, namely the conservation of information. Chapters $2-4$ of this thesis are dedicated to the study of Hawking radiation emitted by the HD SdS black hole (1.27).

1.4 Extra dimensions

Gravitational theories that postulate the existence of extra spatial dimensions appeared shortly after the formulation of GR by the pioneering works of Kaluza and Klein [66, 67] in an effort to unify gravity with electromagnetism. In the late 90s, motivated by the hierarchy problem of gravity, the so-called braneworld-models have emerged. In these models, our observable universe is thought of as a membrane (upon which all regular matter is localized), embedded in a higher dimensional space (which can be probed only by gravity and possibly exotic non-Standard-Model particles). Modern theories that are candidates for a complete theory of gravity (string theory and variants of it), in fact *require* the existence of extra spacelike dimensions beyond the three we observe.

While it is true that, even to date, there is no experimental evidence supporting the existence of extra dimensions, we also have no reason to restrict our theories to only $(3+1)$-dimensional spacetimes; after all Einstein's GR is valid for an arbitrary number of dimensions. Thus, considering Higher-Dimensional (HD) theories is interesting not only from a purely theoretical point of view but as a means of possibly providing useful input for experiments aiming to detect them in the future.

Since the existence of extra dimensions drastically modifies the properties of black holes, it is the goal of this section to provide a short introduction to the HD theories discussed above and to the HD black holes.

1.4.1 The Kaluza-Klein idea

Attempts for unification via extra dimensional theories date back to the works of Kaluza and Klein [66, 67] where they tried to unify gravity and electromagnetism by considering a flat 5-dimensional

space $M(4,1)$. The 15 Degrees Of Freedom (DOF) of such a metric can be decomposed into the usual $4D$ metric tensor (10 DOFs), a 4-vector that is interpreted as the vector potential of electromagnetism (4 DOFs) plus a scalar DOF.

Since we observe only four dimensions in the universe the extra dimension should be "hidden" somehow via a mechanism that reproduces effectively the 4-dimensional gravity we observe. To achieve this, as Klein pointed out, the extra dimension (y) can be "curled up" to a circle of extremely small radius. Mathematically this is realized via the "compactification" of the extra dimension that amounts to imposing the periodic condition

$$y \sim y + 2\pi k L\,, \tag{1.99}$$

where k is an arbitrary integer and L is the radius of the circle of compactification. Indeed, if L is very small[6] the extra dimensions cannot be observed and the world appears four-dimensional. More precisely, the statement that the extra dimension remains hidden can be understood as follows. The imposed periodicity (1.99) on the extra dimension causes the fluctuations of the gravitational field that are called *KK modes* to have discrete masses that are heavier the smaller the radius of compactification L is. To see this, we may expand the $5D$ metric as

$$g_{M\,N}(x^\mu, y) = \sum_k e^{\frac{i\,k\,y}{L}}\, g^k_{M\,N}(x^\mu)\,, \tag{1.100}$$

where henceforth capital (lowercase) letters are used to denote indices that span the five- (four-) dimensional spacetime respectively. Then it can be shown that the 5-dimensional space corresponds to an effective 4-dimensional theory along with an infinite tower of fields with masses $m_k \equiv |k|/L$. Assuming then that the radius of compactification is small we get that the mass of the first KK mode ($k = 1$) is out of reach for the current particle detectors. In this way, only massless modes appear in the low-energy effective theory and the metric can be considered independent of y.

1.4.2 The brane world scenario

Beyond the Kaluza-Klein proposal, there are other theories that allow for a fundamentally higher-dimensional (HD) universe to appear effectively as four-dimensional. This is achieved within the context of the so-called braneworld models that first appeared in the late 90s. In the braneworld models, the four dimensional universe we observe corresponds to a "membrane" that is usually termed the *brane* embeded in a higher-dimensional space called the *bulk*. All standard model particles are confined on the brane while gravity being the geometry of space itself "spreads out" to all dimensions.

The chronologically first brane-world model to appear [8–10] was the *Arkani-Hamed-Dimopoulos-Dvali* (ADD) or equivalently the *Large Extra Dimensions* (LEDs) scenario. The motivation behind

[6] Of the order of the Planck length.

the formulation of the ADD model was the solution to the *hierarchy problem*. This problem refers to the fact that gravity is many orders of magnitude weaker than the rest of the fundamental forces in nature. In the ADD model it is assumed that the fundamental scale of gravity and the energy scales set by the *Standard Model* (SM) of particle physics are essentially the same.

The explanation then as to why gravity appears weaker is that it is the only one of the forces that can probe the extra dimensions of spacetime and as such it gets "diluted". The extra dimensions can be "large" in the sense that they are much larger than the Planck length. By virtue of Gauß's law it can easily be shown that the (fundamental) $(4+n)$-dimensional scale of gravity M_* and the 4-dimensional one M_P are related in the following way:

$$M_*^{n+2} \sim \frac{1}{L^n}\frac{\hbar c}{G}\left(\frac{\hbar}{c}\right)^n = \frac{M_P^2}{L^n}\,, \tag{1.101}$$

where n is the number of extra dimensions and L is the length of the extra dimensions (for simplicity all extra dimensions are assumed to be of the same length). In the last equality we have set $\hbar = c = 1$.

In the second brane-world scenario, [11, 12] called *Warped Extra Dimensions* (WED) or *Randall-Sundrum* (RSI, RSII) model, the SM particles are still confined on a 3-brane while only one extra dimension is sufficient to solve the hierarchy problem. The crucial difference between the WED and LEDs is that, in the former, the extra dimension is not flat but it is "warped". The warping of the extra dimension is supported by the presence of a negative bulk cosmological constant Λ_5. Another important feature of the WEDs is that the extra dimension is $\mathbb{Z}_2$-symmetric and so the bulk is y-symmetric around the location of the brane. The line-element is given by

$$ds^2 = e^{-2|y|/l}\eta_{\mu\nu}dx^\mu dx^\nu + dy^2\,, \tag{1.102}$$

where $l \equiv \sqrt{-6/\Lambda_5}$ is the AdS radius and $\eta_{\mu\nu}$ is the Minkowski metric. The function $e^{-2|y|/l}$ is called *warp factor*. Due to the fact that the warp factor is en *exponentially* decaying function as we move away from the brane at $y = 0$, gravity remains localized close to the brane.

In the first RSI model [11], the gravitational set up consists of two branes, one with positive tension located at $y = 0$ and one with negative tension located at $y = L$. As with the Kaluza Klein model the extra dimension is compactified with period L. The action for the model is

$$S = S_g + S_1 + S_2 \tag{1.103}$$

with

$$S_g = \int dx^4 \int dy \sqrt{-g^{(5)}}\left(\frac{R}{2\kappa_5^2} - \Lambda_5\right)\,, \tag{1.104}$$

where Λ_5 is the cosmological constant. The contributions to the action by the two 3-branes located at $y = 0$ and $y = L$ with respective energy densities σ_1 , σ_2 and Lagrangians $\mathcal{L}_1$, $\mathcal{L}_2$ are

$$S_1 = \int d^4x\sqrt{-g_1}\,(\mathcal{L}_1 - \sigma_1) \tag{1.105}$$

and

$$S_2 = \int d^4x\sqrt{-g_2}\,(\mathcal{L}_2 - \sigma_2)\ . \tag{1.106}$$

In the second RSII model [12], Randall and Sundrum showed that it is possible to effectively obtain $4d$-gravity with an infinite extra dimension L. In this picture the 3-brane located at $y = L$ is sent to infinity and is thus essentially removed from the setup. The action for RSII is

$$S = S_g + S_1\,, \tag{1.107}$$

where the first and second terms in the above equation have been defined in eq. (1.104) and eq. (1.105) respectively.

Higher dimensional black-hole solutions have been found already from the 60s [30, 68] where, as in the LEDs brane-world scenario, the topology of the extra dimensions is flat, or uniformly curved due to the presence of a bulk cosmological constant. The HD SdS black hole of eq. (1.27) belongs to this class of solutions. On the other hand, in WEDs the richer topological structure of the model has, so far, proven to be an insurmountable obstacle towards finding an exact analytic localized on the brane black-hole solution in this context. The chapter 5 of this thesis is dedicated to the search for such a solution in WEDs.

Chapter 2

Greybody factors for higher-dimensional Schwarzschild-de Sitter black holes

Our understanding of black holes changed drastically in the mid-seventies when Steven Hawking considered quantum field theory in curved spacetime and realized for the first time that black holes are not the perfect absorbers they were considered to be [48]. He found that in fact black holes evaporate by radiating particles with a perfect black-body spectrum at the Hawking temperature T_h, exactly at the location of the event horizon when backreaction effects on the background are ignored [69] . The emitted particle flux though has to transverse a non-trivial curved spacetime background until it reaches the distant observer; by that time, the frequency profile of the spectrum is modified to the famous Hawking spectrum that for massless bosons has the following form:

$$\frac{d^2E}{dt\,d\omega} = \frac{1}{2\pi}\sum_l \frac{N_l\,|A|^2\,\omega}{\exp(\omega/T_h)-1}\,. \tag{2.1}$$

The above gives the energy emitted per unit time and unit frequency by the black hole. Also, ω is the energy of the emitted particle, N_l is the multiplicity of states with the same angular-momentum number and T_h is the temperature of the black hole. The term $|A|^2$ encodes all the information about the deviation from the Planck spectrum and has been dubbed *greybody factor* (GF). For pure black-body radiation the GF is a constant and equals the surface of the emitting body while in the case of a black hole it depends on the properties of the emitted particle species and the geometrical background. The main objective of this chapter is to obtain an analytic expression for the GF of spherically-symmetric, uncharged black holes in the presence of a positive cosmological constant in $d = 4 + n$ dimensions. We focus on the emission of massless scalar particles that are non-minimally coupled to gravity and derive the corresponding GF both for bulk and brane propagating fields for an arbitrary angular momentum parameter of the field.

We start by introducing the higher-dimensional black-hole geometry, we obtain the brane-induced metric by projection and study the causal structure to determine the event horizons of this spacetime. Then we solve the equations of motion (EOM) of the scalar field employing an approximate technique of matching its solutions at the two asymptotic radial regimes. The derived complete solution then allows us to compute the GF. Finally we study in depth the profile of the GF in terms of all four parameters that govern the emission namely, the number of extra dimensions n, the cosmological constant Λ, the angular momentum number of the field l and the non-minimal coupling parameter ξ. Also, the low-energy limit of our analytic expressions is thoroughly investigated.

2.1 The $(4+n)$-dimensional Schwarzschild-de Sitter black-hole

2.1.1 Gravitational background

Under the assumption that our universe is fundamentally higher-dimensional and the ever-increasing observational confirmation [70–82] of its expansion at an accelerated rate we are led to consider the Einstein-Hilbert action in $D = 4+n$ dimensions, supplemented by a positive bulk cosmological constant term Λ

$$S_D = \int d^{4+n}x \sqrt{-G} \left(\frac{R_D}{2\kappa_D^2} - \Lambda \right) . \tag{2.2}$$

The determinant of the metric tensor G_{MN} is G while the higher-dimensional gravitational constant $\kappa_D^2 = 1/M_*^{2+n}$ is related to the fundamental scale of gravity M_*. Finally R_D is the D-dimensional Ricci scalar. The observed value for the cosmological constant is $\Lambda \sim 10^{-52} m^{-2}$ although in our analysis we will not be restricted to this specific value but rather consider different values for Λ . Employing the principle of extremal action, the variation of (2.2) with respect to the inverse metric tensor yields the Einstein equations

$$R_{MN} - \frac{1}{2} G_{MN} R_D = -\kappa_D^2 G_{MN} \Lambda \equiv \kappa_D^2 T_{MN} \tag{2.3}$$

where we have identified the r.h.s. of the gravitational equations as the bulk energy-momentum tensor T_{MN}. To calculate the Ricci scalar one can simply contract (2.3) with G^{MN} to find that in n extra dimensions it is given by the following expression:

$$R_D = \frac{2\,(n+4)}{n+2} \kappa_D^2 \Lambda \, . \tag{2.4}$$

Notice that it is directly proportional to the cosmological constant. Let us now assume a general ansatz for a $(4+n)$-dimensional spacetime that is spherically-symmetric and static i.e. there are no time-space mixing terms. Then the line element in such a coordinate system will be

$$ds^2 = G_{MN} dx^M dx^N = -h(r)\, dt^2 + \frac{dr^2}{h(r)} + r^2 d\Omega_{2+n}^2 \, , \tag{2.5}$$

where $d\Omega_{2+n}^2$ is the surface element of a $(2+n)$-dimensional unit sphere given by

$$d\Omega_{2+n}^2 = d\theta_{n+1}^2 + \sin^2\theta_{n+1} \left(d\theta_n^2 + \sin^2\theta_n \left(... + \sin^2\theta_2 \left(d\theta_1^2 + \sin^2\theta_1 \, d\varphi^2 \right) ... \right) \right) , \tag{2.6}$$

with $0 \leq \varphi < 2\pi$ and $0 \leq \theta_i \leq \pi$, for $i = 1, ..., n+1$. In concord with the spherical symmetry of the spacetime, the *metric function*[1] $h(r)$ is a function of the radial coordinate r only and we choose to

[1] Sometimes also referred to as the "gravitational potential" because in the weak field limit the g_{00} metric component is related to the Newtonian potential.

introduce the n extra space-like dimensions in the form of n additional azimuthal coordinates θ_i. In order to specify the functional form of $h(r)$ we need to use the Einstein equations (2.3). To this end, we substitute (2.5) into (2.3) and recover the Tangherlini solution [30] describing a $(4+n)$-dimensional black hole in the presence of a cosmological constant term

$$h(r) = 1 - \frac{\mu}{r^{n+1}} - \frac{2\kappa_D^2\,\Lambda r^2}{(n+3)(n+2)}\,. \tag{2.7}$$

The *mass parameter* μ is related to the mass M of the black hole through the relation [68]

$$\mu = \frac{2\kappa_D^2 M}{(2+n)A_{2+n}}, \quad A_{2+n} = \frac{2\pi^{(n+3)/2}}{\Gamma[(n+3)/2]}\,, \tag{2.8}$$

where A_{2+n} is the surface area of the $(2+n)$-dimensional unit-sphere.

The line element (2.5) with the metric function (2.7), corresponds to the $(4+n)$-dimensional generalization of the *Schwarzschild-de Sitter* (SdS) solution that describes the gravitational field in the exterior of a spherically-symmetric, uncharged mass in the presence of a positive cosmological constant. The invariance of the metric under time translations indicates that the spacetime admits a Killing vector field $K^\mu \sim \partial_t$ that is time-like in the region of spacetime where $h(r) > 0$.

In the limit $\Lambda \to 0$ the last term in eq. (2.7) vanishes and $h(r)$ becomes that of an asymptotically flat $(4+n)$-dimensional Schwarzschild black hole. On the other extreme limit $\mu \to 0$ the black hole is "removed" from the setup and we are left with the pure higher-dimensional de Sitter space.

We have thus far introduced the geometry of the higher-dimensional black hole and a few important comments are in order regarding the fitness of the above metric to adequately describe the Hawking radiation process which is the ultimate goal of this study. Hawking radiation, as we discuss in the introduction, is a semi-classical effect where quantum fields are considered on a classical gravitational background and result in the black hole radiating particles in a very specific way. Of course, each of the particles emitted strips the black hole of an amount of energy equal to the particle's total energy thus reducing its mass and in turn altering the metric upon which the particles propagate. The line element (2.5) is indeed a good approximation to the black-hole background as long as the energy carried away by the field is much smaller than the black-hole mass because only then can we neglect the back-reaction of the particle emission on the spacetime. For the purposes of this study we assume that this is always the case.

The second point we wish to clarify is the following. In order for this black hole to be a higher-dimensional object, it has to be fully submerged in the higher-dimensional space. This means that the black-hole radius r_h has to be much smaller than the characteristic length scale of the extra dimensions[2] L otherwise the black hole is effectively four-dimensional. Also, r_h has to be much larger

[2]Here, for simplicity we assumed that all extra dimensions have the same length scale.

than the Planck scale l_P so that we can safely ignore quantum-gravity effects. Eventually the black-hole radius is assumed to satisfy $l_P \ll r_h \ll L$. This observation, combined with the upper limit for the size of the extra dimensions today, makes clear that the black holes we study in this work are not of astrophysical size but rather miniature black holes that could possibly be created in present or future particle accelerators with sufficient center-of-mass energy higher than the fundamental Planck scale M_* [83].

In the brane-world theories [8–12] the standard model fields are confined on the brane, in order to avoid conflict with observations, while gravity is free to probe the extra dimensions. Then, for fields localized on our observable brane universe the geometry is not described by the line element of (2.5) but rather by a projected-on-the-brane metric. The projection of the bulk metric onto the brane is achieved by assigning to all the extra coordinates the value $\frac{\pi}{2}$. This way the surface element of the unit-sphere reduces to the usual four-dimensional one and the induced metric on the brane is

$$ds^2 = g_{\mu\nu}dx^\mu dx^\nu = -h(r)\,dt^2 + \frac{dr^2}{h(r)} + r^2\left(d\theta^2 + \sin^2\theta\, d\varphi^2\right). \tag{2.9}$$

Finally by performing a direct computation one can verify that the Ricci scalar derived from (2.9) is

$$R_4 = \frac{24\kappa_D^2\Lambda}{(n+2)(n+3)} + \frac{n(n-1)\mu}{r^{n+3}}. \tag{2.10}$$

Notice that the projection procedure does not affect the functional form of $h(r)$ and in this way the effect of the extra-dimensions still enters the geometry of the brane via the metric function. A direct consequence of this is that both line elements (2.5) and (2.9) will share the same causal structure the study of which is the subject of the following section.

2.1.2 Causal structure

To find the locations of the horizons for a given spherically-symmetric spacetime one has to solve $g^{rr} = 0$ because at these radii the timelike Killing vector $\frac{\partial}{\partial t}$ becomes null [15]. So the condition we are looking for is the vanishing of the metric function

$$h(r) = 1 - \frac{\mu}{r^{n+1}} - \frac{2\kappa_D^2\,\Lambda r^2}{(n+3)(n+2)} = 0\,. \tag{2.11}$$

In general this algebraic equation yields $n+3$ roots corresponding to multiple horizons of the higher-dimensional spacetime which at first glance may seem to lead to a very complicated causal structure. Thankfully, not all of these roots are real and positive and thus some of the solutions are non-physical and are discarded. To simplify things even further one can restrict the parameter space of (n, Λ, μ)

in such a way that the following condition is always respected:

$$\mu^2 \tilde{\Lambda}^{(n+1)} \leqslant \frac{4(n+1)^{(n+1)}}{(n+3)^{(n+3)}} \tag{2.12}$$

where we have defined $\tilde{\Lambda} \equiv 2\kappa_D^2 \Lambda/(n+2)(n+3)$. Then, only two real and positive solutions to (2.11) exist [84–86] with the smaller one corresponding to the radius of the black-hole horizon r_h and the larger one to the cosmological-horizon radius r_c.

We are interested in events that satisfy $r_h \leqslant r \leqslant r_c$ so we deal with observers located in the causal part of spacetime between the two horizons. In this region the metric function is positive and thus the space-like (time-like) character of the spatial (temporal) coordinates is preserved while outside the horizons i.e. at $(0, r_h) \cup (r_c, \infty)$ the sign of $h(r)$ is reversed along with the causal character of the coordinates and thus the spacetime is dynamical. In our analysis we shall work in units of r_h and this effectively sets $r_h = 1$. For example the cosmological constant will be measured in units of r_h^{-2} and in the plots that appear throughout this thesis the energy will be parametrised by the dimensionless quantity ωr_h.

To better understand the behavior of the metric function $h(r)$ (2.7) in Fig. 2.1 we fix the black-hole mass parameter $\mu = 1$ and the number of extra dimensions $n = 2$ as the value of the cosmological constant Λ varies from $\Lambda = 10^{-5} r_h^{-2}$ to $\Lambda = 10^{-1} r_h^{-2}$. Care has been taken so that the values considered for μ and Λ are compatible with the constraint (2.12).

Recall that the locations of the two horizons correspond to the roots of $h(r)$ and so in Fig. 2.1(a) the radii at which the curves meet the horizontal axis are the locations of r_h and r_c. As Λ grows, the two horizons are located closer to each other and thus the causal space becomes smaller (in this coordinate system [87]) until a critical value Λ_{crit} is reached and the two horizons *apparently* coincide

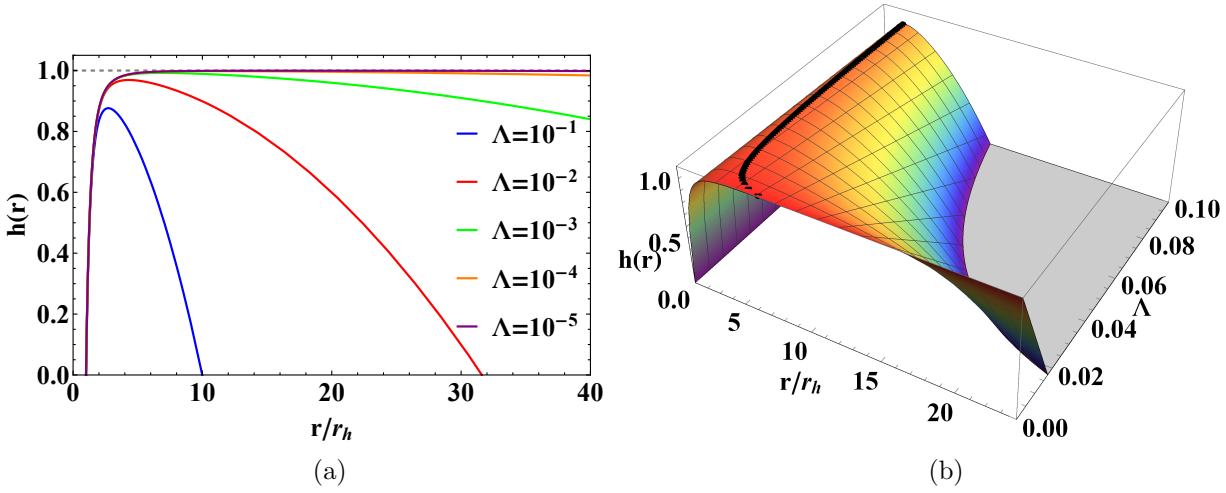

FIGURE 2.1: The metric function (2.7) for $\mu = 1, n = 2$ and (a) various values of the cosmological constant Λ. (b) The location of r_0 (black curve) for all values of $\Lambda \in (10^{-5}, 10^{-1})$.

n	0	1	2	3	4	5
$\Lambda_{crit}(r_h^{-2})$	0.44	1.50	3.26	5.77	9.09	13.23

TABLE 2.1: Indicative values of Λ_{crit} for $\mu = 1$ and for $n \in [1, 5] \cap \mathbb{Z}$.

(See appendix A) when

$$\mu^2 \tilde{\Lambda}_{crit}^{(n+1)} \to \frac{4(n+1)^{(n+1)}}{(n+3)^{(n+3)}}. \tag{2.13}$$

Some indicative values of Λ_{crit} for various n and for $\mu = 1$ are given in Table 2.1. For even larger values of the cosmological constant, the condition (2.12) is violated and thus (2.5) ceases to describe a black hole since there are no horizons.

By inspection of Fig. 2.1(a) it is evident that the metric function (2.7) always exhibits a global maximum at some radius $r_h < r_0 < r_c$. This can also be seen in Fig. 2.1(b), where we plot the metric function for all values of $\Lambda \in (10^{-5}, 10^{-1})$ and the black curve corresponds to the location of r_0 in each case. The exact value of r_0 can be easily calculated as it corresponds to the vanishing of the first derivative of the metric function and has the following expression:

$$r_0 = \left[\frac{(n+1)(n+2)(n+3)\mu}{4\kappa_D^2 \Lambda} \right]^{1/(n+3)}. \tag{2.14}$$

The importance of this radius is that the metric function satisfies $h(r_0) \approx 1$[3] and actually this becomes an increasingly accurate approximation as Λ becomes smaller, something one can also verify from Fig. 2.1. An observer $\mathcal{O}$ located at r_0 in SdS will resemble the asymptotic Minkowski observer $\mathcal{M}$ located at $r \to \infty$ in a pure-Schwarzschild geometry where the metric function is

$$h_{\mathcal{M}}(r) = \lim_{\Lambda \to 0} h_{\mathcal{O}}(r) = 1 - \frac{\mu}{r^{n+1}}, \tag{2.15}$$

and so it is clear that

$$h_{\mathcal{O}}(r_0) \approx 1 = h_{\mathcal{M}}(r \to \infty). \tag{2.16}$$

For $\mathcal{O}$, the gravitational attraction of the black hole and the repulsion of the cosmological constant cancel out and so $\mathcal{O}$ is a non-accelerated observer exactly like $\mathcal{M}$.

The cosmological horizon radius r_c has been identified with the largest of the two roots of the metric function. It is interesting to quantify how much larger r_c is than the black hole radius r_h for a given Λ and n. To this end, in Fig. 2.2(a) we have fixed the mass parameter of the metric function to $\mu = 1$ and computed numerically the value of the ratio of the horizon radii r_c/r_h as Λ ranges from $\Lambda = 0$ to $\Lambda = 6$ (in units of r_h^{-2}) for several values of the number of extra dimensions. The feature that emerges from this figure is that the larger the number of extra dimensions (n), the further away r_c is located

[3] This feature will play an important role in our discussion in chpt. 4 about the various proposals made for the proper definition of the temperature for the Hawking radiation process in asymptotically de Sitter spacetimes.

from r_h for the same value of Λ. So we conclude that the causal region of spacetime available to the SdS observer increases with n. As Λ increases, the ratio becomes smaller until the two horizons are identified ($r_c/r_h = 1$). Thus one realizes that in contrast to the asymptotically flat case where a black hole can be indefinitely large, the presence of a cosmological constant sets an upper limit to the size of the black hole [88, 89]. This limit corresponds to the extremal SdS or *Nariai solution* [90] .

In Fig. 2.2(b) we fixed again the parameter $\mu = 1$ and for an arbitrary number of extra dimensions $n = 1$ we plot the variation of the black-hole horizon radius depicted with the red curve, the cosmological horizon with the purple curve and the "unaccelerated observer" radius r_0 with the blue curve as Λ ranges from $\Lambda = 0r_h^{-2}$ to $\Lambda = 1.5r_h^{-2}$. For small values of Λ we see that the black-hole horizon radius approaches the pure-Schwarzschild radius since the cosmological term contribution to eq. (2.7) becomes negligible in this limit. The observer at the special radius r_0 is located further away from the black-hole horizon r_h the smaller Λ is and approaches the asymptotic observer at infinity in the limit $\Lambda \to 0$. As Λ increases, r_c and r_0 decrease rapidly at first and then their decrease rate becomes milder while r_h exhibits a mild increase through-out the range of the allowed Λ values. A possible interpretation to the latter could be the increase of the internal energy contained by the black hole [91] as the vacuum energy density increases with the cosmological constant. For $\Lambda = 1.5r_h^{-2}$, the maximum allowed value for the cosmological constant (2.13) subject to the constraint of eq. (2.12) has been reached and the two horizons coincide with r_0. Thus we have the apparent "vanishing" of the causal volume of the observable universe (since $(r_c - r_h) \to 0$).

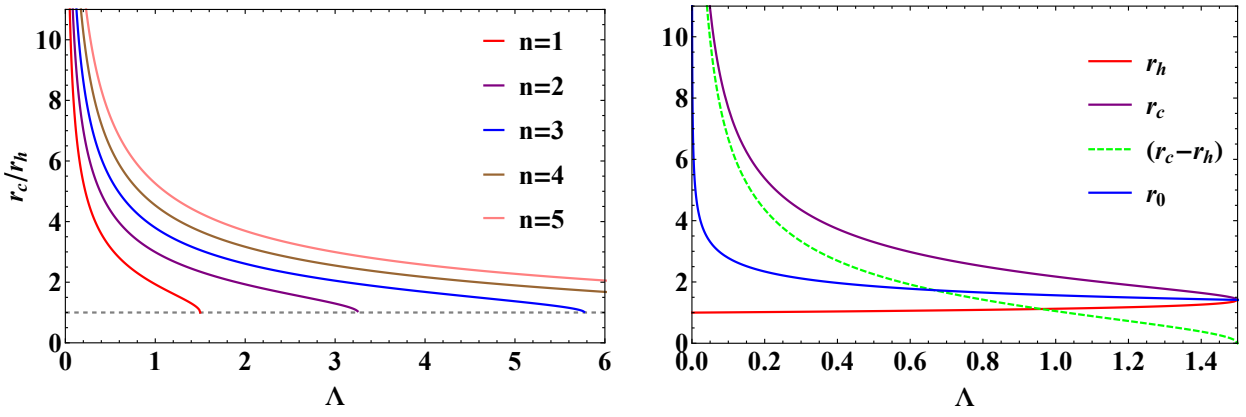

(a) (b)

FIGURE 2.2: For fixed mass parameter $\mu = 1$, **(a)** the ratio r_c/r_h as Λ varies in the range $(1, 6)$ for $n \in [1, 5] \cap \mathbb{Z}$, and **(b)** the values of r_h, r_c, r_0 and $r_c - r_h$ for $n = 1$ and $\Lambda \in (0, 1.5)$.

2.2 Scalar field scattering on the brane

2.2.1 The effective potential

Having specified the geometry of the higher-dimensional curved spacetime, the next step is to introduce the field theory on it. The propagating field will interact with the black hole by means of scattering on the effective potential generated by the non-trivial spacetime curvature [92–94]. Computing the transmission probability of this process will then allow as to obtain the greybody factor. We focus on a free scalar field (that is to say we will not include a self-interaction term in the action) that is massless but couples non-minimally to gravity through an interaction term with the Ricci scalar.

We will first study the case of a brane localized field since it is the phenomenologically more interesting one. The action for brane-bound fields with the features described above reads

$$S_4 = -\frac{1}{2}\int d^4x\,\sqrt{-g}\left[\xi\Phi^2 R_4 + g^{\mu\nu}\partial_\mu\Phi\,\partial_\nu\Phi\right]\,, \tag{2.17}$$

where the induced metric is given in eq. (2.9), the Ricci scalar in eq. (2.10) and the strength of the field coupling to gravity is parametrised by ξ. Varying the action (2.17) we obtain the field equation of motion (EOM) on the brane

$$\frac{1}{\sqrt{-g}}\,\partial_\mu\left(\sqrt{-g}\,g^{\mu\nu}\partial_\nu\Phi\right) = \xi R_4\,\Phi\,. \tag{2.18}$$

Notice at this point that the form of the right-hand-side (r.h.s.) of eq. (2.18) can be interpreted as an effective mass term for the field and taking also into account the expression for the Ricci scalar (2.10) we can see that the "mass" of the field becomes larger with the parameter $\xi\Lambda$ while it vanishes in the asymptotically-flat ($\Lambda \to 0$) and minimal-coupling ($\xi \to 0$) limits.

Because we are dealing with a spherically symmetric spacetime the radial part of the eom is the one that encodes all the important information of the field propagation and is naturally the one we are interested in. So in order to decouple the radial part we introduce the following factorized ansatz for the field:

$$\Phi(t, r, \theta, \varphi) = e^{-i\omega t}\,R(r)\,Y(\theta, \varphi)\,, \tag{2.19}$$

where ω is the energy of the emitted particle, $R(r)$ is the radial part of the field while the angular contribution to the field enters through the scalar spherical harmonics $Y(\theta, \varphi)$. Applying the standard method of separation of variables, the angular EOM corresponds to the eigenvalue equation of the spherical harmonics with eigenvalue $l(l+1)$, where l is the angular momentum quantum number of the emitted particle or *field mode*. The form of the radial part of the field $R(r)$ is thus dictated by

the decoupled differential equation

$$\boxed{\frac{1}{r^2}\frac{d}{dr}\left[h(r)r^2\frac{dR(r)}{dr}\right]+\left[\frac{\omega^2}{h(r)}-\frac{l(l+1)}{r^2}-\xi R_4\right]R(r)=0}\,. \tag{2.20}$$

This is the "master equation" for the calculation of the greybody factor for scalar fields with arbitrary l and ξ and for any values of the spacetime parameters n and Λ.

Before we proceed to the solution, we will study the profile of the *effective potential* induced by the spacetime curvature upon which the field scatters. The importance of this study is twofold. First and most importantly, the barrier is the physical reason behind the form of the Hawking spectrum and thus deserves special attention. Second, many of the qualitative features of the GFwill be encapsulated by the shape of the potential. For example the higher the potential barrier the smaller the GFwill be. This inverse relation between the two is due to the fact that the greybody factor corresponds to the absorption probability for an incoming wave to be absorbed by the black hole after it scatters on the barrier. One can prove [31, 93, 94] that the absorption probability of this problem equals the transmission probability for a wave that emanates from the black-hole horizon and impinges on the effective potential in order to overcome the barrier and contribute to the Hawking radiation.

To specify the expression for the potential we can recast (2.20) into an one-dimensional Schrödinger-like equation and in this way obtain the potential term. After the field redefinition $u(r)=rR(r)$ and using the *tortoise coordinate* r_* that was introduced by Wheeler and is related to r via

$$r_*\equiv\int\frac{dr}{h(r)}\,, \tag{2.21}$$

we obtain

$$-\frac{d^2u(r)}{dr_*^2}+V_{\rm eff}^{\rm brane}\,u(r)=\omega^2\,u(r)\,. \tag{2.22}$$

The effect of the tortoise coordinate is to "push" the locations of the horizons to infinity since it maps the finite radial coordinate interval $r\in[r_h,r_c]$ to the infinite $r_*\in(-\infty,\infty)$. So the black-hole horizon is located at $r_*\to-\infty$ and the cosmological one at $r_*\to\infty$. Equation (2.22) is of the same form as the one derived by Regge and Wheeler in their investigation of the stability of the Schwarzschild black hole [95] against linear perturbations and is often referred to as the *Regge-Wheeler equation*.

Thus the potential that a brane-confined massless scalar particle with angular momentum quantum number l has to overcome is

$$\begin{aligned}V_{\rm eff}^{\rm brane}=&h(r)\left[\frac{l(l+1)}{r^2}+\xi R_4+\frac{1}{r}\frac{dh}{dr}\right]\\ =&h(r)\left\{\frac{l(l+1)}{r^2}+\frac{4\kappa_D^2\Lambda(6\xi-1)}{(n+2)(n+3)}+\frac{\mu}{r^{n+3}}\left[\,(n+1)+\xi n(n-1)\,\right]\right\},\end{aligned} \tag{2.23}$$

where in the last step we have substituted (2.10) and (2.7).

This potential "filters" the particle flux generated on the black-hole horizon giving rise to the Hawking spectrum for a distant observer. Only a portion of the emitted black-body radiation manages to overcome the barrier (either by having energy larger than the peak of the potential or via quantum tunneling) while the rest gets back-scattered into the black hole. The barrier depends on both the spacetime properties n and Λ as well as on the field parameters l and ξ. Perhaps the most important feature of the potential is its proportionality to the metric function $h(r)$. On the location of the horizons we have seen that the metric function vanishes and as a consequence in the vicinity of the horizons the height of the effective barrier is negligible and the field is free. This enables us to express the solution to (2.22) as a superposition of free plane waves.

In (2.23) we see that the shape of the gravitational barrier is determined by the following 5 parameters: the black-hole mass parameter μ, the number of extra spacelike dimensions n, the angular momentum number l, the non-minimal coupling ξ and the cosmological constant Λ. We can use the condition that determines the locations of the horizons to reduce the number of parameters upon which the barrier depends by one. At the location of any of the two horizons (which we collectively denote here with a subscript "i") we can solve for the mass parameter μ and have

$$h(r_i) = 0 \rightarrow \mu = r_i^{n+1}\left(1 - \frac{2\kappa_D^2 \Lambda r_i^2}{(n+2)(n+3)}\right) . \tag{2.24}$$

So, using (2.24) evaluated on the black-hole horizon $r_h = 1$ we can eliminate μ and thus study the dependence of the effective potential eq. (2.23) on n, l, ξ and Λ.

The impact of l on the potential is evident by inspection of (2.23). The peak of the barrier assumes its lowest value for $l = 0$ while for particles with larger values of the parameter l the height increases and this means that they are less probable to overcome the barrier, reach the observer and contribute to the radiation of the black hole. This can be attributed to the spherical symmetry of the background that favors the also spherically-symmetric lowest mode with $l = 0$. This is the reason why this field mode is often referred to as the *dominant mode*. The effect of the other three parameters on the form of the barrier is less evident and so the best way to reveal their effect is to plot the potential.

For the dominant mode of the field with $\xi = 0.5$ and $\Lambda = 0.01$, in Fig. 2.3(a), we present the profile of the effective potential as the number of extra dimensions assumes the values $n = 0, 1, 2, 3, 4, 5, 8$. We notice that the height of the barrier increases with the increase of n and this will in turn lead to the decrease of the emission of brane-localized scalar particles as was also shown in [96]. Regarding the effect of the non-minimal coupling ξ in Fig. 2.3(b) we observe a similar behavior since the barrier also increases with ξ.

Next, in Fig. 2.4, we study the effect of the cosmological constant Λ on the barrier for the dominant field mode ($l = 0$) in the case of two extra dimensions ($n = 2$). The effect here is subtle and to this end we present a plot focusing on the peak of the barrier to better depict this. For minimally coupled fields, Fig. 2.4(b), the barrier is lowered with an increase in Λ and thus the particle emission

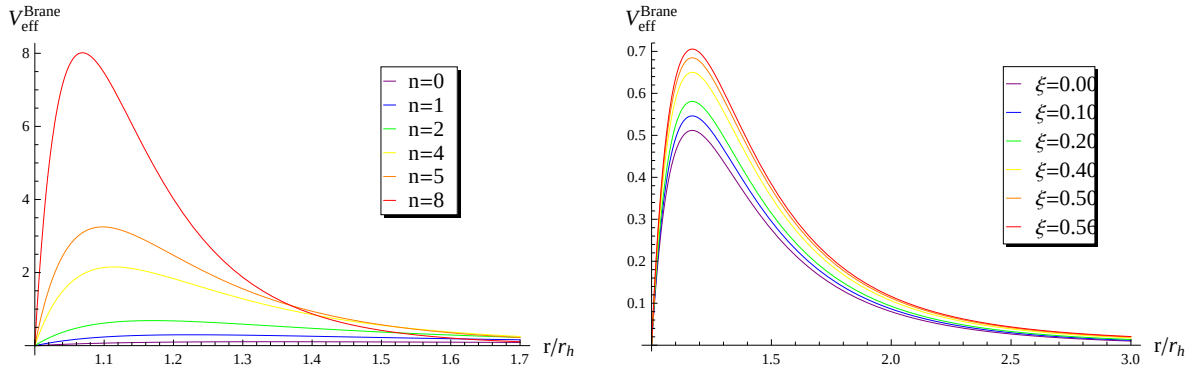

(a) (b)

FIGURE 2.3: Effective potential for brane scalar fields for: **(a)** $l = 0$, $\Lambda = 0.01\, r_h^{-2}$, $\xi = 0.5$ and variable $n = 0, 1, 2, 4, 5, 8$ (from bottom to the top), and **(b)** $l = 0$, $\Lambda = 0.01\, r_h^{-2}$, $n = 2$ and variable $\xi = 0, 0.1, 0.2, 0.4, 0.5, 0.56$ (again, from bottom to top).

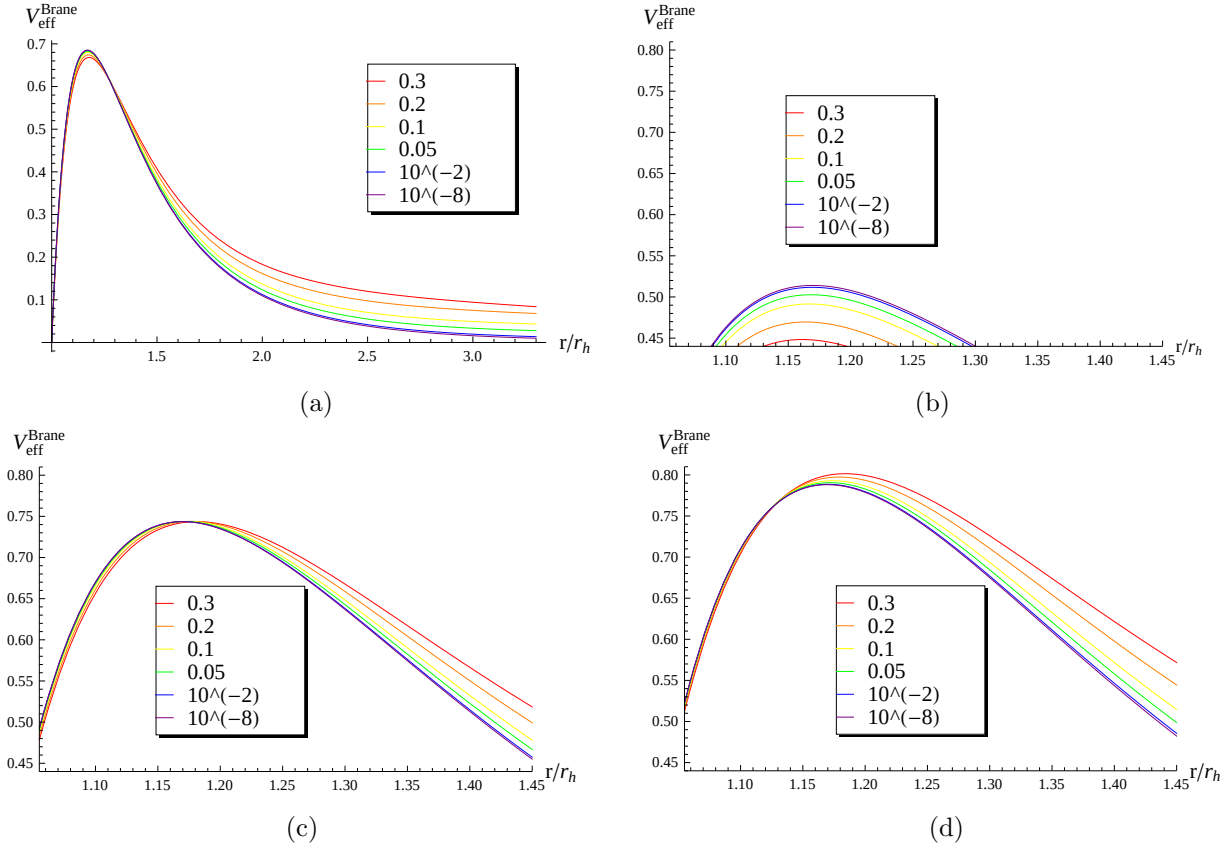

(a) (b)

(c) (d)

FIGURE 2.4: Effective potential for brane scalar fields for $l = 0$, $n = 2$, and variable $\Lambda = 10^{-8}, 10^{-2}, 0.05, 0.1, 0.2, 0.3$ (in units of r_h^{-2}), and **(a)** wide view for $\xi = 0.5$, and magnifications of the peak area for **(b)** $\xi = 0$, **(c)** $\xi = 0.67$ and **(d)** $\xi = 0.8$.

is enhanced. As ξ is "switched-on" the emission-enhancing effect of Λ weakens as Fig. 2.4(a) and 2.4(c) with $\xi = 0.5$ and $\xi = 0.67$ respectively show. Finally for even larger values of ξ as in Fig. 2.4(d) the role of the cosmological constant is reversed and now the effective potential height increases with Λ.

2.2.2 The analytic solution

In this section we proceed with the computation of the greybody factor. The idea is to solve the EOM for the scalar field (2.20) and then express the solution in terms of incoming and outgoing plane wave modes, far away from the black-hole horizon, i.e. close to the cosmological horizon. The greybody factor can then be obtained through the ratio of the amplitudes of the waves. Unfortunately to obtain an exact analytic solution to eq. (2.20) is an extremely difficult task[4] and to our knowledge this has been achieved only in special cases (see for example [97]) albeit under fine tuning of the parameters. We can solve this equation by employing numerical techniques and in fact we are going to do so in the next chapters in order to calculate the exact form of the greybody factors valid for any value of the parameters and throughout the energy range of the emitted particle. Still the analytic calculation is deemed necessary in order to better grasp the physics of the problem and obtain the boundary conditions we are going to use for the numerical solution.

To solve eq. (2.20) analytically we need to invoke an approximate scheme. A long-used approximate method employed in calculations of field scattering by black holes was first introduced by Unruh in 1976 [98] and later used by a series of other authors to solve the Klein-Gordon equation in various black-hole space-times, asymptotically-flat or not (see [99–102] for some indicative works).

In this scheme, assuming that the two horizons are located sufficiently apart, the EOM is solved independently in the vicinity of each of the two horizons. This can be achieved after suitable field and radial coordinate redefinitions that recast the radial differential equation to a familiar equation with known solutions. The two sets of solutions are then smoothly matched in the intermediate region between the horizons to ensure the existence of the complete solution. This is achieved by expanding the asymptotic solutions and identifying the same power terms of the two expansions. In using this method, the parameter space has to be constrained in one hand in order to obtain the solutions close to the horizons and on the other hand for the matching of the solutions. As a consequence the validity of the approximate analytic expressions is rather limited. This approximation procedure is termed *method of matched asymptotic expansions*.

Previous studies that solved (2.20) analytically using the above approximate method were limited in the case of the dominant mode ($l = 0$) for a minimally-coupled scalar field in $(4+n)$ dimensions or for a non-minimally coupled scalar field ($\xi \neq 0$) [93, 96] and arbitrary angular momentum number l but in 4 dimensions [99]. In our analysis we deal with the most general case by considering non-minimal coupling ξ in combination with arbitrary values for l and n.

In order to solve (2.20) close to the black-hole horizon the approach followed so far was to neglect the effect of the cosmological constant in that region in order to simplify the analysis. We have managed to solve the radial EOM in this regime without discarding Λ and thus to obtain more accurate analytic

[4] Even for the simplified form of the equation with $\xi = 0$ or $\Lambda = 0$.

results. To do so we found out that the appropriate redefinition for the radial coordinate is

$$r \to f(r) = \frac{h(r)}{1-\tilde{\Lambda} r^2}\,, \tag{2.25}$$

where, recall that we have previously defined $\tilde{\Lambda} \equiv 2\kappa_D^2 \Lambda/(n+2)(n+3)$. For the rest of our analysis we shall also set $\kappa_D^2 = 1$. The new radial function close to the black-hole horizon behaves as $f(r \approx r_h) \to 0$ because it is proportional to the metric function. On the other hand, the r.h.s.of eq. (2.25) can be expressed as

$$f(r) = 1 - \frac{\mu}{r^{n+1}} \frac{1}{1-\tilde{\Lambda} r^2} = 1 - \left(\frac{r_h}{r}\right)^{n+1} \frac{(1-\tilde{\Lambda} r_h^2)}{(1-\tilde{\Lambda} r^2)} \tag{2.26}$$

thus, far away from the black-hole horizon where we have $r \gg r_h$, $f(r) \approx 1$. An important relation that the derivative of $f(r)$ satisfies is

$$\frac{df}{dr} = \frac{1-f}{r} \frac{A(r)}{1-\tilde{\Lambda} r^2}\,, \tag{2.27}$$

where we have defined $A(r) \equiv (n+1) - (n+3)\tilde{\Lambda} r^2$.

We are now ready to rewrite the radial EOM (2.20) in terms of the new radial coordinate $f(r)$ close to the black-hole horizon as

$$f\,(1-f)\,\frac{d^2R(f)}{df^2} + (1 - B_h\, f)\,\frac{dR(f)}{df} + \left[\,\frac{(\omega r_h)^2}{A_h^2 f} - \frac{\lambda_h\,(1-\tilde{\Lambda} r_h^2)}{A_h^2 (1-f)}\,\right] R(f) = 0\,. \tag{2.28}$$

We used the (super-)subscript "h" to indicate quantities evaluated at $r = r_h$ and we have also defined for reasons of convenience the following factors:

$$B_h \equiv 1 + \frac{n}{A_h}\,(1-\tilde{\Lambda} r_h^2) + \frac{4\tilde{\Lambda} r_h^2}{A_h^2}\,, \qquad \lambda_h = l(l+1) + \xi R_4^{(h)} r_h^2\,. \tag{2.29}$$

Regarding the form of the term in the square brackets of eq. (2.28), see appendix B. Under the following field redefinition:

$$R(f) = f^{\alpha_1} (1-f)^{\beta_1} F(f)\,, \tag{2.30}$$

we can finally recast (2.28) in the familiar form of a hypergeometric differential equation

$$f\,(1-f)\,\frac{d^2F(f)}{df^2} + [c_1 - (1 + a_1 + b_1)\,f]\,\frac{dF(f)}{df} - a_1 b_1\, F(f) = 0\,, \tag{2.31}$$

if we further identify

$$a_1 = \alpha_1 + \beta_1 + B_h - 1 \qquad b_1 = \alpha_1 + \beta_1\,, \qquad c_1 = 1 + 2\alpha_1\,. \tag{2.32}$$

The general solution of (2.31) in combination with the redefinition (2.30) yields the radial part of the field in terms of the coordinate function $f(r)$

$$R_{BH}(f) = A_1 f^{\alpha_1}\,(1-f)^{\beta_1}\,F(a_1,b_1,c_1;f) \\ + A_2\,f^{-\alpha_1}\,(1-f)^{\beta_1}\,F(a_1-c_1+1,b_1-c_1+1,2-c_1;f)\,, \tag{2.33}$$

where the coefficients $A_{1,2}$ are arbitrary constants to be determined by the boundary conditions we will impose on the solution. In order to have the complete solution in the near black-hole horizon regime we have to also specify the values for the power coefficients α_1 and β_1 of eq. (2.30). To do this we need to solve a set of equations that result from the requirement that the term multiplying $F(f)$ in eq. (2.31) does not depend on f since only then we have the form of a hypergeometric differential equation. The set of these two equations is the following:

$$\alpha_1^2 + \frac{\omega^2 r_h^2}{A_h^2} = 0\,, \tag{2.34}$$

and

$$\beta_1^2 + \beta_1\,(B_h - 2) + \frac{\omega^2 r_h^2}{A_h^2} - \frac{\lambda_h\,(1-\tilde{\Lambda} r_h^2)}{A_h^2} = 0\,, \tag{2.35}$$

with the corresponding solutions being

$$\alpha_1^{(\pm)} = \pm\frac{i\omega r_h}{A_h}\,, \tag{2.36}$$

and

$$\beta_1^{(\pm)} = \frac{1}{2}\left[\,(2-B_h) \pm \sqrt{(B_h-2)^2 + \frac{4\lambda_h\,(1-\tilde{\Lambda} r_h^2)}{A_h^2}}\,\right]. \tag{2.37}$$

Close to the black-hole horizon the new radial coordinate $f(r)$, as we have already seen, goes to zero and so we can use one of the properties of the hypergeometric functions, namely $F(a,b,c;0) = 1$ to rewrite (2.33) as

$$R_{BH}(f) \simeq A_1\,f^{\alpha_1} + A_2\,f^{-\alpha_1}\,. \tag{2.38}$$

Since the coefficients A_1 and A_2 are arbitrary we are led to conclude that the two solutions for α_1 (2.36) are equivalent. The reason being we can always interchange A_1 with A_2 in eq. (2.38). Also, due to the vanishing of the effective potential on the horizons of SdS we can express the field as a general superposition of free plane waves in terms of the tortoise coordinate namely

$$R_{BH}(r_*) = \tilde{A}_1\,e^{-i\omega r_*} + \tilde{A}_2\,e^{i\omega r_*}\,. \tag{2.39}$$

Then we can see that (2.38) and (2.39) coincide if $f \propto e^{A_h r_*/r_h}$, so choosing the positive or negative sign of α_1 corresponds to interchanging the in-going with the out-going field modes on the black-hole

horizon. All we have to do then is to simply choose one of the two solutions. We shall choose

$$\alpha_1 = \frac{-i\omega r_h}{A_h}. \tag{2.40}$$

Turning now to the power coefficient β_1 the way to pick one out of the two solutions in (2.37) is to use the convergence criterion for the hypergeometric function,

$$\mathbf{Re}\,(c_1 - a_1 - b_1) > 0, \tag{2.41}$$

which is satisfied if $\beta_1 = \beta_1^{(-)}$. Thus we have completely specified the solution close to r_h. Finally a boundary condition we should impose on the solution close to r_h stems from the natural requirement that *exactly* on the location of the horizon there can only be in-going field modes. This amounts to setting $A_2 = 0$ in eq. (2.38). Of course a second boundary condition can be used in order to specify the remaining arbitrary coefficient A_1 but in fact this is not necessary in deriving the GF because it cancels out of the equations. So to simplify the expressions one can simply set $A_1 = 1$.

Next we focus on the cosmological horizon regime. There in order to bring the radial EOM to a familiar form we work along the lines drawn in previous studies [93, 99] and apply the following approximation to the metric function

$$h(r) = 1 - \left(\frac{r_h}{r}\right)^{(n+1)} - \tilde{\Lambda} r^2 \left[1 - \left(\frac{r_h}{r}\right)^{(n+3)}\right] \simeq 1 - \tilde{\Lambda} r^2\,, \tag{2.42}$$

where we have once again substituted the mass parameter μ via (2.24) evaluated at r_h. By using this asymptotic de Sitter approximation we neglect the effect of the black-hole mass close to r_c. This is indeed a well-justified approximation if the two horizons are located far away from each other and in fact it becomes more accurate the further away r_c is located from r_h. Another factor that acts in favor of the increased validity of the approximation of eq. (2.42) is the value of the parameter of the number of extra dimensions n. This is due to the fact that in the neighborhood of r_c we have $r \gg r_h$ and thus for larger values of n the term r_h/r gets heavily suppressed.

Under the radial coordinate transformation $r \to h(r) \simeq 1 - \tilde{\Lambda} r^2$, eq. (2.20) assumes the following form:

$$h\,(1-h)\,\frac{d^2R}{dh^2} + \left(1 - \frac{5}{2}\,h\right)\frac{dR}{dh} + \frac{1}{4}\left[\frac{(\omega r_c)^2}{h} - \frac{l(l+1)}{(1-h)} - \xi R_4^{(c)} r_c^2\right] R = 0\,, \tag{2.43}$$

where $R_4^{(c)}$ is the 4-dimensional Ricci scalar (2.10) evaluated at $r = r_c$. This time, to bring the EOM in the form of a hypergeometric equation we redefine the field as $R(h) = h^{\alpha_2}(1-h)^{\beta_2} X(h)$ and the hypergeometric indices thus have the following expressions:

$$a_2 = \alpha_2 + \beta_2 + \frac{3}{4} + \sqrt{\frac{9}{16} - \frac{\xi R_4^{(c)} r_c^2}{4}}\,, \tag{2.44}$$

$$b_2 = \alpha_2 + \beta_2 + \frac{3}{4} - \sqrt{\frac{9}{16} - \frac{\xi R_4^{(c)} r_c^2}{4}}\,, \qquad c_2 = 1 + 2\alpha_2\,. \tag{2.45}$$

As for the power coefficients α_2 and β_2, they are determined by the set of equations

$$\alpha_2^2 + \frac{\omega^2 r_c^2}{4} = 0\,, \tag{2.46}$$

and

$$\beta_2^2 + \frac{\beta_2}{2} - \frac{l(l+1)}{4} = 0\,, \tag{2.47}$$

with solutions

$$\alpha_2^{(\pm)} = \pm\frac{i\omega r_c}{2}\,, \qquad \beta_2^{(\pm)} = \frac{1}{4}\Big[-1 \pm (2l+1)\Big]\,. \tag{2.48}$$

Then, in the neighborhood of r_c the general solution for the radial part of the field is given in terms of hypergeometric functions we denote here with $X(h)$ as

$$\begin{aligned} R_C(h) =& B_1\, h^{\alpha_2}\,(1-h)^{\beta_2}\, X(a_2, b_2, c_2; h) \\ &+\; B_2\, h^{-\alpha_2}\,(1-h)^{\beta_2}\, X(a_2 - c_2 + 1, b_2 - c_2 + 1, 2 - c_2; h)\,, \end{aligned} \tag{2.49}$$

where once again the coefficients B_1 and B_2 are arbitrary. The vanishing of $h(r)$ as the cosmological horizon is approached results in the following expression

$$R_C(h) \simeq B_1\, h^{\alpha_2} + B_2\, h^{-\alpha_2} \tag{2.50}$$

where the properties of the hypergeometric functions have been employed once again. Also, close to r_c the vanishing of the effective potential allows for expressing the solution in the form of free plane waves in terms of the tortoise coordinate. For $h = e^{-2r_*/r_c}$ we can write (2.50) as

$$R_C(r_*) \simeq B_1\, e^{\mp i\omega r_*} + B_2\, e^{\pm i\omega r_*} \tag{2.51}$$

In regard now with the power coefficients $\alpha_2^{(\pm)}$, as was the case in the r_h neighborhood, choosing the positive or negative solution simply interchanges the in-going and out-going modes on r_c. On the cosmological horizon, we can have both sets of modes, in contrast to the black-hole horizon where we imposed the purely-in-going-modes condition . Then upon selecting $\alpha_2 = \alpha_2^{(+)}$, the coefficient B_1 (B_2) corresponds to the amplitude of the incoming (outgoing) wave and so the greybody factor is given by the ratio of the coefficients as

$$|A|^2 = 1 - \left|\frac{B_2}{B_1}\right|^2\,. \tag{2.52}$$

Finally since the solution (2.49) has to converge we are led to choose $\beta_2 = -(l+1)/2$ for the second power coefficient and thus fully determine the r_c asymptotic solution to the radial EOM .

The analysis so far boils down to two solutions of (2.20), each being valid close to one of the two

causal boundaries of the SdS spacetime. In order to guarantee the existence of a full solution for all r in $r_h < r < r_c$, we must make sure that these two asymptotic solutions (2.33) and (2.49) can be smoothly "sewn" together at some intermediate value of the radial coordinate r. For this to be possible the parameters of the system, unavoidably, have to be subject to further constraints. Before we can derive these constraints though we must first "stretch" the asymptotic solutions towards the intermediate regime. In the near-r_h solution we take the limit $r \gg r_h$ (or in terms of the new radial coordinate of (2.25) $f \to 1$) and in this way "strech" the solution to large values of r. We use the following hypergeometric function property [103]:

$$\begin{aligned} F(a,b,c;x) =& \frac{\Gamma(c)\,\Gamma(c-a-b)}{\Gamma(c-a)\,\Gamma(c-b)}\,F(a,b,a+b-c+1;1-x) \\ &+(1-f)^{c-a-b}\,\frac{\Gamma(c)\,\Gamma(a+b-c)}{\Gamma(a)\,\Gamma(b)}\,F(c-a,c-b,c-a-b+1;1-x), \end{aligned} \tag{2.53}$$

to change the argument in (2.33) (with $A_2 = 0$) from f to $1-f$. Then in terms of r the "stretched" solution is

$$\begin{aligned} R_{BH}(r) \simeq& A_1\,\frac{\Gamma(c_1)\,\Gamma(a_1+b_1-c_1)}{\Gamma(a_1)\,\Gamma(b_1)}\,\left(\frac{r}{r_h}\right)^{-(l+1)} \\ &+ A_1\,\frac{\Gamma(c_1)\,\Gamma(c_1-a_1-b_1)}{\Gamma(c_1-a_1)\,\Gamma(c_1-b_1)}\,\left(\frac{r}{r_h}\right)^{l} \\ \equiv& \Sigma_1\, r^{-(l+1)} + \Sigma_2\, r^{l}\,. \end{aligned} \tag{2.54}$$

In deriving the last equation we had to use the following approximations valid for small cosmological constant Λ and coupling constant ξ:

$$(1-f)^{\beta_1} \simeq \left(\frac{r_h}{r}\right)^{\beta_1(n+1)} \simeq \left(\frac{r}{r_h}\right)^{l} \tag{2.55}$$

and

$$(1-f)^{\beta_1+c_1-a_1-b_1} \simeq \left(\frac{r_h}{r}\right)^{(2-B_h-\beta_1)(n+1)} \simeq \left(\frac{r}{r_h}\right)^{-(l+1)}\,, \tag{2.56}$$

since in that limit it holds that: $A_h \simeq (n+1)$, $B_h \simeq (2n+1)/(n+1)$ and $\beta_1 \simeq -l/(n+1)$. Note that we only applied these approximations in the powers of the factors $(1-f)$ and not in the gamma function arguments. This way we expect to have an increased validity for our analytical results.

On the near-r_c solution the corresponding "stretching" aims to extending the solution (2.49) towards $r \ll r_c$. To do this, we shift the argument $h \to 1-h$ using the transformation relationship (2.53) of the hypergeometric function and under the following approximations:

$$(1-h)^{\beta_2} \simeq \left(\frac{r}{r_c}\right)^{2\beta_2} = \left(\frac{r}{r_c}\right)^{-(l+1)} \tag{2.57}$$

$$(1-h)^{\beta_2+c_2-a_2-b_2} \simeq \left(\frac{r}{r_c}\right)^{-(1+2\beta_2)} = \left(\frac{r}{r_c}\right)^{l}\,, \tag{2.58}$$

that once again require the smallness of Λ and ξ, we end up with the stretched solution in terms of r

$$\begin{aligned} R_C(r) &\simeq \left(\frac{r}{r_c}\right)^{-(l+1)} \left[B_1 \frac{\Gamma(c_2)\,\Gamma(c_2-a_2-b_2)}{\Gamma(c_2-a_2)\,\Gamma(c_2-b_2)} + B_2 \frac{\Gamma(2-c_2)\,\Gamma(c_2-a_2-b_2)}{\Gamma(1-a_2)\,\Gamma(1-b_2)}\right] \\ &+ \left(\frac{r}{r_c}\right)^{l} \left[B_1 \frac{\Gamma(c_2)\,\Gamma(a_2+b_2-c_2)}{\Gamma(a_2)\,\Gamma(b_2)} + B_2 \frac{\Gamma(2-c_2)\,\Gamma(a_2+b_2-c_2)}{\Gamma(a_2+1-c_2)\,\Gamma(b_2+1-c_2)}\right] \\ &\equiv (\Sigma_3 B_1 + \Sigma_4 B_2)\, r^{-(l+1)} + (\Sigma_5 B_1 + \Sigma_6 B_2)\, r^{l}\,. \end{aligned} \tag{2.59}$$

The matching of the two expansions (2.54) and (2.59) is now possible in the region between the two horizons because they exhibit the same powers of r namely l and $-(l+1)$. Equating the coefficients of r^l and $r^{-(l+1)}$ we find that the field amplitudes $B_{1,2}$ on the cosmological horizon are

$$B_1 = \frac{\Sigma_1\Sigma_6 - \Sigma_2\Sigma_4}{\Sigma_3\Sigma_6 - \Sigma_4\Sigma_5}\,, \qquad B_2 = \frac{\Sigma_2\Sigma_3 - \Sigma_1\Sigma_5}{\Sigma_3\Sigma_6 - \Sigma_4\Sigma_5}\,. \tag{2.60}$$

Having specified the amplitudes then it is straightforward to obtain the final expression for the greybody factor via eq. (2.52)

$$|A^2| = 1 - \left|\frac{\Sigma_2\Sigma_3 - \Sigma_1\Sigma_5}{\Sigma_1\Sigma_6 - \Sigma_2\Sigma_4}\right|^2 . \tag{2.61}$$

The analytic expression we derived for the greybody factor $|A^2|$ for the Hawking radiation process of scalar particles emitted on the brane by a higher-dimensional Schwarzschild-de Sitter black hole (2.61) has an extremely complicated dependence on the parameters of the system namely the two horizon radii r_h and r_c, the coupling constant ξ, the cosmological constant Λ, the number of extra spacelike dimensions n the angular momentum quantum number l as well as on the energy ω of the emitted particle. In order to obtain this solution with the method of the matching of the asymptotic expansions we had to impose some constraints on these parameters. More precisely, ξ and Λ need to be small.

In the next subsection we study the low-energy profile of the approximate analytic result for the greybody factor (2.61).

2.2.3 The low-energy limit of the greybody factor

We now focus in the infrared limit ($\omega \to 0$) of (2.61) for minimal and non-minimal coupling of the scalar field. In the minimally-coupled case and for the dominant mode of the field $l = 0$ we recover the findings of a previous work [96] that reported a non-vanishing low-energy asymptotic limit for the GFOnce the coupling ξ is "switched-on", the low-energy profile drastically changes. As we shall see, non-minimally coupled scalar fields result in the vanishing of the greybody factor expansion around $\omega \to 0$, a feature previously reported for the 4-dimensional case in [99].

The functional dependence of the greybody factor is encoded in the parameters of the hypergeometric functions a_i, b_i and c_i. For the low-energy expansion we found that it is convenient to separate the energy-dependent part of the (a_i, b_i, c_i). More precisely, for the parameters of the near-r_h solution we write

$$a_1 = \delta - \frac{i\omega r_h}{(n+1)}\,, \quad b_1 = \epsilon - \frac{i\omega r_h}{(n+1)}\,, \quad c_1 = 1 - \frac{2i\omega r_h}{(n+1)}\,, \tag{2.62}$$

with the ω-independent parts defined as

$$\delta = \frac{1 + 2n - \sqrt{1 + 4\lambda_h}}{2(n+1)}\,, \tag{2.63}$$

$$\epsilon = \frac{1 - \sqrt{1 + 4\lambda_h}}{2(n+1)}\,. \tag{2.64}$$

For the near-r_c solution's parameters we respectively have the following decomposition:

$$a_2 = \eta_+ + \frac{i\omega r_c}{2}\,, \quad b_2 = \eta_- + \frac{i\omega r_c}{2}\,, \quad c_2 = 1 + i\omega r_c\,, \tag{2.65}$$

where

$$\eta_\pm = \frac{1}{4}\left(1 - 2l \pm \sqrt{9 - 4\xi R_4^{(c)} r_c^2}\right)\,. \tag{2.66}$$

In order to manipulate analytically the low-energy expansion we had to impose a further simplification of the expressions by neglecting terms proportional to Λ in grounds of small cosmological constant. Note that all terms containing both Λ and ξ were kept into play.

Under these simplifications, if we further define $R_H \equiv r_h/(n+1)$ and $R_C \equiv r_c/2$ we can write the Σ_i coefficients that appear in (2.54) and (2.59) in the following compact forms:

$$\Sigma_1 = \frac{r_h^{l+1}\,\Gamma(1 - 2i\omega R_H)\,\Gamma(\delta + \epsilon - 1)}{\Gamma(\delta - i\omega R_H)\,\Gamma(\epsilon - i\omega R_H)}\,, \tag{2.67}$$

$$\Sigma_2 = \frac{r_h^{-l}\,\Gamma(1 - 2i\omega R_H)\,\Gamma(1 - \delta - \epsilon)}{\Gamma(1 - \delta - i\omega R_H)\,\Gamma(1 - \epsilon - i\omega R_H)}\,, \tag{2.68}$$

$$\Sigma_3 = \frac{r_c^{(l+1)}\,\Gamma(1 + 2i\omega R_C)\,\Gamma(1 - \eta_+ - \eta_-)}{\Gamma(1 - \eta_+ + i\omega R_C)\,\Gamma(1 - \eta_- + i\omega R_C)}\,, \tag{2.69}$$

$$\Sigma_4 = \frac{r_c^{(l+1)}\,\Gamma(1 - 2i\omega R_C)\,\Gamma(1 - \eta_+ - \eta_-)}{\Gamma(1 - \eta_+ - i\omega R_C)\,\Gamma(1 - \eta_- - i\omega R_C)} = \overline{\Sigma_3}\,, \tag{2.70}$$

$$\Sigma_5 = \frac{r_c^{-l}\,\Gamma(1 + 2i\omega R_C)\,\Gamma(\eta_+ + \eta_- - 1)}{\Gamma(\eta_+ + i\omega R_C)\,\Gamma(\eta_- + i\omega R_C)}\,, \tag{2.71}$$

$$\Sigma_6 = \frac{r_c^{-l}\,\Gamma(1 - 2i\omega R_C)\,\Gamma(\eta_+ + \eta_- - 1)}{\Gamma(\eta_+ - i\omega R_C)\,\Gamma(\eta_- - i\omega R_C)} = \overline{\Sigma_5}\,. \tag{2.72}$$

We also make use of the following general expressions for the expansion of gamma functions [103]:

$$\Gamma(\hat{a}+i\omega\hat{b}) = \Gamma(\hat{a})\left[1+i\omega\hat{b}\Psi^{(0)}(\hat{a})\right]+\mathcal{O}(\omega^2)\,, \tag{2.73}$$

$$\Gamma(i\omega\hat{b}) = \frac{1}{i\omega\hat{b}}-\gamma+\mathcal{O}(\omega)\,, \tag{2.74}$$

as well as the property $z\Gamma[-z]=-\Gamma[1-z]$. The coefficients $\hat{a}$ and $\hat{b}$ are energy-independent and $\Psi^{(0)}$ is the poly-gamma function. Finally, $\gamma\approx 0.577216$ is the Euler–Mascheroni constant.

We consider first the dominant mode ($l=0$) of a minimally coupled ($\xi=0$) scalar field. In this case the quantities of eq. (2.63),(2.64) and (2.66) assume the following simplified forms

$$\delta=\frac{n}{n+1}\,,\qquad \epsilon=0\,,\qquad \eta_{\pm}=\left(1,-\frac{1}{2}\right)\,. \tag{2.75}$$

Then the power-series expansion of Σ_i coefficients in the energy results in the following approximate expressions:

$$\Sigma_1\approx i\omega r_h^2+\mathcal{O}(\omega^2)\,, \tag{2.76}$$

$$\Sigma_2\approx 1+\frac{i\omega r_h}{n+1}\left[\gamma+\Psi^{(0)}\left(\frac{1}{n+1}\right)\right]+\mathcal{O}(\omega^2)\,, \tag{2.77}$$

$$\Sigma_3\approx i\omega r_c^2+\mathcal{O}(\omega^2)=\overline{\Sigma_4}\,, \tag{2.78}$$

$$\Sigma_5\approx 1+i\omega r_c\,(\log 2-1)+\mathcal{O}(\omega^2)=\overline{\Sigma_6}\,. \tag{2.79}$$

Finally, substitution of these into (2.61) reproduces the low-energy asymptotic limit, often refer to as the *geometric limit* for the greybody factor, reported in previous analyses [93, 96, 99, 104–106]

$$|A^2|=1-\left|\frac{i\omega\,(r_c^2-r_h^2)}{i\omega\,(r_c^2+r_h^2)}\right|^2+\mathcal{O}(\omega)=\frac{4r_h^2r_c^2}{(r_c^2+r_h^2)^2}+\mathcal{O}(\omega)\,. \tag{2.80}$$

The authors of [96] interpreted this characteristic non-vanishing value obtained for the dominant mode of the massless scalar emitted by the black hole in the presence of a cosmological constant as follows: The cosmological horizon creates effectively a finite-size universe for the particles to propagate and since in the infrared limit the field is completely delocalized this results in a finite probability for the particle to traverse the distance between the black-hole horizon and the detector. Of course when the spacetime is asymptotically flat, the observer is located at spatial infinity and thus the probability for the low-energy particle to reach this vanishes as does the geometric limit for $\Lambda\to 0\Rightarrow r_c\to\infty$. We point out that although (2.80) does not exhibit clearly the dependence on n the numerical values of r_h and r_c depend on it as they are solutions of $h(r)=0$ that is an n-dependent equation.

Notice now the dependence of the infrared limit (2.80) on the black-hole and cosmological horizon radii. By studying the infrared limit of the power spectrum that is closely connected with the geometric limit of the GFof a decaying black hole, it is in principle possible to deduce the value of the cosmological

horizon radius and in turn the value of the cosmological constant itself. As a matter of fact, an even more exciting possibility opens-up in the case we observe Hawking radiation by a mini black hole generated possibly in sufficiently energetic particle collisions in a future particle accelerator. By the features of the spectrum we can infer not only the value of Λ but the number of the extra spacelike dimensions (if any!) of our universe since as we have seen GF depend on n as well.

The GFinfrared limit, in the case of a non-minimally coupled scalar field ($\xi \neq 0$) exhibits an entirely different behavior with respect to ω. The coefficients Σ_i are proportional to the combination

$$\frac{\Gamma(1 \pm 2i\omega R)}{\Gamma(\hat{a} \pm i\omega R)\,\Gamma(\hat{b} \pm i\omega R)} = \frac{1 \mp i\omega R\left[2\gamma + \Psi^{(0)}(\hat{a}) + \Psi^{(0)}(\hat{b})\right]}{\Gamma(\hat{a})\,\Gamma(\hat{b})} + \mathcal{O}(\omega^2)\,, \tag{2.81}$$

where we denote by R either R_H or R_C and $\hat{a}$, $\hat{b}$ are again energy-independent. Using (2.81), we can write the combinations of the Σ_i quantities that appear in the expression of the greybody factor (2.61) as

$$\begin{aligned}
\Sigma_1\Sigma_5 &= K\,(1 - i\omega R_C B + i\omega R_H \Gamma)\,,\\
\Sigma_1\Sigma_6 &= K\,(1 + i\omega R_C B + i\omega R_H \Gamma)\,,\\
\Sigma_2\Sigma_3 &= E\,(1 + i\omega R_H Z - i\omega R_C \Theta)\,,\\
\Sigma_2\Sigma_4 &= E\,(1 + i\omega R_H Z + i\omega R_C \Theta)\,,
\end{aligned} \tag{2.82}$$

where we have defined the following quantities:

$$\begin{aligned}
K &\equiv \frac{r_h^{(l+1)} r_c^{-l}\,\Gamma(\delta + \epsilon - 1)\,\Gamma(\eta_+ + \eta_- - 1)}{\Gamma(\delta)\,\Gamma(\epsilon)\,\Gamma(\eta_+)\,\Gamma(\eta_-)}\,,\\
E &\equiv \frac{r_h^{-l} r_c^{l+1}\,\Gamma(1 - \delta - \epsilon)\,\Gamma(1 - \eta_+ - \eta_-)}{\Gamma(1 - \delta)\,\Gamma(1 - \epsilon)\,\Gamma(1 - \eta_+)\Gamma(1 - \eta_-)}\,,
\end{aligned} \tag{2.83}$$

and

$$\begin{aligned}
B &\equiv 2\gamma + \Psi^{(0)}(\eta_+) + \Psi^{(0)}(\eta_-)\,,\\
\Gamma &\equiv 2\gamma + \Psi^{(0)}(\delta) + \Psi^{(0)}(\epsilon)\,,\\
Z &\equiv 2\gamma + \Psi^{(0)}(1 - \delta) + \Psi^{(0)}(1 - \epsilon)\,,\\
\Theta &\equiv 2\gamma + \Psi^{(0)}(1 - \eta_+) + \Psi^{(0)}(1 - \eta_-)\,.
\end{aligned} \tag{2.84}$$

It is straightforward then to get the quantity that appears in the numerator of (2.61)

$$\Sigma_2\Sigma_3 - \Sigma_1\Sigma_5 = (E - K) + i\omega R_H\,(EZ - K\Gamma) + i\omega R_C\,(KB - E\Theta)\,, \tag{2.85}$$

while for the denominator we have

$$\Sigma_1\Sigma_6 - \Sigma_2\Sigma_4 = (K-E) + i\omega R_H\,(K\Gamma - EZ) + i\omega R_C\,(KB - E\Theta)\,. \tag{2.86}$$

From these two last equations one can easily conclude that

$$|\Sigma_2\Sigma_3 - \Sigma_1\Sigma_5|^2 \simeq |\Sigma_1\Sigma_6 - \Sigma_2\Sigma_4|^2 = (K-E)^2 + \mathcal{O}(\omega^2)\,, \tag{2.87}$$

and so if we now substitute eq. (2.87) into eq. (2.61), we see that the first non-vanishing term for non-minimally coupled scalar fields is of order $\mathcal{O}(\omega^2)$ and has the form

$$|A|^2 = \frac{8\pi^2(\omega r_h)^2\lambda_h^l\,[\Gamma(\theta_+)\,\Gamma(\theta_-)]^2\,\Gamma[\frac{1+u}{2(n+1)}]\,\Gamma[\frac{1+2n+u}{2(n+1)}]}{(1+2l)u\left(\cos[\frac{n\pi}{(n+1)}]+\cos[\frac{\pi u}{(n+1)}]\right)\Gamma[\frac{1}{2}+l]^2\,\Gamma[\frac{u}{(n+1)}]^2\,\Gamma[\frac{1+2n-u}{2(n+1)}]\,\Gamma[\frac{1-u}{2(n+1)}]}, \tag{2.88}$$

where $u \equiv \sqrt{(2l+1)^2 + 4\xi R_4^{(h)} r_h^2}$, and

$$\theta_\pm = \frac{1}{4}\left(3 + 2l \pm \sqrt{9 - 4\xi R_4^{(c)} r_c^2}\right)\,. \tag{2.89}$$

We can thus conclude that the low-energy asymptotic value for the greybody factor (2.80) disappears for a non-vanishing coupling constant ξ. Also, since ξ is directly related with the presence of an effective mass for the field (2.18), it becomes clear that only GFs for *massless* fields may exhibit this low-energy non-zero limit.

2.2.4 Plotting the analytic result

In this section we are going to study in depth the profile of the approximate analytic expression we obtained (2.61) for the greybody factor $|A|^2$ for massless scalar fields emitted on the brane by a higher-dimensional SdS black hole. The extremely complicated form of (2.61) makes imperative the analysis using plots. We thoroughly investigate the dependence of the greybody factor on the field parameters ξ and l as well as on the spacetime parameters n and Λ.

In the left panel of Fig. 2.5 we plot $|A|^2$ for minimally coupled fields ($\xi = 0$), with solid curves, as well as with an arbitrary non-minimal coupling ($\xi = 0.3$) depicted with dashed curves. The spacetime parameters are fixed to $n = 2$ extra dimensions and $\Lambda = 0.1$ (in units of r_h^{-2}). The first 5 modes ($l = 0 - 4$) of the field are depicted, with the $l = 0$ one clearly dominating in the low-energy region both for $\xi = 0$ and $\xi \neq 0$. Recall that the height of the effective potential (2.23) increased with the quantum number l of the field and this is clearly reflected here. For larger values of l the transmission probability for particles with up to intermediate values of energy to overcome the barrier is further decreasing.

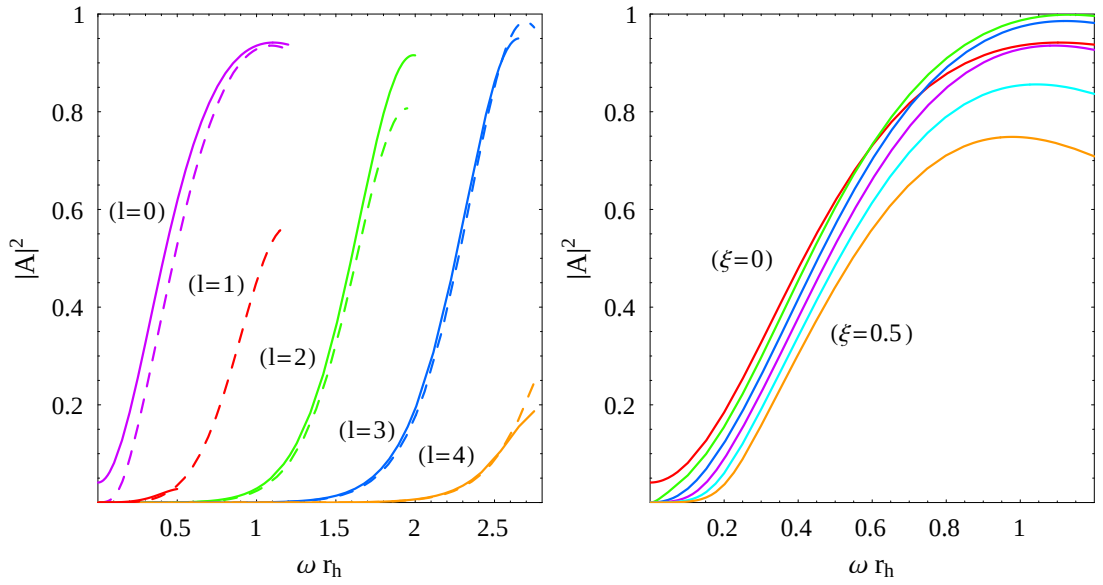

FIGURE 2.5: Greybody factors for brane scalar fields, for $n = 2$ and $\Lambda = 0.1$, and: **(a)** for variable $l = 0, 1, 2, 3, 4$ and $\xi = 0$ (solid lines) or $\xi = 0.3$ (dashed lines); **(b)** for $l = 0$ and variable $\xi = 0, 0.1, 0.2, 0.3, 0.4, 0.5$.

Notice also that the non-vanishing low-energy limit of $|A|^2$ (2.80) in the minimally coupled case is clearly seen for the $l = 0$ mode. As a consequence, the presence of non-minimal coupling affects the most the dominant mode ($l = 0$) in the low-energy limit. Independently of the value of l, we see that for arbitrary $\xi \neq 0$ we have further suppression of the greybody factor compared to the case with $\xi = 0$.

Although the authors of previous works, in order to achieve the matching of the two solutions had to impose constraints on the energy parameter ωr_h in our analysis of the previous section we have only required ξ and Λ to be small . We believe that this contributed in enabling us to extend the curves of the approximate analytic result way beyond the low-energy region, as it can be seen in Fig. 2.5 for example.

The usually imposed low-energy approximation, causes the approximate analytic results to deviate from the exact numerical ones when the energy is increased. Thus, we expect the analytic results we obtained without resorting to the low-ωr_h approximation to be more accurate and deviate from the exact ones only at large values of the energy. Inevitably, a deviation between the exact and approximate results is expected at large energies (even for $\xi \ll 1$ and $\Lambda \ll 1$) due to the presence of poles in the arguments of the gamma functions of the analytic expressions (as is usually the case for the analytic results for greybody factors). These poles, that occur at various values of ωr_h, sometimes result in "abrupt stops" exhibited in the plotting of the curves. One such example can be seen in the $l = 1$ curve (solid) for the minimally coupled field in Fig. 2.5(a) where a pole restricts the plotting of the curve in the low-energy region. The effect of ξ only slightly modifies the profile of the curves with

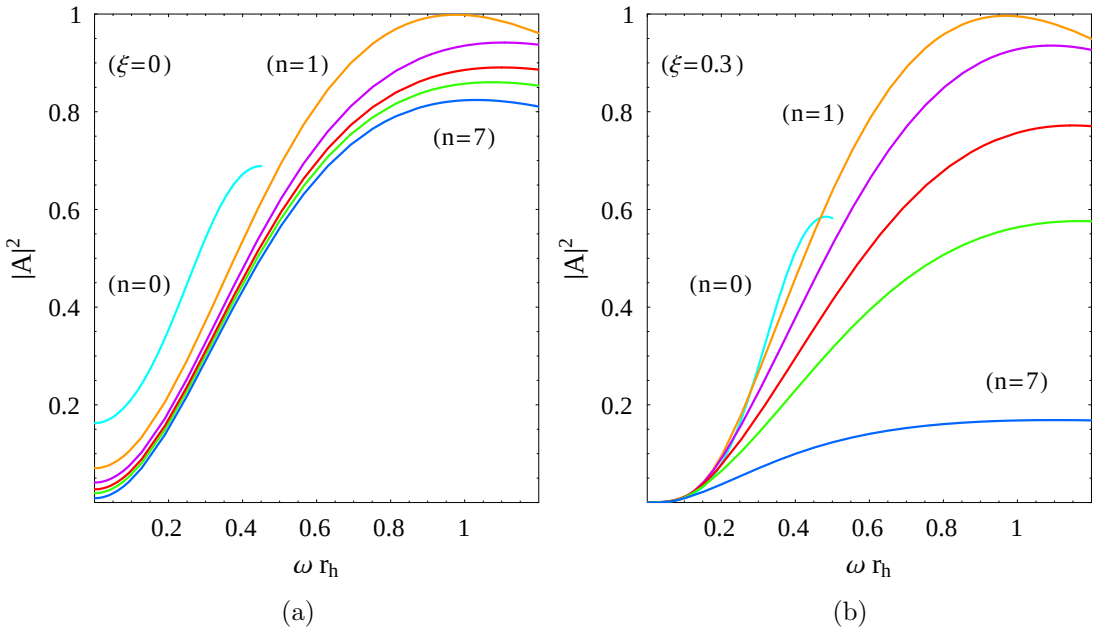

FIGURE 2.6: Greybody factors for brane scalar fields, for $l = 0$, $\Lambda = 0.1$, and variable $n = 0, 1, 2, 3, 4, 7$ and: **(a)** for $\xi = 0$, and **(b)** $\xi = 0.3$.

$l > 0$ but its presence in the arguments of the gamma functions is enough to shift the location of the pole and thus for the non-minimally coupled (dashed curve) $l = 1$ mode of the field, the greybody factor manages to extend up to intermediate values of ωr_h.

To see the effect of the non-minimal coupling parameter ξ on the greybody factor we plot $|A|^2$ for the following values of the parameters: $n = 2$, $\Lambda = 0.1$ and for the dominant mode $l = 0$ in Fig. 2.5(b). The depicted coupling parameter values range from $\xi = 0$ to $\xi = 0.5$ with an increment of $\delta\xi = 0.1$. Clearly, the larger the coupling ξ the more suppressed the greybody factors get and this feature comes as no surprise if one recalls the form of the equation of motion (2.18). The way ξ enters in the r.h.s. of the EOM resembles the mass term of a massive field. This feature is in agreement with the findings of previous works [107–111], that studied the emission of massive scalar particles by various black holes, suggesting that the transmission probability for scattering on the Regge-Wheeler type effective potential is reduced with the mass of the field.

Now, we turn to the effect of the spacetime parameters n and Λ on the greybody factor. We start by plotting the profile of $|A|^2$ with respect to the number of extra dimensions n in Fig. 2.6. Recall that the dependence of the brane-induced metric on n is inherited via the functional form of the metric function (2.7) and so the brane greybody factor depends on n as well. We fix $\Lambda = 0.1$ and work with the dominant field mode ($l = 0$) for the cases of minimal coupling on the left panel and non-minimal coupling with $\xi = 0.3$ on the right panel. For the minimally coupled case, the low-energy asymptotic geometric limit (2.80) that was derived in the previous section can be clearly seen and decreases as n becomes larger. The physical interpretation behind this result is that for fixed values of the black-hole mass and cosmological constant, the two horizons are located further apart with the number of extra

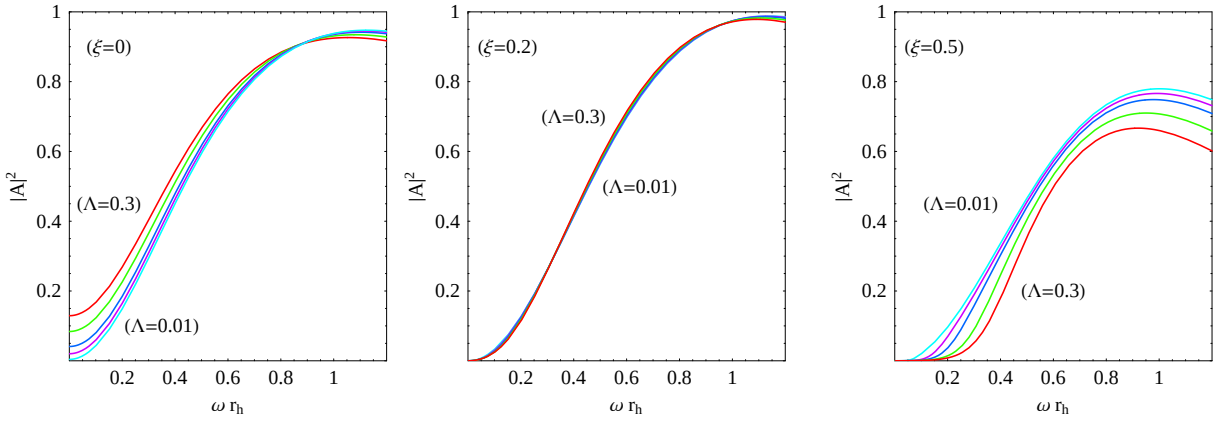

FIGURE 2.7: Greybody factors for brane scalar fields for $l = 0$, $n = 2$, and Λ =0.01, 0.05, 0.1, 0.2, 0.3, and **(a)** for $\xi = 0$, **(b)** $\xi = 0.2$, and **(c)** $\xi = 0.5$.

dimensions; in this way the space that the field has to traverse becomes larger, and as a consequence the greybody factor is decreased. Moving away from the low-energy region we see that for larger values of the ωr_h parameter the suppression of $|A|^2$ with n persists.

The most interesting interplay between the parameters of the system we considered is depicted in Fig 2.7 where the effect of the cosmological constant Λ on the transmission probabilities is studied. We consider once again the dominant mode of the field for $l = 0$, and fix the number of extra dimensions to $n = 2$ while assigning the following values for $\Lambda = 0.01, 0.05, 0.1, 0.2, 0.3$. Then we plot the transmission probability for 3 different values of the non-minimal coupling, namely $\xi = 0, 0.2, 0.5$ in subfigures (a),(b) and (c) respectively.

Starting with the minimal coupling in Fig. 2.7(a) we can clearly see that the low-energy geometric limit of the curves gets larger as Λ grows. The values of the geometric limit depicted in the leftmost panel can be used as a way to constrain the values of Λ. Obviously, as the cosmological constant value grows the approximations we made in the derivation of the analytic result for the greybody factor, that required the smallness of Λ, becomes less valid. See for example (2.42) and recall that the cosmological horizon is located closer to the black-hole horizon for larger values of Λ. Of course increasing the number of extra dimensions n as well restores partially the validity of the approximation because the term $\left(\frac{r_h}{r}\right)^{(n+3)}$ we neglect becomes smaller.

Then, for the dominant field mode in non-minimal coupling we can compare the exact geometric limit value of (2.80) with the low-energy value of our approximate analytic result (2.61) and see how much the two differ for various values of the cosmological constant. It turns out that for $\Lambda > 0.3$ we have a deviation of the order of 10% while for $\Lambda \leq 0.1$ the two values deviate by less than 5%. Finally, notice that the enhancement of the curves with the cosmological constant in Fig. 2.7(a) extends up to intermediate values of the energy parameter while for even larger values of ωr_h the approximate analytic curves are expected to deviate a lot from the exact ones.

Increasing now the value of the field coupling to $\xi = 0.2$ in Fig. 2.7(b) we see that the greybody factor is almost independent of Λ while for even larger values of ξ, for example $\xi = 0.5$ in Fig. 2.7(c), the effect of Λ on the GFis reversed and now the transmission probabilities get suppressed with the cosmological constant. To explain this peculiar behavior of cosmological constant parameter we need to recall where Λ comes into play. On one hand, as we have already discussed previously, the field exhibits an effective mass that is proportional to ξ and Λ (via the Ricci scalar). When the field coupling ξ is not negligible the effective mass increases with Λ and as a consequence the greybody factor gets suppressed. On the other hand, for $\xi \to 0$, the effect of the mass term is diluted and Λ contributes via the metric function $h(r)$ (2.7). As Λ grows, $h(r)$ becomes smaller since the cosmological term contributes with a negative sign. As a consequence, since the effective potential (2.23) is directly proportional to the metric function the barrier gets lowered thus leading to the observed greybody factor enhancement. Obviously for the values of the parameters of Fig. 2.7(b) these two effects cancel each other out.

2.3 Scalar field scattering in the bulk

2.3.1 The effective potential

Following closely along the lines drawn in the previous section with the computation of the greybody factor on the brane we now turn to the GFfor fields propagating in the bulk. We focus again on the emission of massless scalar particles that couple non-minimally to gravity. This time the scalar field will be free to probe the extra dimensions and in this sense it is a higher-dimensional field that depends also on the extra azimuthal coordinates θ_i. Its action will be

$$S_\Phi = -\frac{1}{2}\int d^{4+n}x\,\sqrt{-G}\left[\xi\Phi^2 R_D + \partial_M\Phi\,\partial^M\Phi\right]\,, \tag{2.90}$$

where the higher-dimensional metric tensor G_{MN} components follow immediately from the line element (2.5) and the Ricci scalar is given in (2.4).

Variation of the action (2.90) with respect to the field yields the scalar field equation of motion

$$\frac{1}{\sqrt{-G}}\,\partial_M\left(\sqrt{-G}\,G^{MN}\partial_N\Phi\right) = \xi R_D\,\Phi\,. \tag{2.91}$$

Again we wish to decouple the radial part of the EOM and in order to achieve this we can write the field in the following factorized form:

$$\Phi(t,r,\theta_i,\varphi) = e^{-i\omega t}R(r)\,\tilde{Y}(\theta_i,\varphi)\,, \tag{2.92}$$

where $\tilde{Y}(\theta_i, \varphi)$ are the hyperspherical harmonics [112] satisfying the following eigenvalue equation:

$$\frac{r^2}{\sqrt{-G}}\left[\sum_{j=1}^{n+2}\partial_{\theta_j}\left(\sqrt{-G}G^{\theta_j\theta_j}\partial_{\theta_j}\tilde{Y}(\theta_i,\varphi)\right)\right] = -l(l+n+1)\tilde{Y}(\theta_i,\varphi), \tag{2.93}$$

where the index j runs on all angles θ_i and ϕ. Note that for n extra azimuthal coordinates the determinant of the metric (2.5) is

$$\sqrt{-G} = r^{n+2}\prod_{i=1}^{n}\sin^i\theta_i\,. \tag{2.94}$$

Equation (2.93), as one can easily verify, reduces to the well-known 4-dimensional one upon setting $n = 0$.

Substituting the above field ansatz to eq. (2.91) and using the method of separation of variables we obtain the decoupled radial part of the EOM that describes the propagation of $\Phi(t, r, \theta_i, \varphi)$ in the bulk

$$\boxed{\frac{1}{r^{n+2}}\frac{d}{dr}\left[h(r)r^{n+2}\frac{dR(r)}{dr}\right] + \left[\frac{\omega^2}{h(r)} - \frac{l(l+n+1)}{r^2} - \xi R_D\right]R(r) = 0\,.} \tag{2.95}$$

Under the field redefinition $u(r) = r^{(n+2)/2}R(r)$ and radial coordinate transformation $dr_* = dr/h(r)$ we recast the EOM into a Schrödinger-like equation with the potential term being once again proportional to the metric function. More precisely the form of the potential is

$$V_{\text{eff}}^{\text{bulk}} = h(r)\left[\frac{l(l+n+1)}{r^2} + \xi R_D + \frac{(n+2)}{2r}\frac{dh(r)}{dr} + \frac{n(n+2)h(r)}{4r^2}\right], \tag{2.96}$$

and if we further use (2.7) we can write

$$V_{\text{eff}}^{\text{bulk}} = h(r)\left\{\frac{(2l+n+1)^2-1}{4r^2} + \kappa_D^2\Lambda\,(n+4)\left[\frac{2\xi}{(n+2)} - \frac{1}{2(n+3)}\right] + \frac{(n+2)^2\mu}{4r^{n+3}}\right\}. \tag{2.97}$$

By inspection of (2.97) there are two features of the barrier that one can readily identify. Firstly, we see that, for fields propagating in the bulk, we have the nice property that the potential vanishes at the location of the horizons due to its proportionality to the metric function $h(r)$. This fact, as we have seen in the previous section, is crucial in order to express the field as a superposition of free plane waves and be able to compute the greybody factor as the end product of a scattering problem. The second feature is the increase of the height of the barrier with the angular momentum number l. Still, the potential has a highly non-trivial dependence on the parameters n and ξ, so in order to be able to see their effect on the potential the plots of Fig. 2.8 are necessary.

Similarly to the brane effective potential (2.23) we see that an increase in the number of extra dimensions n as well as an increase in the strength of the coupling of the field ξ results in the raising of the barrier and consequently to a suppression in the total number of particles that contribute to the radiation of the black hole in the bulk. Notice that the effect of ξ is milder for emission in the

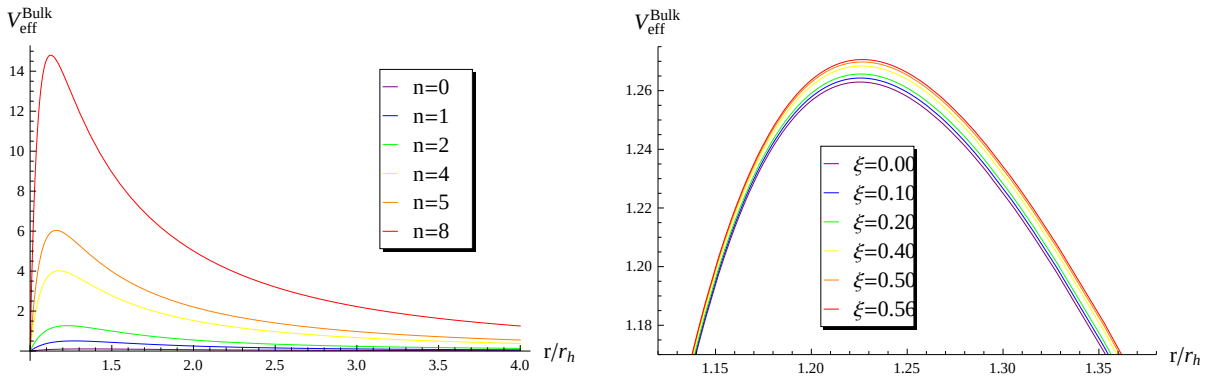

(a) (b)

FIGURE 2.8: Effective potential for bulk scalar fields for: **(a)** $l = 0$, $\Lambda = 0.01$, $\xi = 0.5$ and variable $n = 0, 1, 2, 4, 5, 8$ (from bottom to the top), and **(b)** $l = 0$, $\Lambda = 0.01$, $n = 2$ and variable $\xi = 0, 0.1, 0.2, 0.4, 0.5, 0.56$ (again, from bottom to top).

$\xi \rightarrow$	0.0	0.1	0.2	0.4	0.5	0.56
$n = 1$	1.7048	1.70521	1.70561	1.70642	1.70682	1.70706
2	2.46808	2.31422	2.17869	1.95092	1.85431	1.8009
4	4.09964	3.30647	2.7708	2.09329	1.86547	1.75118
5	4.95021	3.71294	2.97078	2.1228	1.85784	1.72845
8	7.58826	4.6779	3.38132	2.17565	1.84655	1.69292

TABLE 2.2: Bulk-over-brane ratios of the peak values of the effective barriers for $l = 0$ and $\Lambda = 0.01 r_h^{-2}$

bulk in Fig. 2.9(b) compared to brane emission in Fig. 2.3(b) and this is the reason we present the magnification around the area of the peak. The height of the barrier is also located at larger values for the bulk channel compared to the brane one and this indicates a dominance of the latter as the favored channel for emission (at least in this parameters range). For convenience we display in Table 2.2 the bulk-over-brane ratio of the peak values for the effective potentials. We will return to the question of which is the favored channel for scalar particle emission by the higher-dimensional SdS black hole in a following chapter where we compute the bulk-over-brane total and relative emissivities using exact numerical results.

Finally, regarding the effect of the cosmological constant on the effective potential we see in Fig. 2.9 that for small values of the coupling ξ we have a suppression of the barrier with Λ while for larger values of ξ the role of Λ is reversed and leads to an increase of the effective potential. The dual role exhibited by Λ will be studied and analyzed in great detail in a following chapter.

2.3.2 The analytic solution

The form of the master equation (2.95) dictating the scalar field propagation in the bulk is even more complicated than the corresponding brane one (2.20). So, in order to calculate the greybody factor

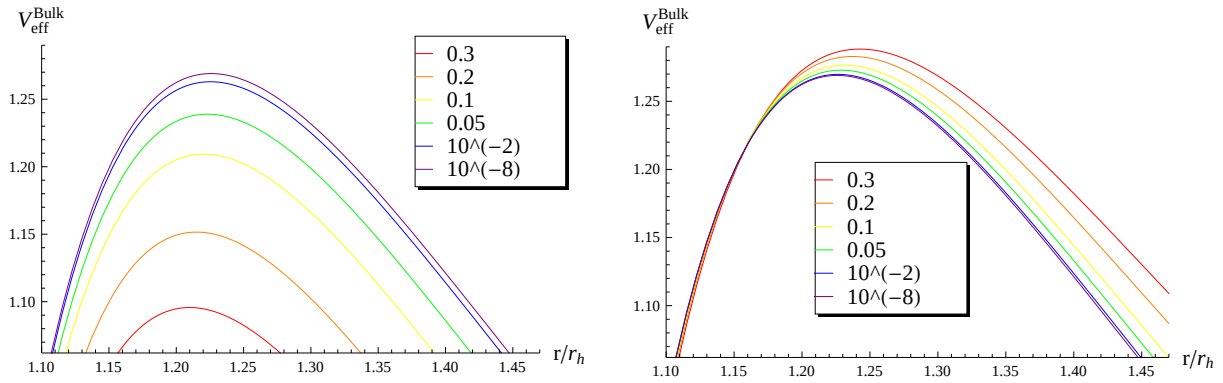

(a) (b)

FIGURE 2.9: Effective potential for bulk scalar fields for $l = 0$, $n = 2$, and variable $\Lambda = 10^{-8}, 10^{-2}, 0.05, 0.1, 0.2, 0.3$: magnifications of the peak area for **(a)** $\xi = 0$, and **(b)** $\xi = 0.5$.

for the bulk channel we employ the same approximate technique with the matching of the expanded asymptotic solutions used in the previous section. We are able to keep the cosmological constant effect on the proximity of the black-hole horizon r_h into play by using the radial coordinate transformation of (2.25), and thus we rewrite eq. (2.95) as

$$f\,(1-f)\,\frac{d^2R}{df^2} + (1 - B_h\,f)\,\frac{dR}{df} + \left[\,\frac{(\omega r_h)^2}{A_h^2} + \frac{(\omega r_h)^2}{A_h^2 f} - \frac{\lambda_h\,(1-\tilde{\Lambda} r_h^2)}{A_h^2(1-f)}\,\right] R = 0 \tag{2.98}$$

where $A_h = (n+1) - (n+3)\,\tilde{\Lambda} r_h^2$, and

$$B_h \equiv 1 + \frac{4\tilde{\Lambda} r_h^2}{A_h^2}\,, \qquad \lambda_h = l(l+n+1) + \xi R_D r_h^2\,. \tag{2.99}$$

To obtain a hypergeometric equation we redefine the field according to $R(f) = f^{\alpha_1}(1-f)^{\beta_1}F(f)$. Then the parameters of the hypergeometric equation are

$$a_1 = \alpha_1 + \beta_1 + \frac{1}{2}\left(B_h - 1 + \sqrt{(B_h-1)^2 - 4\omega^2 r_h^2/A_h^2}\right), \tag{2.100}$$

$$b_1 = \alpha_1 + \beta_1 + \frac{1}{2}\left(B_h - 1 - \sqrt{(B_h-1)^2 - 4\omega^2 r_h^2/A_h^2}\right), \qquad c_1 = 1 + 2\alpha_1\,, \tag{2.101}$$

while the power coefficients α_1 and β_1 have the same functional form with their brane counterparts namely

$$\alpha_1 = -\frac{i\omega r_h}{A_h}\,, \tag{2.102}$$

and

$$\beta_1 = \frac{1}{2}\left[\,(2 - B_h) - \sqrt{(B_h-2)^2 + \frac{4\lambda_h\,(1-\tilde{\Lambda} r_h^2)}{A_h^2}}\,\right]. \tag{2.103}$$

Of course, the quantities B_h and λ_h that appear in (2.102) and (2.103) differ from the corresponding brane ones and are given by eq. (2.99) instead.

The general solution of (2.98) in the neighborhood of the black-hole horizon r_h after imposing the condition that only in-going modes of the field exist on r_h is

$$R_{BH}(f) = A_1 f^{\alpha_1} (1-f)^{\beta_1} F(a_1, b_1, c_1; f). \tag{2.104}$$

Turning now to the cosmological horizon r_c, the form of (2.95) after we change the radial coordinate according to $r \to h(r) \simeq 1 - \tilde{\Lambda} r^2$ is

$$\begin{aligned} h\,(1-h)\,\frac{d^2R}{dh^2} + \left[1 - \frac{(n+5)}{2}\,h\right]\frac{dR}{dh} \\ + \frac{1}{4}\left[\frac{(\omega r_c)^2}{h} - \frac{l(l+n+1)}{(1-h)} - \xi(n+4)(n+3)\right] R = 0\,. \end{aligned} \tag{2.105}$$

Finally redefining the field as $R(h) = h^{\alpha_2}(1-h)^{\beta_2} X(h)$ we recast (2.105) into a hypergeometric equation with the following indices:

$$a_2 = \alpha_2 + \beta_2 + \frac{n+3}{4} + \frac{1}{4}\sqrt{(n+3)^2 - 4\xi(n+4)(n+3)}\,, \tag{2.106}$$

$$b_2 = \alpha_2 + \beta_2 + \frac{n+3}{4} - \frac{1}{4}\sqrt{(n+3)^2 - 4\xi(n+4)(n+3)}\,, \qquad c_2 = 1 + 2\alpha_2\,. \tag{2.107}$$

The power coefficients α_2 and β_2 are now

$$\alpha_2 = \frac{i\omega r_c}{2}\,, \qquad \beta_2 = -\frac{(l+n+1)}{2}\,, \tag{2.108}$$

and the general solution of (2.95) near the cosmological horizon has the same functional form as eq. (2.49).

After this point the analysis in the bulk follows closely the one on the brane. The two asymptotic solutions of the radial EOM in the neighborhood of the horizons are obtained in terms of hypergeometric functions. Then they are stretched towards the intermediate radial regime by employing the small- and large-value expansions of the hypergeometric functions. Finally a matching is achieved under the assumption of small ξ and Λ since the solutions can be once again written in terms of the original radial coordinate r and the terms of equal powers of r be identified. This identification yields the expressions for the coefficients B_1 and B_2 and thus to the analytic expression for the greybody factor in the bulk that is of the same form as that of eq. (2.61), namely

$$|A^2| = 1 - \left|\frac{\Sigma_2\Sigma_3 - \Sigma_1\Sigma_5}{\Sigma_1\Sigma_6 - \Sigma_2\Sigma_4}\right|^2\,, \tag{2.109}$$

where the quantities Σ_i in the bulk, differ from their corresponding brane ones only by the form of the exponents of r_h and r_c. More precisely, in the coefficients Σ_1,Σ_3 and Σ_4 for the brane channel we

have $r_i^{(l+1)}$ while for the bulk channel we have $r_i^{(l+n+1)}$.

2.3.3 The low-energy limit of the greybody factor

We will now study the low-energy limit of the greybody factor (2.61) for the bulk channel. The low-ω asymptotics for both the minimally ($\xi = 0$) and the non-minimally ($\xi \neq 0$) coupled scalar field will be considered. Similarly to the brane case, the sets of the parameters (a_i, b_i, c_i) for the solutions of the hypergeometric equations close to the black-hole horizon r_h and the cosmological horizon r_c will be in the same form as in (2.62) and (2.65). This time, the energy-independent parts $(\delta, \epsilon, \eta_\pm)$ will be

$$\delta = \frac{1}{2}\left[B_h - \sqrt{(B_h-2)^2 + \frac{4\lambda_h}{A_h^2}}\right], \tag{2.110}$$

$$\epsilon = \frac{1}{2}\left[2 - B_h - \sqrt{(B_h-2)^2 + \frac{4\lambda_h}{A_h^2}}\right], \tag{2.111}$$

$$\eta_\pm = \frac{1}{4}\left[1 - 2l - n \pm \sqrt{(n+3)^2 - 4\xi R_D r_c^2}\right]. \tag{2.112}$$

In order to simplify the analysis we have taken the limit of small Λ in the above except in the expression for B_h (2.99). For $\Lambda \to 0, B_h \to 1$ and so we take this limit after we take the low-energy limit of the gamma functions in order to keep the two expansions distinct.

For the dominant mode of the field ($l = 0$) and in the minimal coupling case ($\xi = 0$) the quantities of (2.110)-(2.112) assume the simplified expressions

$$\delta = B_h - 1\,, \qquad \epsilon = 0\,, \qquad \eta_\pm = \left[1, -\frac{(n+1)}{2}\right], \tag{2.113}$$

and the low-energy expansion of the Σ_i quantities yields

$$\Sigma_1 \approx \frac{i\omega r_h^{n+2}}{(n+1)} + \mathcal{O}(\omega^2)\,, \tag{2.114}$$

$$\Sigma_2 \approx \Sigma_5 \approx \Sigma_6 \approx 1 + \mathcal{O}(\omega)\,, \tag{2.115}$$

and

$$\Sigma_3 \approx \frac{i\omega r_c^{n+2}}{(n+1)} + \mathcal{O}(\omega^2) \approx -\Sigma_4\,. \tag{2.116}$$

Upon substituting these expressions in (2.61) we find that the infrared limit of the greybody factor for the bulk channel and for $(\xi, l) = (0, 0)$ is

$$|A^2| = 1 - \left|\frac{i\omega\,(r_c^{n+2} - r_h^{n+2})}{i\omega\,(r_c^{n+2} + r_h^{n+2})}\right|^2 + \mathcal{O}(\omega) = \frac{4(r_h r_c)^{(n+2)}}{(r_c^{n+2} + r_h^{n+2})^2} + \mathcal{O}(\omega)\,. \tag{2.117}$$

The same low-energy geometric limit of the bulk greybody factor has been reported in previous works [93, 96]. Note that due to the appearance of n in the powers of r_h and r_c of the last equation, the bulk geometric limit is suppressed compared to the corresponding brane one. So, the probability for very low-energy particles to overcome the effective potential in the bulk is smaller compared to the brane case.

Finally, since the functional form of the Σ_i quantities in the bulk is the same with the ones in the brane analysis and the arguments there in favor of the vanishing of the greybody factor as $\omega \to 0$ did not include the expressions of $(\delta, \epsilon, \eta_\pm)$ we conclude that, in the bulk also, non-minimally coupled scalar fields result in greybody factors that exhibit vanishing asymptotic values in the low-energy expansion. The first non-vanishing term has the following form:

$$|A|^2 = \frac{16\pi^8 (r_h/r_c)^{l+n/2} \, (\omega r_h)^2 \sec^4(w\pi/2) \, [\Gamma(\theta_+)\,\Gamma(\theta_-)]^{-2}}{\sigma\sqrt{\sigma^2 + 4\xi R_D r_h^2}\left(\cos[\frac{\pi\sigma}{2}] + \cos[\frac{\pi\sqrt{(n+3)^2 - 4\xi R_D r_c^2}}{2}]\right)^2 \Gamma[\frac{\sigma}{2}]^2 \Gamma[w]^2 \, \Gamma[\frac{1-w}{2}]^4}, \tag{2.118}$$

where we have defined the following quantities in order to simplify the expression:

$$\begin{aligned} \sigma &\equiv 2l + n + 1, \\ w &\equiv \frac{\sqrt{(2l+n+1)^2 + 4\xi R_D r_h^2}}{n+1}, \\ \theta_\pm &\equiv \frac{1}{4}\left(1 - 2l - n \pm \sqrt{(n+3)^2 - 4\xi R_D r_c^2}\right) . \end{aligned} \tag{2.119}$$

For $n = 0$ we have confirmed that (2.118) reduces to the previously reported 4-dimensional result of Crispino et al. [99].

2.3.4 Plotting the analytic result

The profile of the approximate analytic expression we obtained for the greybody factor of the bulk channel upon variation of the particle and the spacetime parameters will be now investigated. We start with the particle parameters in Fig. 2.10 where we have fixed $n = 2$ and $\Lambda = 0.1$. In the left panel the dependence of $|A|^2$ on the angular momentum number of the field is depicted with the solid curves corresponding to minimal coupling and the dashed ones to $\xi = 0.3$.

For the dominant field mode the low-energy geometric limit is clearly seen for $\xi = 0$. We observe that the larger the value of l, the more suppressed the transmission probability gets. The effect of the non-minimal coupling further suppresses the curves with the most prominent effect being on the $l = 0$ curve due to the presence of the geometric limit in the low energy regime. As l grows, the greybody factors appear to get less sensitive to the presence of ξ since solid and dashed curves are almost identified. Moving to Fig. 2.10(b) the effect of ξ on the dominant mode is presented. For

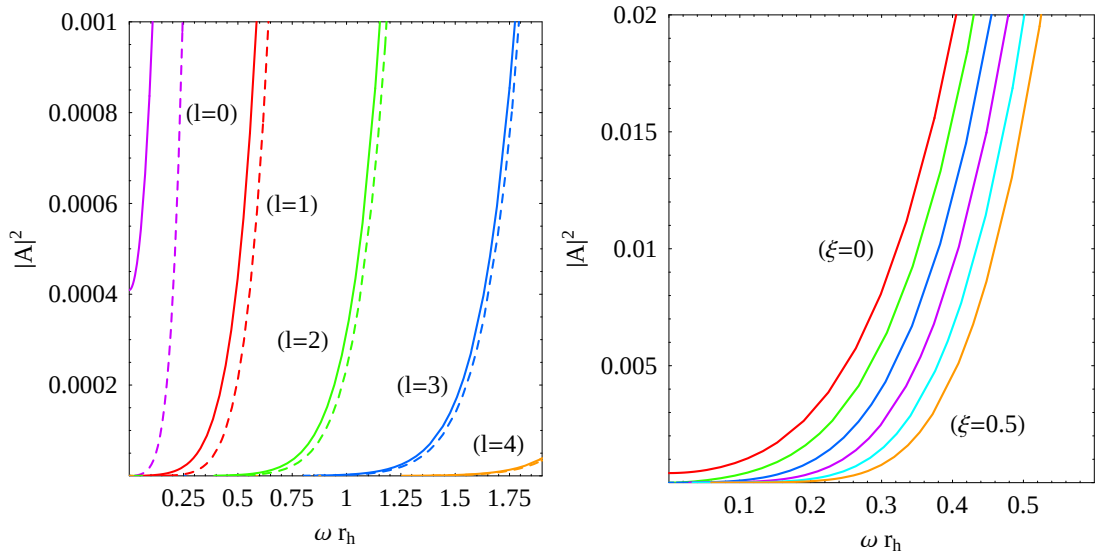

(a) (b)

FIGURE 2.10: Greybody factors for bulk scalar fields, for $n = 2$ and $\Lambda = 0.1$, and: **(a)** for variable $l = 0, 1, 2, 3$ and $\xi = 0$ (solid lines) or $\xi = 0.3$ (dashed lines); **(b)** for $l = 0$ and variable $\xi = 0, 0.1, 0.2, 0.3, 0.4, 0.5$.

this particular value of $\Lambda = 0.1$ an increase in the non-minimal coupling suppresses $|A|^2$. Again for $\xi = 0$ the geometric limit can be seen. Notice also that the geometric limits in the bulk channel (2.117) assume much smaller values compared to their brane counterparts (2.80) and this is a direct by-product of the dependence the former exhibit on n.

In Fig. 2.11, for $\Lambda = 0.1$ and for the dominant mode, the effect of the number of extra dimensions on the greybody factor is presented. Again we have used solid curves to indicate the $\xi = 0$ case and

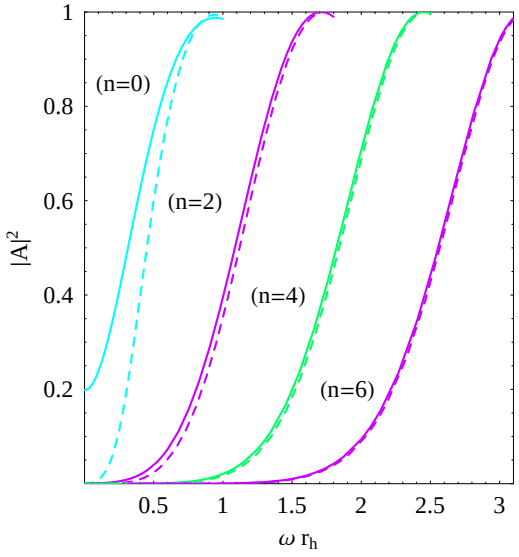

FIGURE 2.11: Greybody factors for bulk scalar fields, for $l = 0$, $\Lambda = 0.1$ and variable $n = 0, 2, 4, 6$ and for $\xi = 0$ (solid lines) and $\xi = 0.3$ (dashed lines).

dashed for the arbitrary choice of $\xi = 0.3$. We were able to plot only curves that correspond to even values of n because of the poles of the gamma functions in our analytic expression. We use the same arbitrary values for the parameters to allow for easier comparison between different plots. A general suppression of $|A|^2$ with n is observed in the bulk channel which is further enhanced in all cases when $\xi \neq 0$ and even more so for the lowest values of n.

Finally in Fig. 2.12 we show the effect of the cosmological constant Λ on the transmission probability for minimally coupled fields on the left panel and for $\xi = 0.5$ on the right. The similar "dual-role" behavior of Λ as the one observed in the brane channel arises. The cosmological constant acts in favor of the enhancement of the greybody factor for low ξ and against it above some critical value for the coupling ξ. Already at $\xi = 0.5$ the effect is reversed as one can see in Fig. 2.12(b).

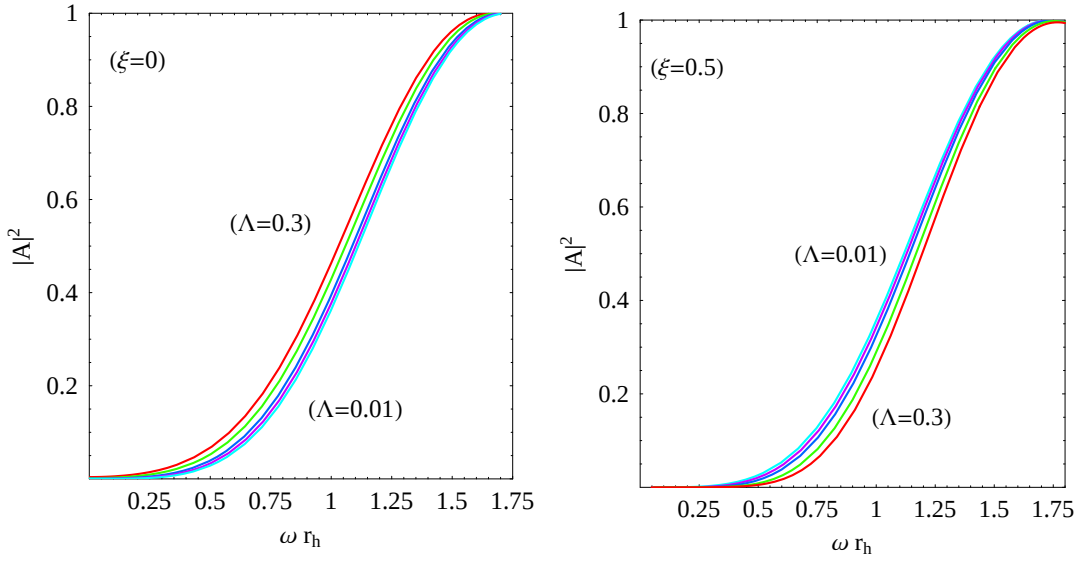

(a) (b)

FIGURE 2.12: Greybody factors for bulk scalar fields for $l = 0$, $n = 2$, and $\Lambda = 0.01$, 0.05, 0.1, 0.2, 0.3, and **(a)** for $\xi = 0$, and **(b)** $\xi = 0.5$.

2.4 Conclusions

In this chapter, we considered scalar fields that propagate in the spacetime of a higher-dimensional Schwarzschild-de Sitter (SdS) black hole. We focused on fields that are massless and couple non-minimally to gravity via an interaction term in the action with the Ricci scalar. In this context, we derived analytic expressions for the greybody factors, both on the brane and in the bulk, that are valid for arbitrary values of the number of extra dimensions (n) and field angular-momentum number (l). In order to solve the Klein-Gordon equation we followed a well-known approximate technique that amounts to matching the asymptotic solutions in the vicinity of the two horizons of the SdS spacetime. Contrary to previous works we were able to keep the effect of the cosmological

constant (Λ) into play in both asymptotic solutions thus increasing the accuracy of our results. As a consequence of applying this method, the analytic results we have obtained are valid in the low- and intermediate-energy regime but for small values of the field coupling (ξ) and cosmological constant. We then thoroughly studied the dependence of the greybody factors on the spacetime parameters n, Λ and field parameters l, ξ. We found that the characteristic non-zero infrared limit of the GF for the dominant field mode ($l = 0$) vanishes in the presence of a non-minimal field coupling both on the brane and in the bulk. Our analysis has also revealed a particularly interesting "dual-role" behavior of Λ that can act either in favor or against the enhancement of the GF depending on the value of ξ.

Chapter 3

The Hawking radiation spectrum of a $(4+n)$-dimensional Schwarzschild-de Sitter black hole

In the previous chapter, the analytic expressions for the greybody factors (g.f.) for a massless scalar field, non-minimally coupled to gravity that propagates in a $(4+n)$-dimensional Schwarzschild-de Sitter (SdS) spacetime were derived. The SdS line element in the bulk is

$$ds^2 = G_{MN}dx^M dx^N = -h(r)\,dt^2 + \frac{dr^2}{h(r)} + r^2 d\Omega^2_{2+n}\,, \tag{3.1}$$

where the metric function is given by

$$h(r) = 1 - \frac{\mu}{r^{n+1}} - \frac{2\kappa_D^2\,\Lambda r^2}{(n+3)(n+2)}\,, \tag{3.2}$$

with μ being the black-hole mass parameter, n the number of extra space-like dimensions and Λ the bulk cosmological constant. For fields confined on the brane, the geometry is described instead by the induced metric

$$ds^2 = g_{\mu\nu}dx^\mu dx^\nu = -h(r)\,dt^2 + \frac{dr^2}{h(r)} + r^2\left(d\theta^2 + \sin^2\theta\, d\varphi^2\right). \tag{3.3}$$

Using a factorized ansatz for the field [eqs. (2.19) and (2.92) for the brane and bulk respectively], we were able to decouple the radial part of the Klein-Gordon equation and obtain the following equations of motion (EOM):

- **On the brane:**

$$\frac{1}{r^2}\frac{d}{dr}\left[h(r)r^2\frac{dR(r)}{dr}\right] + \left[\frac{\omega^2}{h(r)} - \frac{l(l+1)}{r^2} - \xi R_4\right]R(r) = 0\,, \tag{3.4}$$

- **In the bulk:**

$$\frac{1}{r^{n+2}}\frac{d}{dr}\left[h(r)r^{n+2}\frac{dR(r)}{dr}\right] + \left[\frac{\omega^2}{h(r)} - \frac{l(l+n+1)}{r^2} - \xi R_D\right]R(r) = 0\,, \tag{3.5}$$

where $R(r)$ is the radial part of the field, ω is the energy of the emitted particle, l is the angular momentum quantum number of the field, ξ is the non-minimal coupling parameter of the field to

gravity and finally R_4 (2.10) and R_D (2.4) are the Ricci scalars for the brane and bulk geometries respectively.

Since, to our knowledge, exact analytic solutions to eqs. (3.4) and (3.5) cannot be obtained for arbitrary values of the parameters, we had to resort to an approximate method in order to calculate the g.f. The approximations imposed restrict the validity of our analytic results to small values of the cosmological constant Λ, small coupling parameter ξ and in the low-energy regime.

In this chapter we develop a numerical technique in order to extend the previous study and obtain the exact forms of the g.f. for arbitrary values of the parameters. Then, with the exact g.f. in hand we are able to study the Hawking radiation spectrum of the SdS black hole in the bulk and on the brane.

We start by introducing the numerical method we developed in order to calculate the g.f. Then we compare the analytic expressions for the g.f. of chapter 2 with the exact ones and move on to an in-depth study of the Hawking spectrum in both the brane and bulk channels of emission. Finally, for a wide range of the parameters, we calculate the bulk-over-brane relative energy rates and total emissivity ratio in order to see whether the black hole emits the majority of its energy on the brane or in the bulk.

3.1 Numerical calculation of the greybody factors

For the calculation of the g.f. we use the fact that the effective Regge-Wheeler potentials eqs. (2.23) and (2.97) vanish at the locations of the horizons in order to express the field as a superposition of plane waves in these regions. We have seen that the g.f. is then given in terms of the amplitudes of the incoming (B_1) and outgoing (B_2) field modes at the tortoise-coordinate (2.21) infinity $r_* \to \infty$ via the relation

$$|A|^2 = 1 - \left|\frac{B_2}{B_1}\right|^2 . \tag{3.6}$$

So, in order to numerically compute the greybody factor we have to integrate the radial EOMs (3.4) and (3.5) to obtain the exact solutions for the brane and bulk propagating fields and then isolate the amplitudes $B_{1,2}$ at $r_* \to \infty$ i.e. in the vicinity of the cosmological horizon.

Of course, in order to solve eqs. (3.4) and (3.5) two boundary conditions are needed and to specify them we turn to their analytic asymptotic solutions close to the horizons we have already derived in the previous chapter. In the vicinity of the black-hole (r_h) and cosmological (r_c) horizons, the radial part of the field has been found to be of the same functional form both in the bulk and on the brane. The only difference lies in the definition of the indices of the hypergeometric functions [compare eqs. (2.44) and (2.45) with eqs. (2.100) and (2.101)] and the power coefficients [compare eq. (2.48) with eqs. (2.102) and (2.103)]. More precisely, we found that close to the black-hole horizon

and after we impose the condition that purely in-going modes exist at $r \to r_h$, the solution is

$$R_{BH} \simeq A_1 \, f^{\alpha_1} \, , \tag{3.7}$$

where A_1 is an arbitrary constant,

$$f(r) \equiv \frac{h(r)}{1-\tilde{\Lambda} r^2} \quad , \quad \tilde{\Lambda} \equiv \frac{2\Lambda}{(n+2)(n+3)} \, , \tag{3.8}$$

and

$$\alpha_1 = \frac{-i\omega r_h}{A_h} \quad , \quad A_h = (n+1) - (n+3)\tilde{\Lambda} r_h^2 . \tag{3.9}$$

In the limit $r \to r_h$, due to the vanishing of the metric function we have $f \to 0$ and so by re-writing (3.7) as

$$R_{BH} \simeq A_1 \, f^{\alpha_1} = A_1 \, e^{-i(\omega r_h/A_h) \, \ln f} \, , \tag{3.10}$$

we see that the solution indeed describes an in-going field mode close to the black-hole horizon. The amplitude A_1 has no physical significance since it does not appear in the expression of the g.f. and thus has no observable effect. This allows us to normalize the radial solution to unity at the black-hole horizon and obtain in this way the first boundary condition

$$\boxed{R_{BH}(r_h) = 1} \, . \tag{3.11}$$

Evaluating now the first derivative of (3.7) with respect to the original radial coordinate at $r = r_h$ and using (3.11) we obtain the second boundary condition necessary for our numerical analysis

$$\boxed{\left.\frac{dR_{BH}}{dr}\right|_{r_h} = A_1 f^{-i(\omega r_h/A_h) \, \ln f} \left(-\frac{i\omega r_h}{A_h}\right) \left.\frac{A(r)(1-f)}{h(r)\, r}\right|_{r=r_h} \simeq -\frac{i\omega}{h(r)}} \, . \tag{3.12}$$

We now turn to the cosmological horizon (r_c) regime. To obtain the asymptotic solution there, in the analytic approach we used the simplified radial coordinate redefinition $r \to h(r) \approx 1 - \tilde{\Lambda} r^2$ that essentially discards the effect of the black hole close to r_c. Here, since we are dealing with the problem numerically we are not going to resort to this simplification and so we use again eq. (3.8) as the appropriate coordinate redefinition that takes into account both the black-hole mass and the cosmological constant. Then, the asymptotic solution of the EOM close to r_c (in analogy to the $r \to r_h$ case) is

$$R_C \simeq B_1 \, f^{\alpha_2} + B_2 \, f^{-\alpha_2} = B_1 \, e^{-i(\omega r_c/A_c) \ln f} + B_2 \, e^{i(\omega r_c/A_c) \ln f} \, , \tag{3.13}$$

where $\alpha_2 = -i\omega r_c/A_c$ and $A_c = (n+1) - (n+3)\tilde{\Lambda} r_c^2$. This time both incoming and outgoing modes are allowed. Notice that always $A_c < 0$[1] and since $f \to 0$ also close to r_c the amplitude of the incoming (outgoing) field mode is B_1 (B_2); thus the GF is indeed given by eq. (3.6).

Because of the existence of an apparent singularity at $r = r_h$ we start the integration of the EOM not

[1] This can be easily verified by performing a numerical calculation.

exactly at the location of the horizon but in the neighborhood of r_h i.e. at radial distance $r = r_h + \epsilon$ where ϵ is a small positive parameter of the order of $10^{-6} - 10^{-4}$. In order to obtain stable numerical solutions we had to carefully choose not only the value of ϵ but the integration step as well.

With the boundary conditions of eqs. (3.11) and (3.12) imposed at $r = r_h + \epsilon$ the integration of the EOM proceeds until the radial distance $r = r_c - \epsilon$ where the amplitudes $B_{1,2}$ are to be computed.

To isolate the amplitudes of the plane waves close to the cosmological horizon we solved the system of equations consisting of the asymptotic solution eq. (3.13) and its first derivative with respect to r. This way we ended up with the following expressions for the amplitudes:

$$B_1 = \frac{1}{2}\, e^{i(\omega r_c/A_c)\,\ln f} \left[R_C(r) + \frac{iA_c hr}{\omega r_c A(r)(1-f)} \frac{dR_C(r)}{dr} \right], \tag{3.14}$$

$$B_2 = \frac{1}{2}\, e^{-i(\omega r_c/A_c)\,\ln f} \left[R_C(r) - \frac{iA_c hr}{\omega r_c A(r)(1-f)} \frac{dR_C(r)}{dr} \right]. \tag{3.15}$$

By plugging eqs. (3.14) and (3.15) into (3.6) the greybody factor is finally obtained. The numerical code we developed on Wolfram Mathematica [113] can be found in App. C along with detailed comments.

3.1.1 Exact results on the brane

Using the above algorithm we integrated numerically eq. (3.3) and obtained the exact form for the g.f. for scalar fields confined on the brane. Before we move to the study of these results we compare how our approximate analytic expressions stand against the numerical results. In Fig. 3.1 we plot the numerical (analytic) results for the g.f. with solid (dashed) curves. On the left panel we depict the variation with respect to coupling constant ξ while on the right panel we show the variation with respect to the cosmological constant Λ. In both cases, in the low-energy regime the anticipated agreement between the analytic and numerical results is excellent and only for intermediate values of ωr_h deviations start to appear. Recall that the analytic expressions were derived under the assumption of small ξ and Λ. This is also depicted here since as either ξ or Λ ceases to be small the range of agreement between the two sets of curves is reduced.

We would like to point out that a general feature of the analytic results is that they always lie lower than their corresponding numerical counterparts. This is a consequence of the poles that appear in the analytic expressions[2] that tend to "pull-down" the analytic curves. In some cases the poles result in the abrupt termination of the analytic curves while the numerical ones are free of this problem and are thus smooth curves that extend throughout the energy regime.

[2] See also the discussion in §2.2.4 of the previous chapter.

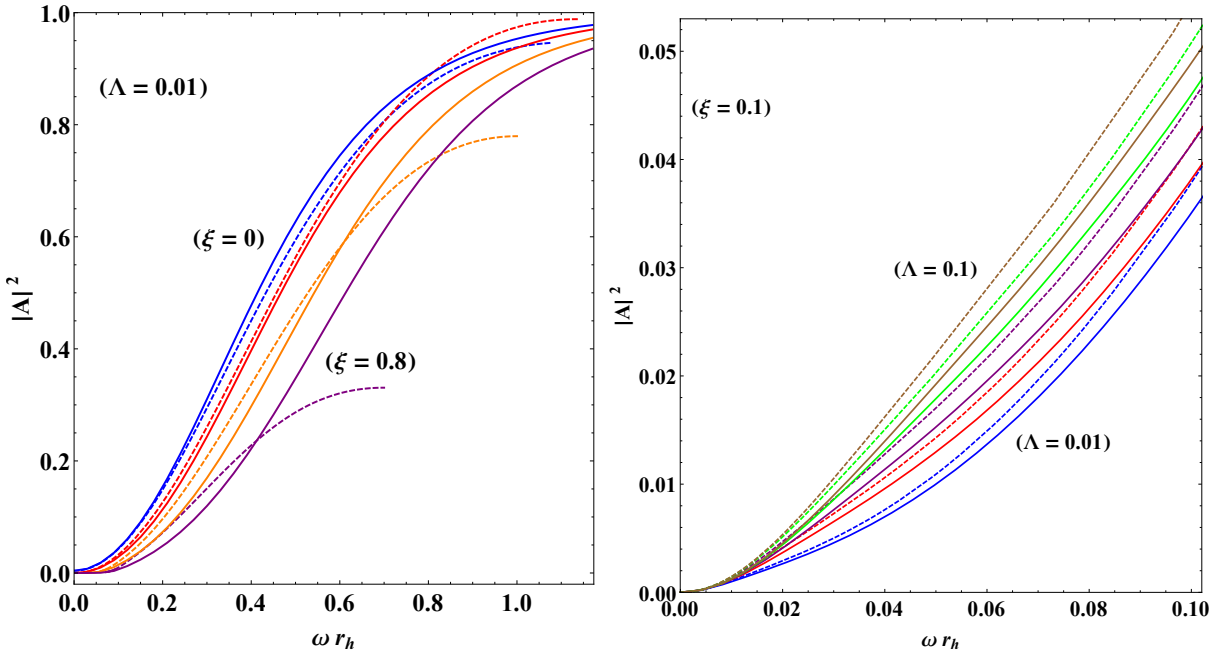

FIGURE 3.1: Greybody factors for brane scalar fields. Analytical (dashed curves) and numerical results (solid curves) for $l = 0, n = 2$ with (a) $\Lambda = 0.01$ (in units of r_h^{-2}) for variable (top to bottom) $\xi = 0, 0.2, 0.5, 0.8$ and (b) $\xi = 0.1$ for variable (bottom to top) $\Lambda = 0.01, 0.03, 0.05, 0.08, 0.1$.

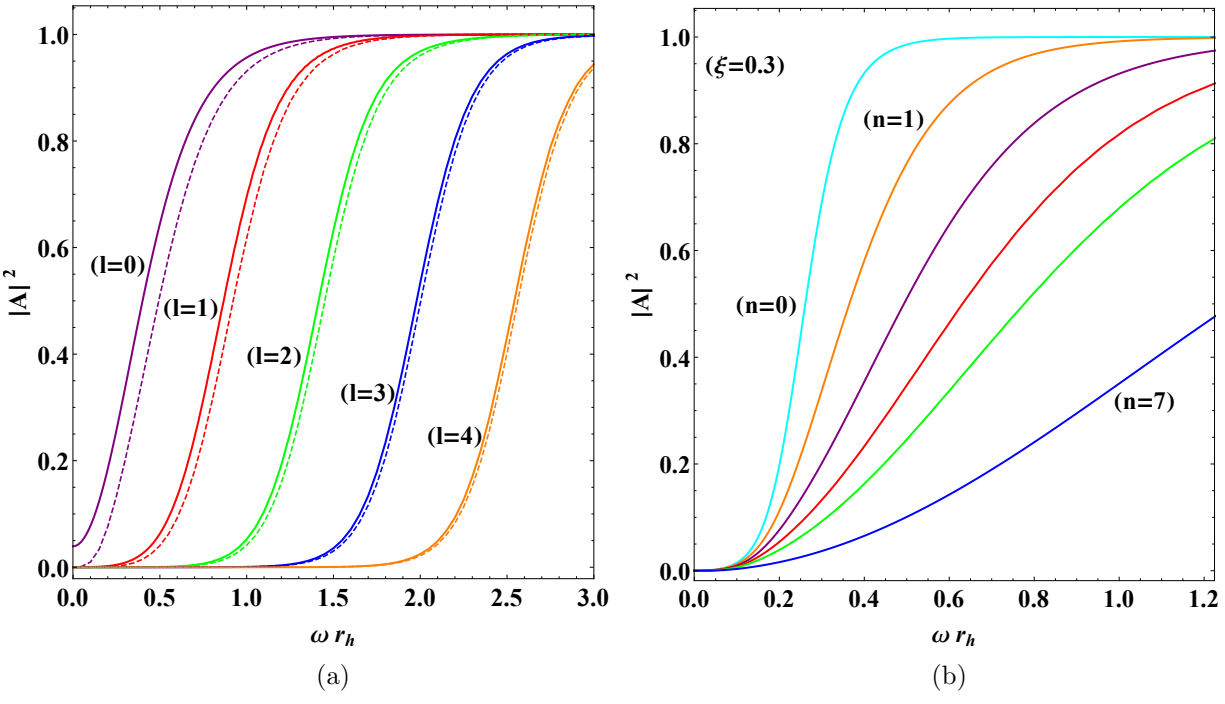

FIGURE 3.2: Greybody factors for brane scalar fields for $\Lambda = 0.1$ and (a) $n = 2$ for variable $l = 0, 1, 2, 3, 4$ and $\xi = 0$ (solid curves) or $\xi = 0.3$ (dashed curves); (b) $l = 0, \xi = 0.3$ for variable (top to bottom) $n = 0, 1, 2, 3, 4, 7$.

In Fig. 3.2(a) we plot the dependence on the angular momentum l parameter of the field. We have used solid and dashed curves to depict the minimal ($\xi = 0$) and non-minimal coupling (with $\xi = 0.3$)

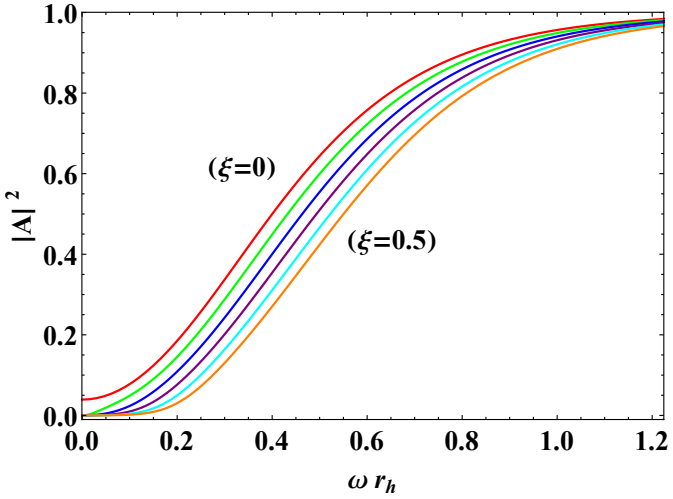

FIGURE 3.3: Greybody factors for brane scalar fields for $l = 0$, $n = 2$, $\Lambda = 0.1$ and variable (top to bottom) $\xi = 0, 0.1, 0.2, 0.3, 0.4, 0.5$.

respectively. Independently of the value of ξ we observe a suppression with l thus the most enhanced g.f. are those for $l = 0$. The presence of a non-vanishing ξ results in the general suppression of the g.f. and the effect of this suppression becomes milder the larger the value of l is. Finally, in the case of minimal coupling, the infrared non-vanishing asymptotic limit of the g.f. (2.80) for the dominant mode ($l = 0$) of the field can be seen.

In Fig. 3.2(b) for the dominant mode ($l = 0$) and for $\xi = 0.3$ we plot the effect of the number of extra dimensions (n) on the g.f. As n increases the usual suppression of the g.f. is observed in agreement to the findings of various previous works. Regarding the agreement with the analytic expressions as n varies we report that the two sets are in excellent agreement in this case as well with deviations appearing as the energy parameter ωr_h and/or n are increased.

Turning now to the effect of the non-minimal coupling (ξ) on the g.f. in Fig. 3.3 we plot the dominant mode with 2 extra space-like dimensions and for $\Lambda = 0.1 r_h^{-2}$ while ξ varies. We see that an increase in the value of ξ results to the suppression g.f. This was also the behavior we observed in the analytic results. The physical interpretation of this result is tied with the effective mass term that appears in the EOM of the scalar field (2.18) [1, 107–111, 114, 115] and is proportional to ξ.

The effect of the cosmological constant on the g.f., as the analytic approach of the previous chapter hints, strongly depends on the value of ξ. To this end we plot in Fig. 3.4 the profile of the numerical results as Λ varies with $l = 0, n = 2$ and for three values of the non-minimal coupling $\xi = 0$, $\xi = 0.2$ and $\xi = 0.5$, in the left, middle and right panel respectively. The dual role of the cosmological constant now becomes evident. For minimal coupling, Λ acts in favor of the enhancement of the g.f. while as ξ becomes larger its role is reversed and eventually above some critical value for ξ the increase in the value of the cosmological constant results in the suppression of the g.f. The two opposing effects that drive this behavior are the following: In one hand Λ enters in the effective mass term that increases the height of the Regge-Wheeler potential (2.23) thus reducing the transmission probability. On the

other hand, Λ also enters in the metric function (3.2) in such a way that $h(r)$ is suppressed with an increasing Λ and since the Regge-Wheeler potential is proportional to $h(r)$ we have the opposing effect. When ξ is small, the effective mass is negligible and the latter effect dominates. The opposite holds for large values of ξ.

3.1.2 Exact results in the bulk

To obtain the exact forms of the GF for scalar fields propagating in the bulk we numerically integrate the radial EOM (3.5) once again by means of the numerical technique we have introduced in the beginning of section 3.1.

In Fig. 3.5 we compare the exact results (solid curves) we obtained with the aforementioned method against the analytic ones (dashed curves) of the previous chapter. For two extra space-like dimensions ($n = 2$) and for the dominant field mode ($l = 0$) we vary the value of ξ in Fig. 3.5(a) and Λ in Fig. 3.5(b). In the region of validity of the analytic results i.e. in the low ωr_h regime and for small values of ξ and Λ the two sets of curves exhibit an impressive agreement. Still the existence of poles in the gamma functions of the analytic expressions result in the discontinuities observed for the dashed curves.

Now we focus solely on the numerical results. We start with the dependence of the bulk GF on the angular momentum l and the number of extra dimensions n in Fig. 3.6. We have fixed the cosmological constant to $\Lambda = 0.1 r_h^{-2}$ and we have used solid curves for the minimal-coupling case ($\xi = 0$) and dashed for an arbitrary non-minimal coupling ($\xi = 0.3$). We observe that the GF get suppressed as l and/or n are increased. Recall that for the dominant field mode ($l = 0$) the asymptotic

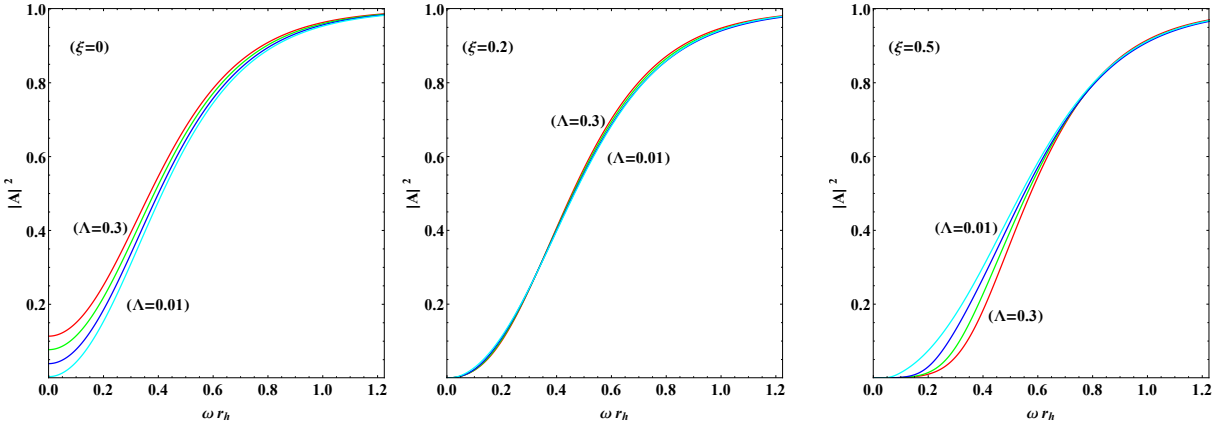

FIGURE 3.4: Greybody factors for brane scalar fields for $l = 0, n = 2$ and $\Lambda = 0.01, 0.1, 0.2, 0.3$ and (a) for $\xi = 0$, (b) $\xi = 0.2$ and (c) $\xi = 0.5$.

infrared limit of the bulk GF is given in terms of the black-hole r_h and cosmological horizon r_c as

$$|A^2| = \frac{4(r_h r_c)^{(n+2)}}{(r_c^{n+2} + r_h^{n+2})^2} \,. \tag{3.16}$$

For $n = 2$ this asymptotic limit is highly suppressed and this is the reason why it can only be seen via a magnification of the low ωr_h regime in Fig. 3.6(a). On the other hand, when $n = 0, 1$ the limit (3.16) is visible in Fig. 3.6(b) for the $l = 0$ mode with minimal coupling.

In both panels of Fig. 3.6 we notice that the effect of the non-minimal coupling on the GF is to further suppress them with the effect becoming milder as l and n assume larger values. Essentially for $l > 3$ and $n > 5$ the presence of ξ plays no role on the profile of the curves since for the considered values of Λ and ξ, the contribution of the "effective mass" term is much smaller than the one of l and n to the potential barrier. . Finally let as point out that the numerical results can be plotted smoothly for all values of n in contrast to the analytic approach where the curves corresponding to odd values of n could not be depicted because of the existence of poles.

In Fig. 3.7 we plot the dependence of the exact results for the bulk GF on the non-minimal coupling of the field ξ with gravity. We study the $l = 0$ mode in $n = 2$ extra dimensions and for $\Lambda = 0.1 r_h^{-2}$. As the field couples more intensely to the Ricci scalar the GF are suppressed mildly thus the scalar particles become less probable to overcome the effective barrier. Notice that we used the same values of the parameters as the ones we used in the brane channel (Fig. 3.3) to further allow us to compare the effect of ξ on the two channels. We see that the effect of the variation of the field coupling is

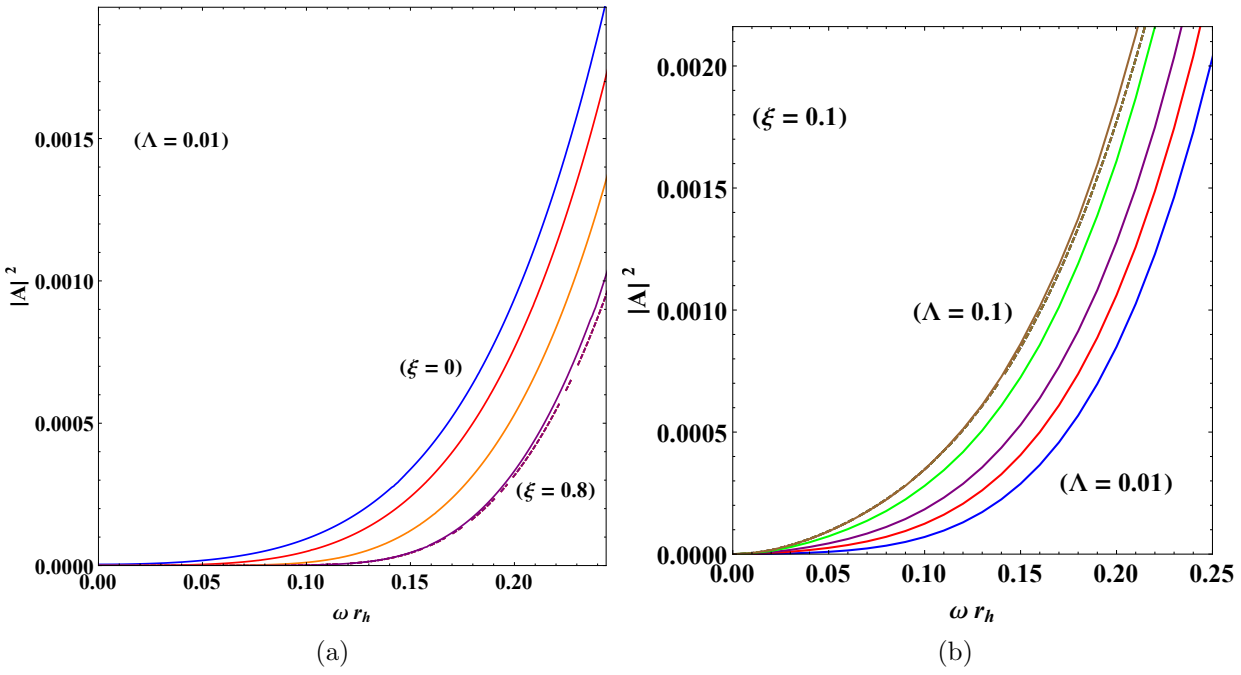

FIGURE 3.5: Greybody factors for bulk scalar fields. Analytical (dashed curves) and numerical (solid curves) results for $l = 0, n = 2$ and: (a) for $\Lambda = 0.01$ and variable $\xi = 0, 0.2, 0.5, 0.8$; (b) for $\xi = 0.1$ and variable $\Lambda = 0.01, 0.03, 0.05, 0.08, 0.1$.

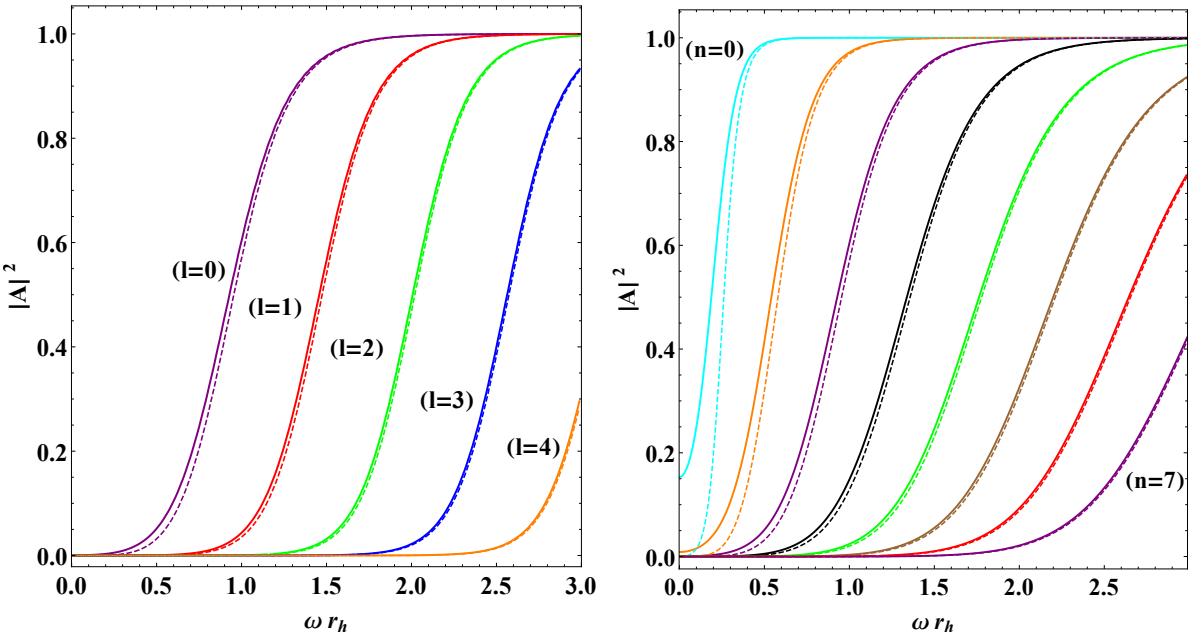

FIGURE 3.6: Greybody factors for bulk scalar fields for $\Lambda = 0.1$, $\xi = 0$ (solid curves) or $\xi = 0.3$ (dashed curves) and: (a) $n = 2$ and variable $l = 0, 1, 2, 3, 4$; (b) $l = 0$ and variable $n = 0, 1, 2, 3, 4, 5, 6, 7$.

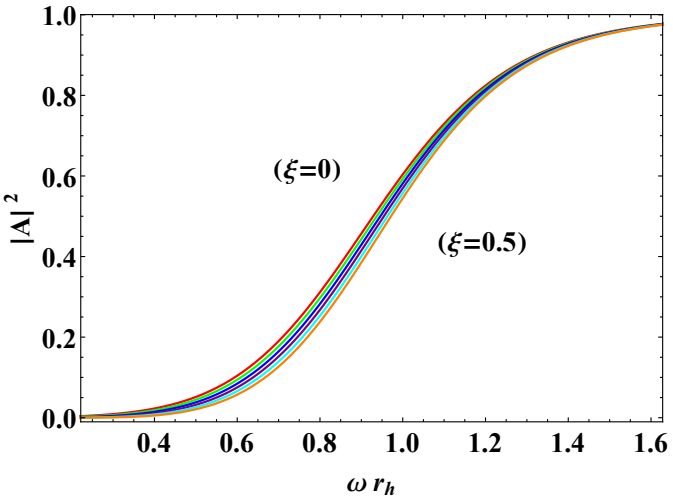

FIGURE 3.7: Greybody factors for bulk scalar fields for $n = 2, \Lambda = 0.1, l = 0$ and variable $\xi = 0, 0.1, 0.2, 0.3, 0.4, 0.5$.

milder in the bulk channel. To interpret this behavior we need to recall what our analytic study of the previous chapter revealed. The effective potential in the bulk is not affected much by ξ (Fig. 2.8) and this is reflected on the GF as well. Still, the role of the effective mass of the field (being proportional to ξ) leads to the observed general suppression of the GF .

To study the effect of the cosmological constant on the GF using the exact results we plotted Fig. 3.8. On the left panel we have the minimal coupling ($\xi = 0$) while on the right panel we have $\xi = 0.5$. We see that in the former case, the effect of Λ is to boost the GF while as the field coupling grows the role of Λ is reversed and acts as a deterring factor at least up to intermediate values of the energy

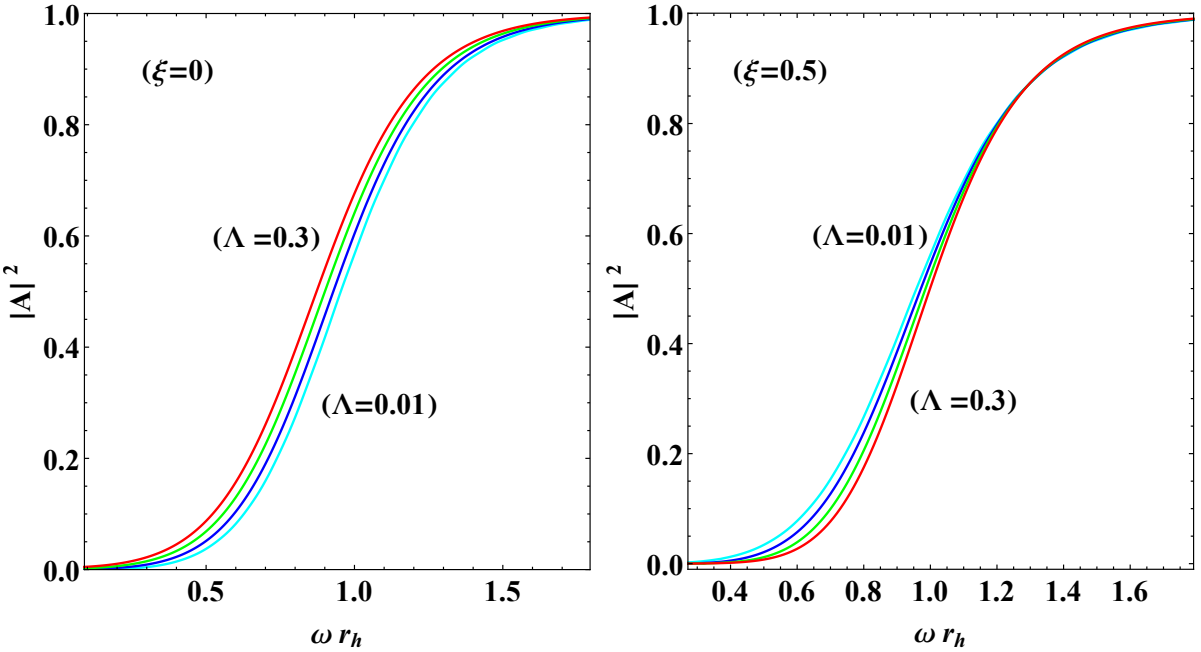

(a) (b)

FIGURE 3.8: Greybody factors for bulk scalar fields for $l = 0, n = 2$ and $\Lambda = 0.01, 0.1, 0.2, 0.3$ and (a) for $\xi = 0$ and (b) $\xi = 0.5$.

parameter ωr_h. It is noteworthy that this dual-role behavior of the cosmological constant has been encapsulated to a very good extend by the analytic results in Fig. 2.12.

3.2 The scalar power spectrum

Now that we have obtained and studied in depth the form of the exact results for the GF for scalar fields propagating in the higher-dimensional SdS spacetime we are able to proceed to the derivation of the Hawking spectrum emitted by such a black hole. The power emitted by the black hole per unit frequency (ω) in the form of scalar particles that a non-accelerated observer measures is given by [96, 116, 117]

$$\frac{d^2E}{dt\,d\omega} = \frac{1}{2\pi}\sum_l \frac{N_l\,|A|^2\,\omega}{\exp(\omega/T_h)-1}\,. \tag{3.17}$$

In the above expression, $|A|^2$ is the GF that corresponds to the transmission probability for scalar particles generated on the horizon of the back hole to overcome the effective barrier and contribute to the radiation. In the case of fermionic fields, the Hawking power spectrum is given by eq. (3.17) with the only difference being the change of sign before 1 in the denominator. The coefficient N_l corresponds to the multiplicity of states with the same angular momentum (l) due to the spherical

symmetry of the spacetime. For fields in n extra spatial dimensions propagating on the brane and in the bulk the multiplicity has respectively the following form [96, 118]:

$$N_l = 2l + 1 \quad , \quad N_l = \frac{(2l+n+1)\,(l+n)!}{l!\,(n+1)!}\,. \tag{3.18}$$

Finally, to account for the non-asymptotic flatness of the SdS spacetime we employed the Bousso-Hawking normalization for the black hole temperature[3] T_{BH} that for the line-element (3.1) has the form [96, 119]

$$T_h = T_{BH} = \frac{1}{\sqrt{h(r_0)}}\,\frac{1}{4\pi r_h}\left[(n+1) - \frac{2\kappa_D^2 \Lambda r_h^2}{(n+2)}\right], \tag{3.19}$$

where r_0 is the location of the non-accelerated observer in SdS [4] given explicitly by

$$r_0 = \left[\frac{(n+1)(n+2)(n+3)\mu}{4\kappa_D^2 \Lambda}\right]^{1/(n+3)}. \tag{3.20}$$

Notice that in order to obtain the power spectrum (3.17) one has to include the contributions of all the field modes l and this translates to the computation of an infinite number of terms. In practice, only the first lowest field modes contribute significantly to the spectrum and this allows as to terminate the series at a finite value of the angular momentum l. This is essential in order to be able to perform a numerical calculation in a finite amount of time!

To illustrate this, in Fig. 3.9 we give an indicative example of the individual contributions to the spectrum by each field mode in the brane channel with $n = 2$, $\Lambda = 0.1\, r_h^{-2}$ and $\xi = 0$. It is evident

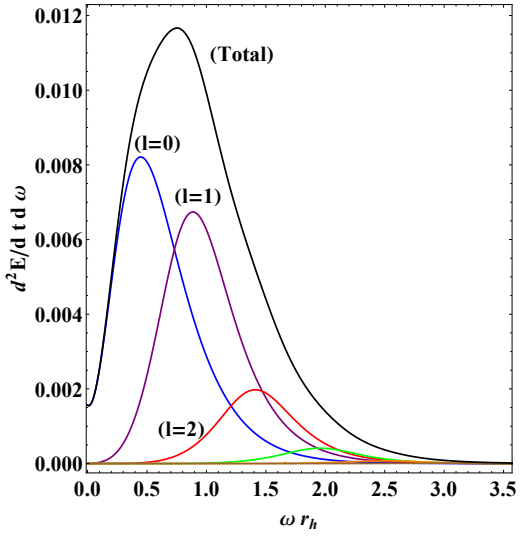

FIGURE 3.9: Energy emission rate curves for brane scalar fields for $n = 2$, $\Lambda = 0.1$, $\xi = 0$ for the first six dominant modes with $l = 0, 1, 2, 3, 4, 5$.

that only the first few modes ($l \leqslant 5$) contribute significantly. We found that in all cases, modes with

[3] A detailed discussion on the black-hole temperature in SdS spacetime is given in the following chapter.
[4] See the discussion on the causal structure of SdS in §2.1.2.

$l = 7$ or higher induce contributions to the spectrum that peak many orders of magnitude lower than the dominant mode ($l = 0$) and thus we terminated the sum at $l = 7$ for the needs of the numerical calculation. The numerical code we developed on Wolfram Mathematica [113] can be found in App. D along with detailed comments.

3.2.1 The power spectrum in the brane channel

We start with the study of the black-hole radiation in the brane channel that is the phenomenologically more interesting one. Since the angular momentum (l) is summed up the only free parameters of the system are now the non-minimal coupling of the field ξ, the cosmological constant Λ and the number of extra dimensions n.

In Fig 3.10(a) we plot the dependence of the power spectrum on n for $\Lambda = 0.1$ and $\xi = 0.3$. Notice that although the GF are suppressed with n [Fig. 3.2(b)] the spectra are clearly enhanced. The reason for this behavior lies in the way the temperature (3.19) gets significantly enhanced with n thus becoming the dominating factor. The observed enhancement of the spectra with the number of extra dimensions was an anticipated result, since a plethora of previous works [96, 116, 120–142] have also reported enhancement of the Hawking radiation with n not only for the SdS case but for other spherically and axially symmetric black holes as well.

In Fig. 3.10(b) the effect of the coupling parameter ξ is depicted for two extra dimensions and $\Lambda = 0.1$. We see that when the field couples to gravity non-minimally, the resulting radiation gets suppressed

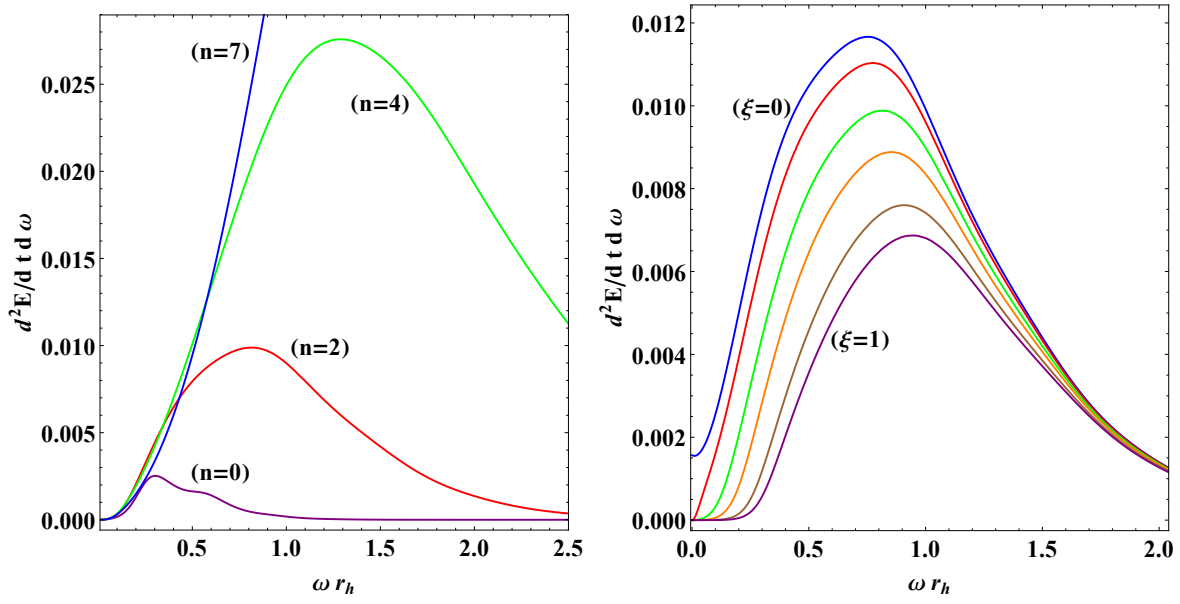

FIGURE 3.10: Energy emission rates for brane scalar fields, for $\Lambda = 0.1$, and: (a) $\xi = 0.3$ and variable $n = 0, 2, 4, 7$; (b) $n = 2$ and variable $\xi = 0, 0.1, 0.3, 0.5, 0.8, 1$.

throughout the energy regime apart from the tail of the curve. This time, the behavior of the spectral curves is in agreement with the behavior of the GF (Fig. 3.3) since the temperature is independent of the field parameters.

For the minimal coupling ($\xi = 0$) the imprint of the non-vanishing low-energy asymptotic limit of the greybody factor (2.80) on the power spectrum is evident. Thus in this case we have a drastic deformation of the power spectrum deviating from the "standard" form by starting from a non-vanishing value in the infrared limit. This feature has also been reported in previous works [93, 96, 99, 106].

We finally point out that the observed suppression with ξ in Fig. 3.10(b) is in excellent agreement with the results reported in [111] where massive scalar fields were considered. As we have seen in the analytic approach, the coupling ξ to the Ricci scalar corresponds to an effective mass term for the scalar field and thus the similar effect on the power spectra comes as no big surprise.

Turning now to the effect of the cosmological constant (Λ) on the spectra we plot in Fig. 3.11 the differential energy emission rate in the brane channel for $n = 2$ extra dimensions, and three different values of the non-minimal coupling parameter ξ as Λ varies. The motivation behind choosing three values for ξ is of course the dual-role behavior of the cosmological constant on the GF we have observed in the analytic approach and verified with the numerical analysis as well.

On the left panel of Fig. 3.11 we have the minimal coupling ($\xi = 0$) and the cosmological constant boosts the particle emission. Also, the infrared asymptotic limits can once again be seen. In Fig. 3.11(b) as the field coupling to gravity is "switched on" the low-energy limit vanishes and the enhancement of the radiation with Λ becomes milder. Finally for an even stronger field coupling we see in Fig. 3.11(b) that as the cosmological constant is increased the enhancement becomes milder still in the high-energy regime while in the low-energy part of the spectrum we observe suppression of

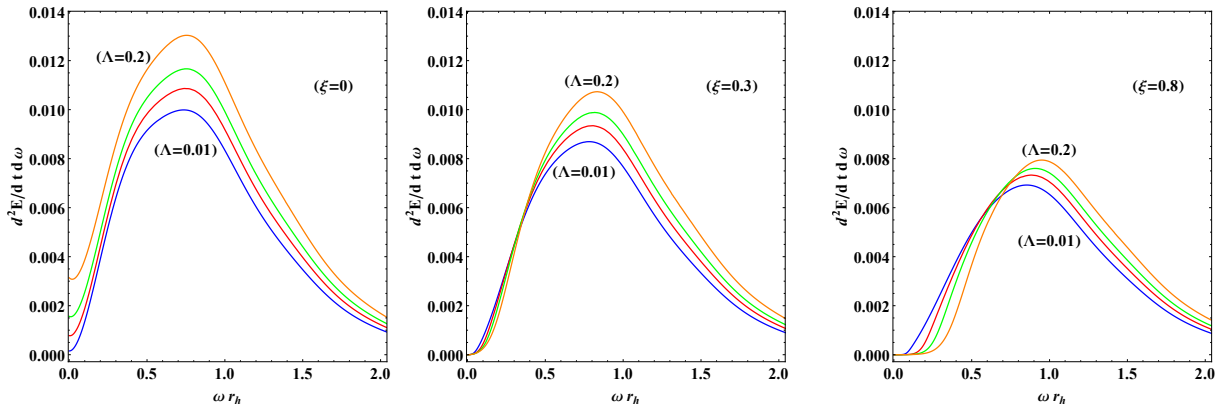

(a) (b) (c)

FIGURE 3.11: Energy emission rates for brane scalar fields for $n = 2$, variable $\Lambda = 0.01, 0.05, 0.1, 0.2$, and for: (a) $\xi = 0$, (b) $\xi = 0.3$, and (c) $\xi = 0.8$.

the low-energy particles that are emitted. Clearly, the effect of the "mass term" is irrelevant for the high-energy modes, that is why the tail of the radiation curve is always enhanced with Λ.

3.2.2 The power spectrum in the bulk channel

We will now study the features of the bulk channel for the higher-dimensional SdS black hole decaying via Hawking radiation in the form of scalar particles. In Fig. 3.12(a) we plot the dependence of the spectrum on the number of extra dimensions (n). By purposely choosing the same values for the parameters $\Lambda = 0.1$ and $\xi = 0.3$ as in Fig. 3.10(a), we are able to compare the bulk and brane channels. We see that as n becomes larger, the bulk radiation becomes enhanced as well even though in a milder way compared to the brane channel. On the other hand, the peaks of the power curves for particles emitted in the bulk are shifted in a more prominent way towards larger values of the energy parameter (ωr_h).

For this specific choice of parameters the power curves in the bulk are located lower than their corresponding brane counterparts thus yielding a brane dominance for the emission process. This observation cannot be generalized because as we shall see in the following sections, the values of the parameters strongly affect the bulk-over-brane relative emission rates and total emissivities.

The effect of ξ on the bulk spectra is depicted in Fig. 3.12(b) and we observe once again a suppression with an increase of the field coupling in accordance with the behavior exhibited by massive particles

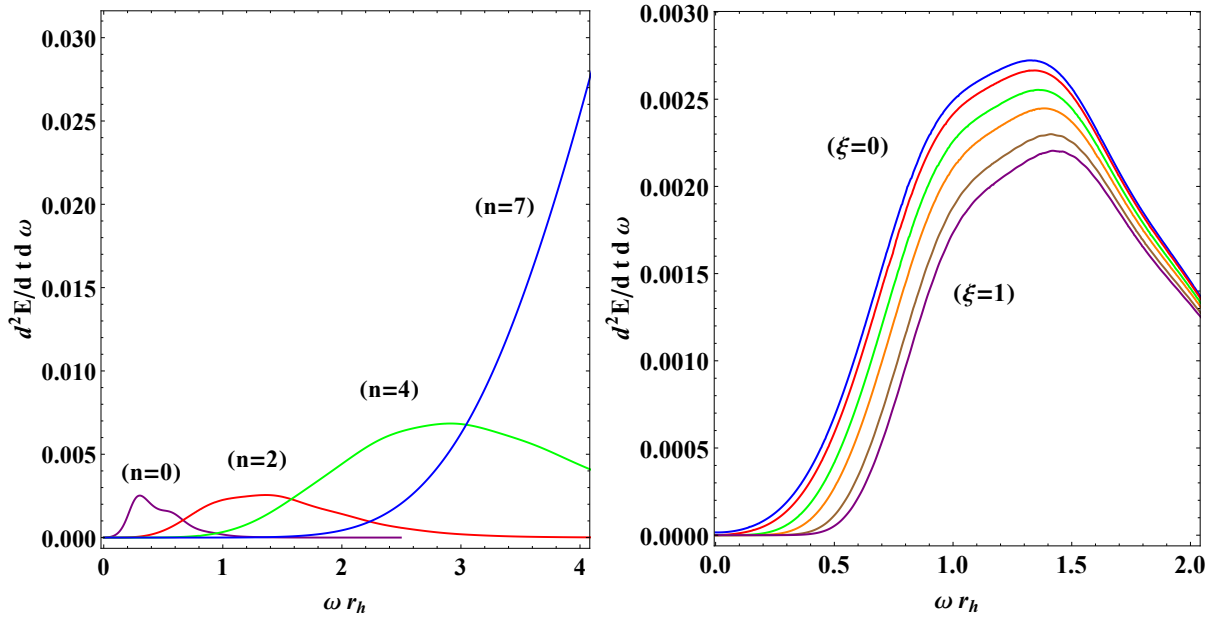

FIGURE 3.12: Energy emission rates for bulk scalar fields for $\Lambda = 0.1$, and: (a) $\xi = 0.3$ and variable $n = 0, 2, 4, 7$; and (b) $n = 2$ and variable $\xi = 0, 0.1, 0.3, 0.5, 0.8, 1$.

in [111]. A low-energy non-vanishing limit when $\xi = 0$ is exhibited by the power spectra in the bulk channel as well but since it stems from the infrared limit of the GF it is highly suppressed in the bulk as we have already seen (at least for the value $\Lambda = 0.1 r_h^{-2}$ we used here).This low-energy limit can be seen when the cosmological constant is slightly larger as is the case with $\Lambda = 0.2 r_h^{-2}$ in Fig. 3.13 where we plot the dependence on Λ for $n = 2$ and three values of the non-minimal coupling parameter (ξ).

The behavior of the bulk power spectra with respect to the variation in Λ is reminiscent of the brane channel. For vanishing values of ξ the cosmological constant boosts the emission throughout the energy regime while as the field coupling becomes stronger the low-energy part of the spectrum gets suppressed with the increase of Λ.

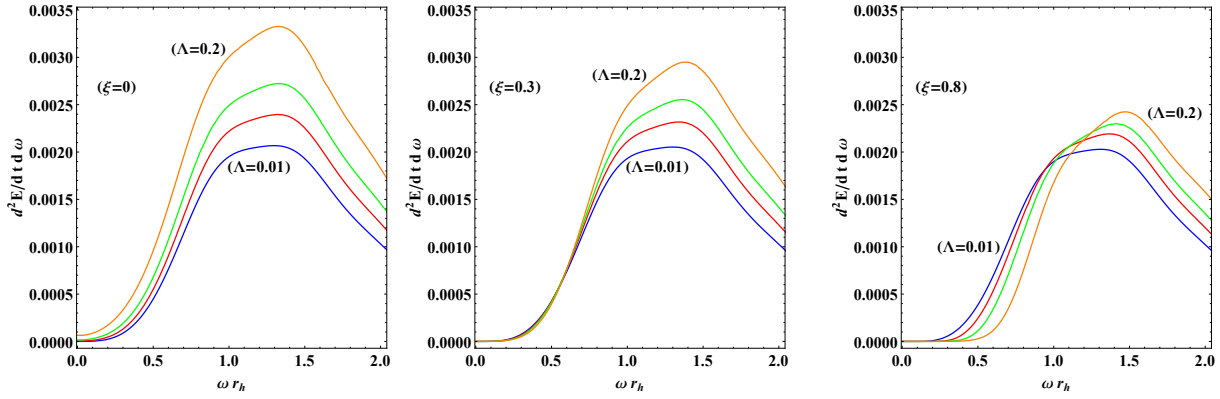

(a) (b) (c)

FIGURE 3.13: Energy emission rates for bulk scalar fields for $n = 2$, variable $\Lambda = 0.01, 0.05, 0.1, 0.2$, and for: (a) $\xi = 0$, (b) $\xi = 0.3$, and (c) $\xi = 0.8$.

3.3 The Bulk-over-brane emissivity

When we studied the exact numerical results for the GF in a previous section, we used the same values of the parameters for both the brane and bulk analyses in order to make the comparison between the two easy. Then, by inspection of the sets of figures 3.2 and 3.6 that depict the dependence of the GF on the angular momentum (l) and the number of extra dimensions (n) on the brane and in the bulk respectively, we can see that the bulk GF are more suppressed than the brane ones. In fact this is a well-known result [116, 120, 143]. However, in our present work we have two more parameters namely the non-minimal coupling of the field to gravity (ξ) and the cosmological constant (Λ). Regarding the former we have seen that it suppresses the GF in both channels while the latter exhibits a more complicated "dual role" behavior that depends on the value of ξ.

The above discussion makes evident that the previously reported bulk-over-brane dominance may be refuted in the more general case we consider here. Thus it is necessary to study the relative emission rates and compare the total emissivities in the two channels a task we undertake in this section.

3.3.1 Relative emission rates

In Fig. 3.14(a) we plot the effect of the non-minimal coupling (ξ) on the bulk-to-brane energy emission ratio when $n = 4$ and $\Lambda = 0.1$. We observe a "dual role" behavior of ξ since in the low-energy regime, the brane channel is favored over the bulk one with an increase of the coupling parameter while beyond the intermediate energy regime the bulk emission is favored and at the same time the effect of ξ on the ratio is deminished.

To better understand this result one may consult the sets of figures 3.10 and 3.12 where it is clear that in the low-energy regime the bulk channel is highly suppressed compared to the brane one and this results in the very small values of the ratio observed in the infrared limit in Fig. 3.14(a). For intermediate values of ωr_h the bulk spectral curves are only slightly lower than the brane ones while in the high energy regime we eventually have a bulk domination. This behavior is again in agreement with the findings of [111] that reported a boost of the bulk emission with the mass of the scalar field.

The cosmological constant effect on the ratio is plotted in Fig. 3.14(b) where again a "dual-role" behavior is evident. In the low-energy regime Λ enhances the emission in the bulk channel while for larger values of ωr_h this effect is reversed favoring the brane channel. In the high-energy regime the value of the cosmological constant appears to only slightly affect the ratio that approaches unity and thus we conclude that both channels are equally favored for the emission of highly energetic particles. This dual-role behavior of Λ is attributed to the presence of a non-vanishing field coupling (here we

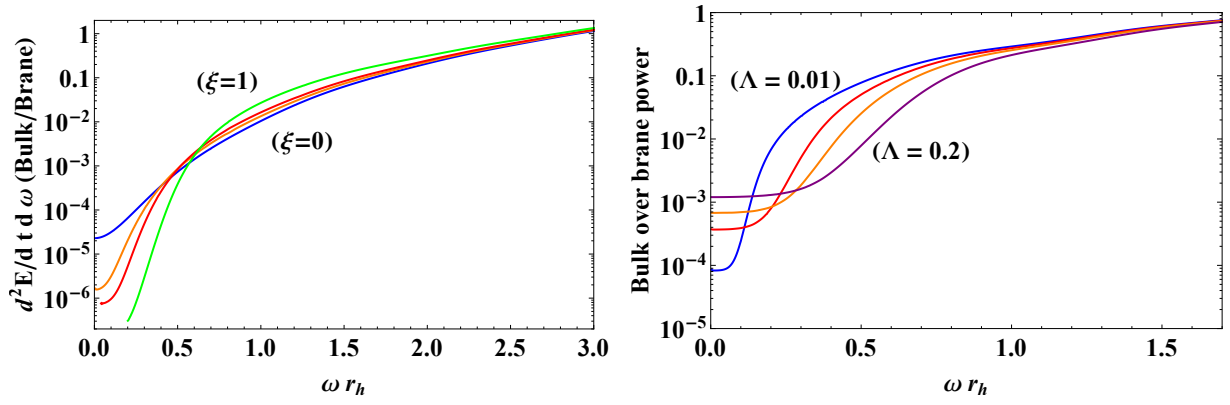

FIGURE 3.14: Bulk-over-brane relative emission rates for: (a) $n = 4$, $\Lambda = 0.1$ and variable $\xi = 0, 0.3, 0.5, 1$, and (b) $\xi = 0.8$, $n = 2$ and variable $\Lambda = 0.01, 0.05, 0.1, 0.2$.

had fixed $\xi = 0.8$) since in a previous study [96] of the bulk-to-brane emission ratio, the minimal-coupling ($\xi = 0$) case was studied and an enhancement of the bulk channel throughout the energy regime has been observed.

Finally we examine the dependence of the bulk-to-brane emission ratio on the number of extra dimensions. In Fig. 3.15, for $\xi = 0.3$ and $\Lambda = 0.2$ we observe that as n is increased the brane channel is boosted in the low-energy region while above intermediate values of ωr_h the bulk channel is significantly favored for all values of n.

3.3.2 Total emissivities

The analysis of the previous section revealed that the bulk-to-brane emission ratio differs by many orders of magnitude when we compare different energy regions or change the values of the parameters. What can we say about the total energy emitted by the black hole on the brane and in the bulk and how is the energy balance between the two channels affected by the parameters?

This is a non-trivial question that cannot be answered by inspection of the bulk-to-brane ratios alone. As an indicative example, we plot Fig. 3.16 where the energy emission rates (e.e.r.) on the brane and in the bulk for $n = 7$, $\Lambda = 0.2$ and for two values of the field coupling $\xi = 0.3$ and $\xi = 1$ are depicted. In Fig. 3.16(a) we observe that the brane emission is favored in the low-energy regime while for $\omega r_h \approx 4.5$ and above the bulk channel becomes the dominant one. This is exactly the picture painted in Fig. 3.15. A similar behavior though can be seen in Fig. 3.16(b), where the field coupling is stronger, but this time the bulk dominance in the high-energy region is so strong that the brane emission is only a small part of the total black-hole emission. It is then clear that in order to study the energy balance between the two channels we need to calculate the *total emissivities* defined as the *total energy per unit time emitted over the whole frequency regime*.

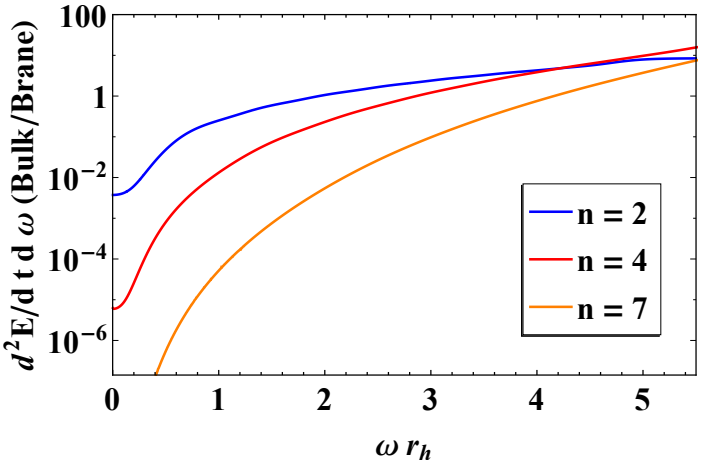

FIGURE 3.15: Bulk-over-brane relative emission rates for $\xi = 0.3$, $\Lambda = 0.2$ and variable $n = 2, 4, 7$.

To this end, for a given set of parameters (n, Λ, ξ) we integrate the brane and bulk e.e.r. throughout the frequency range and compute the bulk-to-brane ratio. Our results are displayed in Tables 3.1 to 3.3.

Regarding the effect of the cosmological constant, we see that for a fixed value of n and as long as the coupling is not larger than $\xi \approx 0.8$ the bulk-over-brane ratio exhibits an enhancement with Λ that becomes gradually less substantial as the value of ξ is increased. This is no longer the "rule" for even larger values of ξ since in some regions of the parameter space we observe the opposite effect.

The non-minimal coupling of the scalar field to gravity in all cases appears to enhance the ratio thus

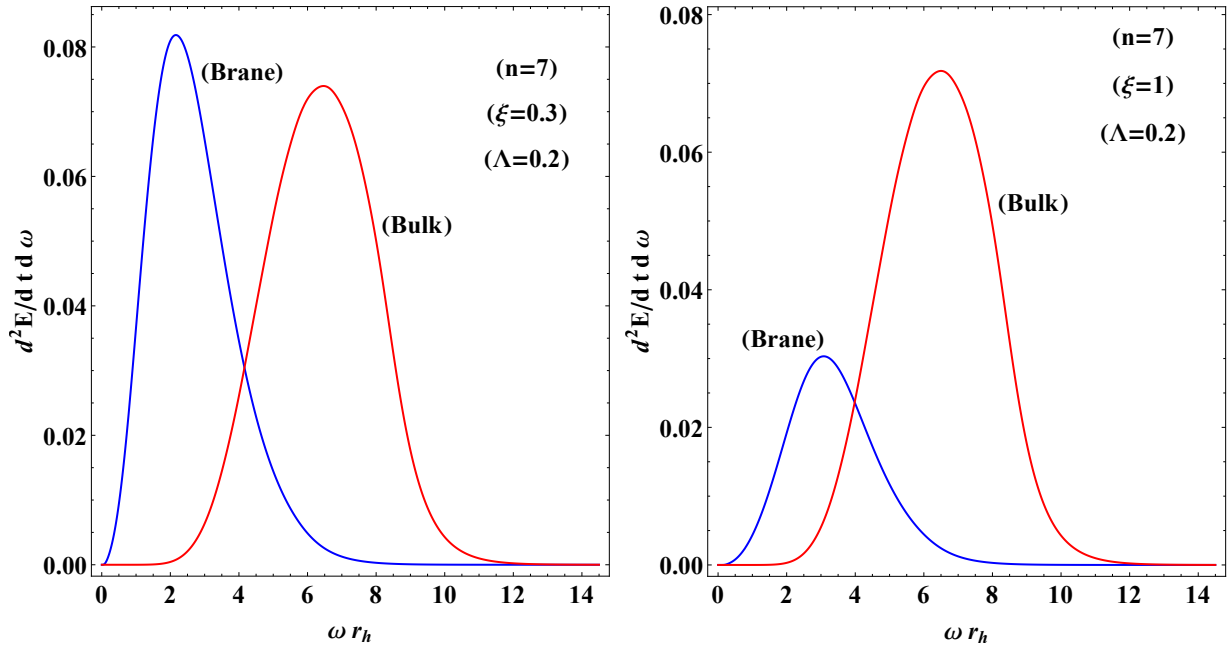

FIGURE 3.16: Power spectra for emission on the brane and in the bulk for $n = 7$, $\Lambda = 0.2$, and: (a) $\xi = 0.3$, and (b) $\xi = 1$.

TABLE 3.1: Bulk over brane total emissivity for $n = 2$

$\xi \rightarrow$	0.0	0.1	0.3	0.5	0.8	1.0
$\Lambda = 0.01$	0.257506	0.269481	0.294391	0.320639	0.362918	0.393068
0.05	0.27356	0.285502	0.309271	0.333195	0.369824	0.394932
0.1	0.288635	0.300295	0.322187	0.343	0.373032	0.392523
0.2	0.314566	0.325492	0.343106	0.357599	0.375749	0.38618

TABLE 3.2: Bulk over brane total emissivity for $n = 4$

$\xi \rightarrow$	0.0	0.1	0.3	0.5	0.8	1.0
$\Lambda = 0.01$	0.247028	0.275432	0.339321	0.413966	0.549627	0.658426
0.05	0.255885	0.284767	0.349056	0.423319	0.556669	0.662449
0.1	0.264557	0.293826	0.358134	0.43146	0.561241	0.662884
0.2	0.279594	0.30942	0.373259	0.444156	0.566328	0.659702

TABLE 3.3: Bulk over brane total emissivity for $n = 7$

$\xi \rightarrow$	0.0	0.1	0.3	0.5	0.8	1.0
$\Lambda = 0.01$	0.779006	0.906992	1.21479	1.60427	2.38062	3.05751
0.05	0.790883	0.92003	1.22955	1.61993	2.39509	3.0686
0.1	0.803103	0.933293	1.24413	1.63466	2.40657	3.07444
0.2	0.824629	0.956511	1.26906	1.65866	2.42208	3.07722

causing more energy to be emitted in the bulk channel the larger the value of ξ. Still, its effect is not enough to tilt the energy balance in favor of the bulk channel at least when n and Λ are small. When the number of extra dimensions assumes large values there is a clear dominance of the bulk with the increase of ξ.

As the number of extra dimensions is increased from $n = 2$ to $n = 4$, in the case of a minimally coupled field ($\xi = 0$) we see that the ratio decreases slightly and then rises again for larger values of n. This behaviour has also been reported in the absence of a cosmological constant for the higher-dimensional Schwarzschild black hole in [116]. For non-vanishing but small values of the coupling $\xi \leqslant 0.1$ we see that this behavior still persists in some regions of the parameter space while for an even stronger field coupling $\xi \geqslant 0.1$ the increase in n clearly favors the enhancement of the bulk channel resulting (in combination with a large value of ξ) to even 3 times more energy being emitted in the bulk than on the brane! This bulk dominance is expected to be further enhanced with even larger values of the field coupling.

3.4 Conclusions

In this chapter, we studied the Hawking radiation spectrum of a higher-dimensional Schwarzschild-de Sitter (SdS) black hole that decays in the form of scalar particles on the brane and in the bulk. The field theory we considered is that of a massless scalar field that exhibits a non-minimal coupling to gravity. To obtain the Hawking spectrum, the exact form of the greybody factors (GF) over the whole energy regime is necessary and their approximate analytic expressions derived in the previous chapter do not suffice. To this end, we developed a numerical technique in order to solve the Klein-Gordon equation and compute the GF valid throughout the energy regime and for arbitrary values of the parameters, namely the field's non-minimal coupling (ξ) and angular momentum (l), the number of extra dimensions (n) and the cosmological constant (Λ). An excellent agreement between the analytic and numerical results is observed in the low-energy regime (and in some cases even beyond that) when ξ and Λ are small. Using the exact GF we computed the Hawking spectrum in both the brane and the bulk and studied in depth its features. We found that the effect of ξ is to suppress the energy emission rates while the role of Λ is "dual" and depends on the value of the field coupling. We finally computed the relative emission rates and total emissivities in the brane and bulk channels of

emission and concluded that the bulk channel becomes the dominant one when a strong field coupling is combined with a large number of extra dimensions.

Chapter 4

The effect of the temperature on the Hawking spectrum of Schwarzschild-de Sitter black holes

Based on Hawking's area theorem [144, 145] stating that the surface area of the classical black-hole horizon can never decrease, Bekenstein conjectured that the entropy contained in the black hole should be related with to the surface area of the event horizon [44]. This observation opened the way to the formulation of the laws of black-hole mechanics [43] that closely resemble the laws of thermodynamics. In this analogy, that remains a mathematical one in the classical level, the internal energy (U) and entropy (S) are related to the mass of the black hole (M) and the surface area of the event horizon (A) respectively. A system that has energy and entropy, inevitably has temperature T associated to it via

$$\frac{1}{T} = \frac{\partial S}{\partial U}\,, \tag{4.1}$$

and so, pursuing this analogy further, it is tempting to assign a temperature to the black hole as well given by

$$\frac{1}{T_h} = \frac{\partial A}{\partial M}\,. \tag{4.2}$$

It is clear that T_h is a geometric quantity since both the surface area of the horizon and the mass of the black hole are related to the geometry. As an example, for the Schwarzschild metric in 4 dimensions $M \sim r_h$ and $A \sim r_h^2$ where r_h is the radius of the event horizon and so $T_h \sim r_h^{-1}$. It turns out that the black-hole temperature is proportional to the surface gravity (κ_h) of the black-hole horizon[1]

$$\boxed{T_h = \frac{\hbar \kappa_h}{2\pi}}\,. \tag{4.3}$$

At first, this formula was considered nothing more than an interesting mathematical consequence of the relation between the first laws of thermodynamics and black-hole mechanics since classical black holes absorb everything and thus are by definition, objects with zero temperature. It was only a few years later that Hawking treated black holes semi-classically [48] and found that when quantum effects are taken into account black holes radiate particles with a thermal spectrum at a temperature given exactly by eq. (4.3). So eventually, T_h was identified with the actual temperature of the black hole! This relation between surface gravity and temperature is not restricted only to the black-hole horizon. For every Killing horizon in a given spacetime, one can associate a temperature proportional to its surface gravity.

[1] For the rest of the thesis we set $\hbar = 1$.

In the case of the Schwarzschild-de Sitter (SdS) spacetime both the black-hole (r_h) and the cosmological (r_c) horizons are Killing horizons and as a consequence each one has its own temperature. In general, as we shall see, the black-hole temperature is larger than the one of the cosmological horizon and so a problem immediately arises. An observer located in the causal part of the SdS spacetime ($r_h < r < r_c$) can never be in true thermal equilibrium since due to the temperature gradient there will be a constant flow of heat from the hotter black-hole horizon towards the colder cosmological horizon.

A second obstacle towards the thermodynamic description of the SdS black hole is the absence of an asymptotically flat observer with respect to whom the surface gravity (and as a consequence the temperature) is *traditionally* defined. Through the years, in order to circumvent these issues, various proposals have been made in the literature regarding the appropriate way to define the SdS black-hole temperature.

In this chapter, we compare six different expressions for the temperature of the HD SdS black hole and study their effect on the differential energy emission rates and the total emissivities on the brane and in the bulk when the field theory is that of a massless scalar field with a non-minimal coupling to gravity. Another important element of this study is that we do not restrict the value of the cosmological constant (Λ) only to small values. Instead we consider values of Λ that span the whole allowed regime up to the Nariai limit. The motivation for this is the radical differences exhibited by the various temperatures in this limit.

Two of these temperatures are "black-hole temperatures" in the sense that involve only the surface gravity of the black-hole event horizon and differ in the way that the Killing vectors are normalized. The other four belong to the category of the recently proposed "effective temperatures" that involve both the black-hole and cosmological horizon surface gravities. One of the four effective temperatures we study, is valid only in 4-dimensions since its derivation is based on 3-dimensional spatial volumes and its generalization in higher-dimensions requires careful consideration. This is why we only introduce it in the final section of the chapter where we focus on the effect of the temperatures on the 4-dimensional Hawking radiation of SdS.

4.1 Black-hole thermodynamics in the presence of a cosmological horizon

The analogy between thermodynamics and black-hole mechanics [43] associates the temperature of the black hole with the geometric quantity of *surface gravity* (κ_h) evaluated at the location of the black-hole event horizon. The physical interpretation of the latter becomes clear only when the spacetime is static. It corresponds to the force (as it is measured by a non-accelerated observer) that has to be exerted on a unit mass in order for it to remain static exactly on the location of the horizon [15, 22].

Mathematically, the surface gravity can be obtained in terms of the underlying symmetries of the metric. Consider an *isometry* of the metric i.e. an infinitesimal coordinate transformation of the form

$$x^{\alpha}(x) \to x^{'\alpha}(x) = x^{\alpha}(x) + \epsilon K^{\alpha}(x)\,,\ \epsilon \ll 1, \tag{4.4}$$

that leaves the metric invariant. The associated vector field K^{α}, that generates this isometry, "points" in the direction along which the metric remains unchanged. Such a field satisfies Killing's equation

$$\nabla^{\mu}K^{\nu} + \nabla^{\nu}K^{\mu} = 0, \tag{4.5}$$

where ∇^{μ} is the covariant derivative and is thus called a *Killing vector field* (KVF). For every isometry of the metric there exists an associated KVF and any linear combination of KVFs with constant coefficients is a KVF since it will still satisfy eq. (4.5). As a consequence, the KVFs are defined up to a normalization constant.

The surface gravity on the black-hole horizon (r_h) is then obtained via the following limit [15, 22, 26, 146]:

$$\kappa_h^2 = -\frac{1}{2}\lim_{r\to r_h}(\nabla^{\mu}K^{\nu})(\nabla_{\mu}K_{\nu}), \tag{4.6}$$

in terms of a KVF K^{μ} that is *timelike* at infinity and becomes *null* on r_h. Thus, in order to associate surface gravity to the horizon the latter has to be a *Killing horizon* defined by the condition that the norm of the KVF vanishes on it.

If the metric is time-independent there is a timelike Killing vector K^{μ} that points in the "time direction" along which the metric is invariant. This KVF will then have the following form [15]:

$$\mathbf{K} = \gamma_t \frac{\partial}{\partial t}, \tag{4.7}$$

where γ_t is a normalization constant.

Turning to the SdS spacetime, that as we have seen is static and so it has a KVF of the form of eq. (4.7), we can compute the norm of K^{μ} to get

$$K^2 = g_{MN}K^M K^N = \gamma_t^2 g_{tt} = -\gamma_t^2 h(r)\,. \tag{4.8}$$

The metric function $h(r)$ (2.7) is positive for all values of the radial coordinate in between the black-hole and cosmological horizon radii. It is then clear that K^{μ} is timelike in the causal patch of SdS and becomes null on the locations of both r_h and r_c. So, the two horizons of SdS are Killing horizons and thus temperature can indeed be associated to each one of them via their corresponding surface gravity.

Substituting eq. (4.7) into eq. (4.6) one concludes that for a general static and spherically symmetric spacetime, the surface gravity (4.6) is [147]

$$\kappa_h = \frac{1}{2}\frac{\gamma_t}{\sqrt{-g_{tt}g_{rr}}}|g_{tt,r}|_{r=r_h} = \frac{1}{2}|\partial_r h(r)|_{r=r_h}\,, \tag{4.9}$$

and consequently can be simply obtained in terms of the first derivative of the metric function with respect to the radial coordinate. Applying eq. (4.9) for the metric function (2.7) we find that the surface gravity on the location of the black-hole horizon of the higher-dimensional SdS black hole is

$$\kappa_h = \frac{\gamma_t}{2r_h}\left[(n+1) - (n+3)\tilde{\Lambda}r_h^2\right]\,, \tag{4.10}$$

where n is the number of extra dimensions, $\tilde{\Lambda} \equiv 2\lambda/(n+2)(n+3)$ and we have used eq. (2.24) evaluated at $r = r_h$ to eliminate the mass parameter μ.

The ambiguity, introduced in the expression of the surface gravity with γ_t, is lifted by appropriately normalizing K^μ at the location of the static observer. For asymptotically-flat black holes, the *static* observer lies in spatial infinity with a four-momentum P^μ that "points" in the direction of time translations. Thus her four-momentum will be proportional to the timelike KVF. Usually, P^μ is normalized as $P^\mu P_\mu = -1$ and this also fixes the normalization of the KVF [15, 148]

$$\lim_{r\to\infty} K^\mu K_\mu = \gamma_t^2 \lim_{r\to\infty}(-g_{tt}) = -\gamma_t^2 = -1\,. \tag{4.11}$$

In the presence of a cosmological horizon, the static observer is located at r_0 (2.14) instead, where the black-hole attraction is canceled exactly by the repulsion of the cosmological constant. In the "naive" approach, the KVF is normalized to unity at r_0 as well [99, 149]. This way, the following expression for the "bare" black-hole temperature is obtained:

$$\boxed{T_0 = \frac{1}{4\pi r_h}\left[(n+1) - (n+3)\tilde{\Lambda}r_h^2\right]}\,, \tag{4.12}$$

and in a similar way the cosmological-horizon temperature in terms of the surface gravity at r_c [50, 85, 96] may be defined

$$\boxed{T_c = \frac{-1}{4\pi r_c}\left[(n+1) - (n+3)\tilde{\Lambda}r_c^2\right]}\,, \tag{4.13}$$

where the minus sign in the last expression has been introduced in order to have a positive-definite temperature . Finally, notice that since $r_h < r_c$ the black-hole temperature will always be larger than the cosmological-horizon one. This is the root of another issue that plagues the SdS thermodynamics namely the absence of thermal equilibrium due to the temperature gradient.

To deal with this problem, the usual approach is to treat the horizons as independent thermodynamic systems [50, 119, 150]. This is indeed a reasonable assumption as long as the value of the cosmological constant is very small so that one may ignore the effect of the cosmological horizon ($r_c \to \infty$). In

this case, the "naive" normalization (4.12) is a very accurate approximation since $h(r_0) \to 1$ and the static SdS observer resembles greatly the asymptotically Minkowski one (see section 2.1.2).

By considering larger values of Λ, the two horizons are located closer, and the bare normalization for the temperature of the black hole is no longer a good approximation. To account for the absence of the asymptotically flat limit, a different normalization for the KVF at r_0 has been proposed by Bousso and Hawking [119]

$$\lim_{r\to r_0} K^\mu K_\mu = \gamma_t^2 \lim_{r\to r_0} (-g_{tt}) = -\gamma_t^2 h(r_0) = -1\,, \tag{4.14}$$

and this amounts to setting $\gamma_t = 1/\sqrt{h(r_0)}$. The temperature obtained with this normalization is also commonly used in the literature [3, 96, 106] and has the following form:

$$\boxed{T_{BH} = \frac{1}{4\pi r_h \sqrt{h(r_0)}} \left[(n+1) - (n+3)\tilde{\Lambda} r_h^2\right]}\,, \tag{4.15}$$

where the value of the metric function $h(r)$ at r_0 is

$$h(r_0) = \frac{1}{n+1} \left[(n+1) - (n+3)\tilde{\Lambda} r_0^2\right]. \tag{4.16}$$

Notice that even this "improved" expression for the SdS black-hole temperature is employed under the assumption of independent horizon thermodynamics since the effect of the temperature of the cosmological horizon on the emission is ignored.

Although in the previous chapter we studied the Hawking radiation of the HD SdS black hole with T_{BH} as the temperature both on the brane and in the bulk, our analysis was restricted to small values of the cosmological constant. Here, the inclusion again of T_{BH} in the study of the effect of the temperatures on the power spectra is twofold. On the one hand, it serves as a reference to the results of the previous chapter and on the other hand it allows for the study of its corresponding spectra when $\Lambda \approx \Lambda_{crit}$, a limit we consider in this chapter.

In Fig. 4.1 we can see the dependence of the two black-hole temperatures T_0 and T_{BH} depicted with blue and red curves respectively as the cosmological constant spans the whole allowed regime up to the critical limit. In the left panel, we have the case of $n = 2$ extra dimensions and we observe that as Λ increases, T_0 gets suppressed according to eq. (4.12). On the other hand the Bousso-Hawking normalized temperature increases. This is a consequence of the fact that as Λ grows the value of $h(r_0)$ decreases (see sec. 2.1.2) resulting in a boost of T_{BH} for nearly all values of Λ.

In the right panel of Fig. 4.1 where $n = 5$ the bare temperature still gets monotonically suppressed while the enhancement of T_{BH} with the cosmological constant is now restricted to the low- and intermediate-Λ regime. Beyond that point, the boosting effect of the lowering of the value of the denominator $h(r_0)$ is not sufficient to counter the rapid decrease of the numerator for large values

of n. Independently of n, T_{BH} is always larger than T_0 throughout the allowed Λ values (see also [106] where a similar comparison has been performed) and the two expressions match only in the limit $\Lambda \to 0$ where $h(r_0) \to 1$. This is the limit of a vanishing cosmological constant and as one would expect, the asymptotic low-Λ value at which the two temperatures coincide corresponds to the temperature of the HD Schwarzschild black hole

$$T_h = \frac{(1+n)}{4\pi r_h}. \tag{4.17}$$

In the other extreme limit where $\Lambda \to \Lambda_{crit}$ [90, 151, 152], the bare temperature vanishes while T_{BH} assumes a non-zero value as a consequence of the simultaneous vanishing of the denominator and numerator of its expression (4.15) that leaves the ratio constant.

To study the effect of the number of extra dimensions on the temperatures, in Fig. 4.2 we consider two fixed values for $\Lambda = 0.1$ and 0.8 (in r_h^{-2}) as n ranges from 0 to 5. Focusing again on the black hole temperatures, we see that they both increase monotonically with n while at the same time, the difference between them decreases as the value of Λ becomes smaller.

The validity of the above two expressions eqs. (4.12) and (4.15) for the temperature gets compromised as the cosmological constant is increased. This is related with the basic requirement that the two horizons be located sufficiently apart in order to ignore the effect of T_c on the emission of the black hole and, consequently, this limits the potential analyses. In an effort to take into account the effect from both of the horizons in the thermodynamic description of the SdS black hole and deal with the absence of thermal equilibrium, the notion of the *effective temperature* appeared in recent years [153]. Contrary to the previous approach where each of the horizons has its own respective first

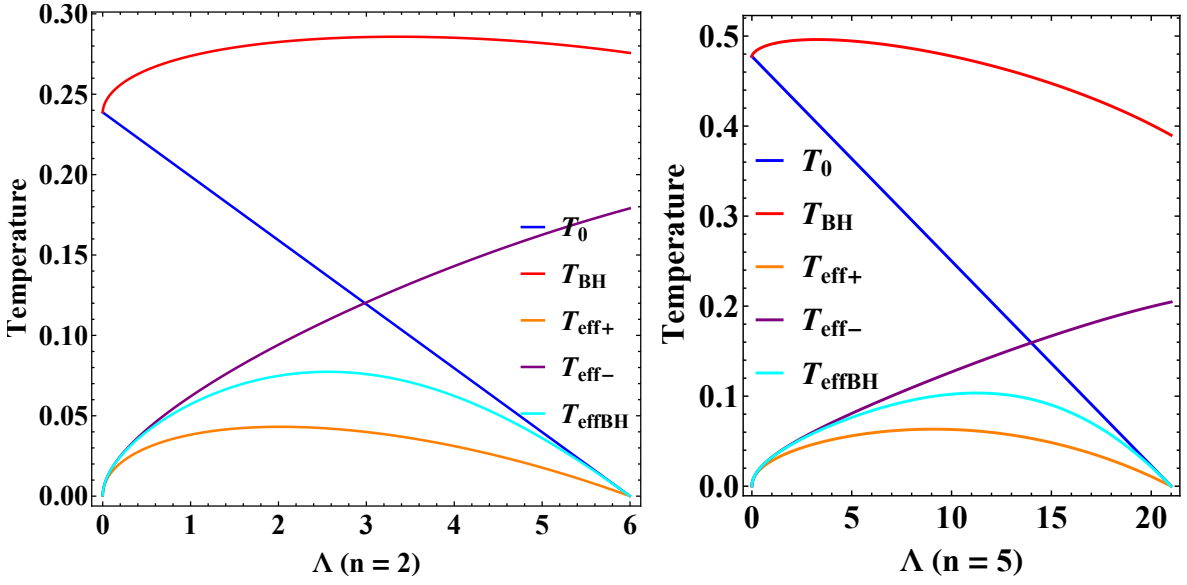

(a) (b)

FIGURE 4.1: Temperatures for a $(4+n)$-dimensional Schwarzschild-de Sitter black hole as a function of the cosmological constant Λ, for: **(a)** $n = 2$, and **(b)** $n = 5$.

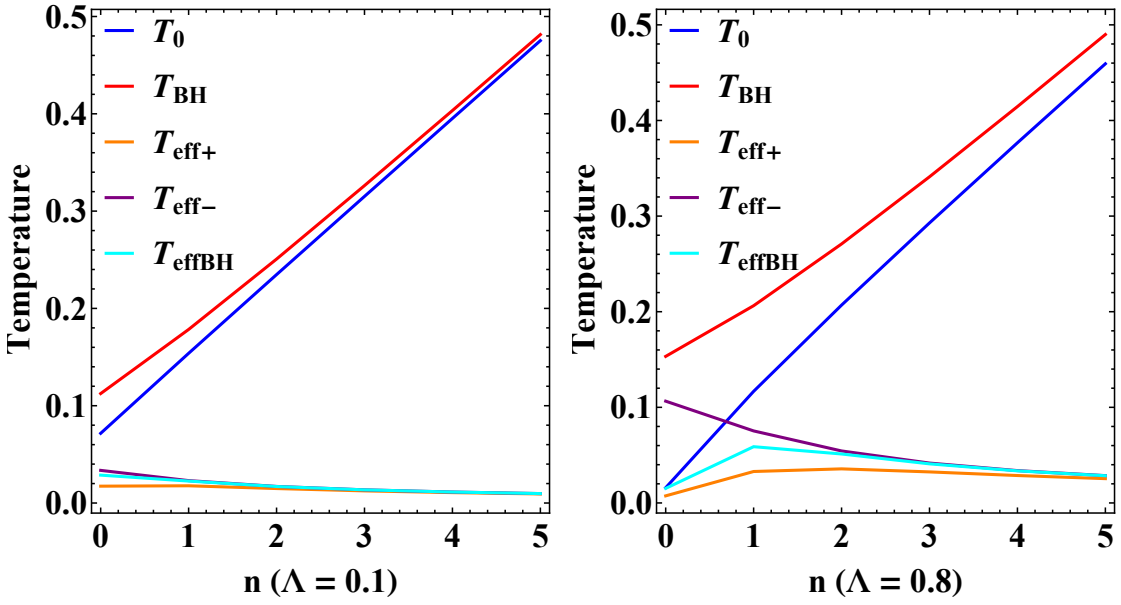

(a) (b)

FIGURE 4.2: Temperatures for a $(4+n)$-dimensional Schwarzschild-de Sitter black hole as a function of the number of extra dimensions n, for: **(a)** $\Lambda = 0.1$, and **(b)** $\Lambda = 0.8$.

thermodynamic law and is studied independently, in the effective thermodynamics proposal a single *postulated* global first law is assigned to the system[2]

$$\delta M = T_{eff}\delta S - P_{eff}\delta V, \tag{4.18}$$

where M is the mass of the black hole, T_{eff} the effective temperature, S is the total gravitational entropy while in the role of pressure we have the cosmological constant $P_{eff} = \Lambda/8\pi$. Finally, the volume V is defined as the thermodynamic conjugate of pressure. In this picture, the system effectively corresponds to a single horizon at temperature T_{eff}.

Depending on the way one interprets the l.h.s. of eq. (4.18) one ends up with different expressions for the black-hole temperature. If the black-hole mass M is identified with the *enthalpy* of the system ($M = -H$) and the total entropy is taken to be the sum of the entropy of the two horizons ($S = S_h + S_c$), then the following effective temperature is obtained [153–158]:

$$T_{eff-} = \left(\frac{1}{T_c} - \frac{1}{T_h}\right)^{-1} = \frac{T_h T_c}{T_h - T_c}\,, \tag{4.19}$$

that is given in terms of both the black-hole (T_h) and cosmological-horizon (T_c) temperatures. In $4+n$ dimensions, after substituting eqs. (4.12) and (4.13) the explicit form of T_{eff-} turns out to be

$$\boxed{T_{eff-} = -\frac{1}{4\pi}\,\frac{(n+1)^2 - (n+1)(n+3)\tilde{\Lambda}(r_h^2 + r_c^2) + (n+3)^2\tilde{\Lambda}^2 r_h^2 r_c^2}{(r_h + r_c)\left[(n+1) - (n+3)\tilde{\Lambda} r_h r_c\right]}}\,. \tag{4.20}$$

[2]Extra "work terms" are included here for more general black holes such ones that are charged and/or rotating.

It is interesting to see what happens to the above expression when we consider the limits $r_h \to 0$ (removing the black hole from the setup) and $r_c \to \infty$ (vanishing cosmological constant). In the former case and according to what one might expect, T_{eff-} reduces to the temperature of the cosmological horizon (4.13). On the other hand, if the limit $r_c \to \infty$ is considered, one does not end up with the black-hole temperature (4.12) but rather with a vanishing result. This shows, that T_{eff-} is valid only for $\Lambda \neq 0$ since the cosmological constant plays the role of the pressure and is always considered to be non-zero and positive in the related analyses. Still, this is not a drawback of the effective approach because the need for such a thermodynamic interpretation arises exactly when $\Lambda \neq 0$.

That is not to say that T_{eff-} is completely free of problems. In more complicated spacetimes such as in the case of the charged SdS, the temperatures of the black-hole (T_h) and cosmological (T_c) horizons are not ordered. This means that depending on the value of the charge we may have $T_h < T_c$, $T_h = T_c$ or even $T_h > T_c$. Thus from eq. (4.19) we see that this effective temperature can be non-positive or even divergent.

The dependence of T_{eff-} on the cosmological constant is shown in Fig. 4.1. We see that it is enhanced with Λ and in the Nariai limit attains a non-zero value, similarly to the Bousso-Hawking normalized black-hole temperature as a consequence of the simultaneous vanishing of its numerator and denominator. Regarding the effect of n on T_{eff-} we see, in Fig. 4.2, that the larger the number of extra dimensions, the more suppressed this effective temperature gets contrary to the behavior exhibited by the black-hole temperatures of eqs. (4.12) and (4.15).

It has been pointed out in [158], that if the total entropy in eq. (4.18) is not taken to be the sum but rather the *difference* between the entropy of the two horizons i.e. $S = S_c - S_h$ then, the corresponding effective temperature

$$T_{eff+} = \left(\frac{1}{T_c} + \frac{1}{T_0}\right)^{-1} = \frac{T_0 T_c}{T_0 + T_c}\,, \tag{4.21}$$

may be defined, that is free of the problems that plague T_{eff-}. This proposal has been characterized as an "ad hoc" one since it can only be justified by the fact that it avoids the pathologies mentioned above.

In Fig. 4.1 we see that in the limit of a vanishing cosmological constant $\Lambda \to 0$, T_{eff+} goes to zero similarly to T_{eff-}, as it is also an effective temperature. Another way to see this is via eq. (4.21) where in this limit, $T_c \to 0$ while $T_0 \neq 0$. As Λ increases, so does T_{eff+} until approximately $0.5\,\Lambda_{crit}$ beyond which point a further increase of Λ results in suppression of T_{eff+}. Finally (and contrary to T_{eff-} this time) in the critical limit, T_{eff+} goes to zero. This vanishing can be seen clearly in eq. (4.21) where due to the fact that $T_0 \to 0$ as $\Lambda \to \Lambda_{crit}$ the numerator vanishes faster than the denominator.

For the $(4+n)$-dimensional SdS black hole the explicit form of eq. (4.21) is

$$\boxed{T_{eff+} = \frac{1}{4\pi}\frac{(n+1)^2-(n+1)(n+3)\tilde{\Lambda}(r_h^2+r_c^2)+(n+3)^2\tilde{\Lambda}^2 r_h^2 r_c^2}{(r_h-r_c)\left[(n+1)+(n+3)\tilde{\Lambda}r_h r_c\right]}}\,. \tag{4.22}$$

Notice that by taking the limit $r_h \to 0$ in the above expression that amounts to removing the black hole from the setup, one recovers the cosmological horizon temperature (4.13), a feature exhibited by T_{eff-} as well.

In [4], inspired by the way that the authors of [158] introduced T_{eff+} in order to deal with the problematic behavior of T_{eff-}, we proposed yet another effective temperature. We have found that if we follow along the calculation that yielded T_{eff-}, by assuming that the total entropy corresponds to the sum of the entropy of the two horizons and merely employ T_{BH} instead of T_0 for the black hole temperature, we end up with

$$T_{effBH} = \left(\frac{1}{T_c}-\frac{1}{T_{BH}}\right)^{-1} = \frac{T_{BH}T_c}{T_{BH}-T_c}\,. \tag{4.23}$$

We believe that this effective temperature is a more "natural" choice compared to T_{eff+}, proposed in [158], since in its derivation the total entropy of the system is obtained as the sum of the entropy on the boundaries. Still, one may argue that the use of the Bousso-Hawking normalization for the black-hole temperature imposes the same normalization for the surface gravity of the cosmological horizon. We have also studied this case and we have found that if one uses $T_{cBH} \equiv T_c/\sqrt{h(r_0)}$ as the temperature for the cosmological horizon, the resultant effective temperature behaves similarly to T_{eff-} for small values of Λ, but is divergent in the critical limit! Of course this is an unacceptable behavior for the temperature and thus this scenario has to be discarded.

By substituting eqs. (4.13) and (4.15) in eq. (4.23) we obtain the following explicit expression for T_{effBH} in $4+n$ dimensions:

$$\boxed{T_{effBH} = -\frac{1}{4\pi}\frac{(n+1)^2-(n+1)(n+3)\tilde{\Lambda}(r_h^2+r_c^2)+(n+3)^2\tilde{\Lambda}^2 r_h^2 r_c^2}{(r_h\sqrt{h(r_0)}+r_c)\left[(n+1)-(n+3)\tilde{\Lambda}r_h r_c\right]}}\,. \tag{4.24}$$

In the limit $r_h \to 0$, the expression above reduces to the temperature of the cosmological horizon (4.13) while for a vanishing cosmological constant it goes to zero similarly to the rest of the effective temperatures. This can be seen both via eq. (4.23) where $T_c \to 0$ while $T_{BH} \neq 0$ and in Fig. 4.1 where the dependence of the temperatures on Λ is depicted. In the Nariai limit, we see that T_{effBH} is vanishing and this is a consequence of the non-zero value of T_{BH} and the fact that $T_c \to 0$ in this limit. To convince oneself that T_c indeed vanishes, one may compare eq. (4.13) with eq. (4.12) and after recalling that in the critical limit $r_h \to r_c$, conclude that $T_0 = T_c$ as $\Lambda \to \Lambda_{crit}$. We also point out the interesting profile of T_{effBH} that matches T_{eff-} and T_0 in the low- and high-Λ regimes respectively as can it can be seen in Fig. 4.1.

Finally, notice that both T_{eff+} and T_{effBH} get monotonically suppressed with the number of extra dimensions as Fig. 4.2 reveals. This of course matches the behavior of T_{eff-} and thus a general conclusion that can be drawn is that all of the effective temperatures we consider in this chapter get suppressed with n.

4.2 Power spectra for minimally-coupled scalar fields.

Now that we have introduced the expressions of various temperatures that are employed in the thermodynamics of the SdS spacetime we turn to the study of their imprint on the Hawking radiation. In this section, we focus on the emission of scalar fields that are non-minimally coupled to gravity and study both the brane and bulk channels of emission. The profile of the spectrum as it appears to the non-accelerated observer located at r_0 (2.14) will be given by the Hawking formula [96, 116, 117]

$$\frac{d^2E}{dt\,d\omega} = \frac{1}{2\pi}\sum_l \frac{N_l\,|A|^2\,\omega}{\exp(\omega/T_h)-1}\,, \tag{4.25}$$

where l is the field angular momentum quantum number, N_l is the multiplicity of states (3.18), $|A|^2$ is the greybody factor (GF), ω is the energy of the emitted particle and T_h is the temperature. In chapter 2 the form of the GF for the HD SdS black hole has been computed analytically albeit employing an approximation scheme and as a result, these expressions are limited in the low-energy regime and for small values of the field coupling ξ and cosmological constant Λ. To compute the power spectra we need the exact form of the GF that is valid for all values of the parameters and throughout the energy regime. The latter has been obtained by means of the numerical technique we developed in chapter 3. Here, we will use these exact forms of the GF to compute the power spectrum for each of the two SdS black-hole temperatures T_0 and T_{BH} as well as for the three effective ones T_{eff-},T_{eff+} and T_{effBH}, and compare the effect that each temperature expression has on the spectrum.

Before we move on to the study of the power spectra, an important comment is in order. The values of the parameters n and Λ used in the figures of this chapter are compatible with the constraint (2.12) that guarantees the existence of only two physical horizons in SdS (even though these values appear to contradict the entries of Table 2.1). To obtain the critical values of Λ_{crit} that are shown in Table 2.1 we had fixed the mass parameter of the metric function (2.7) to $\mu = 1$, while in the analysis of this chapter, we fixed the value of the black-hole horizon $r_h = 1$ and substituted the mass parameter μ via eq. (2.24) evaluated at r_h into eq.(2.12) in order to obtain Λ_{crit}. In Table 4.1 we give the maximum allowed values of Λ corresponding to the Nariai limit, obtained when $r_h = 1$.

4.2.1 Emission on the brane

Starting with the brane channel in Fig. 4.3, we fix the number of extra dimensions to $n = 2$ and use four different values of the cosmological constant namely $\Lambda = 0.8, 2, 4$ and 5 (in units of r_h^{-2}) to plot the power spectra for the various temperatures.

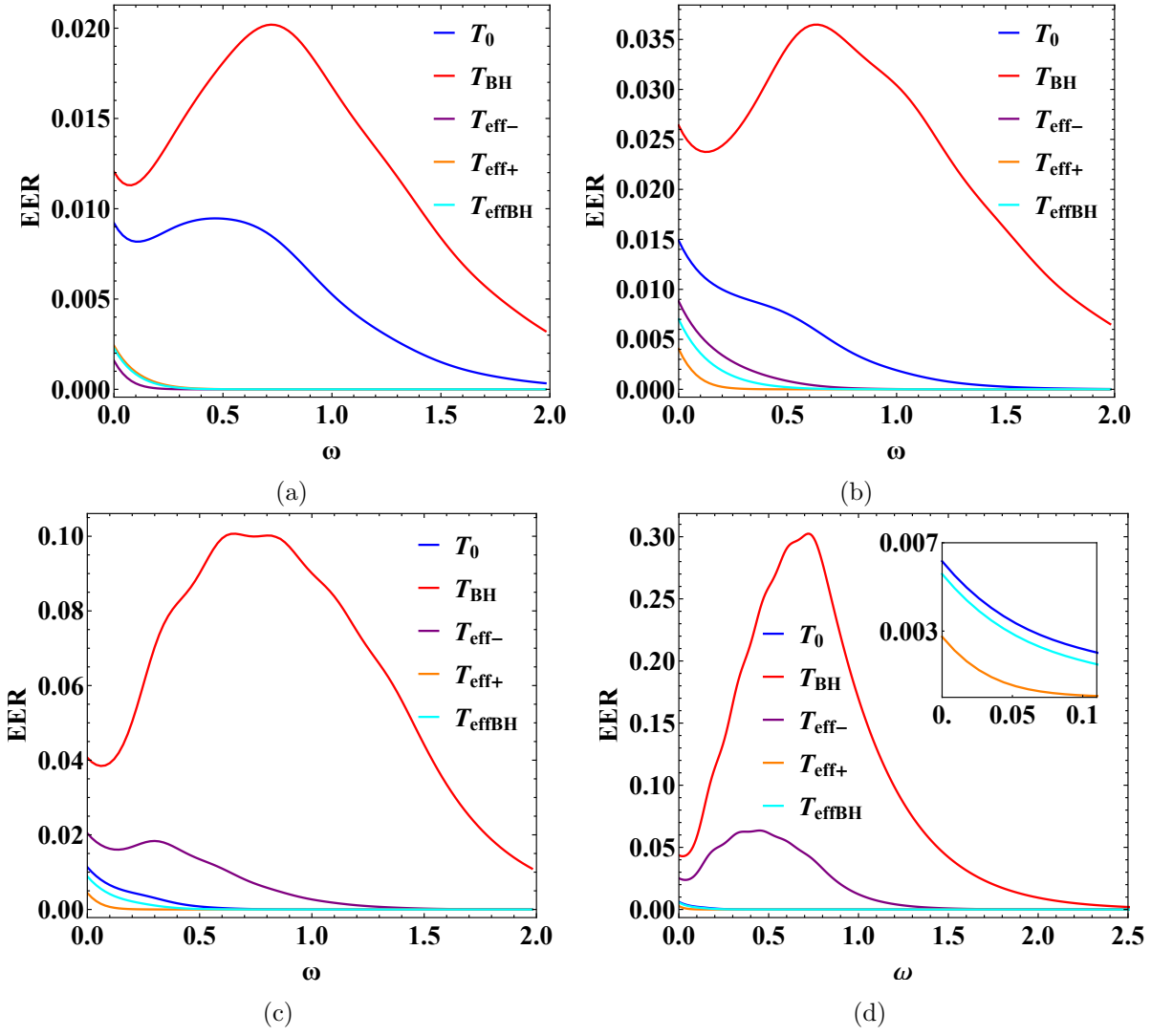

FIGURE 4.3: Energy emission rates for scalar fields on the brane from a 6-dimensional ($n = 2$) Schwarzschild-de Sitter black hole for different temperatures T, and for: **(a)** $\Lambda = 0.8$, **(b)** $\Lambda = 2$, **(c)** $\Lambda = 4$, and **(d)** $\Lambda = 5$ (in units of r_h^{-2}).

Notice that, when $n = 2$ the Nariai limit is reached for $\Lambda = 6\, r_h^{-2}$ (see Table 4.1). So, the four values we have used for Λ (here and in the following figures) have been appropriately chosen in order to

n	0	1	2	3	4	5
$\Lambda_{crit}(r_h^{-2})$	1	3	6	10	15	21

TABLE 4.1: Indicative values of Λ_{crit} for $r_h = 1$ and for $n \in [1, 5] \cap \mathbb{Z}$.

encapsulate the profiles of the spectra away from and close to the critical limit.

In Fig. 4.3(a), we have fixed $\Lambda = 0.8 \approx 0.13\,\Lambda_{crit}$ for which all three of the effective temperatures (see Fig. 4.1) are approximately an order of magnitude smaller than the black hole ones, T_0 and T_{BH}, depicted here with the blue and red curves respectively. It is the smallness of the effective temperatures that leads to the observed heavy suppression of their corresponding differential energy emission rates (EERs). We see that only the black-hole temperatures manage to produce significant emission with the one normalized à la Bousso-Hawking to be the dominant one. In fact, for all values of the cosmological constant, the power spectra corresponding to T_{BH} are always the ones dominating in agreement with Fig. 4.1.

Typically, the form of the EERs is to start from zero in the infrared limit, exhibit a peak for intermediate values of the energy and then fade to zero again in the ultraviolet. So far, in the study of the HD SdS black hole we have seen that the presence of the cosmological constant induces a non-vanishing, low-energy limit for the GF , see eqs. (2.80) and (2.117). This limit results in the radical deviation of the low-energy profile of the spectra as the analysis of the previous chapter has already revealed. Now, in Fig. 4.3 we see that when the temperature is also small, as is the case with the effective temperatures for small values of Λ, the spectra are severally distorted in the intermediate energy regime as well. Notice that the low-energy asymptotic value in these cases is also the maximum value for the EER while as the energy is increased the power curves monotonically decrease to zero. Similar behavior is also observed in the Nariai limit when the temperatures T_0, T_{eff+} and T_{effBH} are employed since they are vanishing close to Λ_{crit}.

By inspection of eq. (4.25) one can see that the low-energy asymptotic limit of the EERs is

$$\left.\frac{d^2E}{dt\,d\omega}\right|_{\omega\to 0} = \frac{1}{2\pi}\sum_l \left.\frac{N_l\,|A|^2\,\omega}{\exp(\omega/T_h)-1}\right|_{\omega\to 0} \approx \frac{|A|^2_{geom}\,T_h}{2\pi}\,, \tag{4.26}$$

where $|A|^2_{geom}$ is the geometric limit of the greybody factor on the brane (2.80), exhibited only for the dominant mode of the field and thus only the $l = 0$ term of the infinite sum contributes. We see that, in the infrared limit, the asymptotic value exhibited by the EERs is proportional to the temperature. This is the reason why we have this "hierarchy" of the infrared limits of the curves (in accordance with Fig. 4.1).

As we have seen in the previous section, the effective temperatures T_{eff-} (purple curve), T_{eff+} (orange curve) and T_{effBH} (cyan curve) are enhanced for intermediate values of Λ . This is why, in Fig. 4.3(b) where $\Lambda = 2 \approx 0.33\,\Lambda_{crit}$ their power spectra are now clearly boosted. Still, for this value of the cosmological constant, it is the black-hole temperatures that produce the most emissive spectra.

As the cosmological constant is further increased in Fig. 4.3(c) to $\Lambda = 4 \approx 0.66\,\Lambda_{crit}$ the curve corresponding to T_{eff-} is greatly enhanced compared to the milder enhancement exhibited by the rest

of the effective temperatures. At the same time, the curve corresponding to the "bare" temperature T_0 gets suppressed and ends up lying below the T_{eff-} one.

Finally, as we approach the Nariai limit with $\Lambda = 5 \approx 0.83\,\Lambda_{crit}$ in Fig. 4.3(d) the effective temperatures T_{eff+} and T_{effBH} as well as T_0 approach zero and so their corresponding emission rates are vanishing. On the other hand, the Bousso-Hawking normalized temperature T_{effBH} and the effective T_{eff-} as we have seen, assume non-vanishing asymptotic values (Fig. 4.1) and thus lead to significant emission. It is worth pointing out that T_{eff-} yields its most enhanced spectra close to the Nariai limit since this temperature is maximized for $\Lambda = \Lambda_{crit}$.

Turning to Fig. 4.4, where we plot the EERs for $n = 5$ ($\Lambda_{crit} = 21\,r_h^{-2}$) and four values of the cosmological constant $\Lambda = 4, 10, 16$ and 18 (in units of r_h^{-2}) we observe a similar behavior to the $n = 2$ case studied above. Regarding the effective temperatures, their power spectra are very suppressed for small values of the cosmological constant and then get slightly boosted as Λ is increased to intermediate values. Close to the critical limit, their corresponding EERs are vanishing save for the one obtained for the temperature T_{eff-} that is again maximized since it asymptotes to a non-vanishing value.

The EER obtained with the "bare" black-hole temperature T_0 becomes gradually suppressed with the increase of Λ until it vanishes in the Nariai limit. On the other hand, the T_{BH} temperature's EER dominates for all the values of the cosmological constant. Even close to the critical limit, where T_{BH} gets slightly suppressed (Fig. 4.1) the latter still yields the most emissive spectrum. Finally, notice that even though the value of T_{BH} is smaller for $\Lambda = 18 r_h^{-2}$ compared to its value when $\Lambda = 16 r_h^{-2}$, as Fig. 4.1 shows, the corresponding EER in Fig. 4.4(d) peaks higher than that of Fig. 4.4(c). The reason behind this behavior is that the profile of the EERs is determined by the combined effect of the value of the temperature and the GF . In the previous chapters, we discovered that for non-minimally coupled scalar fields propagating in the HD SdS spacetime, the GF gets enhanced with the cosmological constant and this is why the power spectrum gets boosted even though the temperature has decreased.

4.2.2 Emission in the bulk

We now turn to the bulk channel of emission in order to study the effect that the different temperatures have on the bulk EERs. Notice that in order to make the comparison between the two channels easier we have used the same values of the parameters n and Λ to plot the spectra.

In Fig. 4.5 we consider two extra spatial dimensions ($n = 2$) and four values of the cosmological constant $\Lambda = 0.8, 2, 4$ and 5 (where for $n = 2$ we have $\Lambda_{crit} = 6\,r_h^{-2}$). The behavior observed here is similar to the brane channel. The Bousso-Hawking normalized temperature (T_{BH}) results to the most emissive black hole even in the bulk under the combined effect of the large numerical value of the temperature and the GF enhancement with Λ. The other black-hole temperature (T_0) yields

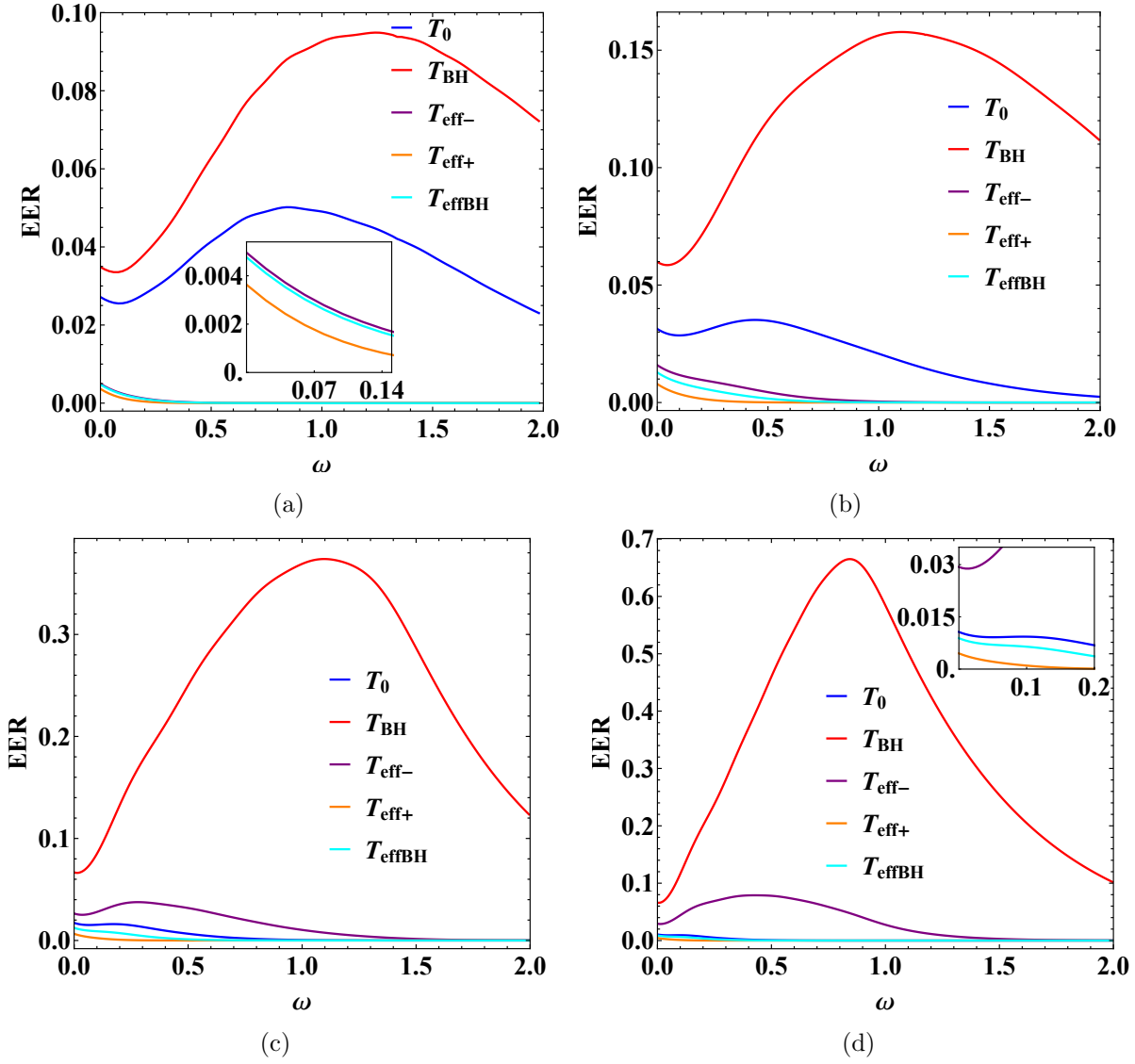

FIGURE 4.4: Energy emission rates for scalar fields on the brane from a 9-dimensional ($n = 5$) Schwarzschild-de Sitter black hole for different temperatures T, and for: **(a)** $\Lambda = 4$, **(b)** $\Lambda = 10$, **(c)** $\Lambda = 16$, and **(d)** $\Lambda = 18$ (in units of r_h^{-2}).

spectra that correspond to a significant amount of emission when Λ is small. For larger values of the cosmological constant, we observe a gradual suppression of its corresponding EERs while as the Nariai limit is approached the emission nearly stops due to the vanishing of the value of T_0 in this limit.

With respect to the effective temperature T_{eff-} we see that its corresponding EER starting from a nearly vanishing spectrum exhibits a gradual enhancement as the value of Λ increases until the critical limit where T_{eff-} obtains its maximum value. In this extreme limit, along with T_{BH}, they are once again the only temperatures that produce non vanishing emission.

Turning now to the impact of the other two "ad hoc" effective temperatures T_{eff+} and T_{effBH} on the emission curves in the bulk, we see that only for intermediate values of Λ we have non-vanishing

power spectra in agreement with the behavior of their corresponding temperatures given in Fig. 4.1.

The typical form of the differential energy emission curves in most cases depicted in Fig. 4.5 remains highly distorted in the bulk channel as well. The combined effect of the low-energy asymptotic limit exhibited by the EERs and the small values of the temperatures are responsible for this distortion of the curves. Only T_{BH} manages to sustain the "typical shape" throughout the allowed values of the cosmological constant, followed by T_0 in the low-Λ regime and T_{eff-} in the critical limit.

If we consider an even larger number of extra dimensions, we see in Fig. 4.6 where $n = 5$ that the EER curves behave similarly to the case with $n = 2$. Comparing the brane (Fig, 4.4) and bulk (Fig. 4.6) channels for a large number of extra dimensions, we observe an important difference. In the bulk, the EERs obtained with the effective temperatures, are always more suppressed than their corresponding ones on the brane. To understand why this is happening, one must recall that for these

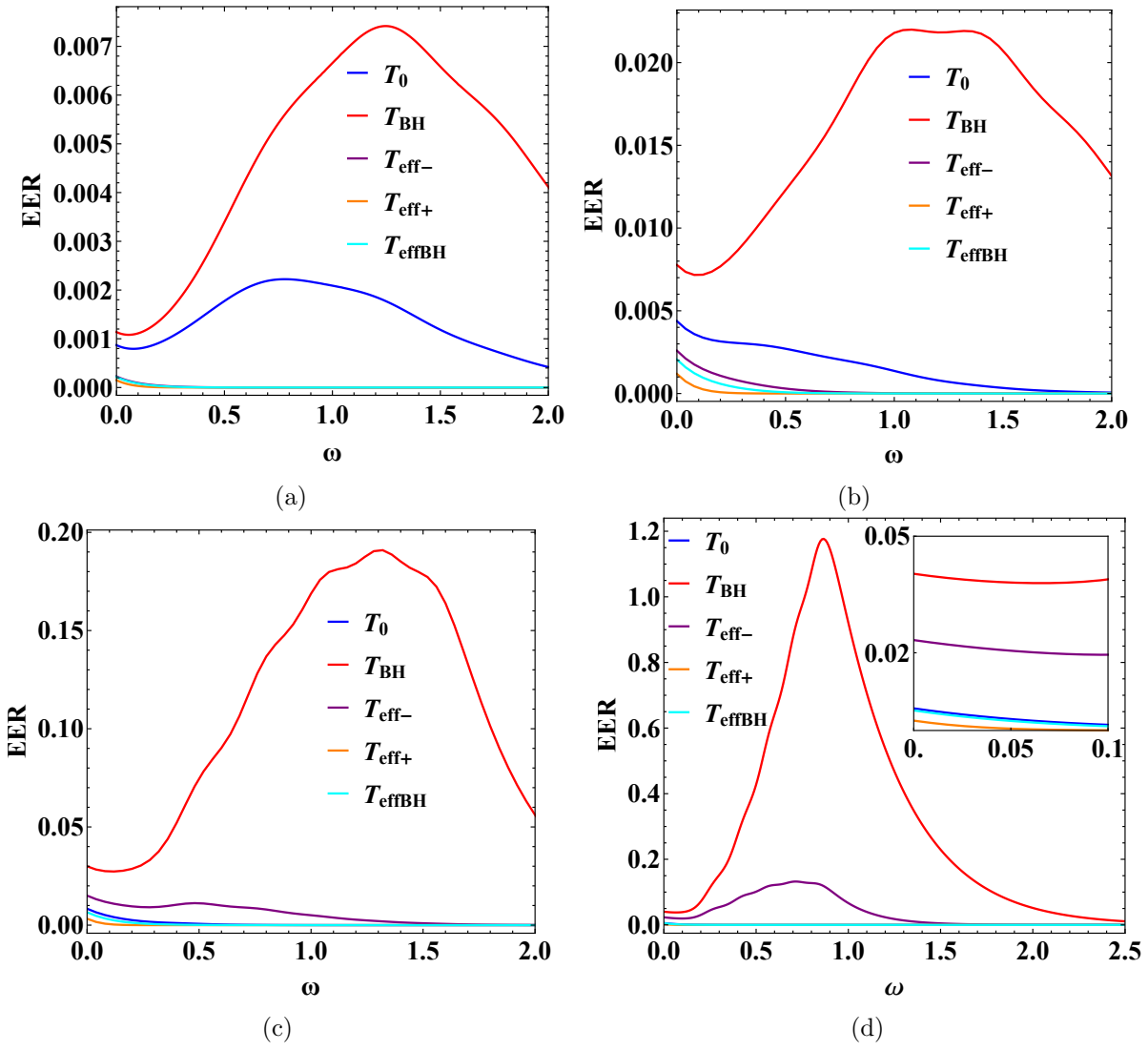

FIGURE 4.5: Energy emission rates for scalar fields in the bulk from a 6-dimensional ($n = 2$) Schwarzschild-de Sitter black hole for different temperatures T, and for: **(a)** $\Lambda = 0.8$, **(b)** $\Lambda = 2$, **(c)** $\Lambda = 4$, and **(d)** $\Lambda = 5$ (in units of r_h^{-2}).

EERs a very important factor that determines the form of the spectra is the low energy-asymptotic limit (4.26). This low-energy limit compensates for the small values of the temperatures and thus helps in "lifting" the curves from vanishing values. Then, a simple inspection of the expressions for the geometric limit ($|A|^2_{geom}$) of the GF , given here in terms of the black-hole (r_h) and cosmological (r_c) horizon radii, on the brane

$$|A|^2_{geom} = \frac{4r_h^2 r_c^2}{(r_c^2 + r_h^2)^2}\,, \tag{4.27}$$

versus the one in the bulk

$$|A|^2_{geom} = \frac{4(r_h r_c)^{(n+2)}}{(r_c^{n+2} + r_h^{n+2})^2}\,, \tag{4.28}$$

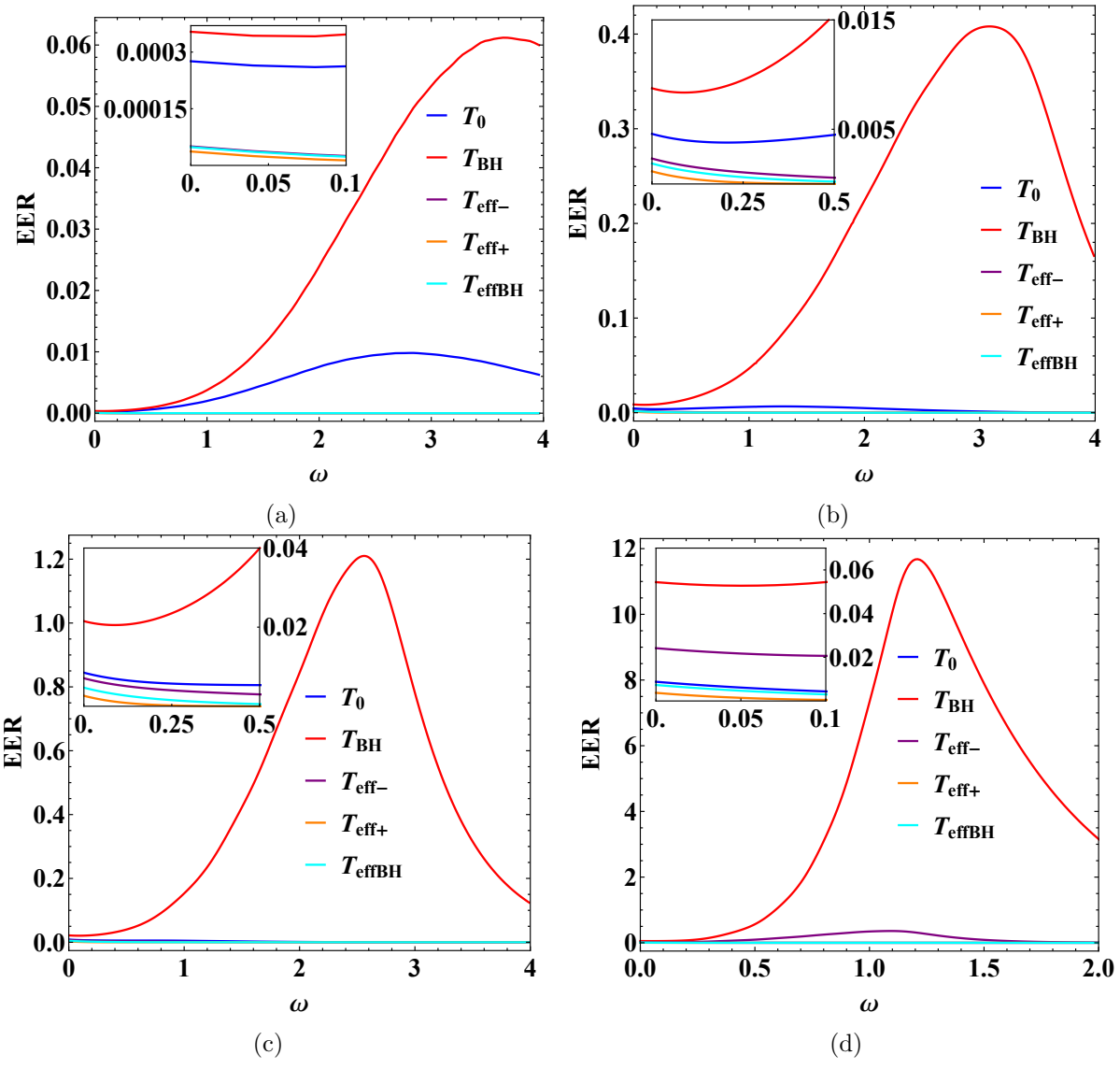

FIGURE 4.6: Energy emission rates for scalar fields in the bulk from a 9-dimensional ($n = 5$) Schwarzschild-de Sitter black hole for different temperatures T, and for: **(a)** $\Lambda = 4$, **(b)** $\Lambda = 10$, **(c)** $\Lambda = 13$ and **(d)** $\Lambda = 18$ (in units of r_h^{-2}).

reveals that as n is increased, the latter gets suppressed compared to the former and this is why the bulk EERs are so much more suppressed than the brane ones for large values of n.

Having completed the study of the power spectra in both the brane and bulk channels for a wide range of values of Λ (even up to the critical limit) we are now in place to draw some conclusions regarding the EERs that correspond to the Bousso-Hawking normalized temperature as an extension of the study performed in the previous chapter. As commented earlier, T_{BH} is the only of the five temperatures considered here, that yields the most typical forms of the power spectra throughout the allowed Λ values. The energy-profile of its corresponding curves as it is depicted in Figs. 4.3-4.6 verifies the results of chapter 3, that the EERs for minimally-coupled scalar fields are enhanced with an increase of the number of extra dimensions and/or with an increase in the value of Λ.

In fact, it is worth pointing out that the cosmological constant boosts the emission of low- and intermediate-energy particles in the following way: First, the low-energy asymptotic limit of the EERs increases with Λ and this boosts the emission of very low-energy particles. Secondly, an effect, that is more evident the larger the number of extra dimensions, is that the peak of the EERs gets shifted towards smaller values of the energy as Λ grows. As a result the intermediate-energy particles become more likely to be emitted.

4.3 Power spectra for non-minimally-coupled scalar fields.

In this section, we consider the propagation of non-minimally coupled scalar fields in the background of the HD SdS black hole again both on the brane and in the bulk. The presence of the field coupling to gravity (ξ), as we have seen in chapter 2, creates an "effective mass" to the otherwise massless scalar field we considered in the previous section. This way, we study in a unified way both the effect of a mass term and a non-minimal coupling to gravity on the spectra.

A second reason that motivates the study of non-minimally coupled fields is based on the conclusions of the previous chapter, indicating that the in the presence of ξ, there is a critical value ξ_{crit} above which the enhancement of the spectra with Λ turns to suppression. Of course, this is a conclusion drawn with the use of the T_{BH} as the temperature of the Hawking radiation and on top of that the study was limited for values of the cosmological constant away from the critical limit. Now, we are going to study the effect of this "dual role" of Λ for values up to Λ_{crit} and also see for the first time how the EERs corresponding to different expressions for the temperature behave in the presence of ξ.

4.3.1 Emission on the brane

In Fig. 4.7 we consider the emission on the brane of a six-dimensional SdS black hole ($n = 2$) when the field coupling is fixed to $\xi = 1$ and the cosmological constant assumes the following four values $\Lambda = 2, 2.8, 4$ and 5 (in units of r_h^{-2}).

A comparison of Fig. 4.7 with Fig. 4.3 shows that a non-zero coupling ξ results in a general suppression of the power spectra. Notice that this is the same effect induced by a mass term for the field [109–111]. As the study of the previous chapters revealed (see figures 3.3 and 3.7), in the non-minimally coupled field case, the larger the value of ξ, the more suppressed the GF gets (a larger value of the field coupling corresponds effectively to a more "massive" field). Thus, the power spectra are universally suppressed regardless of the choice of the expression for the temperature employed.

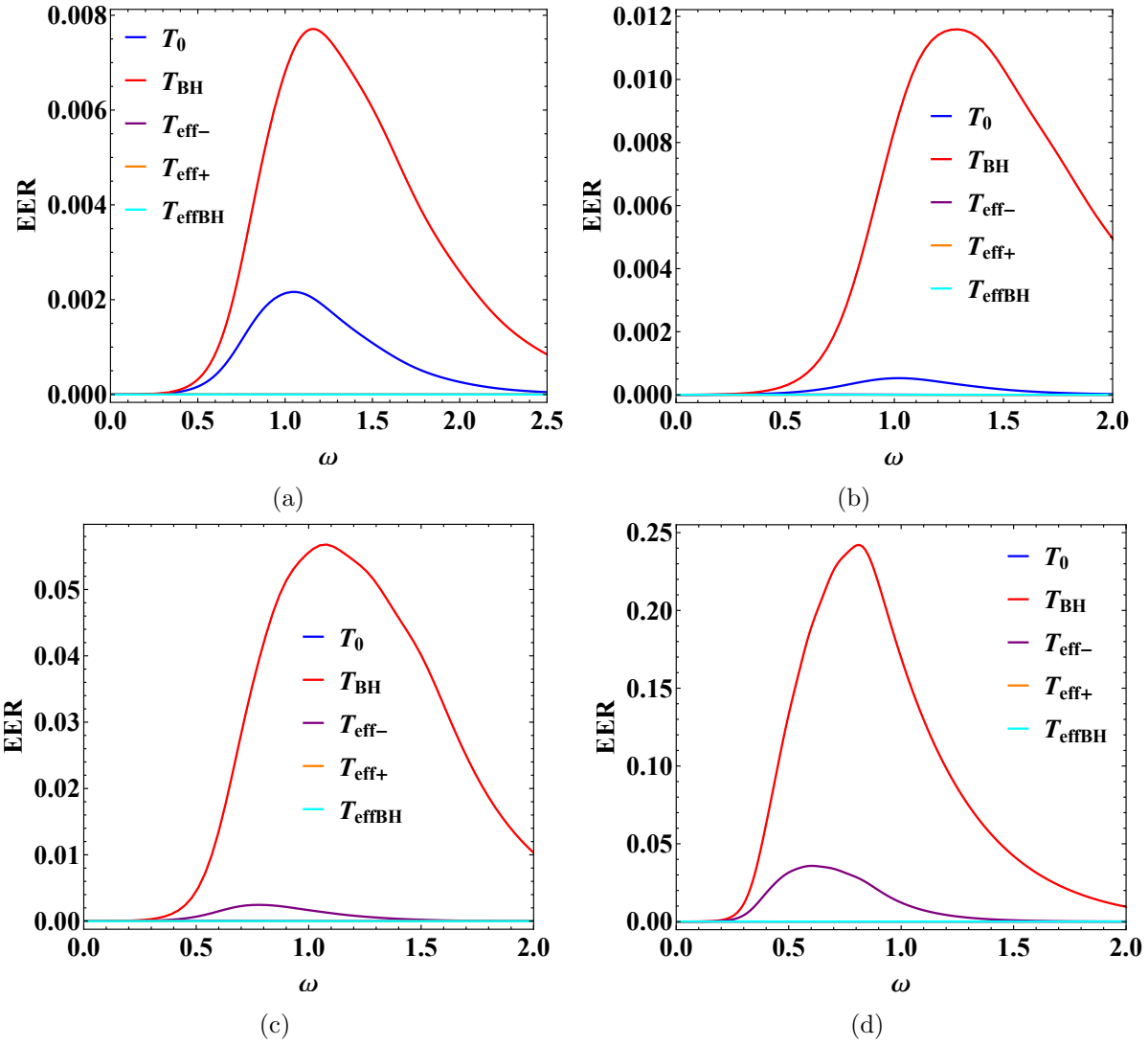

FIGURE 4.7: Energy emission rates for non-minimally coupled brane scalar fields, with $\xi = 1$, from a 6-dimensional ($n = 2$) SdS black hole for different temperatures T, and for: **(a)** $\Lambda = 2$, **(b)** $\Lambda = 2.8$, **(c)** $\Lambda = 4$ and **(d)** $\Lambda = 5$ (in units of r_h^{-2}).

Still, this suppression does not affect all the curves in the same way. A feature one immediately observes in Fig. 4.7, is that the presence of the non-minimal coupling ξ has restored the "typical form" of the power spectra. This is due to the vanishing of the low-energy asymptotic limit of the GF (see chapter 2 for more details) that is responsible for the deformation of the low-energy part of the EERs as we have seen in the previous section. As a consequence, the emission curves corresponding to the effective temperatures and T_0 that exhibit their maxima in the low-energy region get affected the most by a non-vanishing ξ. In contrast, the curves of T_{BH} (and T_{eff-} close to the critical limit) are the ones that are less sensitive to the field coupling.

It is well-known that the presence of a mass for the field (in our case an "effective mass" when $\xi \neq 0$) affects the low-energy region of the EERs by forcing the emission curves to "start rising" from zero at a larger value of ω the more massive the field is. Recall that the magnitude of the effective mass (2.18) is proportional to the product $\xi\Lambda$. So, by naively inspecting the behavior of the power spectrum with T_{BH} as the temperature in Fig. 4.7 one may wonder why as the value of Λ grows, the emission curve "picks up" at smaller values of ω instead. The reason is that T_{BH} gets enhanced with the cosmological constant as depicted in Fig. 4.1 and it is this effect that dominates.

We have performed the same analysis for the brane channel in the case of a larger number of extra dimensions ($n = 5$) and the behavior exhibited by the emission curves follows closely along the one depicted for $n = 2$. The T_{BH} emission curve once again dominates in all cases but due to the larger value of n we observed that in the low-Λ regime the difference between the EERs corresponding to the two black-hole temperatures T_0 and T_{BH} is smaller than the one shown in Fig. 4.7(a). This is a consequence of the fact that the difference between the two temperatures is reduced as n grows (Fig. 4.1).

Again, as the value of Λ is increased, the EER corresponding to the "bare" black-hole temperature gets suppressed until the emission stops at Λ_{crit}. On the other hand, it is exactly in this limit that the emission curve with T_{eff-} as the temperature is maximized and along with the EER corresponding to T_{BH} are the only two curves that produce significant emission.

4.3.2 Emission in the bulk

Turning now to the bulk channel, in Fig. 4.8 we plot the profiles of the emission curves for the various temperatures in $n = 2$ extra dimensions and four values of Λ while the field coupling has been fixed to $\xi = 1$. The power spectrum for the Bousso-Hawking temperature (T_{BH}) clearly dominates. The other black-hole temperature T_0 yields significant amount of emission only for small values of the cosmological constant and is gradually suppressed with an increase in Λ.

The vanishing of the low-energy asymptotic limit of the emission curves due to the presence of ξ in conjunction with the small values of the effective temperatures yields highly suppressed spectra for

these temperatures. Only the curve corresponding to T_{eff-} manages to produce significant emission close to the critical limit. The same behavior for the emission curves in the bulk channel has been observed when the number of extra dimensions is larger ($n = 5$).

Having completed the study of the emission curves both on the brane and in the bulk for minimal and non-minimal coupling of the field as well as for a small and large number of extra dimensions, let us focus once again in the EER of T_{BH} that we had also employed in the study of Hawking radiation in the previous chapter. We would like to address again the question of which is the preferred channel of emission in light of the extended analysis in terms of the range of values for Λ considered in this chapter.

In the minimal coupling case ($\xi = 0$), by comparing the vertical axes of Fig. 4.3 and Fig. 4.5 we

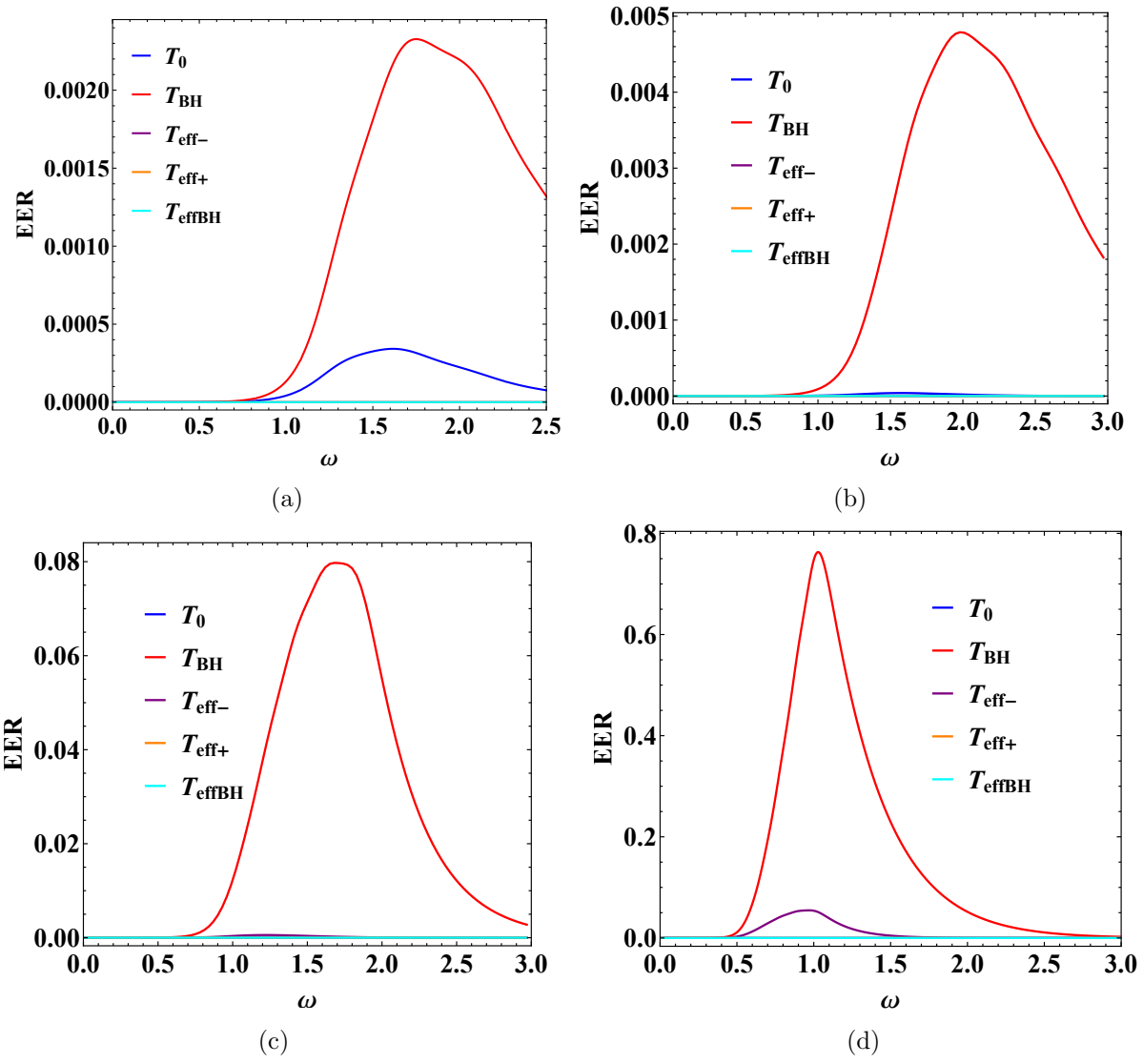

FIGURE 4.8: Energy emission rates for non-minimally coupled bulk scalar fields, with $\xi = 1$, from a 6-dimensional ($n = 2$) SdS black hole for different temperatures T, and for: **(a)** $\Lambda = 2$, **(b)** $\Lambda = 2.8$, **(c)** $\Lambda = 4$ and **(d)** $\Lambda = 5$ (in units of r_h^{-2}).

observe that in the large-Λ regime the bulk channel dominates even for small values of n. This bulk dominance becomes more prominent with n as the comparison between Fig. 4.4 and Fig. 4.6 reveals. For $\xi \neq 0$, by inspection of the vertical axes in Fig. 4.7 and Fig. 4.8 we see that the bulk channel dominates over the brane one for values of Λ larger than approximately $3\, r_h^{-2}$ up until the critical value.

Even though we were able to draw some qualitative conclusions regarding the preferred channel of emission simply by inspection of the profiles of the EERs a more quantitative investigation is deemed necessary. To this end we are led to the calculation of the relative emissivities in the next section.

4.4 Bulk-over-brane relative emissivities

We now focus on the effect the different definitions for the temperature in the SdS spacetime have on the bulk-over brane emissivity ratio. To do this, we integrate the differential energy emission rates throughout the energy regime on the brane and in the bulk and compute their ratio. This way, we are able to conclude which is the preferred channel of emission for the black-hole decay with respect to the values of the parameters of the system (n, Λ and ξ). In the previous chapter the relevant analysis was restricted only to the power spectra obtained with the Bousso-Hawking normalized temperature (4.15) and for values of the cosmological constant far from the critical limit. In this sense the study we perform here supplements and extends the one of section 3.3.2.

The bulk-over-brane emissivity ratio has been computed and the results we obtained for a six-dimensional ($n = 2$) SdS black hole are shown in Tables 4.2 to 4.5. The values for the field coupling and the cosmological constant we employed are respectively $\xi = 0, 0.5, 1, 2$ and $\Lambda = 0.3, 1, 2, 4, 5$. Recall that for $n = 2$ the critical limit corresponds to $\Lambda = 6\, r_h^{-2}$ and so, these values are indicative of the whole allowed range.

Let us start with the bare black-hole temperature T_0 that is the only one of the temperatures we have studied that yields a bulk-over-brane ratio that behaves differently from the rest. When the field is minimally coupled, we observe an enhancement of the bulk channel with the cosmological constant while on the other hand, when ξ is non vanishing, the larger the value of Λ the more favored the brane channel becomes and thus the ratio is decreased. This can be interpreted as a consequence of the

TABLE 4.2: Bulk over brane total emissivity for $n = 2$ and $\xi = 0$

$\Lambda \rightarrow$	0.3	1	2	4	5
T_0	0.259268	0.304247	0.402190	0.663547	0.781833
T_{BH}	0.338245	0.506324	0.798603	1.929660	3.247190
T_{eff-}	0.032997	0.132329	0.319508	0.860880	2.071590
T_{eff+}	0.032507	0.125599	0.298895	0.717772	0.884068
T_{effBH}	0.032950	0.130510	0.309000	0.669669	0.792598

TABLE 4.3: Bulk over brane total emissivity for $n = 2$ and $\xi = 0.5$

$\Lambda \rightarrow$	0.3	1	2	4	5
T_0	0.281627	0.220836	0.160691	0.089933	0.067954
T_{BH}	0.369359	0.450873	0.629061	1.617200	2.962410
T_{eff-}	0.003762	0.012441	0.038311	0.432708	1.710000
T_{eff+}	0.003424	0.008841	0.014009	0.019979	0.021436
T_{effBH}	0.003725	0.011167	0.022578	0.046074	0.052124

TABLE 4.4: Bulk over brane total emissivity for $n = 2$ and $\xi = 1$

$\Lambda \rightarrow$	0.3	1	2	4	5
T_0	0.286455	0.165240	0.089413	0.032550	0.020609
T_{BH}	0.380420	0.387464	0.500779	1.364060	2.704060
T_{eff-}	0.001233	0.003214	0.011410	0.279735	1.433260
T_{eff+}	0.001140	0.002529	0.003787	0.005227	0.005582
T_{effBH}	0.001222	0.002907	0.005497	0.012099	0.013918

TABLE 4.5: Bulk over brane total emissivity for $n = 2$ and $\xi = 2$

$\Lambda \rightarrow$	0.3	1	2	4	5
T_0	0.280978	0.099559	0.035998	0.007446	0.003698
T_{BH}	0.382963	0.287373	0.331984	1.002190	2.289020
T_{eff-}	0.000222	0.000471	0.001935	0.138896	1.045890
T_{eff+}	0.000216	0.000410	0.000580	0.000778	0.000828
T_{effBH}	0.000221	0.000438	0.000738	0.001767	0.002089

vanishing of the low-energy asymptotic limit of the EER when ξ is "switched on". The emission curve with T_0 is among those that exhibit their maximum in the low-energy regime and is thus significantly affected. Clearly the bulk EERs are the ones affected the most in the low-energy region leading to the observed brane channel dominance with Λ.

Turning to the rest of the temperatures, i.e. the three effective ones T_{eff-}, T_{eff+}, T_{effBH} and the Bousso-Hawking normalized one T_{BH}, we observe a similar behavior for the bulk-over-brane ratio. In particular, we see that the brane channel dominates in the low-Λ regime regardless of the value of the field coupling while as Λ assumes larger values, it is the bulk channel that gets enhanced. To understand this, one has to recall firstly that when Λ increases, the peaks of the emission curves in the bulk get shifted towards larger values of the energy and thus more energetic particles are accounted for the emission in this channel. The second factor is that for larger values of Λ the peaks of the emission curves in the bulk are located higher than the corresponding brane ones.

It is interesting to point out the values for the bulk-over-brane ratio obtained when the only two temperatures that asymptote to non-vanishing values in the critical limit (T_{BH} and T_{eff-}) are employed. For these temperatures it is the bulk channel that dominates over the brane even by a factor of 3 close to the critical limit. This bulk dominance has has been anticipated based on the results we obtained in section 3.3.2.

Regarding the effect of the field coupling (ξ) on the ratio, we observe a general suppression, i.e. enhancement of the brane channel of emission, the stronger the field couples to gravity. This effect applies to nearly all values of the cosmological constant as only for small values of Λ the ratio is increased with ξ.

To study the effect of the number of extra dimensions on the bulk-over-brane ratio of emissivities we then set $n = 5$ and for $\xi = 0, 0.5, 1$ and 2 we chose indicative values for $\Lambda = 1, 4, 10, 13$ and $18\, r_h^{-2}$ that once again span the whole allowed range (for $n = 5$ we have $\Lambda_{crit} = 21\, r_h^{-2}$). The results are shown in Tables 4.6 to 4.9.

By inspection of the entries of Tables 4.6 to 4.9 we see that the general behavior we observed in $n = 2$ extra dimensions is exhibited also for $n = 5$ but amplified. As an indicative example, we point out the bulk dominance for T_{BH} and T_{eff-} close to the critical limit for all values of ξ that even yields a bulk-over-brane ratio of approximately 15 when the field is minimally coupled and T_{BH} is employed. Finally, notice that the enhancement of the ratio with ξ that was also observed when $n = 2$ and Λ assumed small values is now sufficient to make the bulk channel the dominant one in this regime for T_{BH} and T_0 (Table 4.9).

TABLE 4.6: Bulk over brane total emissivity for $n = 5$ and $\xi = 0$

$\Lambda \rightarrow$	1	4	10	13	18
T_0	0.296070	0.299653	0.357216	0.422606	0.584868
T_{BH}	0.419245	0.818056	2.578580	4.629670	14.18230
T_{eff-}	0.000267	0.010603	0.140588	0.328066	4.192670
T_{eff+}	0.000265	0.010319	0.137045	0.291825	0.658816
T_{effBH}	0.000267	0.010549	0.134856	0.273098	0.559205

TABLE 4.7: Bulk over brane total emissivity for $n = 5$ and $\xi = 0.5$

$\Lambda \rightarrow$	1	4	10	13	18
T_0	0.468836	0.288097	0.099659	0.054591	0.016835
T_{BH}	0.641474	0.841435	1.770690	3.060490	11.19970
T_{eff-}	$3.152\ 10^{(-6)}$	0.000090	0.002028	0.018275	2.231760
T_{eff+}	$2.898\ 10^{(-6)}$	0.000071	0.000552	0.000923	0.001500
T_{effBH}	$3.139\ 10^{(-6)}$	0.000086	0.000938	0.002127	0.005982

TABLE 4.8: Bulk over brane total emissivity for $n = 5$ and $\xi = 1$

$\Lambda \rightarrow$	1	4	10	13	18
T_0	0.664875	0.248447	0.040067	0.015499	0.002610
T_{BH}	0.890165	0.778299	1.195190	2.049140	9.026680
T_{eff-}	$3.679\ 10^{(-7)}$	0.000007	0.000200	0.003575	1.293840
T_{eff+}	$3.956\ 10^{(-7)}$	0.000006	0.000054	0.000095	0.000164
T_{effBH}	$3.683\ 10^{(-7)}$	0.000007	0.000080	0.000187	0.000616

TABLE 4.9: Bulk over brane total emissivity for $n = 5$ and $\xi = 2$

$\Lambda \rightarrow$	1	4	10	13	18
T_0	1.162700	0.179527	0.009087	0.002170	0.000160
T_{BH}	1.509360	0.632852	0.585960	1.010350	6.207500
T_{eff-}	0.000274	$1.054\ 10^{(-6)}$	$6.508\ 10^{(-6)}$	0.000305	0.514108
T_{eff+}	0.000299	$1.653\ 10^{(-6)}$	$1.827\ 10^{(-6)}$	$3.402\ 10^{(-6)}$	$6.292\ 10^{(-6)}$
T_{effBH}	0.000275	$1.033\ 10^{(-6)}$	$2.328\ 10^{(-6)}$	$5.573\ 10^{(-6)}$	0.000022

4.5 The effect of the temperatures on Hawking radiation in 4 dimensions

As Fig. 4.1 shows, when it comes to the dependence of the temperatures on the number of extra dimensions (n) we have two groups. The first one consists of the black-hole temperatures T_0 (4.12) and T_{BH} (4.15) and the second of the effective ones T_{eff-} (4.19), T_{eff+} (4.21) and T_{effBH} (4.23). The larger n gets, the more the temperatures in each group converge to each other. Thus it is clear, that for the lowest value of $n = 0$ the largest differences between the temperatures appear. So, it is interesting to study their effect on the differential energy emission rates of 4-dimensional ($4d$) SdS black holes.

By setting $n = 0$ in the expressions of the temperatures presented in the introduction, we obtain their $4d$ forms given here for convenience. In terms of the radii of the black-hole (r_h) and cosmological (r_c) horizons we have the bare black-hole and cosmological horizon temperatures respectively:

$$T_0 = \frac{1-\Lambda r_h^2}{4\pi r_h} \quad , \quad T_c = -\frac{1-\Lambda r_c^2}{4\pi r_c} \, , \tag{4.29}$$

where Λ is the value of the cosmological constant. The Bousso-Hawking normalized temperature is

$$T_{BH} = \frac{1}{\sqrt{h(r_0)}} \frac{1-\Lambda r_h^2}{4\pi r_h} \, , \tag{4.30}$$

where $h(r_0)$ is the value of the metric function (2.7) evaluated at the location of the non-accelerated observer in SdS (2.14). The three effective temperatures assume the following simplified forms in $4d$:

$$T_{eff-} = -\frac{(1-\Lambda r_h^2)(1-\Lambda r_c^2)}{4\pi (r_h + r_c)(1-\Lambda r_h r_c)} \, , \tag{4.31}$$

$$T_{eff+} = -\frac{(1-\Lambda r_h^2)(1-\Lambda r_c^2)}{4\pi (r_c - r_h)(1+\Lambda r_h r_c)} \, , \tag{4.32}$$

and

$$T_{effBH} = -\frac{(1-\Lambda r_h^2)(1-\Lambda r_c^2)}{4\pi (r_h \sqrt{h(r_0)} + r_c)(1-\Lambda r_h r_c)} \, . \tag{4.33}$$

Finally, in this $4d$ context, we may further extend our study with the inclusion of one more expression

of an effective temperature. This expression was historically the first one to be proposed in 2009 for the effective description of the SdS thermodynamics by Urano et al.[153]. Employing the Iyer-Wald formalism [159, 160], an effective first law was derived and the black-hole mass was interpreted as the internal energy ($M = U$), the entropy as the sum of the entropy of the two horizons ($S = S_h + S_c$), while the volume corresponding to the causal volume of SdS namely $V = V_c - V_h$. The expression for the effective temperature thusly obtained is

$$T_{effEIW} = \frac{r_h^4\, T_c + r_c^4\, T_0}{(r_h + r_c)\,(r_c^3 - r_h^3)}\,. \tag{4.34}$$

The reason we only study the effect of T_{effEIW} on the EERs in 4 dimensions, is that the derivation of this temperature involves 3-dimensional spatial volumes and may thus only be employed in $4d$.

Taking the limit $r_c \to \infty$ of eq. (4.34) that corresponds to a vanishing cosmological constant, one recovers the black-hole temperature T_0. This is the only temperature of the 4 effective ones that we consider here that has this low-Λ asymptotic limit since all the rest go to zero. By construction, T_{effEIW} requires the presence of the black hole in the setup while the rest require a non-vanishing cosmological constant.

In Fig. 4.9 we plot the dependence of the $4d$ expressions of the six temperatures on the cosmological constant up to the critical limit that for $n = 0$ corresponds to $\Lambda_{crit} = 1\, r_h^{-2}$.

It is the behavior of T_{effEIW} that is the most interesting one in this plot, since the rest of the temperatures behave similarly to their HD expressions and they have already been studied in depth. Still, it is worth mentioning that a comparison with Fig. 4.1 reveals a dominance of T_{BH} for all values

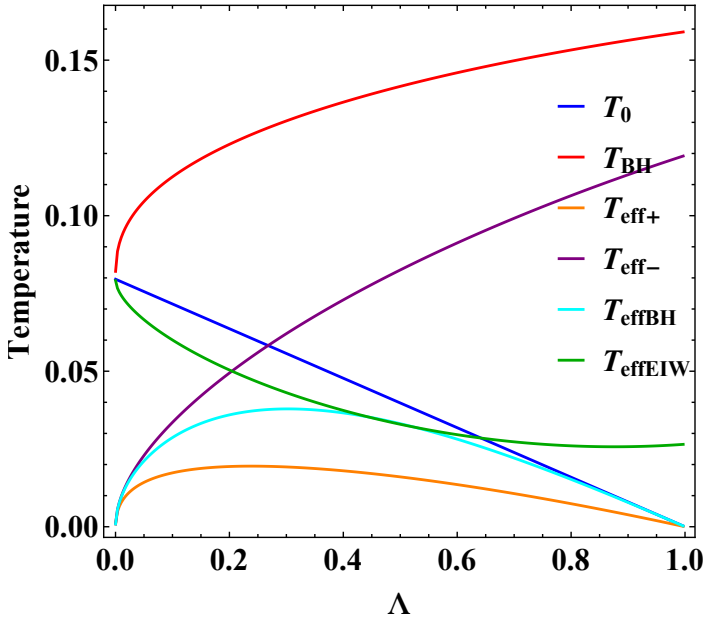

FIGURE 4.9: Temperatures for a Schwarzschild-de Sitter black hole (from top to bottom in the low-Λ regime: T_{BH}, T_0, T_{effEIW}, T_{eff-}, T_{effBH}, and T_{eff+}) as a function of the co- smological constant Λ.

of Λ in four dimensions as well but it is a dominance that is significantly less prominent. This holds for the bare temperature T_0 that also dominated in the low-Λ regime. The reason behind this is that the temperatures T_{BH} and T_0 (including T_{effEIW}), in the limit of a vanishing cosmological constant asymptote to the temperature of the Schwarzschild black hole that in n extra dimensions is

$$T_0|_{\Lambda\to 0} = \frac{(1+n)}{4\pi r_h}\,, \tag{4.35}$$

where the horizon radius is given in terms of the black-hole mass (M) and the fundamental scale of gravity (M_*) via [161]

$$r_h = \frac{1}{\sqrt{\pi}M_*}\left(\frac{M}{M_*}\right)^{\frac{1}{n+1}}\left(\frac{8\Gamma\left(\frac{n+3}{2}\right)}{n+2}\right)^{\frac{1}{n+1}}\,. \tag{4.36}$$

The Schwarzschild black-hole temperature (4.35) is minimized in four dimensions ($n = 0$) as it can be clearly seen in Fig. 4.10 where we plot its variation with respect to the extra dimensions. As a consequence of the above, we anticipate that the EERs of all the temperatures (in the largest part of the allowed Λ values) to be more comparable with each other.

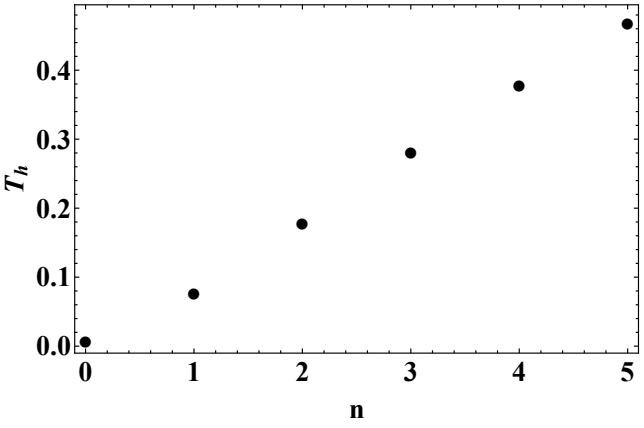

FIGURE 4.10: The Schwarzschild black-hole temperature (4.35) for $M_* = 1$, $M = 5\,M_*$ and $n \in [0, 5]$.

Focusing on the profile of T_{effEIW} in Fig. 4.9, we see that as the cosmological constant increases its value, it is rapidly decreased at first and then more slowly for intermediate values of Λ until it asymptotes to a non-vanishing value at the critical limit along with T_{BH} and T_{eff-}. In contrast to the latter two temperatures that attain their maximum values at Λ_{crit}, the T_{effEIW} is minimized in this limit while exhibiting its maximum at $\Lambda \to 0$ where it is identified with the black-hole temperature T_0.

4.5.1 The 4-dimensional emission spectra

In this section we study the imprint of the six temperatures on the $4d$ differential energy emission rates of the SdS black hole. Starting with the case of a minimally coupled ($\xi = 0$) scalar field in Fig.

4.11 we plot their corresponding EERs for two indicative values of the cosmological constant. The first one $\Lambda = 0.1\, r_h^{-2}$ is far from Λ_{crit}, while the second one $\Lambda = 0.8\, r_h^{-2}$ is appropriate to encapsulate the profile of the spectra close to the critical limit.

Since there is no field coupling in this case, the effective mass is zero and the characteristic infrared asymptotic limit (4.26) of the emission curves is present. For the small value of $\Lambda = 0.1\, r_h^{-2}$ of Fig. 4.11(a) we see that when the Bousso-Hawking normalized temperature is employed, the most emissive spectra are produced in accordance with Fig. 4.9. Also, this is the only emission curve that peaks away from the low-energy limit. All the other temperatures yield EERs that exhibit their maxima at their corresponding low-energy asymptotic limits and monotonically reduce to zero for larger values of the energy.

In Fig. 4.11(b) where the critical limit has been approached, the emission curves corresponding to T_{BH} and T_{eff-} are greatly enhanced since these temperatures are close to their maximum values (Fig. 4.9). All the other power spectra are suppressed with curves that produce insufficient emission due to the small values of their corresponding temperatures. Notice that even though T_{effEIW} asymptotes to a non-vanishing value at the Nariai limit, this value is not large enough to yield an emission curve with the typical profile.

We now "switch on" the field's coupling to gravity ($\xi = 1/6$) in Fig. 4.12 while using the same values for the cosmological constant namely $\Lambda = 0.1\, r_h^{-2}$ and $\Lambda = 0.8\, r_h^{-2}$ to enable easy comparison between different cases.

Comparing Fig. 4.12(a) with Fig. 4.11(a) we see that the presence of ξ suppresses all the emission curves regardless of the temperature employed and it is their low-energy part that gets affected the

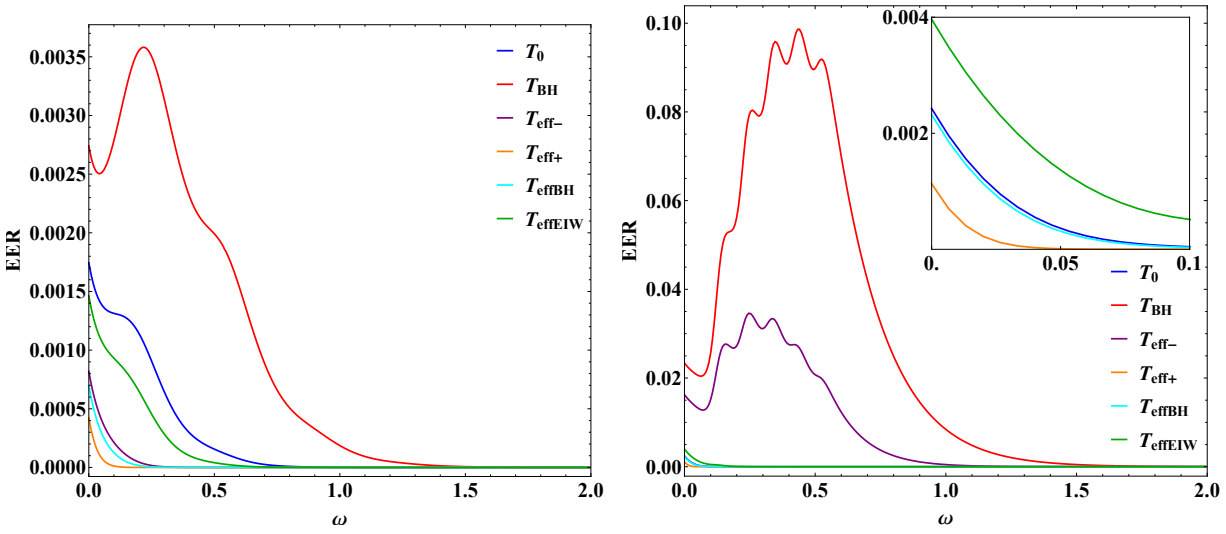

(a) (b)

FIGURE 4.11: Energy emission rates for minimally-coupled scalar fields from a Schwarzschild-de Sitter black hole for: **(a)** $\Lambda = 0.1$ (in units of r_h^{-2}), and $T = T_{BH}, T_0, T_{effEIW}, T_{eff-}, T_{effBH}, T_{eff+}$ (from top to bottom), and **(d)** $\Lambda = 0.8$ and $T = T_{BH}, T_{eff-}$ (from top to bottom, again).

most with the vanishing of low-energy asymptotic limit. This way the curves assume the characteristic form of the EERs where they start from zero in the infrared, exhibit a maximum for intermediate values of the energy and then reduce to zero again in the ultraviolet part of the spectrum. Notice also that in contrast to the higher-dimensional case, in 4-dimensions, all the temperatures for $\Lambda \approx 0.1\Lambda_{crit}$ assume values that are relatively close to each other (Fig. 4.9) and so the power spectra for all of the temperatures can be seen to peak sufficiently above zero.

In Fig. 4.13 we consider the case where the field couples even stronger to gravity with $\xi = 1/2$ and we see that there is a further suppression of the emission curves. We report that the same behavior is observed if we increase the value of ξ even further. Finally, notice that the suppression of the EERs with ξ is more intense for the low-Λ regime compared with the regime close to Λ_{crit}. This observation will play a role in the interpretation of the results we obtained for the total emissivity of the SdS black hole which is the subject of the next subsection.

4.5.2 Total emissivities in 4 dimensions

To calculate the total emissivity (TE) of the SdS black hole we integrate the differential energy emission rate (4.25) throughout the energy regime. This corresponds to evaluating the surface area under the EER curves. We performed this calculation for every one of the six different definitions for the temperature when the field coupling is $\xi = 0, 1/6, 1/2$ and the cosmological constant spans the whole allowed regime with the indicative values $\Lambda = 0.1, 0.3, 0.5$ and 0.8 (in units of r_h^{-2}). Our results are shown in Tables 4.10 to 4.12.

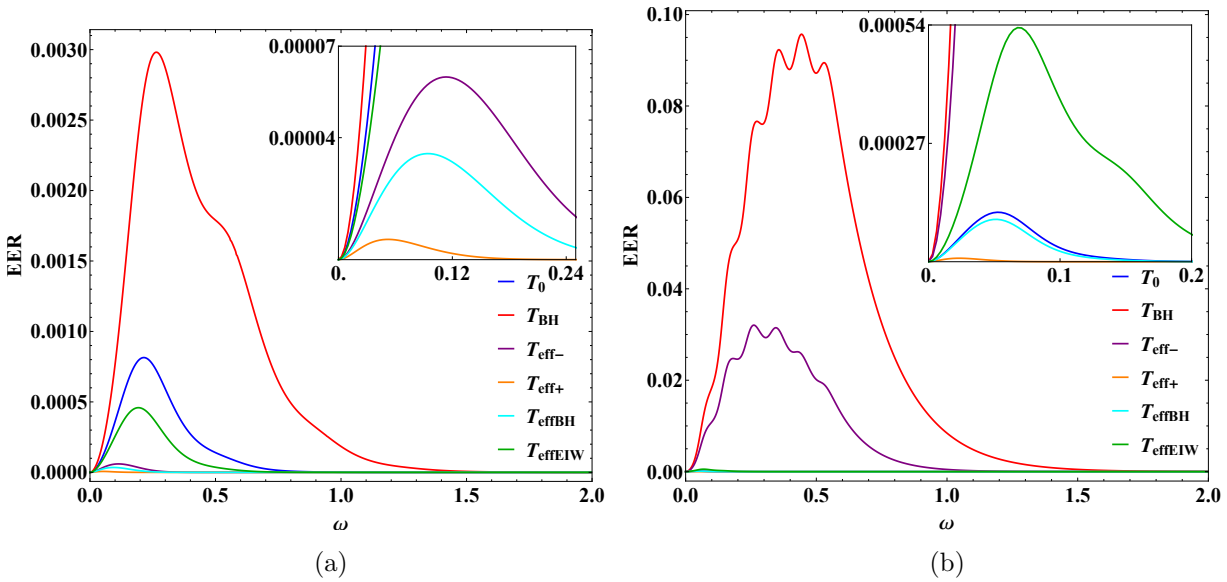

FIGURE 4.12: Energy emission rates for non-minimally-coupled scalar fields with $\xi = 1/6$ from a Schwarzschild-de Sitter black hole for: **(a)** $\Lambda = 0.1$ (in units of r_h^{-2}), and $T = T_{BH}$, T_0, T_{effEIW}, T_{eff-}, T_{effBH}, T_{eff+} (from top to bottom), and **(d)** $\Lambda = 0.8$ and $T = T_{BH}, T_{eff-}$ (from top to bottom, again).

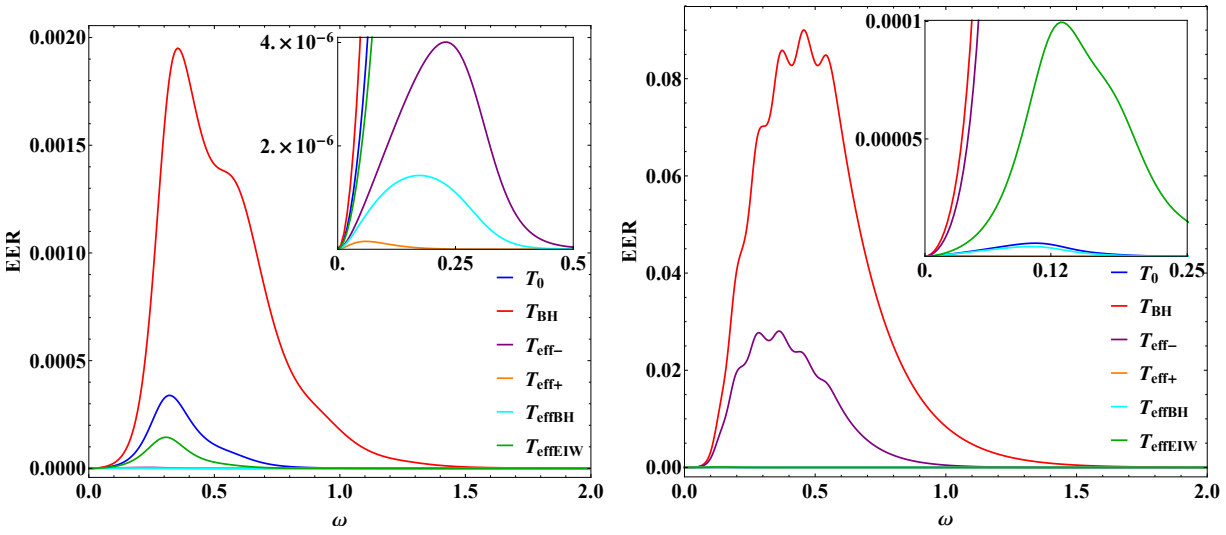

(a) (b)

FIGURE 4.13: Energy emission rates for non-minimally-coupled scalar fields with $\xi = 1/2$ from a Schwarzschild-de Sitter black hole for: **(a)** $\Lambda = 0.1$ (in units of r_h^{-2}), and $T = T_{BH}$, T_0, T_{effEIW}, T_{eff-}, T_{effBH}, T_{eff+} (from top to bottom), and **(d)** $\Lambda = 0.8$ and $T = T_{BH}, T_{eff-}$ (from top to bottom, again).

Starting with the minimally coupled field case ($\xi = 0$), we see that as the cosmological constant increases, the black-hole total emissivity, when the bare temperature T_0 is employed, decreases. Comparing its values at $\Lambda = 0.1\, r_h^{-2}$ and $\Lambda = 0.8\, r_h^{-2}$ we observe the the latter constitutes only the 14% of the former. Similarly, a suppression is observed when the T_{effEIW} temperature is used, only this time the decrease is milder with the total emissivty close to the critical limit being 73% of its value at $\Lambda = 0.1\, r_h^{-2}$.

TABLE 4.10: Total emissivity for $\xi = 0$

$\Lambda \rightarrow$	0.1	0.3	0.5	0.8
T_0	0.000444	0.000487	0.000335	0.000065
T_{BH}	0.001871	0.005432	0.011837	0.054554
T_{eff-}	0.000058	0.000636	0.002106	0.015937
T_{eff+}	0.000013	0.000047	0.000050	0.000014
T_{effBH}	0.000040	0.000200	0.000225	0.000060
T_{effEIW}	0.000266	0.000267	0.000222	0.000196

TABLE 4.11: Total emissivity for $\xi = 1/6$

$\Lambda \rightarrow$	0.1	0.3	0.5	0.8
T_0	0.000228	0.000124	0.000057	$7.5796\ 10^{(-6)}$
T_{BH}	0.001358	0.003647	0.008889	0.050743
T_{eff-}	$9.8980\ 10^{(-6)}$	0.000191	0.001040	0.013964
T_{eff+}	$0.5696\ 10^{(-6)}$	$1.3972\ 10^{(-6)}$	$1.2237\ 10^{(-6)}$	$0.2977\ 10^{(-6)}$
T_{effBH}	$5.0160\ 10^{(-6)}$	0.000026	0.000027	$6.3134\ 10^{(-6)}$
T_{effEIW}	0.000112	0.000044	0.000026	0.000054

TABLE 4.12: Total emissivity for $\xi = 1/2$

$\Lambda \rightarrow$	0.1	0.3	0.5	0.8
T_0	0.000087	0.000021	$6.1253\ 10^{(-6)}$	$0.5443\ 10^{(-6)}$
T_{BH}	0.000837	0.002126	0.006062	0.045459
T_{eff-}	$0.8973\ 10^{(-6)}$	0.000040	0.000433	0.011571
T_{eff+}	$0.0164\ 10^{(-6)}$	$0.0316\ 10^{(-6)}$	$0.0251\ 10^{(-6)}$	$0.0057\ 10^{(-6)}$
T_{effBH}	$0.3206\ 10^{(-6)}$	$1.7945\ 10^{(-6)}$	$1.8766\ 10^{(-6)}$	$0.4070\ 10^{(-6)}$
T_{effEIW}	0.000033	$4.1488\ 10^{(-6)}$	$1.8064\ 10^{(-6)}$	0.000012

In the considered range of Λ values $(0.1 - 0.8\, r_h^{-2})$ and contrary to the behavior of the TEs for T_0 and T_{effEIW}, the temperatures T_{BH} and T_{eff-} result in an enhancement of the TE of the order of 30 and 300 respectively with the increase in Λ. Regarding finally the effect of the "ad hoc" temperatures T_{eff+} and T_{effBH} we see that the TEs get enhanced at first until the intermediate values of Λ and then decrease again as the critical limit is approached. Notice that the behavior of the TEs observed here follows closely the profile of the temperatures as it is depicted in Fig. 4.9.

The effect of the field coupling on the TEs at any given value of the cosmological constant and regardless of the choice for the temperature is to cause suppression. This is in accordance to the interpretation of the non-minimal coupling term of the field equivalently as an effective mass term.

Focusing now to the combined effect of ξ and Λ on the TEs we see that as the cosmological constant increases from $0.1\Lambda_{crit}$ to $0.8\Lambda_{crit}$, the value of ξ modifies differently the enhancement or suppression of the TE. More precisely, we see that when $\xi = 1/6$ and T_0 is employed, the suppression of the TE is of the order of 3% while at a larger coupling $\xi = 1/2$ it is of the order of 0.6% only. For the same variation in Λ $(0.1\, r_h^{-2} \rightarrow 0.8\, r_h^{-2})$ the enhancement caused in the TE when T_{BH} is employed is of the order of 37 for $\xi = 1/6$ while for $\xi = 1/2$, it is of the order of 54.

Finally, the most impressive boost in the enhancement of the TE with an increase of ξ is seen when the effective temperature T_{eff-} is used. At $\xi = 1/2$ the value of the TE close to the critical limit compared with its value in the low-Λ regime appears enhanced by a factor of 1400 and this factor skyrockets to 12000 when $\xi = 1/2$.

4.6 The effect of the higher modes of the field on the EERs close to the Nariai limit

So far in this chapter, we computed the EERs for various temperatures, considering values of the cosmological constant up to the critical limit. In the calculation we took into account only the first 5 scalar field modes because higher modes have insignificant contributions to the spectrum as they

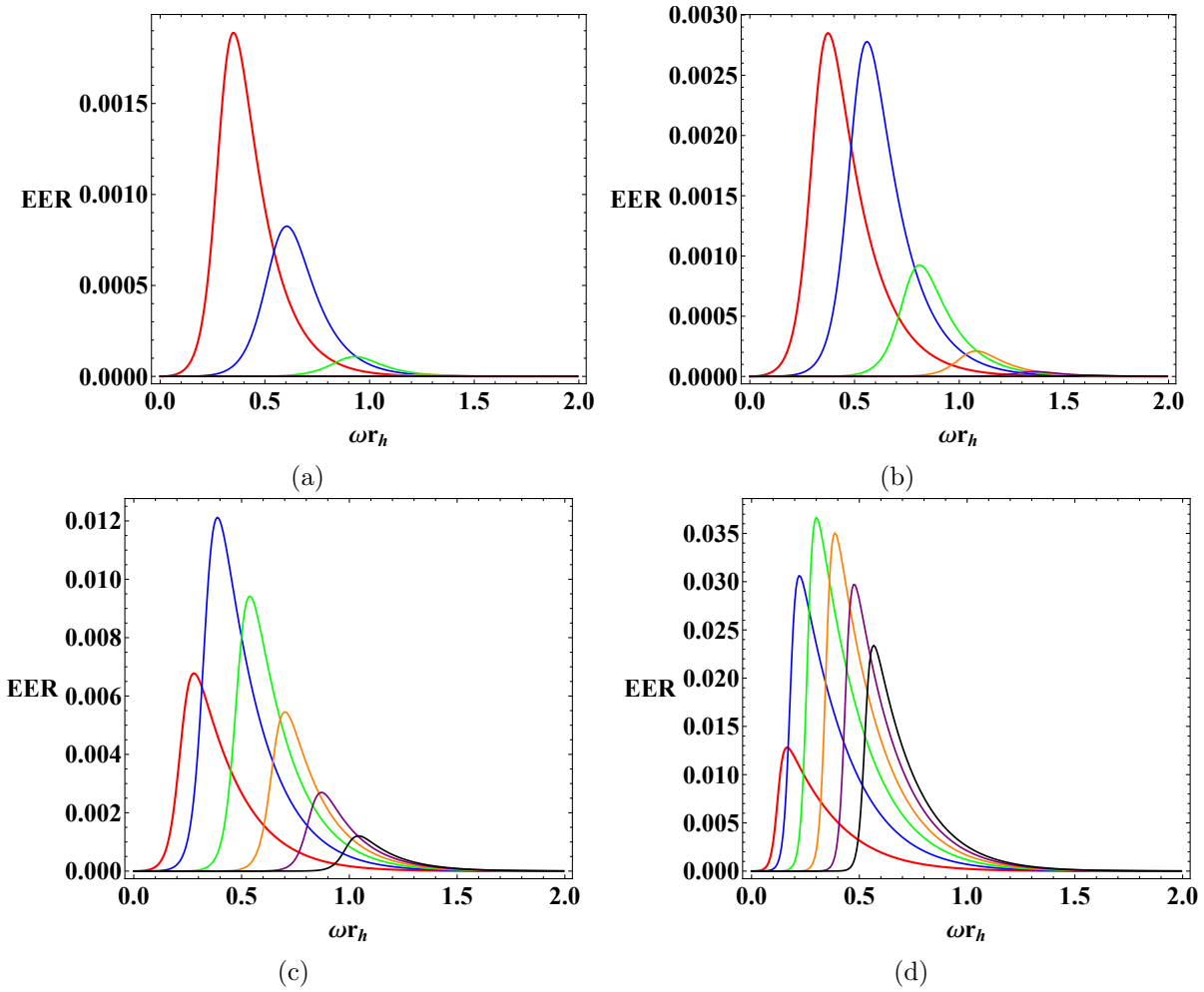

FIGURE 4.14: The first five field modes when T_{BH} is employed and $n = 0$, $\xi = 0.5$ while Λ equals (a) $0.1\,\Lambda_{crit}$, (b) $0.3\,\Lambda_{crit}$, (c) $0.6\,\Lambda_{crit}$ and (d) $0.8\,\Lambda_{crit}$

peak many orders of magnitude below the dominant mode of the field. As we will now demonstrate this is true only far away form the critical limit!

As we can see in Fig. 4.14 where the first five modes are given (the leftmost peak is always $l = 0$ and moving to the right we get one mode number up with each peak), as Λ increases, up until about $0.5\,\Lambda_{crit}$ it is a good approximation to truncate the EER sum to $l = 5$.

Notice in Figs. 4.14(b) that already for $\Lambda = 0.3\,\Lambda_{crit}$ the "dominant mode" ($l = 0$) is comparable with ($l = 1$)! For values of Λ larger than $\sim 0.5\Lambda_{crit}$ higher modes need to be taken into account as they contribute to the "tail" of the emission curve. This is demonstrated in Fig. 4.15 where we used the Bousso-Hawking normalized temperature in four dimensions and for $\Lambda = 0.8\Lambda_{crit}$, $\xi = 0.5$, we plot the EER when we take into account the first 5 (red curve), 13 (blue dashed curve) and 20 (green dashed curve) modes of the field.

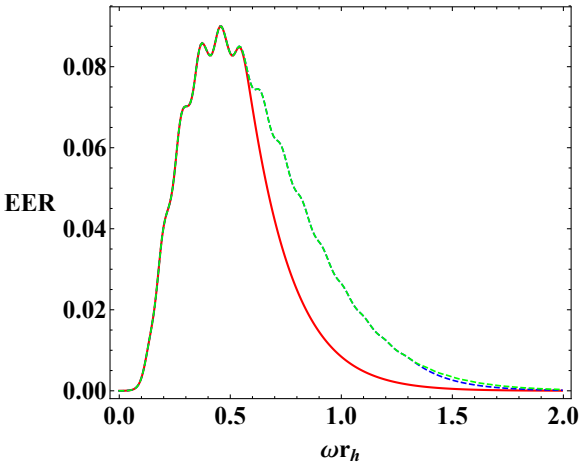

FIGURE 4.15: For T_{BH}, in four dimensions, when $\Lambda = 0.8\Lambda_{crit}$ and $\xi = 0.5$ we give here the first 5 modes ($l = 0 - 5$) summed up with red, ($l = 0 - 13$) with blue dashed and ($l = 0 - 20$) with green dashed.

4.6.1 The enhancement of the higher modes of the field close to Λ_{crit}

We recall here for convenience the formula for the Hawking power spectrum

$$\frac{d^2E}{dt\,d\omega} = \frac{1}{2\pi}\sum_l \frac{N_l\,|A|^2\,\omega}{\exp(\omega/T_h)-1} = \left[\frac{\omega(2\pi)^{-1}}{\exp(\omega/T_h)-1}\right]\left[\sum_l N_l\,|A|^2\right]. \tag{4.37}$$

Obviously, the energy-profile of the EER is determined by the product of the two terms in the square brackets. If we denote the first term with:

$$\Omega(\omega,T_h) \equiv \frac{\omega(2\pi)^{-1}}{\exp(\omega/T_h)-1}, \tag{4.38}$$

then

$$\frac{d^2E}{dt\,d\omega} = \Omega(\omega,T_h)\left[\sum_l N_l\,|A_l|^2\right], \tag{4.39}$$

where $|A_l|^2$ is the GF of the l-th mode of the field. For the Bousso-Hawking normalization of the temperature (4.15), in $n = 2$ dimensions the $\Omega(\omega, T_h)$ function's energy profile as Λ ranges from $\Lambda = 0$ to $\Lambda = \Lambda_{crit} = 6r_h^{-2}$ is depicted in Fig. 4.16.

If we focus now for simplicity on the brane channel, the multiplicity of states will be given by $N_l = 2l + 1$. Then eq. (4.39) for the first few modes is written as

$$\begin{aligned}\frac{d^2E}{dt\,d\omega} &= \Omega(\omega,T_h)\left[N_0\,|A_0|^2 + N_1\,|A_1|^2 + N_2\,|A_2|^2 + N_3\,|A_3|^2 + \ldots\right]\\ &= \Omega(\omega,T_h)\left[|A_0|^2 + 3\,|A_1|^2 + 5\,|A_2|^2 + 7\,|A_3|^2 + \ldots\right].\end{aligned} \tag{4.40}$$

Clearly, the contribution of the GFs of the higher field modes to the spectrum is enhanced due to the monotonic increase in the multiplicity-of-states factor N_l. Let us now define the following function

$A^{(l)} \equiv N_l \, |A_l|^2$. In Fig. 4.17 we give the first four functions $A^{(l)}$ when $n = 2$ and $\xi = 1$. Essentially, these are just the plots for the GF for the first four modes of the field multiplied by some constant number (N_l) that is larger the higher the mode of the field. In the low-Λ and low-(ωr_h) region it is the mode $l = 0$ that dominates as it is expected.

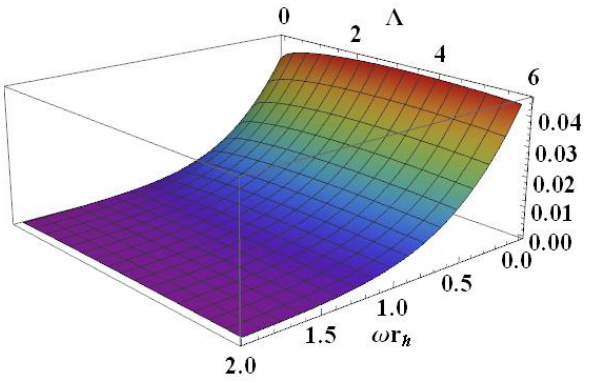

FIGURE 4.16: The $\Omega(\omega, T_h)$ function.

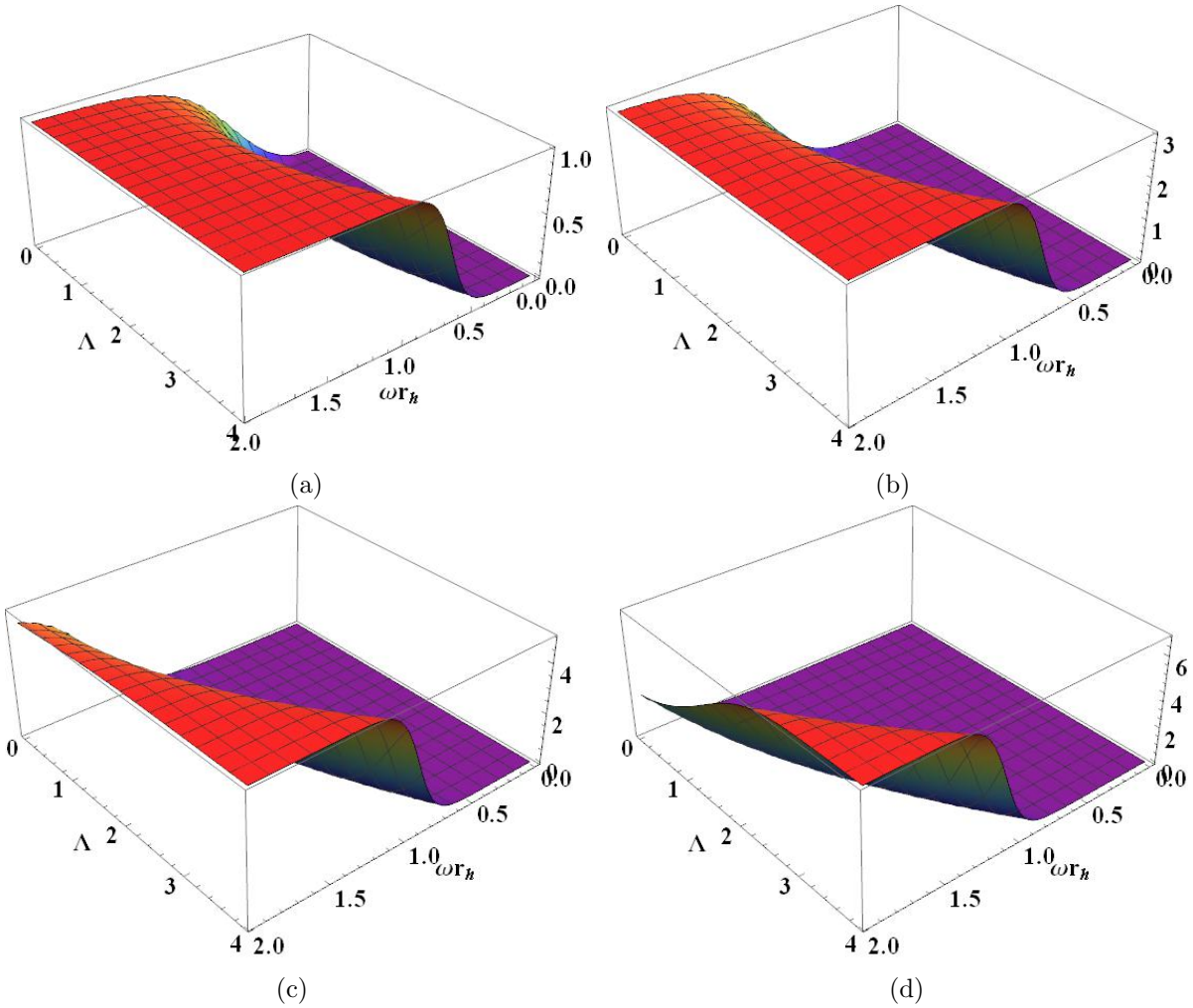

FIGURE 4.17: The functions $A^{(l)} \equiv N_l \, |A_l|^2$ for $n = 2$ and $\xi = 1$, for the mode **(a)** $l = 0$, **(b)** $l = 1$, **(c)** $l = 2$, and **(d)** $l = 3$.

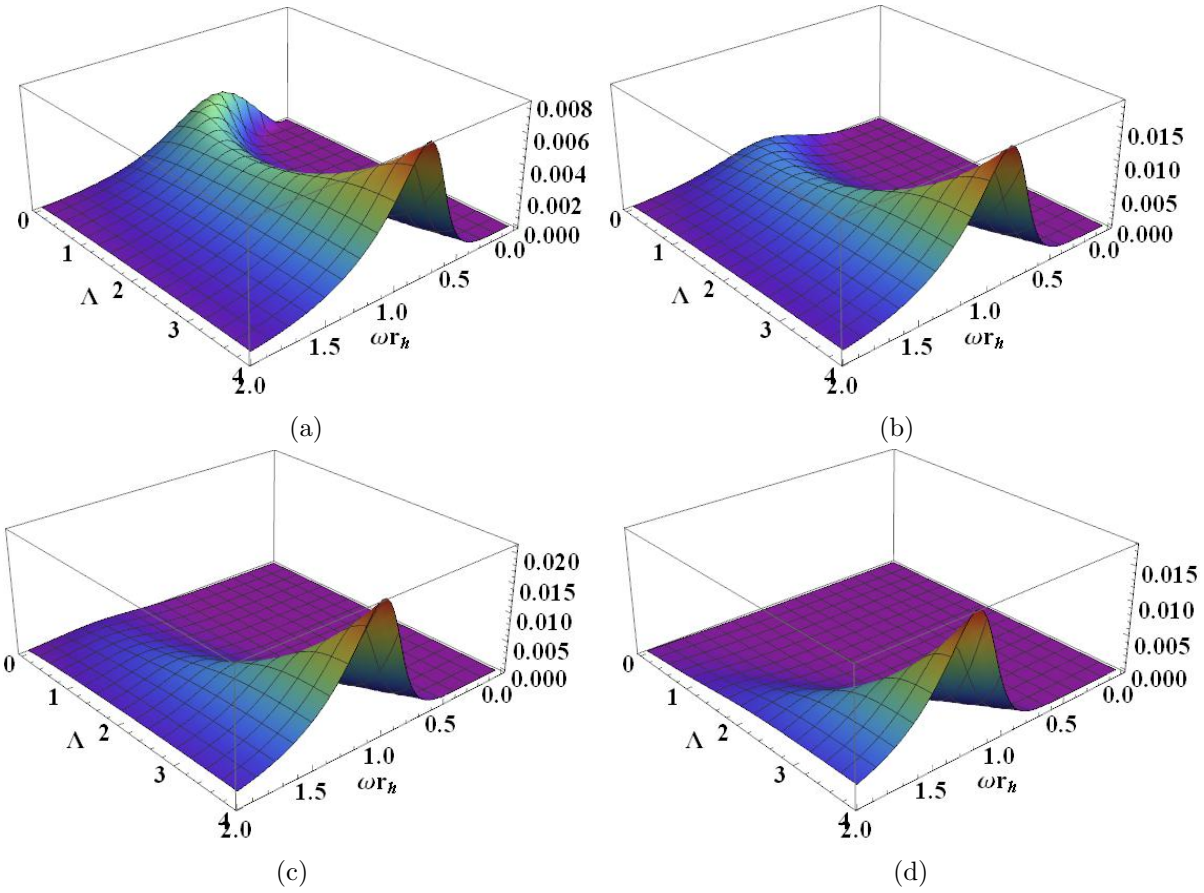

FIGURE 4.18: The functions $S^{(l)} \equiv \Omega(\omega, T_h)A^{(l)}$ for $n = 2$ and $\xi = 1$, for the mode **(a)** $l = 0$, **(b)** $l = 1$, **(c)** $l = 2$, and **(d)** $l = 3$.

Turning now again to eq. (4.40), we write the contribution of each field mode to the *total* EER as

$$\frac{d^2E}{dt\, d\omega} = \Omega(\omega, T_h)A^{(0)} + \Omega(\omega, T_h)A^{(1)} + \Omega(\omega, T_h)A^{(2)} + \ldots \equiv S^{(0)} + S^{(1)} + S^{(2)} + \ldots , \tag{4.41}$$

where we have defined $S^{(l)} \equiv \Omega(\omega, T_h)A^{(l)}$. In this notation, it is then clear that the contribution to the spectrum by the mode $l = 0$ (for example) is quantified in the function $S^{(0)}$ and its energy profile will be the product of Fig. 4.16 and Fig. 4.17(a). The result of the latter multiplication is given in Fig. 4.18(a). Similarly, in the rest of the panels of Fig. 4.18, the higher-mode contributions to the EER are shown. Finally, summing up these 4 modes one gets the EER profile that is depicted in Fig. 4.19.

The way that the product between Figs. 4.16 and 4.17 works is as follows. The $\Omega(\omega, T_h)$ term of Fig. 4.16 "cuts" the high-energy part of the GF because the former vanishes for energy larger than about $\omega r_h = 1.8$ for the case we study here. Then, only the low-energy part of the GFs (or equivalently the functions $A^{(l)}$ of Fig. 4.17) survives in this product. It is the part that "manages to fit under" the surface of Fig. 4.16.

Given the form of the $A^{(l)}$ functions in Fig. 4.17, it is clear that for small values of Λ, only the

dominant mode $l = 0$ manages to "fit under" the surface of Fig. 4.16. On the other hand, for larger values of Λ the higher modes of the field "fit under" the surface of Fig. 4.16 as well. In this case though, due to the multiplicity-of-states factor N_l the small part of $A^{(l)}$ (Fig. 4.17) that fits under the surface of Fig. 4.16 is greatly enhanced compared to the $l = 0 \to N_0 = 1$ mode $A^{(0)}$ and in this way we have the dominance of the higher modes close to the critical limit.

4.6.2 Other black-hole temperatures and higher modes close to Λ_{crit}

In our papers [4, 5], we have studied the power-spectra close to the critical limit but we haven't studied *independently* the forms of the GFs in this limit. In Fig. 4.20 we plot once again the behavior of the first four functions $A^{(l)} \equiv N_l |A_l|^2$, where N_l is the multiplicity of states and $|A_l|^2$ is the GFfor the l-th field mode, this time up to the critical limit.

If we ignore for the moment the scales (determined by N_l), the plots in Fig. 4.20 are just the energy profiles of the GFs for the first four modes on the brane as Λ ranges from 0 to $\Lambda_{crit} = 6$. We see that the dominant mode $l = 0$ indeed dominates in the low energy region for any value of Λ. In the $\Lambda \to \Lambda_{crit}$ regime now, notice that all GFs curves (independently of the value of l) start to "pick up" at very low-energies. If now the scales are also taken into account, it is then evident that close to the critical limit, the higher-modes dominate.

From the discussion of the previous section it is clear that two effects contribute to the extreme amplification of the higher-modes (HMs) in the critical limit. On the one hand we have the magnification of their corresponding GFs ($|A_l|^2$) by a factor of N_l that gets larger with the field mode number l. The second effect comes from the form of the function $\Omega(\omega, T_h)$. In the case of the Bousso-Hawking normalization the profile of Ω is given in Fig. 4.16. Because T_{BH}, and consequently $\Omega(\omega, T_h)$, are non-vanishing in the critical limit the extreme amplification of the GFs of the higher-modes "runs wild" and thus we have a divergent spectrum in this region. A solution then would be to consider a temperature that vanishes in the critical limit in order to counter the effect of the magnification of

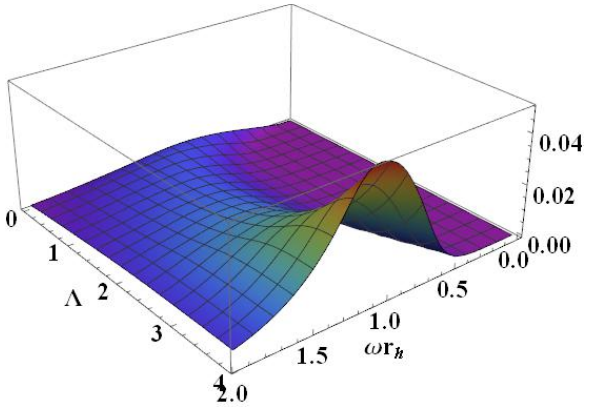

FIGURE 4.19: The contribution of the first four modes of Fig. 4.18 to the EER.

the GFs of the higher modes. One such temperature is of course the bare black-hole one (T_0). For this temperature the function $\Omega(\omega, T_h)$ has the profile shown in Fig. 4.21.

Similarly to the analysis of the previous section, the individual contribution of each field mode l to the total EER will be quantified by the functions $S^{(l)} \equiv \Omega(\omega, T_h)A^{(l)}$. For T_0 as the choice for the

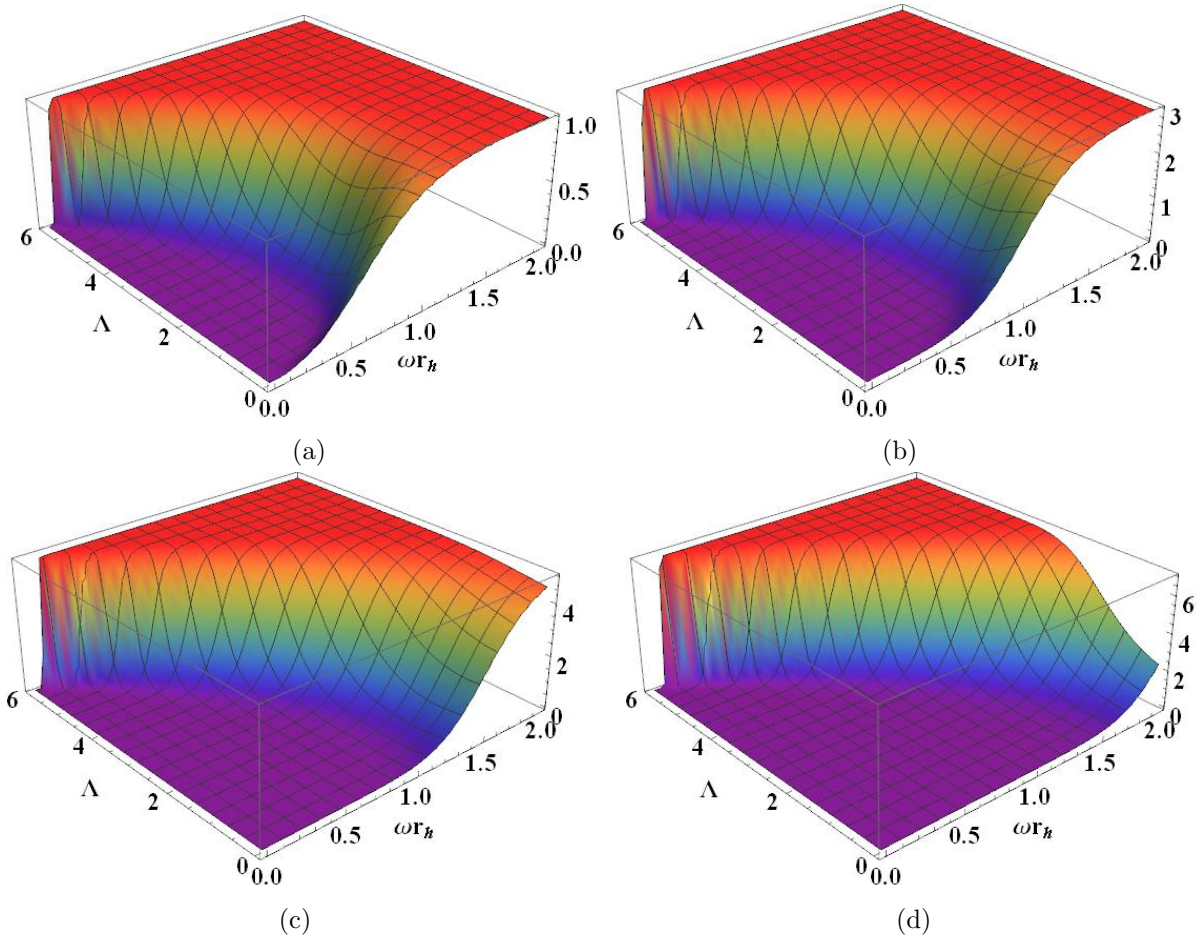

FIGURE 4.20: The functions $A^{(l)} \equiv N_l \, |A_l|^2$ for $n = 2$ and $\xi = 1$. Given here up to Λ_{crit}, for the mode **(a)** $l = 0$, **(b)** $l = 1$, **(c)** $l = 2$, and **(d)** $l = 3$.

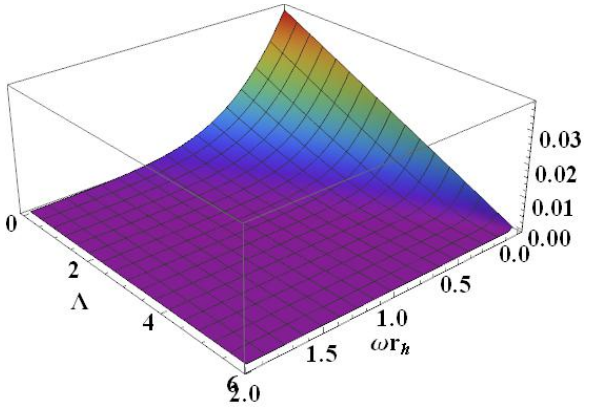

FIGURE 4.21: The $\Omega(\omega, T_h)$ function for the temperature T_0 as Λ ranges from 0 up to the critical limit.

temperature, the first four functions $S^{(l)}$ will have a profile that is given by the product of Fig. 4.21 with each one of the panels in Fig. 4.20. The results (pay attention to the way the 3d plots are oriented with respect to the energy-axis!) are shown in Fig. 4.22. Clearly the higher modes are suppressed for all values of Λ. This is due to the fact that in the region that the surface of Fig. 4.21 is non-zero (and thus allows for non-vanishing contributions of the GFs to the spectrum), namely for small ωr_h and small Λ, the functions $A^{(l)}$ have extremely small values. In fact, the higher the mode number l the corresponding function $A^{(l)}$ moves further away from this region (as Fig. 4.20 clearly shows). On the other hand, close to Λ_{crit} where $A^{(l)}$ are greatly enhanced, the vanishing of $\Omega(\omega, T_h)$ truncates them before they yield any significant contribution to the spectrum. The resultant EER with these first four modes summed is given in Fig. 4.23

Finally, let us consider one last case where the temperature starts from zero at $\Lambda \to 0$, increases to a maximum value and then decreases to zero again in the limit $\Lambda \to \Lambda_{crit}$. We employ the T_{effBH} expression for the temperature as an indicative case with the aforementioned behavior. Then, the profile of $\Omega(\omega, T_h)$ is given in Fig. 4.24.

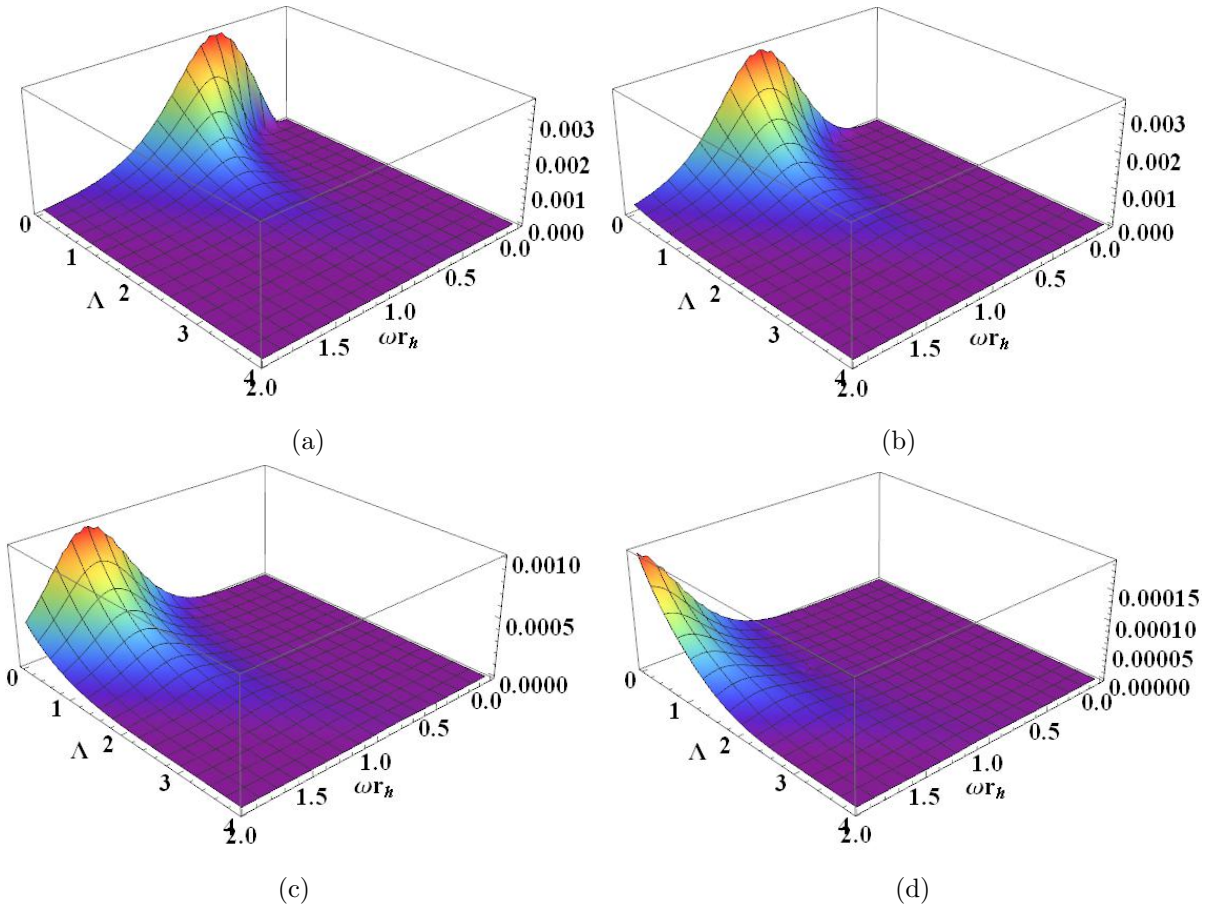

FIGURE 4.22: The functions $S^{(l)} \equiv \Omega(\omega, T_h)A^{(l)}$ for $n = 2$ and $\xi = 1$. For the temperature T_0 and for the mode **(a)** $l = 0$, **(b)** $l = 1$, **(c)** $l = 2$, and **(d)** $l = 3$.

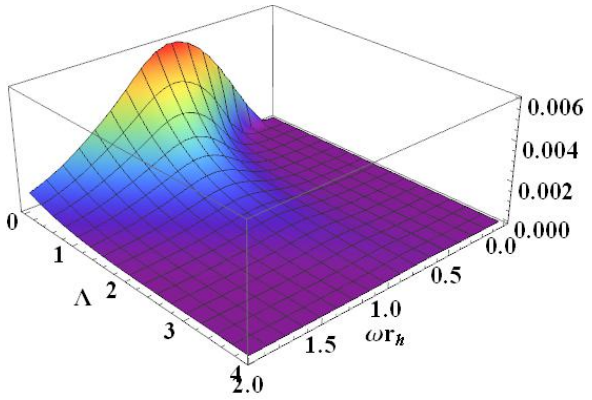

FIGURE 4.23: The contribution of the first four modes of Fig. 4.18 to the EER for $T_h = T_0$.

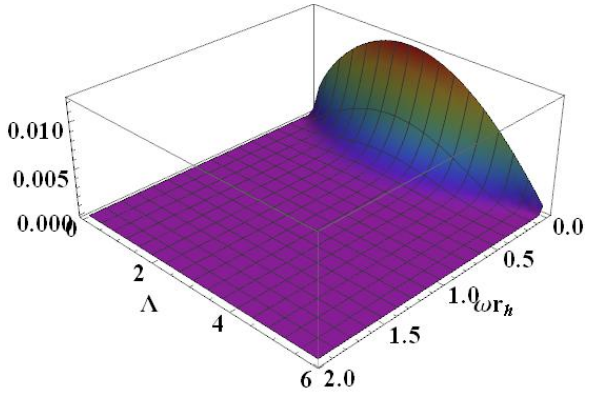

FIGURE 4.24: The $\Omega(\omega, T_h)$ function for the temperature T_{effBH} as Λ ranges from 0 up to the critical limit.

The individual contributions to the EER when $T_h = T_{effBH}$ for the first four modes is shown in Fig. 4.25 while in Fig. 4.26(a), we show the profile of the $S^{(20)}$ that shows that even very large field modes are greatly suppressed due to the fact that the regions on the $(\omega r_h, \Lambda)$ plane where $A^{(20)}$ and $\Omega(\omega, T_{effBH})$ are non vanishing do not overlap significantly and thus $S^{(20)}$ (that corresponds to the product between the two) is highly suppressed. Lastly, the sum of the first four modes modes that are shown in Fig. 4.25 is given in Fig. 4.26(b).

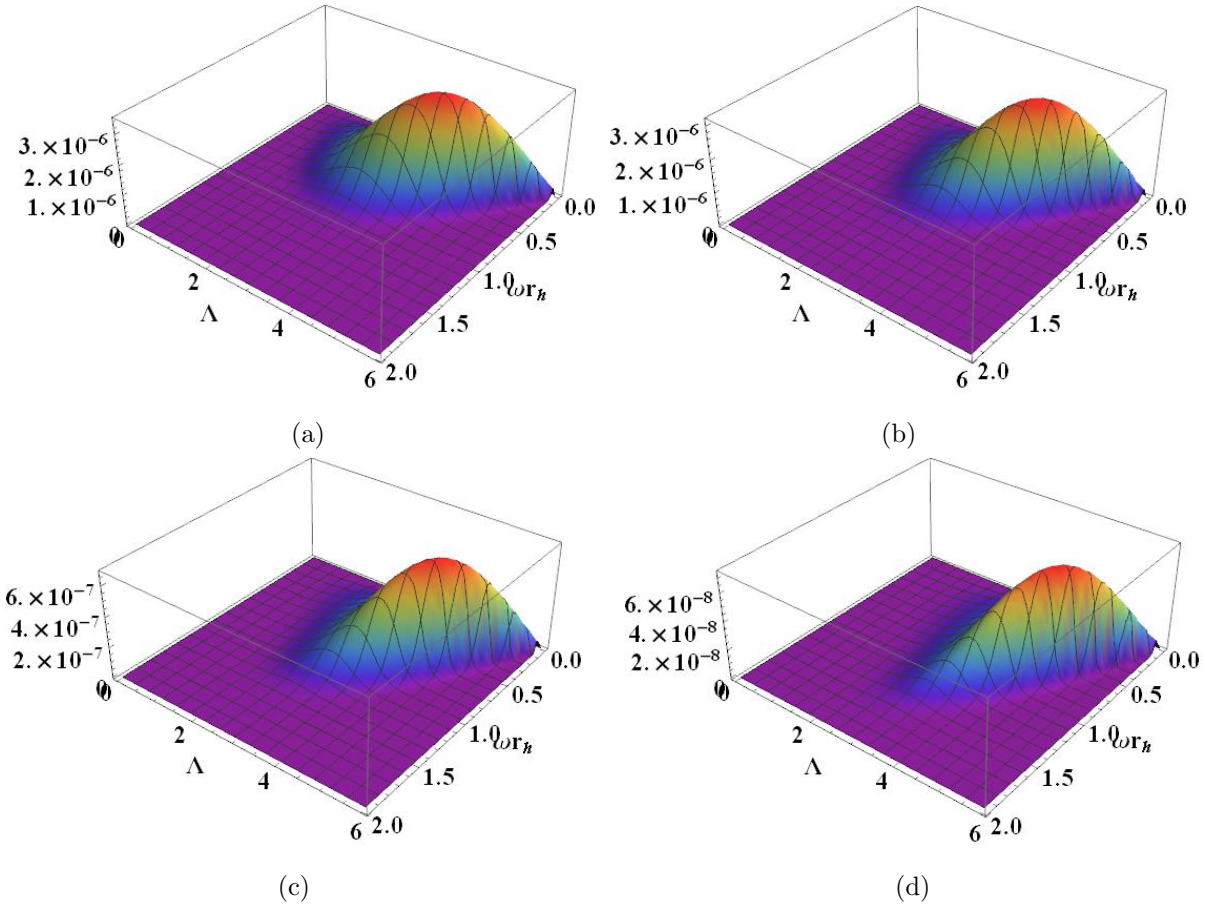

FIGURE 4.25: The functions $S^{(l)} \equiv \Omega(\omega, T_h)A^{(l)}$ for $n = 2$ and $\xi = 1$. For the temperature T_{effBH} and for the mode **(a)** $l = 0$, **(b)** $l = 1$, **(c)** $l = 2$, and **(d)** $l = 3$.

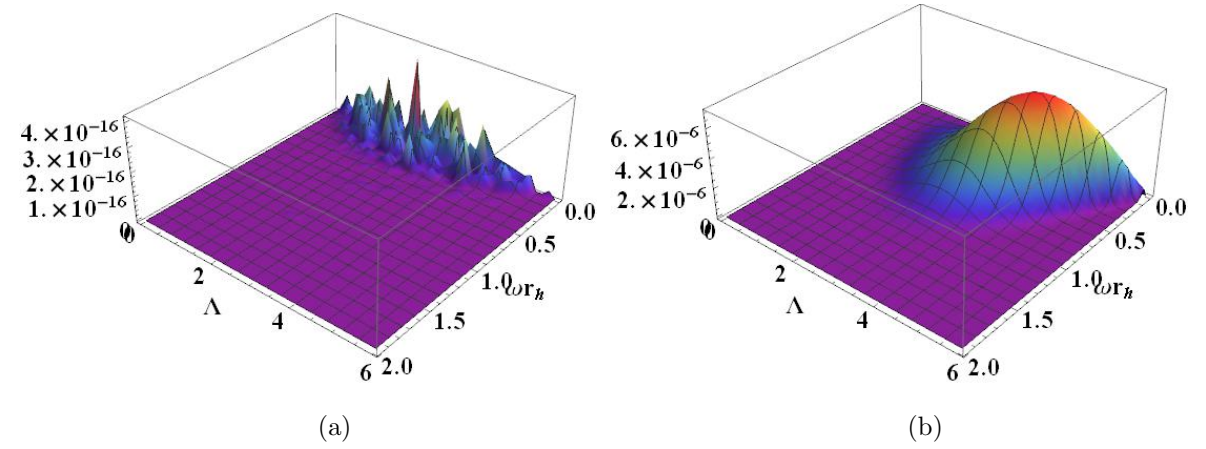

FIGURE 4.26: (a)The $S^{(20)}$ function for the temperature T_{effBH} as Λ ranges from 0 up to the critical limit and (b) hhe contribution of the first four modes of Fig. 4.18 to the EERfor $T_h = T_{effBH}$.

4.6.3 The effect of the field coupling

In Fig. 4.27 we depict the effect of the coupling constant on the GF up to the critical limit. To illustrate this we considered the function $A^{(1)}$.

Let us focus in the low-Λ regime of Fig. 4.27. As we can see, an increase in Λ causes the monotonic enhancement of the greybody factor when the field coupling (ξ) is small [Fig. 4.27(a)]. For larger values of ξ, an increase in Λ causes initially the suppression of the GFs in the low-Λ region while for intermediate-Λ values this effect is reversed, and up to the critical limit the GFs get enhanced with the cosmological constant. Recall that we have already seen this effect where Λ assumes a "dual role" depending on the value of the field's coupling to gravity.

The dual role of the cosmological constant, gives rise to the "U"-shaped profiles of Fig. 4.27. This "U"-shaped profile becomes more prominent with an increase in ξ, and consequently close to Λ_{crit}, we see that the modes yield $A^{(l)}$ that are constrained to a "thinner" region. Thus, for large values of the field coupling we expect the amplification of the high modes contribution to the EER to be reduced (for temperatures that vanish at Λ_{crit}).

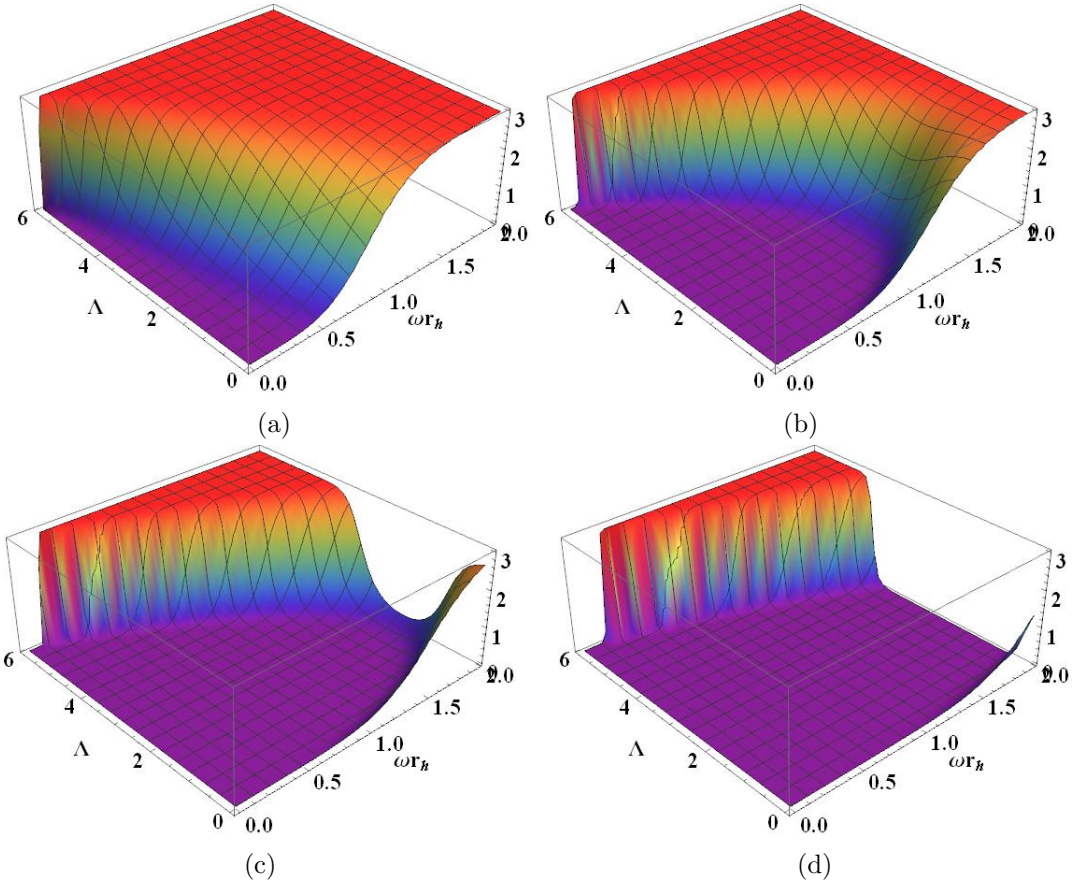

FIGURE 4.27: The function $A^{(1)}$ (i.e. for $l = 1$) for $n = 2$ as **(a)** $\xi = 0.1$, **(b)** $\xi = 2$, **(c)** $\xi = 5$, and **(d)** $\xi = 10$.

4.7 Conclusions

The proper definition of the temperature for the Hawking radiation by Schwarzschild-de Sitter (SdS) black holes is an open subject of debate. The presence of the cosmological horizon endowed with a temperature that is lower than the black-hole one, prevents the system from being in thermal equilibrium. Also, the absence of an asymptotically-flat observer with respect to whom the Killing vectors are usually normalized makes the definition of conserved quantities and the temperature obscure. To circumvent the above issues, various proposals have been made in the literature including a different normalization for the Killing vectors that take into account the non-asymptotic flatness of SdS and the formulation of effective thermodynamic first laws. These approaches yield different temperatures and are employed by various authors "at will".

In this chapter, we compared six different expressions for the SdS temperature as the number of extra dimensions (n) and the cosmological constant (Λ) assume different values. For the latter we considered indicative values that span the whole allowed regime, even up to the Nariai limit. Consequently, we studied the effect of each one of these temperatures on the differential energy emission rates (EERs) and the total emissivity for the higher-dimensional SdS black hole, both on the brane and in the bulk. The underlying field theory we considered is that of a scalar field that couples non-minimally to gravity via the interaction term $\xi\Phi R$ in the action where R is the Ricci scalar and ξ is a free parameter.

We found, that in the limit of a vanishing cosmological constant the temperatures split into two groups. The first group asymptotes to the value of the Schwarzschild black-hole temperature while the second one to zero. In the Nariai limit, the temperatures exhibit once again two distinct behaviors by either going to zero or attaining a non-vanishing value. This is due to the assumptions in the derivation of the temperatures that assume either the black-hole mass or the cosmological constant to be present for the analysis.

The comparison of the EERs revealed that the Bousso-Hawking normalized temperature (T_{BH}) results in the most emissive spectra in all of the (n, Λ, ξ) parameter space while the other temperatures manage to yield significant EERs only in the low- or large-Λ regime. Regarding the results of the bulk-over-brane emissivity ratio, we found that an increase of ξ enhances the brane channel while the effect of Λ is in general the opposite. For the vast majority of the parameter space it is the brane channel that dominates over the bulk. Still, close to the critical limit and for large n, the balance may be tilted in favor of the bulk channel even by a factor of $\mathcal{O}(10)$ when T_{BH} is employed.

Chapter 5

Brane-localized 5-dimensional black-holes: In search for analytic solutions

In the brane-world models, there are two popular theories that describe the structure of the extra dimensional space. In the first one to be proposed [8–10], the so-called *Large Extra Dimensions* (LEDs) scenario, the extra dimensions are flat and black-hole solutions to the Einstein equations are known to exist. As a matter of fact, long before the LEDs were even proposed, higher dimensional black-hole solutions had already been derived [30, 68]. It is in the context of these theories, that the study of the higher-dimensional black holes in the preceding chapters of this thesis has been performed.

Shortly after the LEDs, Lisa Randall and Raman Sundrum, proposed another solution to the hierarchy problem by introducing a single "warped" extra dimension with a $\mathbb{Z}_2$ symmetry that may be finite [11] or infinite [12] in size. This scenario has been termed the *Warped Extra Dimensions* (WEDs) scenario. Contrary to LEDs, in WEDs, no analytic, localized-on-the-brane, regular black-hole solution in five dimensions has been found despite the huge amount of effort put forth by the community [162–168].

In the first attempt towards obtaining such a black-hole solution in the context of WEDs, the authors of [162] considered the following line element:

$$ds^2 = e^{2A(y)}\left[-\left(1-\frac{2m}{r}\right)dt^2+\left(1-\frac{2m}{r}\right)^{-1}dr^2+r^2\left(d\theta^2+\sin^2\theta\, d\varphi^2\right)\right]+dy^2, \tag{5.1}$$

where y is the coordinate corresponding to the extra dimension and $e^{2A(y)}$ is the *warp factor*. The constant parameter m is identified with the black-hole mass[1] since when one considers the location of the brane at $y=0$ and the RS warp function[2] $A(y)=-l^{-1}|y|$, with AdS radius l, the above line-element reduces to the 4-dimensional Schwarzschild metric. Still, the solution of eq. (5.1) does not describe an object that is localized close to the brane in five dimensions. This becomes evident by the singular behavior of the curvature invariants. As an example, consider the Kretschmann scalar for the above geometry (5.1)

$$R^{MNRS}R_{MNRS}=\frac{48e^{-4A(y)}m^2}{r^6}+\dots, \tag{5.2}$$

[1] In contrast to previous chapters where the capital letter "M" has been used for the black-hole mass, here we denote the same quantity with lower-case "m" since M is reserved for the indices of the various higher-dimensional tensorial objects.

[2] This specific choice of $A(y)$ is made here for illustrative reasons.

where "..." in the expression above, is used to indicate extra terms that become sub-dominant in the limit $r \to 0$. It is then clear, that the spacetime singularity located at $r = 0$ extends throughout the extra coordinate range and is not localized close to the brane where the gravitational collapse of ordinary matter took place. In this sense, the line element of eq. (5.1) does not describe a regular brane-localized black hole but rather a new family of solutions that have been termed *black strings*.

Since then, a plethora of works aiming to obtain brane-localized black holes appeared in the literature [169–185]. Even though solutions in lower-dimensional gravity have emerged in some of these analyses, in five dimensions no analytic exact solution exists to date. Numerical solutions in five and six dimensions have been found [186–188] but their validity was restricted to black-holes that are small (or at most of the same order) compared to the scale set by the bulk curvature. More recently, numerical solutions describing large black holes appeared [189, 190], but an analytic solution is still lacking.

The authors of [172, 173] were the first to point out that if the constant mass parameter m gets promoted to a function of the extra coordinate, i.e. $m \to m(y)$, then for an appropriate y-dependence of $m(y)$ that decreases faster than $e^{4A(y)}$, the bulk singularities could potentially be localized close to the brane. In these works it has also been demonstrated that a line element of the Vaidya type [191, 192] is the most appropriate choice since it minimizes the number of bulk spacetime singularities.

Due to the non-trivial dependence of the mass on the coordinates, the metric (5.3) is no longer a vacuum solution to the Einstein equations and thus some form of field content has to be introduced in the bulk to support this solution. In [172, 173] it has also been demonstrated that "conventional" field-theory models such as minimally-coupled scalar or gauge fields are not sufficient to support the aforementioned geometry and at the same time constrain the bulk singularities close to the brane. For a series of other works attempting to find (both analytically and numerically) brane-localized black-holes by introducing some form of bulk or brane matter, or even additional geometric terms see [193–197].

The authors of [198] assumed a line element of the Vaidya type with a mass function $m = m(v, y)$ that depends on both the time (v) and extra dimension (y) coordinates. To support this metric ansatz, they considered a number of bulk scalar field theories, including single and multiple fields that couple minimally or non-minimally to gravity. Unfortunately, they concluded that even for these "unconventional" types of field theories a localized-to-the-brane black hole does not emerge.

In this chapter, we build upon the work done in [198] by considering an even more general mass function that ontop of a dependence on the time and extra dimension coordinates it also exhibits a non-trivial profile along the radial coordinate r. The motivation for this postulated r-dependence of the mass function is the greater flexibility of the field equations that may finally yield a viable solution. Also, by assuming $\partial_r m \neq 0$, a brane-induced geometric background that is richer than the

Schwarzschild one is expected to emerge via the appearance of extra terms in the metric function that are reminiscent of the (anti)de-Sitter ($\sim r^2$) or "Reissner–Nordström" ($\sim r^{-2}$) solutions.

Regarding the bulk field content necessary to support our five dimensional metric, we will consider a plethora of models. We will start with the next-to trivial case of a bulk filled only with a cosmological constant; we then move on to the case of a field theory with one or two scalar fields (interacting or not) that are minimally coupled to gravity. In order to be as general as possible in our analysis, a general potential term will be included in the Lagrangian and the kinetic terms will be canonical, non-canonical or even mixed. Finally we will also consider scalar-tensor gravity where a single scalar field Φ is coupled to the Ricci scalar in the action via a analytic, arbitrary function $f(\Phi)$.

5.1 The gravitational background

We consider the following ansatz for the line element of the five dimensional spacetime:

$$ds^2 = e^{2A(y)}\left[-\left(1-\frac{2m(v,r,y)}{r}\right)dv^2 + 2dvdr + r^2(d\theta^2 + sin^2\theta\, d\phi^2)\right] + dy^2\,, \tag{5.3}$$

where the mass parameter m is a function of the time (v), extra dimension (y) and radial (r) coordinates. The dependence of the mass on y is justified by the non-trivial field content of the bulk, a necessary requirement after all in order for the Einstein equations to be satisfied. Finally, the warp function $A(y)$ is an arbitrary *decreasing* function of y that respects the $\mathbb{Z}_2$ symmetry.

For the line element of eq. (5.3), the non-vanishing components of the mixed Einstein tensor are

$$\begin{aligned}
G^v_{\ v} &= G^r_{\ r} = 6A'^2 + 3A'' - \frac{2}{r^2}\,e^{-2A}\,\partial_r m\,,\\
G^\theta_{\ \theta} &= G^\phi_{\ \phi} = 6A'^2 + 3A'' - \frac{1}{r}\,e^{-2A}\,\partial_r^2 m\,,\\
G^r_{\ v} &= \frac{2}{r^2}\,e^{-2A}\partial_v m - \frac{1}{r}\,(\partial_y^2 m + 4A'\partial_y m)\,,\\
G^y_{\ v} &= e^{2A}\,G^r_{\ y} = \frac{1}{r^2}\,\partial_y m + \frac{1}{r}\,\partial_y\partial_r m\,,\\
G^y_{\ y} &= 6A'^2 - e^{-2A}\big(\frac{2}{r^2}\,\partial_r m + \frac{1}{r}\,\partial_r^2 m\big)\,,\\
G^v_{\ r} &= G^y_{\ r} = G^v_{\ y} = 0\,.
\end{aligned} \tag{5.4}$$

It is imperative to know the forms of the curvature invariants as well, since in order to obtain a black hole that is localized close to the brane, any bulk singularity has to be contained around the location of the brane at $y = 0$. Explicitly, the square of the Riemann and Ricci tensors and the Ricci scalar

for the metric (5.3) are

$$R_{MNRS}R^{MNRS} = 40A'^4 + 32A'^2A'' + 16A''^2 + \frac{48e^{-4A}m^2}{r^6} - \frac{8A'^2e^{-2A}}{r}\left(\partial_r^2 m + \frac{2}{r}\,\partial_r m\right) + \frac{4e^{-4A}}{r^2}\left[(\partial_r^2 m)^2 + \frac{4m}{r^2}(\partial_r^2 m - \frac{4}{r}\,\partial_r m) - \frac{4}{r}\,\partial_r m\,\partial_r^2 m + \frac{8}{r^2}\,(\partial_r m)^2\right], \tag{5.5}$$

$$\begin{aligned} R_{MN}R^{MN} &= 80A'^4 + 64A'^2A'' + 20A''^2 \\ &- \frac{4e^{-2A}}{r}\left(\partial_r^2 m + \frac{2}{r}\,\partial_r m\right)(A'' + 4A'^2) + \frac{2e^{-4A}}{r^2}\left[(\partial_r^2 m)^2 + \frac{4}{r^2}(\partial_r m)^2\right], \end{aligned} \tag{5.6}$$

and

$$R = -20A'^2 - 8A'' + \frac{2e^{-2A}}{r}\left(\partial_r^2 m + \frac{2}{r}\,\partial_r m\right), \tag{5.7}$$

respectively. We point out that these expressions smoothly reduce to the ones given in [198] upon setting $\partial_r m = 0$.

Notice that by postulating that the mass depends on the radial coordinate as well, the curvature invariants become more complicated as they now also contain terms proportional to $\partial_r m \neq 0$ and $\partial_r^2 m \neq 0$. All of these extra terms are singular at $r = 0$ and also extend to all values of y since they are at the same time proportional to the warp factor. This latter feature, is the one that ensures that even these terms may be localized close to the brane with an appropriate profile of the mass along the extra coordinate i.e. one that decreases faster than the warp factor as we "move away" from the location of the brane.

In the rest of this chapter, we consider various field theories in the bulk and investigate whether they can support the geometric background of eq. (5.3) and at the same time yield a mass function that eliminates the singularities of the curvature invariants at a finite coordinate distance from the brane.

5.2 In the presence of a bulk cosmological constant

The action functional in five dimensions is composed of the usual Einstein-Hilbert term supplemented by a matter Lagrangian $\mathcal{L}_m$ that is specified each time by the field content of the theory at hand

$$\mathcal{S} = \int d^4x\, dy\, \sqrt{-g}\, \left(\frac{R}{2\kappa_5^2} - \mathcal{L}_m\right). \tag{5.8}$$

In the above, g is the metric determinant, R is the Ricci scalar, while κ_5^2 is the 5-dimensional gravitational constant. The variation of eq. (5.8) with respect to the bulk metric g_{MN} yields the Einstein

field equations

$$G_{MN} \equiv R_{MN} - \frac{1}{2}\, g_{MN}\, R = \kappa_5^2\, T_{MN}\,, \tag{5.9}$$

where as usual, the bulk energy-momentum tensor T_{MN}, is defined via the variation of $\mathcal{L}_m$ with respect to the metric as follows:

$$T_{MN} \equiv \frac{2}{\sqrt{-g}}\, \frac{\delta(\sqrt{-g}\,\mathcal{L}_m)}{\delta g^{MN}}\,. \tag{5.10}$$

For the rest of the chapter it is understood that we set $\kappa_5^2 = 1$ unless otherwise stated.

In this section, we consider the simplest case where the only contribution to T_{MN} comes from the presence of a bulk cosmological constant (Λ_B).

$$T_{MN} \equiv -g_{MN}\Lambda_B\,, \tag{5.11}$$

and so, the mixed components of the energy-momentum tensor will be given by

$$T^M_{\ N} = -\delta^M_{\ N}\Lambda_B\,. \tag{5.12}$$

The last equation, imposes some constraints on the Einstein tensor via eq. (5.9). In particular one of the requirements is that all mixed diagonal components of $G^M_{\ N}$ in eq. (5.4) be equal to each other. Then, from[3] $G^v_{\ v} = G^\theta_{\ \theta}$ we find that the mass function should satisfy the following differential equation:

$$\partial_r^2 m = \frac{2}{r}\,\partial_r m\,, \tag{5.13}$$

that can be easily integrated to give the solution

$$m(v,r,y) = B(v,y)\, r^3 + C(v,y)\,. \tag{5.14}$$

This expression for the mass, when introduced in eq. (5.3) yields an interesting metric function with a "Schwarzschild-like" term $C(v,y)/r$ and an "(anti)de-Sitter-like" term $B(v,y)r^2$. Still, another constraint imposed on the Einstein tensor by the form of $T^M_{\ N}$ in eq. (5.12) is that the off-diagonal components of $G^M_{\ N}$ should vanish. Thus from $G^y_{\ v} = T^y_{\ v} = 0$ we have

$$\frac{1}{r^2}\,\partial_y m + \frac{1}{r}\,\partial_y\partial_r m = 0\,. \tag{5.15}$$

Unfortunately, the solution (5.14) fails to satisfy this constraint as well since its substitution into eq. (5.15) results to

$$4r^3\partial_y B + \partial_y C = 0\,, \tag{5.16}$$

that can only hold if $\partial_y B = \partial_y C = 0$ and thus the dependence of the mass function on the extra

[3] Often in this thesis we also employ the alternative notation $\binom{M}{N}$ to symbolize the $G^M_{\ N} = T^M_{\ N}$ component of the Einstein's field equations (5.9).

coordinate is removed. This is of course a non-acceptable requirement since the mass has to be y-dependent in order for the localization of the singularity close to the brane to occur.

5.3 Minimally-coupled scalar field theories

Here, we study the case of a bulk filled with either a single scalar field or two interacting scalar fields that are minimally coupled to gravity. We will also assume the presence of a general potential in the Lagrangian as well as a general kinetic term that encompasses both canonical and non-canonical kinetic terms for the field.

5.3.1 A single scalar field with a general Lagrangian

When the bulk is filled with a single scalar field we may write the Lagrangian as

$$\mathcal{L}_\phi = \sum_{n=1} f_n(\phi) \left(\partial^M \phi \, \partial_M \phi\right)^n + V(\phi)\,, \tag{5.17}$$

where $f_n(\phi)$ are arbitrary and analytic functions of the field ϕ and it is understood that the general potential $V(\phi)$ may include the bulk cosmological constant Λ_B. Notice that when $n = 1$ and $f_1(\phi) = 1$ the Lagrangian (5.17) reduces to the one of a single scalar field with a canonical kinetic term while for arbitrary n, the general kinetic term is a mixture of canonical and non-canonical kinetic terms.

The energy-momentum tensor corresponding to the Lagrangian (5.17) is straightforwardly computed via eq. (5.10) and it turns out to have the following expression:

$$T_{MN} = 2 \sum_{n=1} n \, f_n(\phi) \left(\partial^P \phi \, \partial_P \phi\right)^{n-1} \partial_M \phi \, \partial_N \phi - g_{MN} \, \mathcal{L}_\phi. \tag{5.18}$$

We assume that the scalar field is spherically symmetric meaning that it does not depend on the angular coordinates θ and ϕ; other than that, in the most general case it depends on the rest of the coordinates i.e. $\phi = \phi(v, r, y)$.

From the off-diagonal component of the Einstein equations $G^v_{\ r} = T^v_{\ r}$ we obtain

$$2\, e^{-2A} \sum_{n=1} n \, f_n(\phi) \left(\partial^P \phi \, \partial_P \phi\right)^{n-1} (\partial_r \phi)^2 = 0\,. \tag{5.19}$$

If we reasonably assume that the warp factor and the functions $f_n(\phi)$ are non-vanishing the latter requires that the field does not depend on the radial coordinate

$$\partial_r \phi = 0 \;\rightarrow\; \phi = \phi(v, y)\,. \tag{5.20}$$

Under this simplification, the following two equations are obtained from the Einstein's EOMs :

$$G^{v}_{\ v} = T^{v}_{\ v} \ \Rightarrow \ 6A'^{2} + 3A'' - \frac{2}{r^{2}}\, e^{-2A}\, \partial_{r} m = -\mathcal{L}_{\phi}\,, \tag{5.21}$$

$$G^{\theta}_{\ \theta} = T^{\theta}_{\ \theta} \ \Rightarrow \ 6A'^{2} + 3A'' - \frac{1}{r}\, e^{-2A}\, \partial_{r}^{2} m = -\mathcal{L}_{\phi}\,. \tag{5.22}$$

Combining these two equations, we once again end up with eq. (5.13) and thus with the functional form of the mass given in eq. (5.14). Substituting this solution to the $G^{y}_{\ v} = T^{y}_{\ v}$ component of the EOMs we obtain the following constraint:

$$4r\partial_{y}B + \frac{\partial_{y}C}{r^{2}} = 2\sum_{n} n\, f_{n}(\phi)\, (\partial_{P}\phi\, \partial^{P}\phi)^{n-1}\, \partial_{y}\phi\, \partial_{v}\phi\,. \tag{5.23}$$

The r-independence of the scalar field makes the right hand side (r.h.s.) of the last equation r-independent. So, the only way that the left hand side (l.h.s.) is also r-independent is by demanding that $\partial_{y}B = 0$ and $\partial_{y}C = 0$. But these conditions once again remove completely the necessary y-dependence of the mass function. Notice also that the potential $V(\phi)$ and the functions $f_{n}(\phi)$ remained unspecified throughout the analysis of this section and thus we may conclude that any Lagrangian with the general form of eq. (5.17) fails to support the line element (5.3).

Finally, we point out that one unavoidably ends up with the solution of eq. (5.14) for the mass due to the constraint $T^{v}_{\ v} = T^{\theta}_{\ \theta}$, that holds for both eq. (5.12) and eq. (5.18) (for $\partial_{r}\phi = 0$). In the next subsection, this constraint will be avoided by considering two interacting scalar fields.

5.3.2 Two interacting scalar fields

Let us now consider a slightly more complicated scenario in which the field content in the bulk is composed of two interacting scalar fields that are non-minimally coupled to gravity. For the moment we will focus only on fields with canonical kinetic terms described by the Lagrangian

$$\mathcal{L}_{sc} = f^{(1)}(\phi,\chi)\, \partial^{M}\phi\, \partial_{M}\phi + f^{(2)}(\phi,\chi)\, \partial^{M}\chi\, \partial_{M}\chi + V(\phi,\chi)\,, \tag{5.24}$$

where the two scalar fields are denoted here with ϕ and χ respectively, the functions $f^{(1,2)}$ are again arbitrary, analytic and depending on both fields, while $V(\phi,\chi)$ is a general potential. The energy-momentum tensor for this Lagrangian has the following form:

$$T_{MN} = 2f^{(1)}(\phi,\chi)\, \partial_{M}\phi\, \partial_{N}\phi + 2f^{(2)}(\phi,\chi)\, \partial_{M}\chi\, \partial_{N}\chi - g_{MN}\, \mathcal{L}_{sc}\,. \tag{5.25}$$

Due to the vanishing of the respective components of the Einstein tensor (5.4), the off-diagonal components $T^{v}_{\ r}\,, T^{y}_{\ r}$ and $T^{v}_{\ y}$ need to also vanish. As a consequence, the following two independent

constraints for the scalar fields are obtained:

$$f^{(1)}(\phi,\chi)\,(\partial_r\phi)^2 + f^{(2)}(\phi,\chi)\,(\partial_r\chi)^2 = 0\,, \tag{5.26}$$

$$f^{(1)}(\phi,\chi)\,\partial_r\phi\partial_y\phi + f^{(2)}(\phi,\chi)\,\partial_r\chi\partial_y\chi = 0\,, \tag{5.27}$$

while at the same time, the diagonal components of the Einstein's EOMs $G^v_{\ v} = T^v_{\ v}$ and $G^\theta_{\ \theta} = T^\theta_{\ \theta}$, yield respectively

$$6A'^2 + 3A'' - \frac{2}{r^2}\,e^{-2A}\,\partial_r m = 2e^{-2A}\left[f^{(1)}(\phi,\chi)\,\partial_r\phi\,\partial_v\phi + f^{(2)}(\phi,\chi)\,\partial_r\chi\partial_v\chi\right] - \mathcal{L}_{sc}\,, \tag{5.28}$$

$$6A'^2 + 3A'' - \frac{1}{r}\,e^{-2A}\,\partial_r^2 m = -\mathcal{L}_{sc}\,. \tag{5.29}$$

Observe, at this point, that the components $T^v_{\ v}$ and $T^\theta_{\ \theta}$ of the energy-momentum tensor i.e. the l.h.s. of the last two equations, are different. This is a consequence of the non-vanishing of the term in the square brackets of eq. (5.28) since this is not imposed by any constraint. This way, and in conjunction with the discussion of the previous section, the solution of eq. (5.14) is now in general avoided.

Subtracting now eq. (5.29) from eq. (5.28) we find

$$\frac{1}{r}\,\partial_r^2 m - \frac{2}{r^2}\,\partial_r m = 2\Big[f^{(1)}(\phi,\chi)\,\partial_r\phi\,\partial_v\phi + f^{(2)}(\phi,\chi)\,\partial_r\chi\partial_v\chi\Big]\,. \tag{5.30}$$

In order to check whether this differential equation for the mass can produce a solution that exhibits the desired properties, it is convenient to consider individually the following cases for the scalar fields.

- **One of the scalar fields is r-independent.** Then via eq. (5.26), it becomes evident that the other field is r-independent as well. If in turn, both fields do not depend on the radial coordinate, then eq. (5.30) reduces to eq. (5.13) with the corresponding solution that is given by eq. (5.14). The $\binom{y}{v}$ component of the field equations is written explicitly as

$$\frac{\partial_y m}{r^2} + \frac{\partial_r\partial_y m}{r} = 2\left[f_1^{(1)}(\phi,\chi)\partial_y\phi\partial_v\phi + f_1^{(2)}(\phi,\chi)\partial_y\chi\partial_v\chi\right], \tag{5.31}$$

  and the r.h.s. has no dependence on the radial coordinate. This requires that the l.h.s. is also r-independent and so, it is necessary to demand $\partial_y B = 0$ and $\partial_y C = 0$ removing this way the y-dependence of the mass.

- **One of the scalar fields is y-independent.** In this case, the constraint (5.27) requires the other scalar field be either r- or y-independent. We have already excluded the former case in the discussion above. Then we are dealing with the case that the fields satisfy $\partial_y\phi = 0$ and $\partial_y\chi = 0$ and consequently the r.h.s. of eq. (5.31) is zero. The resulting solution for the mass function is

$$m(v,r,y) = \frac{E(v,y)}{r} + D(v,r)\,. \tag{5.32}$$

Upon substituting this mass in the metric function of eq. (5.3) a term $D(v,r)/r$ and a "Reissner–Nordström-like" term $E(v,y)/r^2$ emerge. Unfortunately, plugging eq. (5.32) into eq. (5.30) and keeping in mind that the r.h.s. is y-independent, we are forced to impose the condition $\partial_y E(v,y)=0$ and in this way render the mass y-independent once again.

- **One of the scalar fields is v-independent.** Contrary to the previous two cases, by assuming that one of the two fields does not depend on the time variable, we find that the constraints imposed by the Einstein equations do not require the same to hold for the other field as well. In fact, in order to guarantee that eq. (5.30) and eq. (5.31) do not reduce to eq. (5.13) and eq. (5.15) respectively that yield a non viable solution, one of the two fields necessarily has to be dynamic.

To deal with the most general case, we consider that both of the (spherically-symmetric) fields depend on all of the coordinates i.e. $\phi=\phi(v,y,r)$ and $\chi=\chi(v,y,r)$. We may then solve eq. (5.26) for one of the coupling functions to get

$$f^{(1)}=-f^{(2)}\,\frac{(\partial_r\chi)^2}{(\partial_r\phi)^2}\,, \tag{5.33}$$

and then substitute this into eq. (5.27) to obtain the following constraint:

$$\partial_r\phi\,\partial_y\chi-\partial_r\chi\,\partial_y\phi=0\,. \tag{5.34}$$

Substituting these last two equations in the $\binom{y}{y}$ component of the EOMs

$$6A'^2-\frac{e^{-2A}}{r}\left(\partial_r^2 m+\frac{2}{r}\,\partial_r m\right)=2\left[f^{(1)}(\phi,\chi)\,(\partial_y\phi)^2+f^{(2)}(\phi,\chi)\,(\partial_y\chi)^2\right]-\mathcal{L}_{sc}\,, \tag{5.35}$$

we find that the term in the square brackets vanishes. Combining then eq. (5.35) with the $\binom{\theta}{\theta}$ component (5.29) we end up with

$$\frac{2}{r^2}\,\partial_r m=-3A''\,e^{2A}\,, \tag{5.36}$$

that readily leads to the following solution for the mass function:

$$m(v,r,y)=-\frac{A''}{2}\,e^{2A}r^3+m_0(v,y)\,. \tag{5.37}$$

This mass function gives rise to a "Schwarzschild-like" term $m_0(v,y)/r$ and a "(anti)de-Sitter" one $-A''e^{2A}r^2/2$ when substituted into the metric function but fails to "pass" from the rest of the constraints. When eq. (5.37) is plugged into eq. (5.30), the l.h.s. vanishes and so we obtain

$$f^{(1)}\,\partial_r\phi\,\partial_v\phi+f^{(2)}\,\partial_r\chi\,\partial_v\chi=0\,, \tag{5.38}$$

which via eq. (5.33) gives

$$\partial_r\phi\,\partial_v\chi-\partial_r\chi\,\partial_v\phi=0\,. \tag{5.39}$$

Using eqs. (5.34) and (5.39) into the $\binom{y}{v}$ component (5.31) of the EOMs we have a vanishing r.h.s. and then, the l.h.s. upon substitution of the mass (5.37) yields

$$-2r\partial_y(A''e^{2A}) + \frac{1}{r^2}\,\partial_y m_0 = 0\,. \tag{5.40}$$

This last condition, once again imposes the y-independence of the mass function.

If we now include non-canonical kinetic terms for the fields in the Lagrangian it is trivial to exclude this case as well. The form of $\mathcal{L}_{sc}$ is now

$$\mathcal{L}_{sc} = \sum_{n=1} f_n^{(1)}(\phi,\chi)\left(\partial^M\phi\partial_M\phi\right)^n + \sum_{n=1} f_n^{(2)}(\phi,\chi)\left(\partial^M\chi\partial_M\chi\right)^n + V(\phi,\chi)\,, \tag{5.41}$$

while the energy-momentum tensor turns out to be

$$\begin{aligned} T_{MN} \;=\; & 2\sum_{n=1} n\, f_n^{(1)}(\phi,\chi)\left(\partial^P\phi\partial_P\phi\right)^{n-1}\partial_M\phi\partial_N\phi \\ & +2\sum_{n=1} n\, f_n^{(2)}(\phi,\chi)\left(\partial^P\chi\partial_P\chi\right)^{n-1}\partial_M\chi\partial_N\chi - g_{MN}\,\mathcal{L}_{sc}\,. \end{aligned} \tag{5.42}$$

If one employs the following redefinitions for the coefficients of $\partial_M\phi\partial_N\phi$ and $\partial_M\chi\partial_N\chi$ in the last equation:

$$\tilde{f}^{(1)}(\phi,\chi) \;=\; \sum_{n=1} n f_n^{(1)}(\phi,\chi)\left(\partial^M\phi\partial_M\phi\right)^{n-1}\,, \tag{5.43}$$

$$\tilde{f}^{(2)}(\phi,\chi) \;=\; \sum_{n=1} n f_n^{(2)}(\phi,\chi)\left(\partial^M\chi\partial_M\chi\right)^{n-1}\,, \tag{5.44}$$

it becomes clear that the expression of the energy-momentum tensor (5.42) is equivalent to eq. (5.25). Since the coupling functions $f^{(1,2)}(\phi,\chi)$ played no role in the analysis of this section we conclude that, two interacting bulk scalar fields described by the general Lagrangian of eq. (5.41) are not sufficient to produce a viable solution for the mass function with the required y-dependence.

5.3.3 Two interacting scalar fields with mixed kinetic terms

Next, we turn to a more unconventional field theory described by the following Lagrangian:

$$\mathcal{L}_{sc} = f^{(1)}(\phi,\chi)\,\partial^M\phi\partial_M\phi + f^{(2)}(\phi,\chi)\,\partial^M\chi\partial_M\chi + f^{(3)}(\phi,\chi)\,\partial^M\phi\partial_M\chi + V(\phi,\chi)\,, \tag{5.45}$$

where two scalar fields ϕ and χ are employed with mixed kinetic terms and a general potential $V(\phi,\chi)$. The corresponding energy-momentum tensor is then given by

$$\begin{aligned} T_{MN} &= 2f^{(1)}(\phi,\chi)\,\partial_M\phi\partial_N\phi + 2f^{(2)}(\phi,\chi)\,\partial_M\chi\partial_N\chi \\ &\quad + f^{(3)}(\phi,\chi)\,[\partial_M\phi\partial_N\chi + \partial_M\chi\partial_N\phi] - g_{MN}\,\mathcal{L}_{sc}\,. \end{aligned} \tag{5.46}$$

As a consequence of the vanishing of the $\binom{v}{r}$, $\binom{v}{y}$ and $\binom{y}{r}$ field equations due to the vanishing of the corresponding Einstein tensor components, the following two independent constraints are imposed on the fields via (5.46):

$$f^{(1)}(\phi,\chi)\,(\partial_r\phi)^2 + f^{(2)}(\phi,\chi)\,(\partial_r\chi)^2 + f^{(3)}(\phi,\chi)\,\partial_r\phi\partial_r\chi = 0\,, \tag{5.47}$$

$$2f^{(1)}(\phi,\chi)\,\partial_r\phi\partial_y\phi + 2f^{(2)}(\phi,\chi)\,\partial_r\chi\partial_y\chi + f^{(3)}(\phi,\chi)\,[\partial_r\phi\partial_y\chi + \partial_y\phi\partial_r\chi] = 0\,. \tag{5.48}$$

It is easy to see that, similarly to the case studied in the previous subsection, if one of the fields is assumed to be r- or y-independent, then the above set of constraints imposes the same coordinate independence on the second field as well. Then, the dependence of the mass on the extra coordinate is eliminated . We are thus once again led to consider the case that both scalar fields depend on all of the coordinates i.e. $\phi = \phi(v,y,r)$ and $\chi = \chi(v,y,r)$.

We may then solve the system of eqs. (5.47) and (5.48), to obtain

$$f^{(2)} = f^{(1)}\,\frac{(\partial_r\phi)^2}{(\partial_r\chi)^2}\,, \qquad\qquad f^{(3)} = -2f^{(1)}\,\frac{\partial_r\phi}{\partial_r\chi}\,, \tag{5.49}$$

and with these rewrite the (yv) and (rv) components of the field equations respectively as

$$\frac{\partial_y m}{r^2} + \frac{\partial_r\partial_y m}{r} = \frac{2f^{(1)}}{(\partial_r\chi)^2}\,(\partial_v\phi\partial_r\chi - \partial_r\phi\partial_v\chi)\,(\partial_y\phi\partial_r\chi - \partial_r\phi\partial_y\chi)\,, \tag{5.50}$$

and

$$\frac{2\partial_v m}{r^2} - \frac{e^{2A}}{r}\left(4A'\partial_y m + \partial_y^2 m\right) = \frac{2f^{(1)}}{(\partial_r\chi)^2}\,(\partial_v\phi\partial_r\chi - \partial_r\phi\partial_v\chi)^2\,. \tag{5.51}$$

By rearranging the $(\theta\theta)$ and (yy) components of the field equations, the following equation is obtained:

$$\frac{2e^{-2A}}{r^2}\,\partial_r m + 3A'' = -\frac{2f^{(1)}}{(\partial_r\chi)^2}\,(\partial_y\phi\partial_r\chi - \partial_r\phi\partial_y\chi)^2\,. \tag{5.52}$$

Now, appropriately combining eqs. (5.50),(5.51) and (5.52) we are able to eliminate the dependence on $f^{(1)}$ as well as on the derivatives of the fields, and thus end up with the following differential equation for the mass function:

$$\boxed{\left(\frac{\partial_y m}{r^2} + \frac{\partial_r\partial_y m}{r}\right)^2 = \left(\frac{2e^{-2A}}{r^2}\,\partial_r m + 3A''\right)\left[\frac{e^{2A}}{r}\left(4A'\partial_y m + \partial_y^2 m\right) - \frac{2\partial_v m}{r^2}\right]}\,. \tag{5.53}$$

Eq. (5.53) is the "master equation" that any mass function compatible with the constraints imposed by the field equations has to satisfy when the field theory is described by eq. (5.45).

To obtain the form of $m(v, y, r)$, we start by rearranging the components (vv) and $(\theta\theta)$ of the field equations to get

$$\frac{1}{r}\,\partial_r^2 m - \frac{2}{r^2}\,\partial_r m = 2f^{(1)}\partial_r\phi\,\partial_v\phi + 2f^{(2)}\partial_r\chi\partial_v\chi + f^{(3)}(\partial_r\phi\partial_v\chi + \partial_r\chi\partial_v\phi)\,. \tag{5.54}$$

Then, using eq. (5.49), we find that the r.h.s. of the last equation vanishes and as a result the solution for the mass function is once again given by

$$m(v, r, y) = B(v, y)\, r^3 + C(v, y)\,. \tag{5.55}$$

This mass function of course has to satisfy the master equation given above. Upon substitution of eq. (5.55) into eq. (5.53), we find that as long as $\partial_y C = 0$, this mass is indeed a solution while maintaining a y-dependence via the term $B(v, y)\, r^3$. Unfortunately, when this term is plugged into the metric function, it generates a "(anti)de-Sitter"-like term with a y-dependence and not a "Schwarzschild"-like one, that is associated with the singular terms in the curvature invariants and consequently with the possibility of the localization of the singularity.

5.4 Non-minimally coupled scalar field

In this final section, we turn to the case of a single bulk scalar field that is non-minimally coupled with gravity. The action will be (we re-introduce the five-dimensional gravitational constant only for the following three equations and then set $\kappa_5^2 = 1$ for the remaining of the section)

$$\mathcal{S} = \int d^4x\, dy\, \sqrt{-g}\left[\frac{f(\Phi)}{2\kappa_5^2}R - \frac{1}{2}(\nabla\Phi)^2 - V(\Phi) - \Lambda_B\right]\,, \tag{5.56}$$

where $f(\Phi)$ is a analytic and positive-definite function of the scalar field. The corresponding field equations are

$$f(\Phi)\left(R_{MN} - \frac{1}{2}\,g_{MN}R\right) = \kappa_5^2\left(\mathbb{T}^{(\Phi)}_{MN} - g_{MN}\Lambda_B\right)\,, \tag{5.57}$$

and the generalized energy-momentum tensor of the scalar field has been defined as

$$\mathbb{T}^{(\Phi)}_{MN} \equiv \nabla_M\Phi\nabla_N\Phi - g_{MN}\left[\frac{1}{2}(\nabla\Phi)^2 + V(\Phi)\right] + \frac{1}{\kappa_5^2}\left[\nabla_M\nabla_N f(\Phi) - g_{MN}\nabla^2 f(\Phi)\right]\,. \tag{5.58}$$

For a spherically symmetric scalar field i.e. $\Phi = \Phi(v, y, r)$, the off-diagonal components of the field equations are

$$\binom{v}{r} \Rightarrow (1 + f'')(\partial_r\Phi)^2 + f'\,\partial_r^2\Phi = 0\,, \tag{5.59}$$

$$\binom{y}{r} = \binom{v}{y} \Rightarrow (1+f'')\partial_y\Phi\,\partial_r\Phi + f'\,\partial_y\partial_r\Phi - A'f'\partial_r\Phi = 0\,, \tag{5.60}$$

$$\binom{y}{v} = \binom{r}{y} \Rightarrow (1+f'')\partial_y\Phi\,\partial_v\Phi + f'\,\partial_y\partial_v\Phi - A'f'\partial_v\Phi - \frac{\partial_y m}{r}f'\partial_r\Phi = \frac{f}{r}\,(\frac{\partial_y m}{r} + \partial_y\partial_r m)\,, \tag{5.61}$$

$$\begin{aligned}\binom{r}{v} \Rightarrow (1-\frac{2m}{r})\big[(1+f'')\partial_v\Phi\,\partial_r\Phi + f'\,\partial_v\partial_r\Phi\big] + (1+f'')(\partial_v\Phi)^2 + f'\,\partial_v^2\Phi - \frac{\partial_v m}{r}f'\partial_r\Phi \\ +\frac{f'}{r}\,\partial_v\Phi\,\big(\partial_r m - \frac{m}{r}\big) + \frac{\partial_y m}{r}\,e^{2A}f'\partial_y\Phi = f\big[\frac{2}{r^2}\,\partial_v m - \frac{e^{2A}}{r}\,(\partial_y^2 m + 4A'\partial_y m)\big]\,,\end{aligned} \tag{5.62}$$

where, in the above, a prime indicates differentiation with respect to the argument i.e. $f' \equiv df(\Phi)/d\Phi$ and $A' \equiv dA(y)/dy$. The diagonal components of the Einstein equations yield the following three independent equations:

$$\begin{aligned}\binom{v}{v} \Rightarrow e^{-2A}\big[(1+f'')\,\partial_v\Phi\,\partial_r\Phi + f'\,\partial_v\partial_r\Phi + \frac{f'}{r}\,\partial_r\Phi\,(\frac{m}{r} - \partial_r m)\big] \\ +A'f'\,\partial_y\Phi - (\mathcal{L}_\Phi + \Box f + \Lambda_B) = f\,\big(6A'^2 + 3A'' - \frac{2e^{-2A}}{r^2}\,\partial_r m\big),\end{aligned} \tag{5.63}$$

$$\begin{aligned}\binom{\theta}{\theta} \Rightarrow \frac{e^{-2A}}{r}\,f'\big[\partial_v\Phi + \big(1-\frac{2m}{r}\big)\,\partial_r\Phi\big] + A'f'\,\partial_y\Phi - (\mathcal{L}_\Phi + \Box f + \Lambda_B) \\ = f\,\big(6A'^2 + 3A'' - \frac{e^{-2A}}{r}\,\partial_r^2 m\big),\end{aligned} \tag{5.64}$$

$$\binom{y}{y} \Rightarrow (1+f'')(\partial_y\Phi)^2 + f'\,\partial_y^2\Phi - (\mathcal{L}_\Phi + \Box f + \Lambda_B) = f\big[6A'^2 - \frac{e^{-2A}}{r}\big(\partial_r^2 m + \frac{2}{r}\,\partial_r m\big)\big]\,, \tag{5.65}$$

where

$$\mathcal{L}_\Phi \equiv \frac{1}{2}(\nabla\Phi)^2 + V(\Phi) = \frac{e^{-2A}}{2}\Big[2\,\partial_v\Phi\,\partial_r\Phi + \Big(1-\frac{2m}{r}\Big)\,(\partial_r\Phi)^2\Big] + \frac{1}{2}\,(\partial_y\Phi)^2 + V(\Phi)\,, \tag{5.66}$$

and

$$\Box f = e^{-2A}\,\partial_v\partial_r f + \frac{e^{-2A}}{r^2}\,\partial_r\Big[r^2\partial_v f + r^2\big(1-\frac{2m}{r}\big)\,\partial_r f\Big] + e^{-4A}\partial_y\big(e^{4A}\,\partial_y f\big)\,. \tag{5.67}$$

By combining eqs. (5.63) and (5.64) we end up with the constraint

$$(1+f'')\partial_v\Phi\,\partial_r\Phi + f'\,\partial_v\partial_r\Phi = \frac{f'}{r}\Big[\partial_v\Phi + (1-\frac{3m}{r} + \partial_r m)\,\partial_r\Phi\Big] + \frac{f}{r}\big(\partial_r^2 m - \frac{2}{r}\,\partial_r m\big)\,, \tag{5.68}$$

that does not depend on the complicated quantities of eqs. (5.66) and (5.67).

Let us first study the simplest cases where the bulk scalar field Φ depends on only one of the coordinates v, y or r and see if such a field can satisfy the constraints of eqs. (5.59)-(5.62) and eqs. (5.63)-(5.65).

- **The field depends only on the time coordinate $\Phi = \Phi(v)$.** Then, by combining eqs. (5.63) and (5.65), one ends up with

$$\partial_r^2 m = -3e^{2A} A'' r \,, \tag{5.69}$$

and after integrating once with respect to the radial coordinate, we obtain

$$\partial_r m = -\frac{3}{2}\, e^{2A} A'' r^2 + m_0(v, y). \tag{5.70}$$

Plugging in turn this expression for the mass function into the constraint of eq. (5.68) the following relation is obtained:

$$\frac{\partial_v f}{f} = \frac{2}{r}\, m_0(v, y)\,. \tag{5.71}$$

This equation cannot be satisfied since the l.h.s. is a pure function of the time coordinate while the r.h.s. depends on the rest of the coordinates as well.

- **The field depends only on the extra-dimension coordinate $\Phi = \Phi(y)$.** For such a field dependence, the l.h.s. of eq. (5.61) vanishes and thus we have the solution

$$m(v, r, y) = \frac{C(v, y)}{r} + D(v, r)\,. \tag{5.72}$$

Substitution of this mass function into eq. (5.68) requires its y-independence and this is in contrast with our main assumption that the mass has a non-trivial profile along the extra dimension.

- **The field depends only on the radial coordinate $\Phi = \Phi(r)$.** In this case, eq. (5.60) requires that either the warp function $A'(y) = 0$ or the coupling function $f'(\Phi) = 0$. In the former case there is no warping of the metric with the extra coordinate while in the latter we have once again the minimally coupled field theory of the previous section.

Consequently we are forced to assume that the field depends on more that one coordinates. Let us now study independently the special cases that the field depends on two of the coordinates and search for a viable solution before considering the most general case of $\Phi = \Phi(v, y, r)$.

- **The $\Phi = \Phi(v, r)$ case.** From (5.60) we have once again either $A'(y) = 0$ or $f'(\Phi) = 0$ that has already been discarded in the case of $\Phi(r)$ we studied previously.

- **The $\Phi = \Phi(v, y)$ case.** In this case, the constraint of eq. (5.68) can be written as

$$\partial_r^2 m - \frac{2}{r}\, \partial_r m = -\frac{f'}{f}\, \partial_v \Phi \,, \tag{5.73}$$

where in the r.h.s. we have an arbitrary function of v and y that we shall denote by $C(v,y) \equiv -\frac{f'}{f}\,\partial_v\Phi$. Integrating then twice with respect to the radial coordinate r we obtain the following solution:

$$m(v,r,y) = -C(v,y)\,\frac{r^2}{2} + D(v,y)\,\frac{r^3}{3} + E(v,y)\,, \tag{5.74}$$

in terms of the also arbitrary functions $D(v,y)$ and $E(v,y)$. Now, the combination of eqs. (5.63) and (5.65) gives the following constraint:

$$(1+f'')(\partial_y\Phi)^2 + f'\,\partial_y^2\Phi - A'f'\,\partial_y\Phi + 3fA'' = -\frac{f}{r}\,e^{-2A}\,\partial_r^2 m\,, \tag{5.75}$$

and since $A = A(y)$ and $f = f(v,y)$ the l.h.s. of this equation is r-independent, contrary to the r.h.s. that has a dependence on the radial coordinate. Substituting the expression for the mass function (5.74) into eq. (5.75), in order for the r.h.s. to be also r-independent, it is required that the condition $C(v,y) = 0$ holds. This last condition though cannot be satisfied since via eq. (5.73), we have that $C(v,y) \propto \partial_v\Phi \neq 0$.

- **The $\Phi = \Phi(r,y)$ case.** For such a coordinate dependence of the field we find that eq. (5.61) gets simplified to

$$(\partial_r f)\,\partial_y m + f\,(\frac{\partial_y m}{r} + \partial_r\partial_y m) = 0\,, \tag{5.76}$$

while eq. (5.68) is now

$$(\partial_r f)\Big(1 - \frac{3m}{r} + \partial_r m\Big) + f\big(\partial_r^2 m - \frac{2}{r}\,\partial_r m\big) = 0\,. \tag{5.77}$$

Equations (5.76) and (5.77), constitute a homogeneous linear system of equations with respect to the functions f and $\partial_r f$. Consequently, to allow for additional solutions beyond the trivial one $(f, \partial_r f) = (0,0)$ to exist, the determinant of the system should vanish. The latter requirement translates to the following constraint:

$$\left(\frac{\partial_y m}{r} + \partial_r\partial_y m\right)\left(1 - \frac{3m}{r} + \partial_r m\right) - \partial_y m\,\left(\partial_r^2 m - \frac{2}{r}\,\partial_r m\right) = 0\,. \tag{5.78}$$

To further proceed, we now write the mass function as a *finite* series of powers of the radial coordinate containing both positive and negative order coefficients. More precisely we write the mass function as

$$m(v,r,y) = \sum_n \alpha_n(v,y)\,r^n\,,\ n \in \mathbb{Z}\,. \tag{5.79}$$

Substitution of eq. (5.79) into eq. (5.78) yields

$$\sum_\ell (\partial_y\alpha_\ell)\,r^{\ell-1}\left[(\ell+1) + \sum_n \alpha_n\,r^{n-1}(n-\ell+1)(n-3)\right] = 0\,. \tag{5.80}$$

The most trivial way to satisfy this last equation is of course to require $\partial_y\alpha_\ell\,\forall\,\ell$. Unfortunately

this removes the y-dependence of the mass and so it is the quantity in the square brackets that has to vanish instead. The only way for this to happen is by removing the r-dependence introduced by the second term. It is clear then than the only two allowed powers for the radial coordinate are $n = 1$ and $n = 3$. The substitution of the mass into the metric function leads to

$$1 - \frac{2m}{r} = 1 - 2\alpha_1 - 2\alpha_3 r^2 \,, \tag{5.81}$$

and clearly does not yield a "black-hole" term but only a variant of an "(anti)de-Sitter" one.

Thus, the final case left to consider for the spherically-symmetric bulk scalar field is for it to depend on all three of the coordinates i.e. $\Phi = \Phi(v, r, y)$. Starting from eq. (5.59) we have

$$1 + f''(\Phi) = -f'(\Phi)\,\frac{\partial_r^2 \Phi}{(\partial_r \Phi)^2} \,, \tag{5.82}$$

and after substituting this result into eq. (5.60) we end up with

$$A' = \partial_r \left(\frac{\partial_y \Phi}{\partial_r \Phi} \right) . \tag{5.83}$$

Integrating then once with respect to the radial coordinate we find

$$\partial_y \Phi = \partial_r \Phi \big[A'(y)\, r + F(v, y) \big] \,, \tag{5.84}$$

where $F(v, y)$ is an arbitrary function. Substituting $\partial_y \Phi$ via eq. (5.84) into eq. (5.61) and combining the resultant equation with eq. (5.68) we find the following differential equation for f:

$$\begin{aligned} \partial_r f \left[(A' r + F) \left(1 - \frac{3m}{r} + \partial_r m \right) + r \partial_v F - \partial_y m + F \frac{\partial_v \Phi}{\partial_r \Phi} \right] \\ + f \left[(A' r + F) \left(\partial_r^2 m - \frac{2}{r}\, \partial_r m \right) - \frac{1}{r}\, \partial_y m - \partial_r \partial_y m \right] = \partial_r f A_1 + f A_2 = 0 \,. \end{aligned} \tag{5.85}$$

In the last equality we symbolized the coefficients of $\partial_r f$ and f with A_1 and A_2 respectively for convenience. If we now combine eqs. (5.64) with (5.65) and use eq. (5.82) to substitute $1 + f''$, the following differential equation is obtained:

$$\partial_r f \left[1 - \frac{2m}{r} - r e^{2A} \left(A'' r + \partial_y F \right) + \frac{\partial_v \Phi}{\partial_r \Phi} \right] + f \left(-3 A'' r e^{2A} - \frac{2}{r}\, \partial_r m \right) = \partial_r f B_1 + f B_2 = 0 \,. \tag{5.86}$$

Similarly to the previous equation, B_1 and B_2 are the coefficients of $\partial_r f$ and f respectively. The requirement of the vanishing of the determinant of the homogeneous system of eqs. (5.85) and (5.86) reads $A_1 B_2 - B_1 A_2 = 0$ or equivalently it may be written as

$$\frac{A_1}{B_1} = \frac{A_2}{B_2} \equiv G(v, r, y) \,, \tag{5.87}$$

for an arbitrary function $G(v,r,y)$ that depends on all of the coordinates. The second equality of the last relation is written explicitly as

$$(A'r+F)\left(\partial_r^2 m-\frac{2}{r}\,\partial_r m\right)-\frac{1}{r}\,\partial_y m-\partial_r\partial_y m=G(v,r,y)\left(-3A''re^{2A}-\frac{2}{r}\,\partial_r m\right). \tag{5.88}$$

If we now employ the form of the mass function given in eq. (5.79) the coefficients A_2 and B_2 will be polynomials of the radial coordinate. Then, via eq. (5.87) the arbitrary function will also be a polynomial that can be written as

$$G(v,r,y)=\sum_{\ell} g_\ell(v,y)\,r^\ell\,,\ \ l\in\mathbb{Z} \tag{5.89}$$

where the sum in ℓ is *finite* and may contain terms of both positive and negative order.

If we finally use the polynomial expressions for the mass (5.79) and $G(v,r,y)$ (5.89) in eq. (5.88) we end up with the following constraint:

$$\begin{aligned}\sum_n\Big[n(n-3)\alpha_n A'-(n+1)\,\partial_y\alpha_n\Big]r^{n-1}+\sum_n\alpha_n F n(n-3)\,r^{n-2}\\ =-3\sum_\ell g_\ell A''e^{2A}r^{\ell+1}-2\sum_{\ell,n}g_\ell\alpha_n n\,r^{\ell+n-2}\,.\end{aligned} \tag{5.90}$$

Now we will consider various choices for the parameters n and ℓ that are compatible with the constraint of eq. (5.90) and see if, for each one of these choices, an acceptable solution emerges for the mass function.

- $(n,l)=(3,1)$**.** In this case the substitution of the resultant mass into the metric function does not generate a black-hole term but a modified (anti)de-Sitter one.
- $(n,l)=(4,1)$**.** For this choice of the parameters we also have terms of the same order in r that appear in eq. (5.90) but again the corresponding mass does not describe a black hole on the brane.
- $n=0$**.** Though this choice is consistent with eq. (5.90) the corresponding mass function does not depend on the radial coordinate and is thus reduced to the case $m=m(v,y)$ that was studied in [198], or even to the black-string solutions [162] if the condition $\partial_y\alpha_n=0$ is furthermore imposed.

We may also consider other special cases that lead to the vanishing of the determinant of the system of eqs. (5.85) and (5.86).

- **The two differential eqs.** (5.85) **and** (5.86) **reduce to one.** Then the arbitrary function defined in eq. (5.87) will be $G(v,r,y)=1$ and this means that it does not depend on the radial

coordinate. Consequently via eq. (5.89) we are led to choose $\ell = 0$ and for this value of ℓ, eq. (5.90) requires that the other parameter n is either $n = 2$ or $n = 3$. For both these cases the metric function does not contain a black-hole term.

One of the rows or the columns of the determinant has zero entries.

- ⋆ If $A_2 = B_2 = 0$ one ends up with the solution of eq. (5.37) for the mass function with $\partial_y m_0 = 0$ that removes its y-dependence entirely thus rendering the solution insufficient to localize the bulk singularities.
- ⋆ If on the other hand we start with the condition $A_1 = B_1 = 0$, then eqs. (5.85) and (5.86) lead again to $A_2 = B_2 = 0$ and to the conclusion of the previous point.
- ⋆ Considering the case $A_1 = A_2 = 0$, we have from $A_2 = 0$ and the polynomial form of the mass function (5.79) that the following condition: $Fn(n-3) = 0$ should hold. The latter singles out three values for n. The obvious ones are $n = 3$ and $n = 0$. The third one is obtained if we further substitute $F = 0$ into $A_2 = 0$. The latter equation is then r-independent for $n = 1$. In any case, all these three values of n yield a mass that does not depend on the extra-dimension coordinate since the condition $\partial_y \alpha_n = 0$ has to be also imposed.
- ⋆ The final case is $B_1 = B_2 = 0$. Solving $B_2 = 0$ for the mass we obtain eq. (5.37). Then, substituting this into the second condition $B_1 = 0$ we find

$$\frac{\partial_v \Phi}{\partial_r \Phi} = \frac{2m_0(v,y)}{r} - 1 + r\partial_y F e^{2A}\,. \tag{5.91}$$

Plugging then this last relation along with eq. (5.37) into eq. (5.85), we end up with the following constraint:

$$\sum_\ell f_\ell\, r^{\ell+2}\, \frac{(\ell+4)}{2}\, \partial_y\Big(A'' e^{2A}\Big) + \sum_\ell f_\ell\, r^\ell\, \ell \left(A' + \partial_v F + F\partial_y F\, e^{2A}\right) - \sum_\ell f_\ell\, r^{\ell-1} \Big[3\ell A' m_0 + (\ell+1)\partial_y m_0\Big] - \sum_\ell f_\ell\, r^{\ell-2}\, \ell\, F m_0 = 0\,, \tag{5.92}$$

where we have also written the function f as a polynomial with respect to r of the form

$$f(v,r,y) = \sum_\ell f_\ell(v,y)\, r^\ell\,. \tag{5.93}$$

In order now for eq. (5.92) to hold, each individual term should vanish. From the condition $Fm_0 = 0$ then, we have either $F = 0$ that leads to $A'(y) = 0$ or $m_0 = 0$ that removes the y-dependence of the mass.

Based on the results of the study performed in this section we are led to the conclusion that even the most general spherically-symmetric bulk field that is non-minimally coupled to gravity is incompatible with the line element of eq. (5.3).

Finally, the interested reader is refered to the recent master's thesis [199] where, in an effort to obtain analytic brane-localized black-hole solutions with the metric ansatz of eq. (5.3), an even more complicated Lagrangian was considered. More precisely, the bulk field content consisted of two interacting scalar fields $\phi(v, y, r)$ and $\chi(v, y, r)$ that couple non-minimally to gravity via a general function $f(\phi, \chi)$. Nevertheless, the results of that study dictated that even such a general Lagrangian is not sufficient for localization to occur.

5.5 Conclusions

In the context of warped extra dimensions, analytic 5-dimensional localized-on-the-brane black-hole solutions are still elusive. In an effort to obtain such solutions, we extended previous studies by considering a generalized Vaidya ansatz for the metric where the mass parameter (m) depends on the time (v), extra dimension (y) and radial (r) coordinates. Of course, in order to satisfy the Einstein equations, an appropriate field content has to be introduced in the bulk. Then in principle, a mass function $m = m(v, y, r)$ may emerge from the field equations that corresponds to a black hole on the brane with a singularity that extends over a finite distance along the extra dimension.

With the prospect of obtaining such a solution, we studied a plethora of scalar field models that source the bulk energy-momentum tensor. Starting from the simplest possible non-trivial case, we assumed a bulk filled only with a cosmological constant. We then turned to the cases of a single scalar field and two interacting scalar fields minimally-coupled to gravity in conjunction with a general potential and general kinetic terms (including both canonical and non-canonical ones as well as mixed kinetic terms in the case of two scalars). Finally, we also considered a field theory of a non-minimally coupled bulk scalar field (Φ) that couples to the Ricci scalar via an arbitrary analytic function $f(\Phi)$.

In some of the above cases, solutions to the mass function that are compatible with the constraints imposed by the field equations have been found. When these solutions are substituted into the metric function, physically interesting terms such as "Schwarzschild-like", ($\sim r^{-1}$), "(anti)de-Sitter-like" ($\sim r^2$) or "Reissner–Nordström-like" ($\sim r^{-2}$) do emerge on the brane. Unfortunately, whenever such solutions exist, the profile of the mass along the extra dimension is not suitable to localize the black-hole singularity close to the brane.

Chapter 6

Conclusions

In this final chapter, we present the conclusions of the study performed in this dissertation.

In Chapter 2, we considered the propagation of scalar particles in the gravitational field of the Higher-dimensional (HD) Schwarzschild-de Sitter (SdS) black hole, both on the brane and in the bulk. The field theory we considered is that of a massless scalar field Φ that is non-minimally coupled to gravity via an interaction term in the action ($\xi\Phi^2 R$) with the Ricci scalar R. By deriving the Equation Of Motion (EOM) for the scalar field we found that an "effective mass" term appears that is proportional to the product of ξ and the cosmological constant Λ. This way our analysis incorporates the case of massive particles as well.

By employing a well-known matching technique of the two asymptotic solutions to the radial EOM of Φ close to the black hole (r_h) and cosmological (r_c) horizons, we derived approximate analytic expressions for the Greybody Factors (GF). Contrary to previous similar studies where the matching of the two asymptotic solutions demands a low-energy approximation, this was not necessary in our case and so our analytic results exhibit an extended range of validity. In addition, with an appropriately chosen new radial coordinate, the effect of the cosmological constant was taken into account both close and far away from r_h, while previous studies discard the effect of Λ close to r_h in order to simplify the calculation. Still, in order to have a matching of the two asymptotic solutions we had to assume small values for ξ and Λ. Other than that, our results are valid for an arbitrary number (n) of extra spacelike dimensions and partial mode (l) of the field.

We started by deriving the GFs for scalar fields propagating on the brane and studying its low-energy limit for both minimally and non-minimally coupled fields. In the former case and for the dominant mode ($l = 0$) of the field, we showed that our general expression reproduces the non-vanishing asymptotic limit exhibited by the GFs in the presence of a cosmological constant. We were able to show analytically that when the field coupling $\xi \neq 0$, in the limit $\omega \to 0$, the aforementioned asymptotic limit vanishes and the first non-zero contribution comes from the $\mathcal{O}(\omega^2)$ term which we also derived and presented.

Then, we studied the energy-profile of the full expressions for the GFs with respect to the particle (l, ξ) and spacetime (n, Λ) parameters. We found that as either of the two particle parameters or the number of extra dimensions increase the GFs get suppressed on the brane. With respect to Λ, we found that it can act in favor or against the enhancement of the GFs depending crucially on the

value of the field coupling. For small field couplings, the GFs get enhanced with an increase of the cosmological constant while the opposite effect is observed for large values of ξ.

We then turned to the study of a scalar field propagating in the bulk. By performing the corresponding analysis we once again obtained the approximate analytic expressions for the GFs, valid for arbitrary l and ξ. In the case of minimal coupling and for the dominant mode of the field the corresponding low-energy asymptotic limit of the GF is recovered from our expressions. Again, we have shown that when $\xi \neq 0$, this limit vanishes with the first non-zero term being of $\mathcal{O}(\omega^2)$. By studying the energy-profile of the bulk GFs on the parameters l, n, ξ and Λ, we found that they follow the same pattern as the brane GFs with the main characteristic being the milder dependence on ξ.

In Chapter 3, we developed a numerical technique to compute the exact expressions for the GFs in the case of a massless scalar field non-minimally coupled to gravity propagating in the HD SdS spacetime both on the brane and in the bulk. To achieve this, we numerically integrated the brane and bulk EOMs for Φ and obtained the corresponding radial part of the field which was then used to determine the transmission probabilities (GFs). To set the boundary conditions necessary for the integration of the EOMs we used the asymptotic analytic expressions of the previous chapter. We then compared the exact results we obtained via this method against our approximate analytic results, and we have indeed found that for small values of ξ and Λ the two sets of results are in excellent agreement. Deviations between the exact and approximate results appear as either ξ, Λ or the value of the energy are increased beyond the allowed regimes.

The exact analytic results for the GFs verified the behavior we have observed with the approximate analytic expressions, namely that an increase in any of the parameters ξ, l or n results in suppression of the GFs both on the brane and in the bulk. The cosmological constant on the other assumes a "dual role" and its effect on the transmission probabilities depends on the value of ξ - this is also a feature that had been exhibited by the analytic results. The reason behind this behavior is that Λ corresponds to the vacuum energy density that enhances the particle emission but on the other hand it is simultaneously proportional to the effective mass of the field, thus suppressing the emission of particles. As our analysis revealed, the effective mass is also proportional to the non-minimal coupling ξ and for this reason, when $\xi \ll 1$, it is the former effect of Λ that dominates.

With the exact forms of the brane and bulk GFs that are valid for arbitrary values of the field and spacetime parameters, we were then able to calculate the corresponding differential Energy Emission Rates (EERs) for Hawking radiation by the HD SdS black hole that decays in the form of scalar particles in the brane and bulk channels of emission. The dependence of the Hawking spectrum on the parameters comes from the GF as well as from the expression for the temperature. More precisely, the temperature depends on the spacetime parameters n and Λ. In this study we have employed the Bousso-Hawking normalization for the temperature (T_{BH}) to account for the non-asymptotic flatness of the SdS spacetime.

We found that in both channels, the increase in the number of extra dimensions causes the enhancement of the emission even though the GFs get suppressed with n. This behavior is due to the enhancement of T_{BH} with n that dominates over the effect of the GF. The field coupling ξ (that can be interpreted as an effective mass term) caused the suppression of the EERs throughout the energy regime. Finally with respect to the effect of the cosmological constant we found that the dual-role behavior is also reflected on the EERs. When the field couples weakly with gravity, there is a global enhancement of the emission with Λ throughout the energy regime while for larger values of ξ the low-energy part of the spectrum gets suppressed.

By computing the relative energy rates we showed that for small ξ and Λ it is the brane channel that dominates in the low- and intermediate-energy regime while as ξ is increased the bulk channel gets boosted. The combined effect of an increased ξ and a large value of n results in the dominance of the bulk channel over the brane one. This has been one of the very few times where the brane channel becomes sub-dominant (see also [200]) and this is caused by the presence of the non-trivial interaction of the field with the gravity.

In Chapter 4 we turned to the effect of the temperature on the EERs of the HD SdS black hole. Due to the presence of a cosmological horizon endowed with a temperature that is in principle different from the black-hole one, the SdS spacetime is in absence of true thermal equilibrium and an asymptotically flat limit. To deal with these issues various proposals appeared in the literature regarding the appropriate definition of the temperature in SdS. We considered two different black-hole temperatures. The *bare black-hole temperature* T_0 in which the timelike Killing Vector Field (KVF) K^μ that is associated with the surface gravity is normalized "naively" to $K^\mu K_\mu = -1$ as in the asymptotically flat case. On the other hand, the *Bousso-Hawking normalized temperature* T_{BH} takes into account the non-asymptotic flatness by appropriately normalizing K^μ. We also considered three *effective temperatures* T_{eff-}, T_{eff+} and T_{effBH} that are combinations of the black-hole and cosmological horizon temperatures and are derived via effective thermodynamic first laws where the cosmological constant plays the role of the pressure of the system.

We started by studying the dependence of the above set of five temperatures on the cosmological constant and the number of extra dimensions. The former parameter assumed values from zero up to the critical limit Λ_{crit} (Nariai limit) that is the maximum allowed value of Λ, for a given n, that yields only two horizons for the SdS spacetime. In the limit $\Lambda \to 0$, T_0 and T_{BH} reduce to the HD Schwarzschild temperature while the effective ones vanish. This is due to the fact that in their construction the cosmological constant (pressure of the system) is assumed to be non-vanishing. In the other extreme limit $\Lambda \to \Lambda_{crit}$, only T_{BH} and T_{eff-} asymptote to a non-vanishing value while the rest of the temperatures vanish. The same Λ-profile of the temperatures is observed as n is increased with the black-hole temperatures getting a significant enhancement. In all cases, it is the Bousso-Hawking normalized temperature that dominates throughout the allowed Λ range.

Then we studied the effect of each of the temperatures on the EERs both on the brane and in the bulk for indicative values of Λ that span the whole allowed regime and for a small ($n = 2$) and large ($n = 5$) value of the number of extra dimensions. We found that the spectra follow closely the behavior of their corresponding temperature. The most dominant spectra are produced when the T_{BH} temperature is employed. In the low-Λ regime the most emissive spectra are produced by T_{BH} and T_0 while close to the critical limit, the T_{BH} and T_{eff-} temperatures give the dominant emission curves. The temperatures T_{eff+} and T_{effBH} yield a non-negligible spectrum only for intermediate values of Λ.

When there is no field coupling to gravity ($\xi = 0$), the non-zero low-energy ($\omega \to 0$) asymptotic value of the GFs for the dominant mode results to EERs that are non-vanishing in this limit. Consequently, a significant number of soft particles are expected to be emitted. For the case of the effective temperatures it is in fact this part of the energy spectrum that contributes the most to their total emissivity since the peaks of the EER curves are located close to $\omega \to 0$. When $\xi \neq 0$ the emission curves return to their "usual" shape where they vanish in the limits $\omega \to 0$ and $\omega \to \infty$ while exhibiting a peak at intermediate values of ω.

The analysis performed in this chapter not only serves as a comparison between the emission curves obtained for various temperatures but it also provides information about the EERs close to the critical limit. By computing the total emissivities in the two channels for the above five temperatures, we found that as Λ is increased the bulk channel gets enhanced over the brane one (except for T_0 when $\xi \neq 0$) and becomes the dominant one as the critical limit is approached and the temperature is non-vanishing i.e. for T_{BH} and T_{eff-}. When the number of extra dimensions is also increased, the bulk dominated for the bare black-hole temperature T_0 as well.

As a conclusion the choice of temperature greatly affects the obtained EERs for scalar particle emission by the HD SdS black hole. While some of the proposed temperatures do not produce significant emission rates, others do so only in the low- or large-Λ regimes. In any case, and throughout the allowed range of parameters, the Bousso-Hawking normalized temperature yields the most enhanced EERs.

Finally, in Chapter 5 we turned to the quest for obtaining analytic, 5-dimensional, localized on the brane black-hole solutions in the Warped Extra Dimensions (WEDs) scenario. By extending previous analyses [173, 198], we considered a metric ansatz that reduces to a Schwarzschild-like metric at the location of the brane with a mass parameter that on top of the time and extra dimension (y) coordinates also depends on the radial coordinate (r). This ansatz allows for greater flexibility of the field equations and also allows for additional terms in the metric function beyond the Schwarzschild one such as Reissner-Nordstrom-like ($\sim r^{-2}$) or (anti-)de Sitter-like ($\sim r^2$) to emerge. Even though the extra-coordinate dependence of the mass function yields extra singular terms in the curvature invariants, an appropriate solution for the mass function, i.e. one that decreases fast enough as we move away from the brane, can localize them close to $y = 0$.

To support this metric ansatz we considered a plethora of field theory models in the bulk that source the energy momentum tensor ($T_{\mu\nu}$) in Einstein's field equations. We started with a bulk filled with a cosmological constant and we found that even though a Schwarzschild-(A)dS type of metric function is allowed, the y-dependence of the mass that is necessary to localize the singularity close to the brane is prohibited. The isotropy of $T_{\mu\nu}$ along all five coordinates imposed this constraint.

Next we considered a single bulk scalar field with either canonical or non-canonical kinetic term but the y-independence of the mass function is also required in this case by the constraints imposed by the field equations, and this prevented a viable solution from emerging.

We then moved on to consider two interacting scalar fields with canonical or non-canonical kinetic terms and we thus avoided the total isotropy of $T_{\mu\nu}$. Unfortunately the rest of the constraints required that the terms generating the anisotropy of $T_{\mu\nu}$ should vanish and this translated to a y-independent mass function once again. The next step was to consider mixed kinetic terms for the two scalar fields. This way we avoided the isotropy of the energy momentum tensor and obtained a Schwarzschild-(A)dS (S(A)dS) type of solution with y-dependent mass function. Still, in the metric function, the y-dependence appears as a multiplicative factor in the term $\sim r^2$ and not in the $\sim r^{-1}$ one that is associated with the bulk singularities. So this case also had to be discarded.

In the final section of Chapter 5, we considered a general coupling function $f(\Phi)$ between the bulk scalar field Φ and the Ricci scalar along with a general potential and a cosmological constant term in the action. In this case, solutions resembling S(A)dS or Reissner–Nordström emerged but the complete set of constrains trivialized the mass function or the black-hole spacetime itself.

Appendix A

The proper distance between r_h and r_c in the Nariai limit

In this appendix, following [87, 201] we show that the *apparent* coalescence of the black hole horizon r_h and the cosmological horizon r_c in the Schwarzschild-de Sitter (SdS) metric in the critical limit, does not mean that the physical space between the horizons reduces to zero. Consider the SdS metric in four dimensions for reasons of simplicity

$$ds^2 = -h(r)dt^2 + \frac{1}{h(r)}dr^2 + r^2 d\Omega_2 \quad , \quad h(r) \equiv 1 - \frac{2m}{r} - \frac{\Lambda}{3}r^2 \,. \tag{A.1}$$

Then, there are only two horizons if the black-hole mass (m) and the cosmological constant (Λ) satisfy $0 < m < \frac{1}{3}\Lambda^{-1/2}$ while the critical limit, in which the two horizons meet, is given in terms of an infinitesimal parameter ϵ as

$$9m^2\Lambda = 1 - 3\epsilon^2 \quad , \quad 0 \leqslant \epsilon \ll 1 \,, \tag{A.2}$$

and so we have that the horizons are identified in the limit $\epsilon \to 0$. Under the following redefinitions for the time and radial coordinates in eq. (A.1),

$$t = \frac{1}{\epsilon\sqrt{\Lambda}}\psi \quad , \quad r = \frac{1}{\sqrt{\Lambda}}\left[1 - \epsilon\cos\chi - \frac{1}{6}\epsilon^2\right] \,, \tag{A.3}$$

to first order in ϵ the metric can be re-cast into

$$ds^2 = \frac{1}{\Lambda}\left[-\left(1 + \frac{2}{3}\epsilon\cos\chi\right)\sin\chi^2 d\psi^2 + \left(1 - \frac{2}{3}\epsilon\cos\chi\right)d\chi^2 + (1 - 2\epsilon\cos\chi)\, d\Omega_2^2\right] \,, \tag{A.4}$$

where the locations of the Killing horizons in these coordinates are determined by the vanishing of the metric function, i.e. $g_{tt} = 0$, and are $\chi = 0$ for the black-hole horizon and $\chi = \pi$ for the cosmological horizon.

Now, it is easy to see that the proper distance between the two horizons is non zero since in the limit $\epsilon \to 0$ we have

$$\int_0^\pi \frac{1}{\sqrt{\Lambda}}\sqrt{1 - \frac{2}{3}\epsilon\cos\chi}\, d\chi \simeq \int_0^\pi \frac{1}{\sqrt{\Lambda}}\left(1 - \frac{1}{3}\epsilon\cos\chi\right)d\chi = \frac{\pi}{\sqrt{\Lambda}} \neq 0 \,. \tag{A.5}$$

Appendix B

The manipulation of the energy dependence of the radial EOM

In this appendix, we present the various ways in which one may write the radial EOM for the scalar field that propagates in the HD SdS spacetime eq. (2.28) in order to obtain the most "reasonable" expressions for the GFs. For convenience we re-write the EOM here

$$f\,(1-f)\,\frac{d^2R(f)}{df^2}+(1-B_h\,f)\,\frac{dR(f)}{df}+\left[\,\frac{(\omega r_h)^2}{A_h^2 f}-\frac{\lambda_h\,(1-\tilde{\Lambda}r_h^2)}{A_h^2(1-f)}\,\right]R(f)=0\,. \tag{B.1}$$

We use this EOM to illustrate the method but keep in mind that this also applies to the asymptotic form of the EOM close to the cosmological horizon as well and for fields that propagate on the brane and in the bulk. Let us focus on the form of the term in the square brackets (in this appendix we use the letter A to indicate this term). During the process of recasting the radial EOM for the scalar field into the hypergeometric equation of eq. (2.31)

$$f\,(1-f)\,\frac{d^2F(f)}{df^2}+[c_1-(1+a_1+b_1)\,f]\,\frac{dF(f)}{df}-a_1b_1\,F(f)=0\,, \tag{B.2}$$

the term A in general is not of the form given in eq. (B.1) but rather

$$A\equiv\left[\,\frac{(\omega r_h)^2}{A_h^2 f(1-f)}-\frac{\lambda_h\,(1-\tilde{\Lambda}r_h^2)}{A_h^2(1-f)}\,\right]. \tag{B.3}$$

Clearly, the form of A as it is given in eq. (B.1) is one of the mathematically equivalent ways that one may write (B.3) in the near-horizon ($f\to 0$) limit. Still, the way one chooses to write this term affects the energy-profiles of the obtained GFs due to the fact that the locations of the poles that appear in the gamma functions in the solution for GF change. Consequently some choices are "less appropriate" than others, in the sense that they result in the abrupt termination of the GF curves or yield curves that do not asymptote to the value 1 in the high-energy limit as is the typical behavior of the GFs.

Let us start by recalling the form of the parameters a_1 and b_1 of eq. (B.2) that appear in the arguments of the gamma functions of the analytic expressions for the GF (we re-write them here for convenience)

$$a_1=\alpha_1+\beta_1+B_h-1\qquad b_1=\alpha_1+\beta_1\,,\qquad c_1=1+2\alpha_1\,. \tag{B.4}$$

After the field redefinition (2.30), namely $R(f) = f^{\alpha_1}(1-f)^{\beta_1}F(f)$, that takes us from eq. (B.1) to eq. (B.2), the energy dependence of the first term in eq. (B.3) is distributed to the parameters a_1 and b_1 via the form of α_h and β_h. The latter two parameters are determined by the requirement that the coefficient of $F(f)$ in eq. (B.2) should not depend on f which is guaranteed by imposing the vanishing of the coefficients of the non-zero powers of f that appear in the product $a_1 b_1$. So it is clear that the way one writes the coefficient A close to the horizon affects the form of α_h and β_h which in tern determine a_1 and b_1 that appear in the analytic GF expressions.

Using the fact that close to the horizon $f \to 0$ or equivalently $(1-f) \to 1$ we may multiply "at will" the first term in eq. (B.3) with unity i.e. $1 \sim (1-f)$ and this way "split" the energy dependence of $(\omega r_h)^2$ to terms with various powers of f.

As an example consider the following case:

$$\frac{(\omega r_h)^2}{A_h^2 f(1-f)} = \frac{(\omega r_h)^2(1-f)}{A_h^2 f} = -\frac{(\omega r_h)^2}{A_h^2} + \frac{(\omega r_h)^2}{A_h^2}\frac{1}{f}\,. \tag{B.5}$$

This way the parameters that characterize the solution assume the following forms:

$$\alpha_1 = -\frac{i\omega r_h}{A_h}$$

$$\beta_1 = \frac{1}{2}\left[2 - B_h\right] - \frac{1}{2}\sqrt{(B_h-2)^2 + \frac{4\lambda_h(1-\Lambda r_h^2)}{A_h^2}}$$

$$a_1 = (\alpha_h + \beta_h) + \frac{1}{2}\left[B_h - 1\right] + \frac{1}{2}\sqrt{(B_h-1)^2 - 4\left(\frac{\omega r_h}{A_h}\right)^2}$$

$$b_1 = (\alpha_h + \beta_h) + \frac{1}{2}\left[B_h - 1\right] - \frac{1}{2}\sqrt{(B_h-1)^2 - 4\left(\frac{\omega r_h}{A_h}\right)^2}$$

$$c_1 = 2\alpha_h + 1$$

Another way to write the first term of eq. (B.3) is

$$\frac{(\omega r_h)^2}{A_h^2 f(1-f)} = \left(\frac{\omega r_h}{A_h}\right)^2 \frac{1}{f} + \left(\frac{\omega r_h}{A_h}\right)^2 \frac{1}{(1-f)}\,. \tag{B.6}$$

In this case, the parameters assume the following forms:

$$\alpha_h = -\frac{i\omega r_h}{A_h}$$

$$B_h = 1 + \frac{4\Lambda r_h^2}{A_h^2}$$

$$\beta_h = \frac{1}{2}\left[(2 - B_h) - \sqrt{(B_h - 2)^2 + \frac{4(\lambda_h(1 - \Lambda r_h^2) - (\omega r_h)^2)}{A_h^2}}\right]$$

$$a_1 = \alpha_h + \beta_h$$

$$b_1 = \alpha_h + \beta_h + (B_h - 1)$$

$$c_1 = 1 - \frac{2i\omega r_h}{A_h}$$

We have found that the "best results" for the GFs are obtained upon writing (B.3) as in eq. (B.1). The curves produced for the GF with the choice we made (B.1) in the manipulation of the A term, are affected the less by the existence of poles. Finally, our choice is further justified by the impressive agreement between the analytic results we obtained and the exact numerical ones.

Appendix C

Numerical code for the calculation of the greybody factors

In this Appendix, we present the numerical code we developed in the context of [3] in order to derive the exact forms for the greybody factors (GF) in the case of a massless scalar field that exhibits a non-minimal coupling with gravity and propagates in the higher-dimensional Schwarzschild-de Sitter spacetime. The exact forms of the GF in the case of brane-confined as well as for bulk-propagating fields may be computed with the following algorithm:

```
SetDirectory[NotebookDirectory[]];
$TemporaryDirectory = NotebookDirectory[];
(* ---------------------- Input of the parameters -
 (START) ------------------------------------------------ *)

Λ = 0.1; (* The value of the cosmological constant. *)
ξ = 0.1; (* The non-minimal coupling parameter. *)
n = 2; (* The number of extra dimensions. *)
l = 0; (* The angular momentum quantum number. *)
rh = 1;(* The black-hole horizon radius. *)

BoundaryConditions = 2;
(* Variable that discriminates between the different choices for the boundary conditions. *)
radialeom = "bulk";
(* Variable that discriminates between the bulk and brane radial equations of motion *)

ε = 10^(-5); (* The infinitesimal radial distance from the horizons. *)

w0 = 0.000001;(* Initial value of the energy for the integration of the radial eom. *)
wmax = 1.5;(* Final value of the energy for the integration of the radial eom. *)
datapoints = 200; (* Variable that determines the number of
 data points the code generates in the energy interval: (wmax-w0). *)
dw = wmax / datapoints; (* The integration step for the solution of the radial eom. *)

(* ---------------------- Input of the parameters -
 (END) ------------------------------------------------ *)

If[radialeom == "brane",
 filename = "GFdatafilebrane.txt";]
If[radialeom == "bulk",
 filename = "GFdatafilebulk.txt";](* The name of the file containing the generated data. *)

Clear[rc];
Lam = 2 Λ / ((n + 2) (n + 3));
hr = 1 - (1 - Lam) / r^(n + 1) - Lam r^2;
(* The metric function after using h(rh)=0 and rh=1 to eliminate the mass parameter μ. *)
roots = NSolve[hr == 0, r] ;
list = Table[0 j , {j, 1, n + 3}]; (* The roots of the metric function. *)
Do[If[Im[r /. roots[[i, 1]]] == 0, list[[i]] = r /. roots[[i, 1]]], {i, 1, n + 3}];
rc = Max[list]; (* Sorting and isolating the root corresponding to the cosmological
 horizon radius in a systematic way valid for any choice of the parameters of the system.*)

Ah = (n + 1) - (n + 3) Lam rh^2;
(* The quantity Ah (defined in eq. ... ) evaluated at the location of the black-hole horizon *)
Ac = (n + 1) - (n + 3) Lam rc^2;
(* The quantity Ah (defined in eq. ... ) at the location of the cosmological horizon *)

af[x_, w_] := 1;
bf[x_, w_] := -I w rh (n + 1 - (n + 3) Lam x^2)
    (1 - (1 - (1 - Lam) / x^(n + 1) - Lam x^2) / (1 - Lam x^2)) / (Ah x (1 - (1 - Lam) / x^(n + 1) - Lam x^2));


near = rh + ε; (* The final value of the radial coordinate for the solution of the eom. *)
far = rc - ε; (* The initial value of the radial coordinate for the solution of the eom. *)



OpenWrite[filename];

For[w = w0, w < wmax, w = w + dw, (* For each value of w in the
```

```
   range (wmax-w0) we compute the corresponding value of the greybody factor. *)


  (* ---------------------- Solution of the radial eom on the brane -
   (START) ------------------------------------------------- *)
  If[radialeom == "brane",
   radialfn[r] =
     NDSolve[{(1 - (1 - Lam) / r^(n + 1) - Lam r^2) D[r^2 (1 - (1 - Lam) / r^(n + 1) - Lam r^2) R'[r], r] +
          (w^2 r^2 - (l (l + 1) + ξ r^2 (12 Lam + n (n - 1) (1 - Lam) / r^(n + 3)))
               (1 - (1 - Lam) / r^(n + 1) - Lam r^2)) R[r] == 0, R[near] == af[near, w], R'[near] == bf[near, w]},
      R[r], {r, near, far}, AccuracyGoal → Infinity, MaxSteps → Infinity];
   (* ---------------------- Solution of the radial eom on the brane -
    (END) ------------------------------------------------- *)
   ,
   (* ---------------------- Solution of the radial eom in the bulk -
    (START) ------------------------------------------------- *)
   radialfn[r] = NDSolve[{(hr) D[r^(n + 2) (hr) R'[r], r] +
         (w^2 r^(n + 2) - (hr) (l (l + n + 1) r^(n) + ξ r^(n + 2) ((n + 3) (n + 4) Lam))) R[r] == 0,
      R[near] == af[near, w], R'[near] == bf[near, w]}, R[r], {r, near, far},
     AccuracyGoal → Infinity, MaxSteps → Infinity];
   (* ---------------------- Solution of the radial eom in the bulk -
    (END) ------------------------------------------------- *)
  ];

  (* ---------------------- Boundary conditions -
   (START) ------------------------------------------------- *)
  (* First set *)
  If[BoundaryConditions == 1,
   Rfn[r] = R[r] /. radialfn[r];
   ffn[r] = Ac (1 - (1 - Lam) / r^(n + 1) - Lam r^2) r
     D[Rfn[r], r] / (w rc ((n + 1) - (n + 3) Lam r^2) (1 - (1 - (1 - Lam) / r^(n + 1) - Lam r^2) / (1 - Lam r^2)));
   pfn[w] = (1 / 2) Exp[-I w rc Log[(1 - (1 - Lam) / r^(n + 1) - Lam r^2) / (1 - Lam r^2)] / Ac]
      (Rfn[r] - I ffn[r]) /. r → far;
   qfn[w] = (1 / 2) Exp[I w rc Log[(1 - (1 - Lam) / r^(n + 1) - Lam r^2) / (1 - Lam r^2)] / Ac]
      (Rfn[r] + I ffn[r]) /. r → far;
   greyfn = (1 - Abs[(pfn[w])^2 / (qfn[w])^2]);
  ];
  (* Second set *)
  If[BoundaryConditions == 2,
   Rfn[r] = R[r] /. radialfn[r];
   ffn[r] = 2 (1 - (1 - Lam) / r^(n + 1) - Lam r^2) D[Rfn[r], r] / (w rc D[1 - (1 - Lam) / r^(n + 1) - Lam r^2, r]);
   pfn[w] = (1 / 2) Exp[-I w rc Log[1 - (1 - Lam) / r^(n + 1) - Lam r^2] / 2] (Rfn[r] - I ffn[r]) /. r → far;
   qfn[w] = (1 / 2) Exp[I w rc Log[1 - (1 - Lam) / r^(n + 1) - Lam r^2] / 2] (Rfn[r] + I ffn[r]) /. r → far;
   greyfn = (1 - Abs[(qfn[w])^2 / (pfn[w])^2]);
  ];
  (* ---------------------- Boundary conditions -
   (END) ------------------------------------------------- *)

  Write[filename, {w, Abs[greyfn[[1]]]}];
  (* For[w] end *)];
Close[filename];


(* ---------------------- Plotting the greybody factor -
 (START) ------------------------------------------------- *)
horLabel = "ωr_h";
verLabel = "|A|^2";

ListPlot[ReadList[filename],
 PlotStyle → {Thick},
```

```
 (*PlotLegends→Placed[{"n="<>ToString[n]},{0.85,0.63}],*)
 Joined → True,
 ImageSize → 550,
 PerformanceGoal → "Quality",
 Frame → True,
 LabelStyle → {FontFamily → "Times", FontSize → 24, Bold},
 FrameLabel → {horLabel, Rotate[verLabel, -Pi / 2]},
 FrameStyle → Directive[Black, Opacity[1.5]]
]
(* ---------------------- Plotting the greybody factor -
 (END) ------------------------------------------------- *)
```

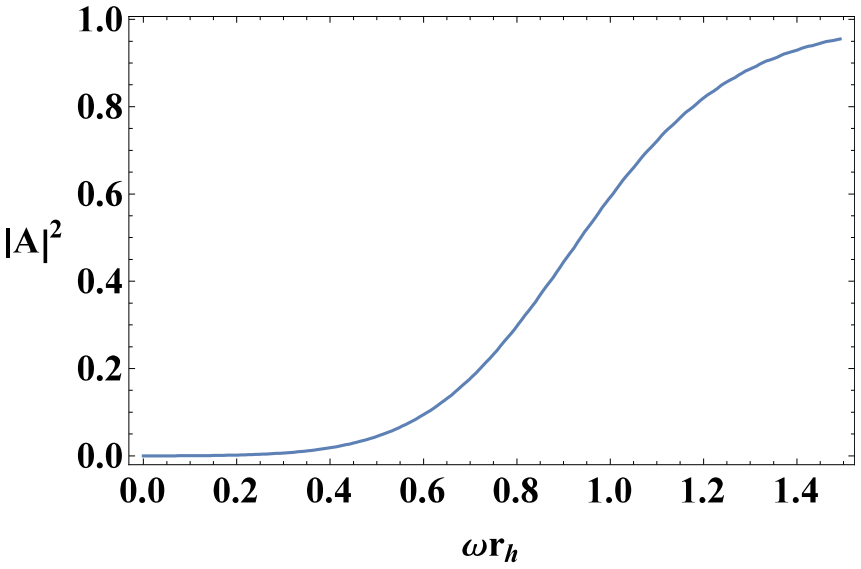

Appendix D

Numerical code for the calculation of the differential energy emission rates

In this Appendix, we present the numerical code we developed in the context of [3] in order to derive the differential energy emission rates (EERs) for the Hawking radiation of a higher-dimensional Schwarzschild-de Sitter black hole. The following algorithm is suitable to calculate the EERs for both the brane and bulk channels of emission:

```
SetDirectory[NotebookDirectory[]];
$TemporaryDirectory = NotebookDirectory[];
(* ---------------------- Input of the parameters -
 (START) ------------------------------------------------- *)

Λ = 0.1; (* The value of the cosmological constant. *)
ξ = 0.1; (* The non-minimal coupling parameter. *)
n = 1; (* The number of extra dimensions. *)
lmin = 0;(* The dominant mode of the field *)
lmax = 0; (* The upper cut-off in the l- summation of the power spectrum *)
rh = 1;(* The black-hole horizon radius. *)

BoundaryConditions = 1;
(* Variable that discriminates between the different choices for the boundary conditions. *)
radialeom = "bulk";(* Variable that discriminates between the bulk and brane radial equations of motion *)

ε = 10^(-5); (* The infinitesimal radial distance from the horizons. *)

w0 = 0.000001;(* Initial value of the energy for the integration of the radial eom. *)
wmax = 1.5;(* Final value of the energy for the integration of the radial eom. *)
datapoints = 50; (* Variable that determines the number of
 data points the code generates in the energy interval: (wmax-w0). *)
dw = wmax / datapoints; (* The integration step for the solution of the radial eom. *)

(* ---------------------- Input of the parameters -
 (END) ------------------------------------------------- *)

If[radialeom == "brane",
 filename = "EERdatafilebrane.txt";]
If[radialeom == "bulk",
 filename = "EERdatafilebulk.txt";](* The name of the file containing the generated data. *)

Clear[rc];
Lam = 2 Λ / ((n + 2) (n + 3));
hr = 1 - (1 - Lam) / r^(n + 1) - Lam r^2;
(* The metric function after using h(rh)=0 and rh=1 to eliminate the mass parameter μ. *)
roots = NSolve[hr == 0, r] ;
list = Table[0 j , {j, 1, n + 3}]; (* The roots of the metric function. *)
Do[If[Im[r /. roots[[i, 1]]] == 0, list[[i]] = r /. roots[[i, 1]]], {i, 1, n + 3}];
rc = Max[list]; (* Sorting and isolating the root corresponding to the cosmological
 horizon radius in a systematic way valid for any choice of the parameters of the system.*)


(*Calculating the radius of the preferred non-accelerated observer (PNAO) *)
Clear[Tbh];
roots2 = NSolve[D[1 - (1 - Lam) / r^(n + 1) - Lam r^2, r] == 0, r] ;
list2 = Table[0 j , {j, 1, n + 3}];
Do[If[Im[r /. roots2[[i, 1]]] == 0, list2[[i]] = r /. roots2[[i, 1]]], {i, 1, n + 3}];
r0 = Max[list2];
dh0 = (1 - (1 - Lam) / r^(n + 1) - Lam r^2) /. {r → r0};

(* Defining the surface gravity of the horizons *)
kh =  (2 rh)^(-1) ((n + 1) - 2 Λ rh^2 / (n + 2));
kc = - (2 rc)^(-1) ((n + 1) - 2 Λ rc^2 / (n + 2));

 (* The Bousso-Hawking temperature*)
Tbh = (Sqrt[dh0])^(-1) kh / (2 Pi);
```

```
Ah = (n + 1) - (n + 3) Lam rh^2;
(* The quantity Ah (defined in eq. ... ) evaluated at the location of the black-hole horizon *)
Ac = (n + 1) - (n + 3) Lam rc^2;
(* The quantity Ah (defined in eq. ... ) at the location of the cosmological horizon *)

af[x_, w_] := 1;
bf[x_, w_] := -I w rh (n + 1 - (n + 3) Lam x^2)
    (1 - (1 - (1 - Lam) / x^(n + 1) - Lam x^2) / (1 - Lam x^2)) / (Ah x (1 - (1 - Lam) / x^(n + 1) - Lam x^2));


near = rh + ε; (* The final value of the radial coordinate for the solution of the eom. *)
far = rc - ε; (* The initial value of the radial coordinate for the solution of the eom. *)



OpenWrite[filename];

For[w = w0, w < wmax, w = w + dw, (* For each value of w in the
   range (wmax-w0) we compute the corresponding value of the greybody factor. *)
  Clear[EER]; EER = 0; Do[

   (* ---------------------- Solution of the radial eom on the brane -
    (START) ------------------------------------------------- *)
   If[radialeom == "brane",
    radialfn[r] = NDSolve[{(1 - (1 - Lam) / r^(n + 1) - Lam r^2) D[r^2 (1 - (1 - Lam) / r^(n + 1) - Lam r^2) R'[r], r] +
          (w^2 r^2 - (l (l + 1) + ξ r^2 (12 Lam + n (n - 1) (1 - Lam) / r^(n + 3))) (1 - (1 - Lam) / r^(n + 1) - Lam r^2))
           R[r] == 0, R[near] == af[near, w], R'[near] == bf[near, w]},
       R[r], {r, near, far}, AccuracyGoal → Infinity, MaxSteps → Infinity];
    (* ---------------------- Solution of the radial eom on the brane -
     (END) ------------------------------------------------- *)
    ,
    (* ---------------------- Solution of the radial eom in the bulk -
     (START) ------------------------------------------------- *)
    radialfn[r] = NDSolve[{(hr) D[r^(n + 2) (hr) R'[r], r] + (w^2 r^(n + 2) -
              (hr) (l (l + n + 1) r^(n) + ξ r^(n + 2) ((n + 3) (n + 4) Lam))) R[r] == 0, R[near] == af[near, w],
        R'[near] == bf[near, w]}, R[r], {r, near, far}, AccuracyGoal → Infinity, MaxSteps → Infinity];
    (* ---------------------- Solution of the radial eom in the bulk -
     (END) ------------------------------------------------- *)
   ];

   (* ---------------------- Boundary conditions -
    (START) ------------------------------------------------- *)
   (* First set *)
   If[BoundaryConditions == 1,
    Rfn[r] = R[r] /. radialfn[r];
    ffn[r] = Ac (1 - (1 - Lam) / r^(n + 1) - Lam r^2) r
      D[Rfn[r], r] / (w rc ((n + 1) - (n + 3) Lam r^2) (1 - (1 - (1 - Lam) / r^(n + 1) - Lam r^2) / (1 - Lam r^2)));
    pfn[w] = (1 / 2) Exp[-I w rc Log[(1 - (1 - Lam) / r^(n + 1) - Lam r^2) / (1 - Lam r^2)] / Ac]
       (Rfn[r] - I ffn[r]) /. r → far;
    qfn[w] = (1 / 2) Exp[I w rc Log[(1 - (1 - Lam) / r^(n + 1) - Lam r^2) / (1 - Lam r^2)] / Ac]
       (Rfn[r] + I ffn[r]) /. r → far;
    greyfn = (1 - Abs[(pfn[w])^2 / (qfn[w])^2]);
   ];
   (* Second set *)
```

```
    If[BoundaryConditions == 2,
     Rfn[r] = R[r] /. radialfn[r];
     ffn[r] = 2 (1 - (1 - Lam) / r^(n + 1) - Lam r^2) D[Rfn[r], r] / (w rc D[1 - (1 - Lam) / r^(n + 1) - Lam r^2, r]);
     pfn[w] = (1 / 2) Exp[-I w rc Log[1 - (1 - Lam) / r^(n + 1) - Lam r^2] / 2] (Rfn[r] - I ffn[r]) /. r → far;
     qfn[w] = (1 / 2) Exp[I w rc Log[1 - (1 - Lam) / r^(n + 1) - Lam r^2] / 2] (Rfn[r] + I ffn[r]) /. r → far;
     greyfn = (1 - Abs[(qfn[w])^2 / (pfn[w])^2]);
    ];
    (* ---------------------- Boundary conditions -
     (END) ---------------------------------------------------- *)

    If[radialeom == "brane", (* With this conditional function,
     we define the "multiplicity of states" coefficient Nl on the brane and in the bulk. *)
     Nl = 2 l + 1,
     Nl = (2 l + n + 1) Factorial[l + n] / Factorial[l] / Factorial[n + 1]
    ];


    EER = EER + (Abs[greyfn[[1]]] Nl w / (Exp[w / Tbh] - 1) / (2 π));


    , {l, lmin, lmax}];

   Write[filename, {w, EER}];
    (* For[w] end *)];
Close[filename];


(* ---------------------- Plotting the energy emission rate -
  (START) ---------------------------------------------------- *)
horLabel = "ωr_h";
verLabel = "EER";

ListPlot[ReadList[filename],
 PlotStyle → {Thick},
 (*PlotLegends→Placed[{"n="<>ToString[n]},{0.85,0.63}],*)
 Joined → True,
 ImageSize → 550,
 PerformanceGoal → "Quality",
 Frame → True,
 LabelStyle → {FontFamily → "Times", FontSize → 24, Bold},
 FrameLabel → {horLabel, Rotate[verLabel, -Pi / 2]},
 FrameStyle → Directive[Black, Opacity[1.5]]
]
(* ---------------------- Plotting the energy emission rate -
  (END) ---------------------------------------------------- *)
```

Out[44]=

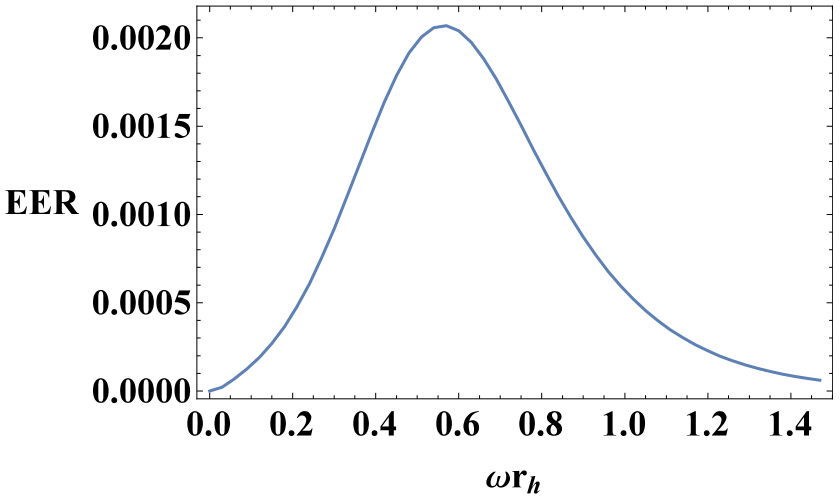

Bibliography

[1] Panagiota Kanti, Thomas Pappas, and Nikolaos Pappas. Greybody factors for scalar fields emitted by a higher-dimensional Schwarzschild–de Sitter black hole. *Phys. Rev.*, D90(12):124077, 2014. doi:10.1103/PhysRevD.90.124077.

[2] P. Kanti, N. Pappas, and T. Pappas. On the localisation of four-dimensional brane-world black holes: II. The general case. *Class. Quant. Grav.*, 33(1):015003, 2016. doi:10.1088/0264-9381/33/1/015003.

[3] T. Pappas, P. Kanti, and N. Pappas. Hawking radiation spectra for scalar fields by a higher-dimensional Schwarzschild–de Sitter black hole. *Phys. Rev.*, D94(2):024035, 2016. doi:10.1103/PhysRevD.94.024035.

[4] Panagiota Kanti and Thomas Pappas. Effective temperatures and radiation spectra for a higher-dimensional Schwarzschild–de Sitter black hole. *Phys. Rev.*, D96(2):024038, 2017. doi:10.1103/PhysRevD.96.024038.

[5] Thomas Pappas and Panagiota Kanti. Schwarzschild–de Sitter spacetime: The role of temperature in the emission of Hawking radiation. *Phys. Lett.*, B775:140–146, 2017. doi:10.1016/j.physletb.2017.10.058.

[6] Alexandros Karam, Thomas Pappas, and Kyriakos Tamvakis. Frame-dependence of higher-order inflationary observables in scalar-tensor theories. *Phys. Rev.*, D96(6):064036, 2017. doi:10.1103/PhysRevD.96.064036.

[7] Alexandros Karam, Luca Marzola, Thomas Pappas, Antonio Racioppi, and Kyriakos Tamvakis. Constant-Roll (Quasi-)Linear Inflation. *JCAP*, 1805(05):011, 2018. doi:10.1088/1475-7516/2018/05/011.

[8] Ignatios Antoniadis, Nima Arkani-Hamed, Savas Dimopoulos, and G. R. Dvali. New dimensions at a millimeter to a Fermi and superstrings at a TeV. *Phys. Lett.*, B436:257–263, 1998. doi:10.1016/S0370-2693(98)00860-0.

[9] Nima Arkani-Hamed, Savas Dimopoulos, and G. R. Dvali. The Hierarchy problem and new dimensions at a millimeter. *Phys. Lett.*, B429:263–272, 1998. doi:10.1016/S0370-2693(98)00466-3.

[10] Nima Arkani-Hamed, Savas Dimopoulos, and G. R. Dvali. Phenomenology, astrophysics and cosmology of theories with submillimeter dimensions and TeV scale quantum gravity. *Phys. Rev.*, D59:086004, 1999. doi:10.1103/PhysRevD.59.086004.

[11] Lisa Randall and Raman Sundrum. A Large mass hierarchy from a small extra dimension. *Phys. Rev. Lett.*, 83:3370–3373, 1999. doi:10.1103/PhysRevLett.83.3370.

[12] Lisa Randall and Raman Sundrum. An Alternative to compactification. *Phys. Rev. Lett.*, 83: 4690–4693, 1999. doi:10.1103/PhysRevLett.83.4690.

[13] Albert Einstein. The Foundation of the General Theory of Relativity. *Annalen Phys.*, 49(7):769–822, 1916. doi:10.1002/andp.200590044, 10.1002/andp.19163540702. [Annalen Phys.14,517(2005)].

[14] Clifford M. Will. The Confrontation between General Relativity and Experiment. *Living Rev. Rel.*, 17:4, 2014. doi:10.12942/lrr-2014-4.

[15] Sean Carroll. *Spacetime and Geometry: An Introduction to General Relativity*. Pearson, 2003. ISBN 978-0805387322.

[16] Hans C. Ohanian and Remo Ruffini. *Gravitation and Spacetime*. Cambridge University Press, 2013. ISBN 978-1107012943.

[17] Ray d'Inverno. *Introducing Einstein's Relativity*. Clarendon Press, 1992. ISBN 978-0198596868.

[18] T. Padmanabhan. *Gravitation: Foundations and Frontiers*. Cambridge University Press, 2010. ISBN 978-0521882231.

[19] Øyvind Grøn. Lecture notes on the general theory of relativity: From Newton's attractive gravity to the repulsive gravity of vacuum energy. 2009. doi:10.1007/978-0-387-88134-8. [Lect. Notes Phys.772,pp. 1(2009)].

[20] Anthony Zee. *Einstein Gravity in a Nutshell*. Princeton University Press, 1st edition edition, 2013. ISBN 978-0691145587.

[21] Norbert Straumann. *General Relativity*. Springer Netherlands, 2013. ISBN 978-94-007-5409-6.

[22] Robert M. Wald. *General Relativity*. University of Chicago Press, 1984.

[23] Jerry B. Griffiths and Jiří Podolský. *Exact Space-Times in Einstein's General Relativity*. Cambridge University Press, 2012. ISBN 9781107406186.

[24] Martin M. Lipschutz. *Schaum's Outline of Differential Geometry*. McGraw-Hill Education, 1 edition edition, 1969. ISBN 978-0070379855.

[25] Barrett O'Neill. *Elementary Differential Geometry*. Academic Press, 2 edition edition, (April 10, 2006). ISBN 978-0120887354.

[26] Eric Poisson. *A Relativist's Toolkit The Mathematics of Black-Hole Mechanics*. Cambridge University Press, 2009. ISBN 9780511606601.

[27] Albert Einstein. Cosmological Considerations in the General Theory of Relativity. *Sitzungsber. Preuss. Akad. Wiss. Berlin (Math. Phys.)*, 1917:142–152, 1917.

[28] Karl Schwarzschild. On the gravitational field of a mass point according to Einstein's theory. *Sitzungsber. Preuss. Akad. Wiss. Berlin (Math. Phys.)*, 1916:189–196, 1916.

[29] G. D. Birkhoff and R. E. Langer. *Relativity and Modern Physics*. Harvard U. Press Cambridge, MA, 1923.

[30] F. R. Tangherlini. Schwarzschild field in n dimensions and the dimensionality of space problem. *Nuovo Cim.*, 27:636–651, 1963. doi:10.1007/BF02784569.

[31] Valeri Frolov and Igor Novikov. *Black hole physics: basic concepts and new developments*, volume 96. Springer Science & Business Media, 2012.

[32] Eleftherios Papantonopoulos, editor. *Physics of Black Holes A Guided Tour*. Springer-Verlag Berlin Heidelberg, 2009. ISBN 978-3-540-88459-0.

[33] Valeri P. Frolov and Andrei Zelnikov. *Introduction to Black Hole Physics*. Oxford University Press, 2011. ISBN 978-0198729112.

[34] Derek J Raine and Edwin Thomas. *Black Holes: A Student Text*. Imperial College Press, 3 edition edition, 2014. ISBN 978-1783264827.

[35] Andrew Strominger. Les Houches lectures on black holes. In *NATO Advanced Study Institute: Les Houches Summer School, Session 62: Fluctuating Geometries in Statistical Mechanics and Field Theory Les Houches, France, August 2-September 9, 1994*, 1994.

[36] Xavier Calmet, editor. *Quantum aspects of black holes*, volume 178. Springer, 2015. ISBN 9783319108513, 9783319108520. doi:10.1007/978-3-319-10852-0. URL http://www.springer.com/978-3-319-10851-3.

[37] M. Parsa, A. Eckart, B. Shahzamanian, V. Karas, M. Zajacek, J. A. Zensus, and C. Straubmeier. Investigating the relativistic motion of the stars near the supermassive black hole in the galactic center. doi:10.3847/1538-4357/aa7bf0.

[38] B. P. Abbott et al. Observation of Gravitational Waves from a Binary Black Hole Merger. *Phys. Rev. Lett.*, 116(6):061102, 2016. doi:10.1103/PhysRevLett.116.061102.

[39] Angelo Ricarte and Jason Dexter. The Event Horizon Telescope: exploring strong gravity and accretion physics. *Mon. Not. Roy. Astron. Soc.*, 446:1973–1987, 2015. doi:10.1093/mnras/stu2128.

[40] R. Penrose. Gravitational collapse: The role of general relativity. *Riv. Nuovo Cim.*, 1:252–276, 1969. [Gen. Rel. Grav.34,1141(2002)].

[41] W. Rindler. Kruskal Space and the Uniformly Accelerated Frame. *Am. J. Phys.*, 34:1174, 1966. doi:10.1119/1.1972547.

[42] Ivan Booth. Black hole boundaries. *Can. J. Phys.*, 83:1073–1099, 2005. doi:10.1139/p05-063.

[43] James M. Bardeen, B. Carter, and S. W. Hawking. The Four laws of black hole mechanics. *Commun. Math. Phys.*, 31:161–170, 1973. doi:10.1007/BF01645742.

[44] Jacob D. Bekenstein. Black holes and entropy. *Phys. Rev.*, D7:2333–2346, 1973. doi:10.1103/PhysRevD.7.2333.

[45] J. D. Bekenstein. Transcendence of the law of baryon-number conservation in black hole physics. *Phys. Rev. Lett.*, 28:452–455, 1972. doi:10.1103/PhysRevLett.28.452.

[46] C. Teitelboim. Nonmeasurability of the lepton number of a black hole. *Lett. Nuovo Cim.*, 3S2: 397–400, 1972. doi:10.1007/BF02826050. [Lett. Nuovo Cim.3,397(1972)].

[47] J. D. Bekenstein. Novel "no-scalar-hair" theorem for black holes. *Phys. Rev.*, D51(12):R6608, 1995. doi:10.1103/PhysRevD.51.R6608.

[48] S. W. Hawking. Particle Creation by Black Holes. *Commun. Math. Phys.*, 43:199–220, 1975. doi:10.1007/BF02345020. [,167(1975)].

[49] W. G. Unruh. Notes on black hole evaporation. *Phys. Rev.*, D14:870, 1976. doi:10.1103/PhysRevD.14.870.

[50] G. W. Gibbons and S. W. Hawking. Action Integrals and Partition Functions in Quantum Gravity. *Phys. Rev.*, D15:2752–2756, 1977. doi:10.1103/PhysRevD.15.2752.

[51] G. W. Gibbons and M. J. Perry. Black Holes and Thermal Green's Functions. *Proc. Roy. Soc. Lond.*, A358:467–494, 1978. doi:10.1098/rspa.1978.0022.

[52] Bryce S. DeWitt. Quantum Field Theory in Curved Space-Time. *Phys. Rept.*, 19:295–357, 1975. doi:10.1016/0370-1573(75)90051-4.

[53] C. J. Isham. Quantum Field Theory in Curved Space Times: An Overview. In *8th Texas Symposium on Relativistic Astrophysics Boston, Mass., December 13-17, 1976*, page 114, 1977.

[54] N. D. Birrell and P. C. W. Davies. *Quantum Fields in Curved Space*. Cambridge University Press, 1984. ISBN 978-0521278584.

[55] S. A. Fulling. Aspects of Quantum Field Theory in Curved Space-time. *London Math. Soc. Student Texts*, 17:1–315, 1989.

[56] Robert M. Wald. *Quantum Field Theory in Curved Space-Time and Black Hole Thermodynamics*. Chicago Lectures in Physics. University of Chicago Press, Chicago, IL, 1995. ISBN 9780226870274.

[57] L. H. Ford. Quantum field theory in curved space-time. In *Particles and fields. Proceedings, 9th Jorge Andre Swieca Summer School, Campos do Jordao, Brazil, February 16-28, 1997*, pages 345–388, 1997.

[58] Andreas Wipf. Quantum fields near black holes. *Lect. Notes Phys.*, 514:385–415, 1998. doi:10.1007/978-3-540-49535-2_19.

[59] Jennie H. Traschen. An Introduction to black hole evaporation. In *Mathematical methods in physics. Proceedings, Winter School, Londrina, Brazil, August 17-26, 1999*, 1999.

[60] Ted Jacobson. Introduction to quantum fields in curved space-time and the Hawking effect. In *Lectures on quantum gravity. Proceedings, School of Quantum Gravity, Valdivia, Chile, January 4-14, 2002*, pages 39–89, 2003. doi:10.1007/0-387-24992-3_2.

[61] Leonard Parker and David Toms. *Quantum Field Theory in Curved Spacetime: Quantized Fields and Gravity*. Cambridge University Press, 2009. ISBN 978-0521877879.

[62] Don N. Page. Hawking radiation and black hole thermodynamics. *New J. Phys.*, 7:203, 2005. doi:10.1088/1367-2630/7/1/203.

[63] N. N. Bogolyubov. A New method in the theory of superconductivity. I. *Sov. Phys. JETP*, 7: 41–46, 1958. [Front. Phys.6,399(1961)].

[64] Panagiota Kanti. *Black holes in the framework of the four-dimensional effective theory of heterotic superstrings at low-energies*. PhD thesis, Ioannina U., 1998.

[65] Samir D. Mathur. The Information paradox: A Pedagogical introduction. *Class. Quant. Grav.*, 26:224001, 2009. doi:10.1088/0264-9381/26/22/224001.

[66] Theodor Kaluza. Zum Unitätsproblem der Physik. *Sitzungsber. Preuss. Akad. Wiss. Berlin (Math. Phys.)*, 1921:966–972, 1921.

[67] Oskar Klein. Quantum Theory and Five-Dimensional Theory of Relativity. (In German and English). *Z. Phys.*, 37:895–906, 1926. doi:10.1007/BF01397481. [,76(1926)].

[68] Robert C. Myers and M. J. Perry. Black Holes in Higher Dimensional Space-Times. *Annals Phys.*, 172:304, 1986. doi:10.1016/0003-4916(86)90186-7.

[69] R. Balbinot. Hawking radiation and the back reaction - a first approach. *Class. Quant. Grav.*, 1(5):573–577, 1984. doi:10.1088/0264-9381/1/5/010.

[70] S. Perlmutter et al. Measurements of Omega and Lambda from 42 high redshift supernovae. *Astrophys. J.*, 517:565–586, 1999. doi:10.1086/307221.

[71] Adam G. Riess et al. Observational evidence from supernovae for an accelerating universe and a cosmological constant. *Astron. J.*, 116:1009–1038, 1998. doi:10.1086/300499.

[72] P. Ruiz-Lapuente, A. Burkert, and R. Canal. Type Ia supernova scenarios and the Hubble sequence. *Astrophys. J.*, 447:L69, 1995. doi:10.1086/309564.

[73] David Branch. Type Ia supernovae and the Hubble constant. *Ann. Rev. Astron. Astrophys.*, 36: 17–55, 1998. doi:10.1146/annurev.astro.36.1.17.

[74] Robert A. Knop et al. New constraints on Omega(M), Omega(lambda), and w from an independent set of eleven high-redshift supernovae observed with HST. *Astrophys. J.*, 598:102, 2003. doi:10.1086/378560.

[75] Adam G. Riess et al. Type Ia supernova discoveries at z > 1 from the Hubble Space Telescope: Evidence for past deceleration and constraints on dark energy evolution. *Astrophys. J.*, 607: 665–687, 2004. doi:10.1086/383612.

[76] A. D. Miller, R. Caldwell, M. J. Devlin, W. B. Dorwart, T. Herbig, M. R. Nolta, L. A. Page, J. Puchalla, E. Torbet, and H. T. Tran. A measurement of the angular power spectrum of the cmb from l = 100 to 400. *Astrophys. J.*, 524:L1–L4, 1999. doi:10.1086/312293.

[77] P. de Bernardis et al. A Flat universe from high resolution maps of the cosmic microwave background radiation. *Nature*, 404:955–959, 2000. doi:10.1038/35010035.

[78] S. Hanany et al. MAXIMA-1: A Measurement of the cosmic microwave background anisotropy on angular scales of 10 arcminutes to 5 degrees. *Astrophys. J.*, 545:L5, 2000. doi:10.1086/317322.

[79] N. W. Halverson et al. DASI first results: A Measurement of the cosmic microwave background angular power spectrum. *Astrophys. J.*, 568:38–45, 2002. doi:10.1086/338879.

[80] Will J. Percival et al. The 2dF Galaxy Redshift Survey: The Power spectrum and the matter content of the Universe. *Mon. Not. Roy. Astron. Soc.*, 327:1297, 2001. doi:10.1046/j.1365-8711.2001.04827.x.

[81] Raul Jimenez, Licia Verde, Tommaso Treu, and Daniel Stern. Constraints on the equation of state of dark energy and the Hubble constant from stellar ages and the CMB. *Astrophys. J.*, 593:622–629, 2003. doi:10.1086/376595.

[82] Daniel Stern, Raul Jimenez, Licia Verde, Marc Kamionkowski, and S. Adam Stanford. Cosmic Chronometers: Constraining the Equation of State of Dark Energy. I: H(z) Measurements. *JCAP*, 1002:008, 2010. doi:10.1088/1475-7516/2010/02/008.

[83] Panagiota Kanti. Black Holes at the LHC. *Lect. Notes Phys.*, 769:387–423, 2009. doi:10.1007/978-3-540-88460-6_10.

[84] C. Molina. Quasinormal modes of d-dimensional spherical black holes with near extreme cosmological constant. *Phys. Rev.*, D68:064007, 2003. doi:10.1103/PhysRevD.68.064007.

[85] G. W. Gibbons and S. W. Hawking. Cosmological Event Horizons, Thermodynamics, and Particle Creation. *Phys. Rev.*, D15:2738–2751, 1977. doi:10.1103/PhysRevD.15.2738.

[86] Z. Stuchlik and S. Hledik. Some properties of the Schwarzschild-de Sitter and Schwarzschild - anti-de Sitter space-times. *Phys. Rev.*, D60:044006, 1999. doi:10.1103/PhysRevD.60.044006.

[87] Paul H. Ginsparg and Malcolm J. Perry. Semiclassical Perdurance of de Sitter Space. *Nucl. Phys.*, B222:245–268, 1983. doi:10.1016/0550-3213(83)90636-3.

[88] T. Shiromizu, K. Nakao, Hideo Kodama, and Kei-Ichi Maeda. Can large black holes collide in de Sitter space-time? An inflationary scenario of an inhomogeneous universe. *Phys. Rev.*, D47: R3099–R3102, 1993. doi:10.1103/PhysRevD.47.R3099.

[89] Sean A. Hayward, Tetsuya Shiromizu, and Ken-ichi Nakao. A Cosmological constant limits the size of black holes. *Phys. Rev.*, D49:5080–5085, 1994. doi:10.1103/PhysRevD.49.5080.

[90] Hidekazu Nariai. On a new cosmological solution of einstein's field equations of gravitation. *Science reports of the Tohoku University 1st ser. Physics, chemistry, astronomy*, 35(1):62–67, 1951.

[91] Brian P. Dolan. Black holes and Boyle's law — The thermodynamics of the cosmological constant. *Mod. Phys. Lett.*, A30(03n04):1540002, 2015. doi:10.1142/S0217732315400027.

[92] J. A. H. Futterman, F. A. Handler, and R. A. Matzner. *Scattering From Black Holes*. Cambridge University Press, 2012. ISBN 9781139245395, 9780521112109.

[93] Troels Harmark, Jose Natario, and Ricardo Schiappa. Greybody Factors for d-Dimensional Black Holes. *Adv. Theor. Math. Phys.*, 14(3):727–794, 2010. doi:10.4310/ATMP.2010.v14.n3.a1.

[94] Petarpa Boonserm. *Rigorous bounds on Transmission, Reflection, and Bogoliubov coefficients*. PhD thesis, Victoria U., Wellington, 2009. URL http://inspirehep.net/record/1325687/files/arXiv:0907.0045.pdf.

[95] Tullio Regge and John A. Wheeler. Stability of a Schwarzschild singularity. *Phys. Rev.*, 108: 1063–1069, 1957. doi:10.1103/PhysRev.108.1063.

[96] P. Kanti, Julien Grain, and A. Barrau. Bulk and brane decay of a (4+n)-dimensional Schwarzschild-de-Sitter black hole: Scalar radiation. *Phys. Rev.*, D71:104002, 2005. doi:10.1103/PhysRevD.71.104002.

[97] G. V. Kraniotis. The Klein–Gordon–Fock equation in the curved spacetime of the Kerr–Newman (anti) de Sitter black hole. *Class. Quant. Grav.*, 33(22):225011, 2016. doi:10.1088/0264-9381/33/22/225011.

[98] W. G. Unruh. Absorption Cross-Section of Small Black Holes. *Phys. Rev.*, D14:3251–3259, 1976. doi:10.1103/PhysRevD.14.3251.

[99] Luís C. B. Crispino, Atsushi Higuchi, Ednilton S. Oliveira, and Jorge V. Rocha. Greybody factors for nonminimally coupled scalar fields in Schwarzschild–de Sitter spacetime. *Phys. Rev.*, D87:104034, 2013. doi:10.1103/PhysRevD.87.104034.

[100] Vitor Cardoso and Oscar J. C. Dias. Small Kerr-anti-de Sitter black holes are unstable. *Phys. Rev.*, D70:084011, 2004. doi:10.1103/PhysRevD.70.084011.

[101] Juan Martin Maldacena and Andrew Strominger. Universal low-energy dynamics for rotating black holes. *Phys. Rev.*, D56:4975–4983, 1997. doi:10.1103/PhysRevD.56.4975.

[102] Don N. Page. Particle Emission Rates from a Black Hole: Massless Particles from an Uncharged, Nonrotating Hole. *Phys. Rev.*, D13:198–206, 1976. doi:10.1103/PhysRevD.13.198.

[103] Milton Abramowitz and Irene A. Stegun. *Handbook of Mathematical Functions: with Formulas, Graphs, and Mathematical Tables*. Dover Publications, 1965. ISBN 978-0486612720.

[104] Patrick R. Brady, Chris M. Chambers, William Krivan, and Pablo Laguna. Telling tails in the presence of a cosmological constant. *Phys. Rev.*, D55:7538–7545, 1997. doi:10.1103/PhysRevD.55.7538.

[105] Molin Liu, Benhai Yu, Rumin Wang, and Lixin Xu. Scattering of scalar perturbations with cosmological constant in low-energy and high-energy regimes. *Mod. Phys. Lett.*, 25:2431–2445, 2010. doi:10.1142/S0217732310033621.

[106] Shao-Feng Wu, Shao-yu Yin, Guo-Hong Yang, and Peng-Ming Zhang. Energy and entropy radiated by a black hole embedded in de-Sitter braneworld. *Phys. Rev.*, D78:084010, 2008. doi:10.1103/PhysRevD.78.084010.

[107] Ey-lee Jung, Sung-Hoon Kim, and D. K. Park. Absorption cross-section for S wave massive scalar. *Phys. Lett.*, B586:390–396, 2004. doi:10.1016/j.physletb.2004.02.001.

[108] Eylee Jung, SungHoon Kim, and D. K. Park. Low-energy absorption cross section for massive scalar and Dirac fermion by (4+n)-dimensional Schwarzschild black hole. *JHEP*, 09:005, 2004. doi:10.1088/1126-6708/2004/09/005.

[109] Marco O. P. Sampaio. Charge and mass effects on the evaporation of higher-dimensional rotating black holes. *JHEP*, 10:008, 2009. doi:10.1088/1126-6708/2009/10/008.

[110] Marco O. P. Sampaio. Distributions of charged massive scalars and fermions from evaporating higher-dimensional black holes. *JHEP*, 02:042, 2010. doi:10.1007/JHEP02(2010)042.

[111] P. Kanti and N. Pappas. Emission of Massive Scalar Fields by a Higher-Dimensional Rotating Black-Hole. *Phys. Rev.*, D82:024039, 2010. doi:10.1103/PhysRevD.82.024039.

[112] Claus Müller. *Spherical Harmonics*. Springer-Verlag Berlin Heidelberg, 1966. ISBN 978-3-540-37174-8.

[113] Wolfram Research, Inc. Mathematica, Version 11.3. Champaign, IL, 2018.

[114] Don N. Page. Particle Emission Rates from a Black Hole. 3. Charged Leptons from a Nonrotating Hole. *Phys. Rev.*, D16:2402–2411, 1977. doi:10.1103/PhysRevD.16.2402.

[115] Eylee Jung, SungHoon Kim, and D. K. Park. Proof of universality for the absorption of massive scalar by the higher-dimensional Reissner-Nordstrom black holes. *Phys. Lett.*, B602:105–111, 2004. doi:10.1016/j.physletb.2004.09.067.

[116] Chris M. Harris and Panagiota Kanti. Hawking radiation from a (4+n)-dimensional black hole: Exact results for the Schwarzschild phase. *JHEP*, 10:014, 2003. doi:10.1088/1126-6708/2003/10/014.

[117] Panagiota Kanti. Black holes in theories with large extra dimensions: A Review. *Int. J. Mod. Phys.*, A19:4899–4951, 2004. doi:10.1142/S0217751X04018324.

[118] Myron Bander and Claude Itzykson. GROUP THEORY AND THE HYDROGEN ATOM. *Rev. Mod. Phys.*, 38:330–345, 1966. doi:10.1103/RevModPhys.38.330.

[119] Raphael Bousso and Stephen W. Hawking. Pair creation of black holes during inflation. *Phys. Rev.*, D54:6312–6322, 1996. doi:10.1103/PhysRevD.54.6312.

[120] Panagiota Kanti and John March-Russell. Calculable corrections to brane black hole decay. 1. The scalar case. *Phys. Rev.*, D66:024023, 2002. doi:10.1103/PhysRevD.66.024023.

[121] Daisuke Ida, Kin-ya Oda, and Seong Chan Park. Rotating black holes at future colliders: Greybody factors for brane fields. *Phys. Rev.*, D67:064025, 2003. doi:10.1103/PhysRevD.67.064025, 10.1103/PhysRevD.69.049901. [Erratum: Phys. Rev.D69,049901(2004)].

[122] Valeri P. Frolov and Dejan Stojkovic. Quantum radiation from a five-dimensional rotating black hole. *Phys. Rev.*, D67:084004, 2003. doi:10.1103/PhysRevD.67.084004.

[123] G. Duffy, C. Harris, P. Kanti, and E. Winstanley. Brane decay of a (4+n)-dimensional rotating black hole: Spin-0 particles. *JHEP*, 09:049, 2005. doi:10.1088/1126-6708/2005/09/049.

[124] Hidefumi Nomura, Shijun Yoshida, Makoto Tanabe, and Kei-ichi Maeda. The Fate of a five-dimensional rotating black hole via Hawking radiation. *Prog. Theor. Phys.*, 114:707–712, 2005. doi:10.1143/PTP.114.707.

[125] Eylee Jung and D. K. Park. Bulk versus brane in the absorption and emission: 5-D rotating black hole case. *Nucl. Phys.*, B731:171–187, 2005. doi:10.1016/j.nuclphysb.2005.10.012.

[126] Daisuke Ida, Kin-ya Oda, and Seong Chan Park. Rotating black holes at future colliders. II. Anisotropic scalar field emission. *Phys. Rev.*, D71:124039, 2005. doi:10.1103/PhysRevD.71.124039.

[127] Daisuke Ida, Kin-ya Oda, and Seong Chan Park. Rotating black holes at future colliders. III. Determination of black hole evolution. *Phys. Rev.*, D73:124022, 2006. doi:10.1103/PhysRevD.73.124022.

[128] Alan S. Cornell, Wade Naylor, and Misao Sasaki. Graviton emission from a higher-dimensional black hole. *JHEP*, 02:012, 2006. doi:10.1088/1126-6708/2006/02/012.

[129] Vitor Cardoso, Marco Cavaglia, and Leonardo Gualtieri. Black Hole Particle Emission in Higher-Dimensional Spacetimes. *Phys. Rev. Lett.*, 96:071301, 2006. doi:10.1103/PhysRevLett.96.219902, 10.1103/PhysRevLett.96.071301. [Erratum: Phys. Rev. Lett.96,219902(2006)].

[130] Vitor Cardoso, Marco Cavaglia, and Leonardo Gualtieri. Hawking emission of gravitons in higher dimensions: Non-rotating black holes. *JHEP*, 02:021, 2006. doi:10.1088/1126-6708/2006/02/021.

[131] S. Creek, O. Efthimiou, P. Kanti, and K. Tamvakis. Graviton emission in the bulk from a higher-dimensional Schwarzschild black hole. *Phys. Lett.*, B635:39–49, 2006. doi:10.1016/j.physletb.2006.02.030.

[132] Marc Casals, S. R. Dolan, P. Kanti, and E. Winstanley. Brane Decay of a (4+n)-Dimensional Rotating Black Hole. III. Spin-1/2 particles. *JHEP*, 03:019, 2007. doi:10.1088/1126-6708/2007/03/019.

[133] Eylee Jung and D. K. Park. Validity of Emparan-Horowitz-Myers argument in Hawking radiation into massless spin-2 fields. *Mod. Phys. Lett.*, A22:1635–1642, 2007. doi:10.1142/S021773230702405X.

[134] S. Creek, O. Efthimiou, P. Kanti, and K. Tamvakis. Greybody factors for brane scalar fields in a rotating black-hole background. *Phys. Rev.*, D75:084043, 2007. doi:10.1103/PhysRevD.75.084043.

[135] S. Creek, O. Efthimiou, P. Kanti, and K. Tamvakis. Greybody factors in a rotating black-hole background. II. Fermions and gauge bosons. *Phys. Rev.*, D76:104013, 2007. doi:10.1103/PhysRevD.76.104013.

[136] S. Creek, O. Efthimiou, P. Kanti, and K. Tamvakis. Scalar Emission in the Bulk in a Rotating Black Hole Background. *Phys. Lett.*, B656:102–111, 2007. doi:10.1016/j.physletb.2007.09.050.

[137] M. Casals, S. R. Dolan, P. Kanti, and E. Winstanley. Bulk Emission of Scalars by a Rotating Black Hole. *JHEP*, 06:071, 2008. doi:10.1088/1126-6708/2008/06/071.

[138] Songbai Chen, Bin Wang, Ru-Keng Su, and W. Y Pauchy Hwang. Greybody factors for rotating black holes on codimension-2 branes. *JHEP*, 03:019, 2008. doi:10.1088/1126-6708/2008/03/019.

[139] Hideo Kodama. Superradiance and Instability of Black Holes. *Prog. Theor. Phys. Suppl.*, 172: 11–20, 2008. doi:10.1143/PTPS.172.11.

[140] Jason Doukas, H. T. Cho, A. S. Cornell, and Wade Naylor. Graviton emission from simply rotating Kerr-de Sitter black holes: Transverse traceless tensor graviton modes. *Phys. Rev.*, D80:045021, 2009. doi:10.1103/PhysRevD.80.045021.

[141] P. Kanti, H. Kodama, R. A. Konoplya, N. Pappas, and A. Zhidenko. Graviton Emission in the Bulk by a Simply Rotating Black Hole. *Phys. Rev.*, D80:084016, 2009. doi:10.1103/PhysRevD.80.084016.

[142] Antonino Flachi, Misao Sasaki, and Takahiro Tanaka. Spin polarization effects in micro black hole evaporation. *JHEP*, 05:031, 2009. doi:10.1088/1126-6708/2009/05/031.

[143] Panagiota Kanti and John March-Russell. Calculable corrections to brane black hole decay. 2. Greybody factors for spin 1/2 and 1. *Phys. Rev.*, D67:104019, 2003. doi:10.1103/PhysRevD.67.104019.

[144] S. W. Hawking. Gravitational radiation from colliding black holes. *Phys. Rev. Lett.*, 26:1344–1346, 1971. doi:10.1103/PhysRevLett.26.1344.

[145] S. W. Hawking. Black holes in general relativity. *Commun. Math. Phys.*, 25:152–166, 1972. doi:10.1007/BF01877517.

[146] S. W. Hawking and G. F. R. Ellis. *The Large Scale Structure of Space-Time*. Cambridge Monographs on Mathematical Physics. Cambridge University Press, 2011. ISBN 9780521200165, 9780521099066, 9780511826306, 9780521099066. doi:10.1017/CBO9780511524646.

[147] James W. York, Jr. Black Hole in Thermal Equilibrium With a Scalar Field: The Back Reaction. *Phys. Rev.*, D31:775, 1985. doi:10.1103/PhysRevD.31.775.

[148] William Ballik and Kayll Lake. Vector volume and black holes. *Phys. Rev.*, D88(10):104038, 2013. doi:10.1103/PhysRevD.88.104038.

[149] J. Labbe, A. Barrau, and Julien Grain. Phenomenology of black hole evaporation with a cosmological constant. *PoS*, HEP2005:013, 2006.

[150] Yuichi Sekiwa. Thermodynamics of de Sitter black holes: Thermal cosmological constant. *Phys. Rev.*, D73:084009, 2006. doi:10.1103/PhysRevD.73.084009.

[151] L. J. Romans. Supersymmetric, cold and lukewarm black holes in cosmological Einstein-Maxwell theory. *Nucl. Phys.*, B383:395–415, 1992. doi:10.1016/0550-3213(92)90684-4.

[152] David Kastor and Jennie H. Traschen. Cosmological multi - black hole solutions. *Phys. Rev.*, D47:5370–5375, 1993. doi:10.1103/PhysRevD.47.5370.

[153] Miho Urano, Akira Tomimatsu, and Hiromi Saida. Mechanical First Law of Black Hole Spacetimes with Cosmological Constant and Its Application to Schwarzschild-de Sitter Spacetime. *Class. Quant. Grav.*, 26:105010, 2009. doi:10.1088/0264-9381/26/10/105010.

[154] S. Shankaranarayanan. Temperature and entropy of Schwarzschild-de Sitter space-time. *Phys. Rev.*, D67:084026, 2003. doi:10.1103/PhysRevD.67.084026.

[155] Sourav Bhattacharya and Amitabha Lahiri. Mass function and particle creation in Schwarzschild-de Sitter spacetime. *Eur. Phys. J.*, C73:2673, 2013. doi:10.1140/epjc/s10052-013-2673-6.

[156] Sourav Bhattacharya. A note on entropy of de Sitter black holes. *Eur. Phys. J.*, C76(3):112, 2016. doi:10.1140/epjc/s10052-016-3955-6.

[157] Huai-Fan Li, Meng-Sen Ma, and Ya-Qin Ma. Thermodynamic properties of black holes in de Sitter space. *Mod. Phys. Lett.*, A32(02):1750017, 2016. doi:10.1142/S0217732317500171.

[158] David Kubiznak, Robert B. Mann, and Mae Teo. Black hole chemistry: thermodynamics with Lambda. *Class. Quant. Grav.*, 34(6):063001, 2017. doi:10.1088/1361-6382/aa5c69.

[159] Vivek Iyer and Robert M. Wald. Some properties of Noether charge and a proposal for dynamical black hole entropy. *Phys. Rev.*, D50:846–864, 1994. doi:10.1103/PhysRevD.50.846.

[160] Robert M. Wald. Black hole entropy is the Noether charge. *Phys. Rev.*, D48(8):R3427–R3431, 1993. doi:10.1103/PhysRevD.48.R3427.

[161] Philip C. Argyres, Savas Dimopoulos, and John March-Russell. Black holes and submillimeter dimensions. *Phys. Lett.*, B441:96–104, 1998. doi:10.1016/S0370-2693(98)01184-8.

[162] A. Chamblin, S. W. Hawking, and H. S. Reall. Brane world black holes. *Phys. Rev.*, D61:065007, 2000. doi:10.1103/PhysRevD.61.065007.

[163] Roy Maartens. Brane world gravity. *Living Rev. Rel.*, 7:7, 2004. doi:10.12942/lrr-2004-7.

[164] Archan S. Majumdar and N. Mukherjee. Braneworld black holes in cosmology and astrophysics. *Int. J. Mod. Phys.*, D14:1095, 2005. doi:10.1142/S0218271805006948.

[165] Panagiota Kanti. Brane-World Black Holes. *J. Phys. Conf. Ser.*, 189:012020, 2009. doi:10.1088/1742-6596/189/1/012020.

[166] Ruth Gregory. Braneworld black holes. *Lect. Notes Phys.*, 769:259–298, 2009. doi:10.1007/978-3-540-88460-6_7.

[167] Nikolaos D. Pappas. The black hole challenge in Randall-Sundrum II model. 2014.

[168] Panagiota Kanti and Elizabeth Winstanley. Hawking Radiation from Higher-Dimensional Black Holes. *Fundam. Theor. Phys.*, 178:229–265, 2015. doi:10.1007/978-3-319-10852-0_8.

[169] Naresh Dadhich, Roy Maartens, Philippos Papadopoulos, and Vahid Rezania. Black holes on the brane. *Phys. Lett.*, B487:1–6, 2000. doi:10.1016/S0370-2693(00)00798-X.

[170] Roberto Emparan, Gary T. Horowitz, and Robert C. Myers. Exact description of black holes on branes. *JHEP*, 01:007, 2000. doi:10.1088/1126-6708/2000/01/007.

[171] G. Kofinas, E. Papantonopoulos, and Vassilios Zamarias. Black hole solutions in brane worlds with induced gravity. *Phys. Rev.*, D66:104028, 2002. doi:10.1103/PhysRevD.66.104028.

[172] Panagiota Kanti and Kyriakos Tamvakis. Quest for localized 4-D black holes in brane worlds. *Phys. Rev.*, D65:084010, 2002. doi:10.1103/PhysRevD.65.084010.

[173] P. Kanti, I. Olasagasti, and K. Tamvakis. Quest for localized 4-D black holes in brane worlds. 2. Removing the bulk singularities. *Phys. Rev.*, D68:124001, 2003. doi:10.1103/PhysRevD.68.124001.

[174] Roberto Casadio, Alessandro Fabbri, and Lorenzo Mazzacurati. New black holes in the brane world? *Phys. Rev.*, D65:084040, 2002. doi:10.1103/PhysRevD.65.084040.

[175] Valeri P. Frolov, Martin Snajdr, and Dejan Stojkovic. Interaction of a brane with a moving bulk black hole. *Phys. Rev.*, D68:044002, 2003. doi:10.1103/PhysRevD.68.044002.

[176] D. Karasik, C. Sahabandu, P. Suranyi, and L. C. R. Wijewardhana. Small black holes on branes: Is the horizon regular or singular? *Phys. Rev.*, D70:064007, 2004. doi:10.1103/PhysRevD.70.064007.

[177] Christophe Galfard, Cristiano Germani, and Akihiro Ishibashi. Asymptotically AdS brane black holes. *Phys. Rev.*, D73:064014, 2006. doi:10.1103/PhysRevD.73.064014.

[178] Simon Creek, Ruth Gregory, Panagiota Kanti, and Bina Mistry. Braneworld stars and black holes. *Class. Quant. Grav.*, 23:6633–6658, 2006. doi:10.1088/0264-9381/23/23/004.

[179] Mohamed Anber and Lorenzo Sorbo. New exact solutions on the Randall-Sundrum 2-brane: lumps of dark radiation and accelerated black holes. *JHEP*, 07:098, 2008. doi:10.1088/1126-6708/2008/07/098.

[180] R. Casadio and J. Ovalle. Brane-world stars and (microscopic) black holes. *Phys. Lett.*, B715: 251–255, 2012. doi:10.1016/j.physletb.2012.07.041.

[181] J Ovalle and F Linares. Tolman IV solution in the Randall-Sundrum Braneworld. *Phys. Rev.*, D88(10):104026, 2013. doi:10.1103/PhysRevD.88.104026.

[182] Jorge Ovalle, László Á. Gergely, and Roberto Casadio. Brane-world stars with a solid crust and vacuum exterior. *Class. Quant. Grav.*, 32:045015, 2015. doi:10.1088/0264-9381/32/4/045015.

[183] Roberto Casadio, Jorge Ovalle, and Roldão da Rocha. The Minimal Geometric Deformation Approach Extended. *Class. Quant. Grav.*, 32(21):215020, 2015. doi:10.1088/0264-9381/32/21/215020.

[184] Tiberiu Harko and Matthew J. Lake. Null fluid collapse in brane world models. *Phys. Rev.*, D89:064038, 2014. doi:10.1103/PhysRevD.89.064038.

[185] André M. Kuerten and Roldão da Rocha. Probing topologically charged black holes on brane worlds in $f(\mathrm{R})$ bulk. *Gen. Rel. Grav.*, 48(7):90, 2016. doi:10.1007/s10714-016-2092-8.

[186] Hideaki Kudoh, Takahiro Tanaka, and Takashi Nakamura. Small localized black holes in brane world: Formulation and numerical method. *Phys. Rev.*, D68:024035, 2003. doi:10.1103/PhysRevD.68.024035.

[187] Hideaki Kudoh. Six-dimensional localized black holes: Numerical solutions. *Phys. Rev.*, D69:104019, 2004. doi:10.1103/PhysRevD.70.029901, 10.1103/PhysRevD.69.104019. [Erratum: Phys. Rev.D70,029901(2004)].

[188] Norihiro Tanahashi and Takahiro Tanaka. Time-symmetric initial data of large brane-localized black hole in RS-II model. *JHEP*, 03:041, 2008. doi:10.1088/1126-6708/2008/03/041.

[189] Pau Figueras and Toby Wiseman. Gravity and large black holes in Randall-Sundrum II braneworlds. *Phys. Rev. Lett.*, 107:081101, 2011. doi:10.1103/PhysRevLett.107.081101.

[190] Shohreh Abdolrahimi, Céline Cattoën, Don N. Page, and Shima Yaghoobpour-Tari. Spectral methods in general relativity and large Randall-Sundrum II black holes. *JCAP*, 1306:039, 2013. doi:10.1088/1475-7516/2013/06/039.

[191] P. Vaidya. The Gravitational Field of a Radiating Star. *Proc. Natl. Inst. Sci. India*, A33:264, 1951.

[192] P. C. Vaidya. Newtonian Time in General Relativity. *Nature*, 171:260–261, 1953. doi:10.1038/171260a0.

[193] Bertha Cuadros-Melgar, Eleftherios Papantonopoulos, Minas Tsoukalas, and Vassilios Zamarias. BTZ Like-String on Codimension-2 Braneworlds in the Thin Brane Limit. *Phys. Rev. Lett.*, 100: 221601, 2008. doi:10.1103/PhysRevLett.100.221601.

[194] Malihe Heydari-Fard and Hamid R. Sepangi. Spherically symmetric solutions and gravitational collapse in brane-worlds. *JCAP*, 0902:029, 2009. doi:10.1088/1475-7516/2009/02/029.

[195] De-Chang Dai and Dejan Stojkovic. Analytic solution for a static black hole in RSII model. *Phys. Lett.*, B704:354–359, 2011. doi:10.1016/j.physletb.2011.09.038.

[196] Burkhard Kleihaus, Jutta Kunz, Eugen Radu, and Daniel Senkbeil. Electric charge on the brane? *Phys. Rev.*, D83:104050, 2011. doi:10.1103/PhysRevD.83.104050.

[197] A. A. Andrianov and M. A. Kurkov. Black holes in the brane world: Some exact solutions. *Theor. Math. Phys.*, 169:1629–1642, 2011. doi:10.1007/s11232-011-0140-9, 10.4213/tmf6731. [Teor. Mat. Fiz.169,307(2011)].

[198] P. Kanti, N. Pappas, and K. Zuleta. On the localization of four-dimensional brane-world black holes. *Class. Quant. Grav.*, 30:235017, 2013. doi:10.1088/0264-9381/30/23/235017.

[199] Theodoros Nakas. Searching for Localized Black-Hole solutions in Brane-World models. Master's thesis, Ioannina U., 2017. URL http://inspirehep.net/record/1611667/files/arXiv:1707.08351.pdf.

[200] Julien Grain, A. Barrau, and P. Kanti. Exact results for evaporating black holes in curvature-squared lovelock gravity: Gauss-Bonnet greybody factors. *Phys. Rev.*, D72:104016, 2005. doi:10.1103/PhysRevD.72.104016.

[201] Raphael Bousso and Stephen W. Hawking. (Anti)evaporation of Schwarzschild-de Sitter black holes. *Phys. Rev.*, D57:2436–2442, 1998. doi:10.1103/PhysRevD.57.2436.